RICE UNIVERSITY

Assessing Photocatalytic Oxidation Using Modified TiO_2 Nanomaterials for Virus Inactivation in Drinking Water: Mechanisms and Application

by

Michael Vincent Liga

A THESIS SUBMITTED
IN PARTIAL FULFILLMENT OF THE
REQUIREMENTS FOR THE DEGREE

Doctor of Philosophy

APPROVED, THESIS COMMITTEE

Qilin Li,
Associate Professor, Civil and
Environmental Engineering

Pedro J. J. Alvarez, Department Chair and
George R. Brown Professor of
Engineering, Civil and Environmental
Engineering

Andrew R. Barron, Charles W. Duncan, Jr.
Welch Chair of Chemistry and Professor
of Materials Science

Yizhi J. Tao, Associate Professor,
Biochemistry and Cell Biology

HOUSTON, TEXAS
November 2012

ABSTRACT

Assessing Photocatalytic Oxidation Using Modified TiO_2 Nanomaterials for Virus Inactivation in Drinking Water: Mechanisms and Application

by

Michael Vincent Liga

Photocatalytic oxidation is an alternative water treatment method under consideration for disinfecting water. Chlorine disinfection can form harmful byproducts, and some viruses (e.g. adenoviruses) are resistant to other alternative disinfection methods. Photocatalytic oxidation using nano-sized photocatalytic particles (e.g. TiO_2, fullerene) holds promise; however, it is limited by its low efficiency and long required treatment times. This research focuses on improving virus inactivation by photocatalytic oxidation by modifying catalysts for improved activity, by analyzing virus inactivation kinetics, and by elucidating the inactivation mechanisms of adenovirus serotype 2 (AdV2) and bacteriophage MS2.

Modifying TiO_2 with silver (nAg/TiO_2) or silica (SiO_2-TiO_2) improves the inactivation kinetics of bacteriophage MS2 by a factor of 3-10. nAg/ TiO_2 increases hydroxyl radical (HO•) production while SiO_2 increases the adsorption of MS2 to TiO_2. These results suggest that modifying the photocatalyst surface to increase contaminant adsorption is an important improvement strategy along with increasing HO• production.

The inactivation kinetics of AdV2 by P25 TiO_2 is much slower than the MS2 inactivation kinetics and displays a strong shoulder, which is not present in the MS2 kinetics. nAg/TiO_2 initially improves the inactivation rate of AdV2. SiO_2-TiO_2 reduces the AdV2 inactivation kinetics since adsorption is not significantly enhanced, as it is with MS2. Amino-C_{60} is highly effective for AdV2 inactivation under visible light irradiation, making it a good material for use in solar disinfection systems. The efficacy of amino-fullerene also demonstrates that singlet oxygen is effective for AdV2 inactivation.

When exposed to irradiated TiO_2, AdV2 hexon proteins are heavily damaged resulting in the release of DNA. DNA damage is also present but may occur after capsids break. With MS2, the host interaction protein is rapidly damaged, but not the coat protein. The kinetics of MS2 inactivation are rapid since it may quickly lose its ability to attach to host cells, while AdV2 kinetics are slower since the entire capsid must undergo heavy oxidation before inactivation occurs. Adenovirus inactivation likely occurs through breaching the capsid followed by radical attack of DNA and core proteins.

Acknowledgments

I sincerely thank my advisor, Qilin Li, for her advice and support throughout my studies at Rice. My time here has greatly expanded my critical thinking and scientific abilities, which could not have occurred without her support and guidance. I would like to thank my committee members, Dr. Andrew R. Barron, Dr. Pedro J. J. Alvarez, and Dr. Yizhi Jane Tao for their advice and collaboration with my research. I also thank my lab mates and fellow graduate students for their friendship, collaboration, and advice as I pursued my degree. Most notably I thank Alison and Michael Contreras, Jacques Mathieu, Sen Wang, Xiaolei Qu, Cong Yu, Jinjian Wu, Huma Jafry, and Samuel Maguire-Boyle.

Finally I thank my family supporting me through this process and providing my inspiration to succeed. I am forever grateful to my wife, Angela, for providing the bulk of our family's finances while I pursued my research and for putting up with my long work hours and hectic schedule. To my dear children, Vivian and Oscar, your smiles and love kept me sane and motivated to finish this thesis. I thank my parents for providing the foundation I have built my life on, and I thank my siblings, Christopher and Michelle, for their encouragement.

This research was supported by the Center for Biological and Environmental Nanotechnology at Rice University and the US NAVY, with additional funding provided by E. I. du Pont de Nemours and Company .

Contents

List of Figures

List of Tables

Nomenclature

$^1O_2$	singlet oxygen
AdV	human adenovirus
AdV2	human adenovirus serotype 2
CT	disinfectant concentration * exposure time (mg L^{-1} $min^{-1)}$
HO•	hydroxyl radical
k	rate constant (“true”) or rate constant in Hom equation
k'	pseudo first order rate constant ($time^{-1}$)
K	adsorption equilibrium constant
m	parameter in Hom equation
MS2	bacteriophage MS2
n	parameter in Hom equation
N	virus titer (PFU/mL)
N_0	virus titer after dark stirring with nanoparticles (PFU/mL)
N_s	virus titer in supernatant of virus – nanoparticle Mixture
PFU	Plaque Forming Units
q_{max}	maximum adsorption density of viruses on catalyst particles (PFU/g)

q_e	equilibrium adsorption density of viruses on catalyst particles (PFU/g)
t	time
$TCID_{50}$	50% tissue culture infective dose

Chapter 1

Introduction

Viruses, and human adenoviruses in particular, commonly occur in the environment and are resistant to several drinking and wastewater treatment processes. Worldwide, there are 1.58 million deaths annually due to diarrheal disease attributed to unsafe water supply, sanitation, and poor hygiene, with a large fraction of these attributed to viruses [1]. In 2005 the USEPA placed adenoviruses on their Contaminant Candidate List 2, indicating the need for specific regulation of these viruses [2]. At the same time, the USEPA further limited the acceptable content of disinfection byproducts (BDBPs) present in drinking water [3]. To avoid DBP formation, highly effective free chlorine disinfection has been replaced with alternative processes, such as combined chlorine and/or UV irradiation. Unfortunately adenoviruses are highly resistant to both these treatment methods and increases the treatment time/cost necessary to produce safe water [4, 5].

Another alternative treatment process, photocatalytic oxidation using a high efficiency nanosized photocatalyst (e.g. titanium dioxide (TiO_2), fullerene), has the potential to inactivate viruses more effectively than other methods while limiting the production of DBPs [6, 7]. It may also be used in conjunction with UV disinfection to shorten the required treatment times. While a large volume of work has been published regarding photocatalytic degradation of chemical compounds by TiO_2 based materials, little research has been conducted on the inactivation of microorganisms, especially viruses. Two limited studies exist on the inactivation of pathogenic mammalian viruses (human poliovirus and murine norovirus [8, 9]) which demonstrate that photocatalytic oxidation may be a viable strategy for virus disinfection; however, these relatively simple viruses are highly susceptible to UV_{254} irradiation and are not a good choice for demonstrating the suitability of this treatment method. Demonstrating improvements to the inactivation efficiency of UV_{254} (and other method) resistant viruses would lower treatment costs and reduce the risk of disease caused by virus transmission in drinking water. This research assesses and improves TiO_2 based photocatalytic oxidation for virus inactivation in drinking water disinfection. This will be accomplished by completing three main research objectives:

1. Identify modifications to TiO_2 that result in enhanced virus inactivation efficiency and elucidate the improvement mechanisms

2. Demonstrate photocatalytic inactivation of human adenovirus using neat and modified TiO_2 and amino-fullerenes and describe the inactivation kinetics

3. Determine the biological inactivation mechanism of adenovirus and a common surrogate virus, MS2, by TiO_2. Determine how differences in virus structure and inactivation mechanism translate into differences in inactivation kinetics.

Most studies available on the photocatalytic inactivation of viruses rely on TiO_2 in some form as the photocatalyst due to its low cost, stability, non-toxicity, and high oxidation potential. However, TiO_2 is limited by its high rate of charge recombination, which reduces its efficiency. This results in low inactivation rates and thus long treatment times required to achieve adequate disinfection levels. The first research objective of this study is to identify modifications to TiO_2 that result in enhanced virus inactivation efficiency and elucidating the improvement mechanisms. Catalysts are assayed for virus inactivation potential as suspended particles in a UV-A photoreactor. A surrogate pathogen, bacteriophage MS2, is initially used for identifying improved catalysts due to its ease of propagation and assay and its common role as a surrogate in water disinfection studies. Catalyst modifications leading to enhanced activity against MS2 are assayed against human adenovirus serotype 2 (AdV2).

AdV has been shown to survive for long periods in environmental waters and to resist traditional and some advanced drinking and wastewater treatment methods. No studies to date have been published on the photocatalytic inactivation of AdV. The second objective of this study is to demonstrate AdV2 photocatalytic inactivation and describe the kinetics resulting from application of neat and modified TiO_2 and amino-fullerene catalysts. Virus inactivation is assayed in suspended particle systems in a UV-A photoreactor. Along with demonstrating the inactivation of AdV2, this study evaluates

the suitability of MS2 as a suitable surrogate for photocatalytic disinfection studies. This will is accomplished by comparing the inactivation kinetics and (biological) mechanism of inactivation.

The third objective of this study is to investigate the (biological) inactivation mechanism of AdV2 and MS2 by photocatalytic oxidation. Disinfectants which produce the most rapid adenovirus inactivation act through protein damage [10-13]. Demonstrating that photocatalytic oxidation inactivates adenoviruses through protein damage would give further support to its development as an alternative disinfection method. While capsid and genetic damage are known to occur during TiO_2 photocatalytic oxidation, the amount of damage and specific damage location required to inactivate any virus is not known. There are no studies which determine whether it is damage to protein and/or genetic material that is ultimately responsible for complete inactivation. In addition, there are no reports on specific damage sites to virus protein or DNA by photocatalytic oxidation. In this study sodium dodecyl sulfate polyacrylamide gel electrophoresis (SDS-PAGE) is used to quantify the extent and location of protein damage, which is compared to the virus survival ratios. Polymerase Chain Reaction (PCR) methods are used to identify damage to the virus genetic material. Knowledge of the inactivation mechanism can be used to design advanced catalysts, design treatment systems that rely on multiple inactivation mechanisms, and aid in selecting a suitable surrogate pathogen for further disinfection studies and reactor validation protocols.

1.1. Thesis Organization

This thesis is organized according to the progression with which the three main objectives listed in the introduction were investigated. Chapter 2 consists of a literature review which details the occurrence of viruses in the aquatic environment and viral disease outbreaks associated with drinking water, drinking water treatment requirements, the survival of adenoviruses during water treatment processes, studies of adenovirus disinfection in water, and TiO_2 based photocatalytic oxidation as an alternative disinfection method. Chapter 3 consists of a published journal article entitled *Virus inactivation by silver doped titanium dioxide nanoparticles for drinking water treatment* (Water Research, volume 45, 2011, pages 535-544). This study reveals that silver modified TiO_2 can improve the virus inactivation kinetics by increasing the production of hydroxyl free radical (HO•). Chapter 4 is a journal manuscript in preparation for submission to the journal Environmental Science and Technology entitled *Silica Decorated TiO_2 for Virus Inactivation in Drinking Water – Green Synthesis Method and Mechanisms of Enhanced Inactivation Kinetics*. In this study a simple and "green" method of modifying TiO_2 nanoparticle surface with silica nanoparticles is developed. The modified catalysts improve virus inactivation kinetics by increasing adsorption of viruses to the catalyst. Chapter 5 is a journal manuscript being prepared for submission to the journal Water Research entitled *Kinetics of human adenovirus disinfection by titanium dioxide nanoparticles for drinking water treatment*. The research from this study evaluates the inactivation kinetics of AdV2 by TiO_2 under several conditions and identifies a kinetic model suitable for describing the data. Chapter 6 consists of a journal manuscript in preparation for submission to the journal Water Research entitled

Inactivation of human adenovirus by modified photocatalytic nanomaterials. This study evaluates both the silver and silica modified TiO_2 materials developed in Chapters 3 and 4 for the inactivation of AdV2. An amino-modified fullerene catalyst is also investigated for its potential to inactivate AdV2. Chapter 7 is a journal manuscript in preparation for submission to the journal Applied and Environmental Microbiology entitled *Inactivation mechanism of adenovirus type 2 and bacteriophage MS2 by TiO_2 – based photocatalytic oxidation*. This study investigates the damage of virus proteins and genetic material resulting from treatment with TiO_2 nanoparticles. Finally, Chapter 8 consists of an overarching conclusion of this thesis. After the references, three appendices are included which consist of published journal articles in which I performed major roles in research, data analysis, and manuscript preparation, but am listed as second author.

Chapter 2

Literature Review

2.1. Occurrence of pathogenic viruses in the environment

Viruses commonly occur in wastewater and drinking water sources (surface and ground). There are several reports available concerning the detection and quantification of adenoviruses and other pathogenic viruses in surface and ground water sources. As will be revealed later, adenoviruses are particularly resistant to several water treatment processes. Because of this they are likely released to the environment in great numbers through treated and untreated sewage discharge. The purpose of this section is to emphasize that pathogenic viruses, especially adenoviruses, are commonly present in the environment and must be controlled for in drinking water treatment.

The detection of viruses in waters is often accomplished through direct application of PCR methods. A positive result indicates the presence of viral genomes, not infectious viruses. Several studies reviewed here report using this method to detect

viruses, leaving the question of whether positive results in the water analyzed pose a health risk. Recently, Charles et al. (2009) investigated this question by concurrently measuring spiked groundwater samples for infective viruses via cell culture systems and viral genomes via PCR [14]. The most persistent virus tested, adenovirus serotype 2 (AdV2), was found to remain infective in groundwater up to 364 days and its genome detectable for up to 672 days by PCR. The decline of infectious AdV2 showed biphasic kinetics, with a rapid drop in infectivity occurring over 1 month and a small subset of the population remaining infective up to one year. The enteroviruses poliovirus 3 and Coxsackie virus B1 remained infective for 140 and 70 days, respectively, and are detectable by PCR for 364 days. While PCR was unable to distinguish the initial rapid loss of infectivity observed with AdV2, the fact that some remains infective for over half the detection time (364 out of 672 days) supports the use of this method for evaluating the health hazards of contaminated water. The reports of adenovirus detection discussed next relied on PCR detection in several instances. The long survivability and detection time by PCR of AdV2 should be considered when reviewing these reports.

Viruses are commonly detected in groundwater sources. In 1980, Keswick and Gerba republished a review on viruses in groundwater [15]. The studies cited within document the occurrence of several virus types, including polio, echo, coxsackie, and rota viruses in several different countries. In U.S. groundwater, a study of 448 wells in 35 states revealed 4.8% of samples tested positive for active viruses (enteroviruses) as determined by cell culture techniques, 31.5% were found to contain viral nucleic acids (enteroviruses, rotavirus, hepatitis A, norovirus) after rt-PCR analysis, and 20.7% of samples contained bacteriophages capable of replicating in one (or more) of bacterial

hosts [16]. As these viruses are commonly transmitted via the fecal-oral route, it is likely that sewage has contaminated these aquifers to some degree. A more recent study reports the transport of adenovirus DNA up to 10 km offshore of the Florida Keys, where septic systems are commonly used for waste [17]. Unlike fecal indicator bacteria, enteric viruses are not able to replicate in the environment outside of their human hosts, ensuring that their presence in the environment is linked with sewage contamination. High flow rate aquifers are especially susceptible to contamination. One study detected enteroviruses and reoviruses at 2-156 most probable number (MPN) in 88% of water samples taken from high flow rate karst aquifers in Tennessee [18].

Surface waters are also frequently contaminated with pathogenic viruses. For example, in the Ruhr and Rhine rivers in Germany, PCR analysis revealed (9.4 - 2.3) x 10^4 genetic equivalents / L of adenoviruses and human polyomavirues in 97.5% of samples, group A rotaviruses in 90% of samples, group II noroviruses in 31.7% of samples, and enteroviruses in one sample [19]. A review of adenovirus detection studies in natural waters as well as recreational facilities across the glove reveals that the pathogen is ubiquitous in the environment [20]. In Jiang's (2006) review, adenovirus detection is reported in Japan, South Korea, Australia, New Zealand, France , and Spain. There are many other reports available regarding virus detection in the environment; however, these are sufficient to conclude that viruses and adenoviruses are commonly present in drinking water sources and must be adequately treated [20].

The above studies highlight the need to adequately treat surface and groundwater to inactivate viruses. This may be especially true for small groundwater systems in rural

locations where treatment is minimal and the residence time in the distribution system is short, leaving little time for residual disinfectant to act.

2.2. Disease outbreaks associated with viruses in drinking water

With the previous studies in section 2.1 demonstrating the ubiquity of viruses in the environment, it is no surprise that in 2004 the WHO estimated that there are 1.58 million deaths annually due to diarrheal disease attributed to unsafe water supply, sanitation, and poor hygiene. While other pathogens may also play a role, viruses are a major cause of diarrheal disease. While most of these deaths occur in developing nations, viral outbreaks still occur in the United States. In the United States just between 2003 and 2005 there were four reported waterborne disease outbreaks attributed to viruses in drinking water affecting 282 people [21, 22].

The public health risk posed by viruses has been recognized around the world for decades. This concern (as well as others) has prompted most countries to regulate drinking and waste water treatment processes. Various agencies, such as the US Environmental Protection Agency (USEPA) and the World Health Organization (WHO), provide specific guidelines and recommendations for water treatment.

2.3. Drinking water treatment requirements and recommendations

The USEPA requires treatment systems capable of providing 4 log (99.99%) removal of viruses for all surface water sources [2] and groundwater sources with a history of contamination or other deficiencies [23]. Traditional chlorine disinfection,

while highly effective for viral inactivation, produces harmful disinfection byproducts (DBPs) when organic compounds are present in the water. The toxicity of DBPs has prompted stricter regulations concerning the acceptable levels of these compounds [3]. Although UV disinfection has not been found to form DBPs, some viruses, such as adenoviruses, are highly resistant to UV disinfection [5]. As a result, the USEPA has increased the UV fluence requirements for 4 log removal of viruses from 40 mJ/cm^2 to 186 mJ/cm^2 [2]. This has become a major barrier for the application of UV disinfection in drinking water treatment due to the high energy (cost) requirement. Increasing the efficiency of the UV process for adenovirus inactivation with a high efficiency photocatalyst could dramatically lower energy usage treatment costs.

The limitation of free chlorine disinfection to prevent DBP formation has created a new problem, achieving adequate levels of adenovirus disinfection. This virus is commonly detected in the environment (section 2.1) and is resistant to several alternative disinfection techniques. While existing drinking water regulations are generally considered adequate, the persistence of adenovirus to the final effluent of several drinking and waste water treatment plants has been documented.

2.4. Properties of human adenoviruses and bacteriophage MS2

Adenoviruses are much more complex than other water-borne viruses, which may lead to their resistance to many disinfection methods. In contrast, bacteriophage MS2, which is commonly used as a surrogate in disinfection studies due to its similarity to other water-borne viruses [24-26] and relative resistance to some disinfection methods [27-29], is relatively simple when compared to adenoviruses.

2.4.1. Properties of adenoviruses

Adenovirus is different from most waterborne pathogenic viruses in that its genome is dsDNA rather than RNA. This enables the virus to utilize the DNA repair enzymes present in host cells to repair damage to its own genome (e.g. from UV disinfection methods) thus increasing its resistance to disinfectants which act through genetic damage [5]. The genome is relatively large, containing 30-40 kb [30]. The 51 human serotypes are known to infect the pulmonary, gastrointestinal, and ocular body systems. Along with the gastrointestinal strains (AdV 40 and 41), the respiratory strains may be transmitted through the fecal-oral route as well through pulmonary secretions [5]. Respiratory serotypes (e.g. type 2) have been identified in the environment and are as much a concern as the enteric serotypes [20].

The virus structure is rather large and complex when compared to other waterborne viruses and common surrogate pathogens, such as MS2. The virus size varies with the serotype, but is generally stated to be 70-100 nm in diameter [31]. There are 3 major capsid proteins (Hexon, Penton base, Fibre), 4 minor capsid associated proteins (IIIa, VI, VIII, IX), 5 DNA associated core proteins (V, VII, Mu Terminal protein, IVa2) and 1 core protease [30]. The capsid proteins are the most likely target for photocatalytic oxidation. The Fibre protein is responsible for infection, and damage to it may render the viral particle non-infective. Damage to hexons may directly inactivate the virions or enable easy access for ROS to enter the core and damage the core proteins and/or DNA.

The adenovirus lifecycle essentially consists of attachment to a host cell, and transport to the nucleus, where early (e.g. E1A protein production) and late (e.g. genetic copying) processes occur. A simplified lifecycle schematic is shown in Figure 2-1.

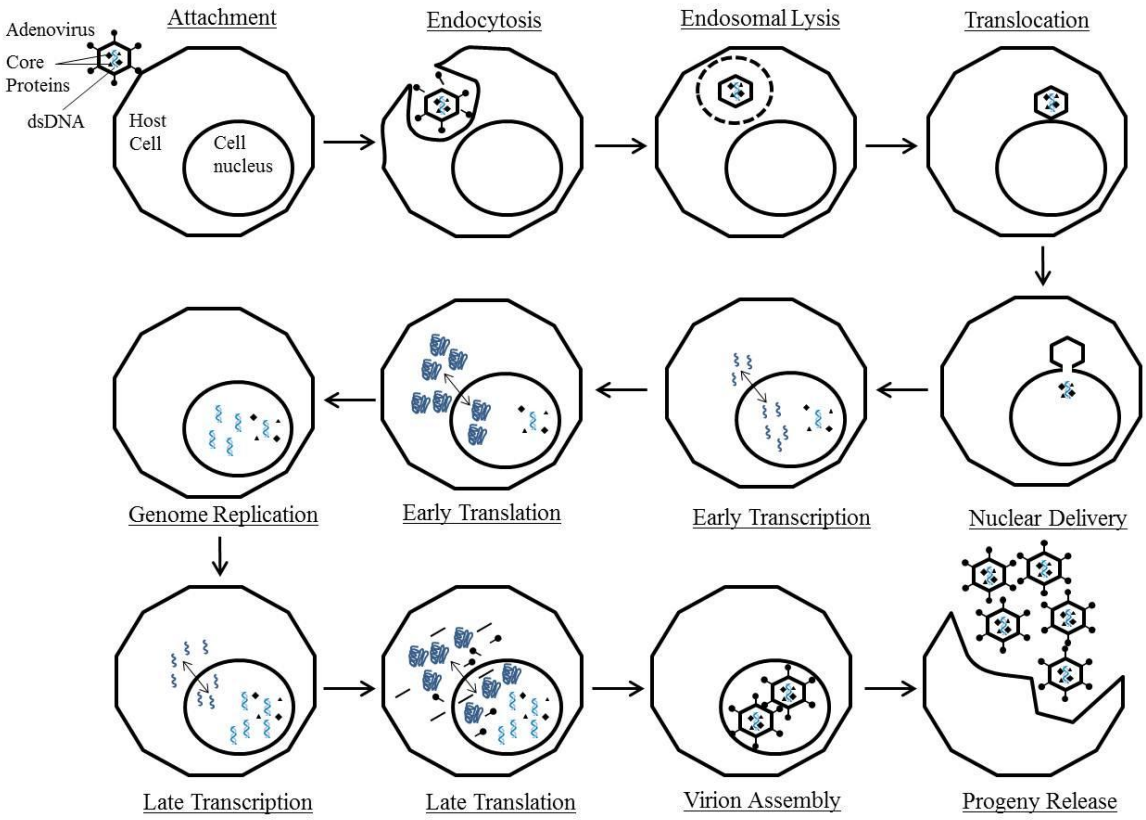

Figure 2-1 Simplified schematic of adenovirus lifecycle. Adapted from [4, 32]

2.4.2. Properties of bacteriophage MS2

Bacteriophage MS2 is a relatively small (~25 nm in diameter) virus containing positive-sense ssRNA that is 3,569 nucleotides long [33]. The capsid forms an icosahedral shape and consists of 2 proteins: coat (180 copies) and A (1 copy) [33]. The A protein, also denoted the maturation protein, interacts with host cells (F+ *E. coli*) by

attaching to the bacterial pilus, after which the virus injects its genome and A protein into the cell [33, 34]. The A protein is attached to the genome at both the 5' and 3' ends [35]. While it is known that the A protein is exposed to the capsid surface [34], the exact location is unknown, although it is hypothesized to be at a vertex of the icosahedron [36]. During photocatalytic oxidation of MS2, the virus may be inactivated by damaging the A protein and preventing interaction with host cells or inhibiting lifecycle processes after the A protein enters the host. Damage to the coat proteins can expose the RNA to damaging ROS or change the capsid conformation and preventing the A protein from interacting with bacterial pili.

2.5. Survival of adenoviruses during drinking and wastewater treatment processes

The studies reviewed here document the resistance of adenoviruses to water treatment processes. They further highlight the problem that adenoviruses pose to providing safe drinking water. In several studies, adenoviruses were observed to persist to the final effluent of several drinking and waste water treatment plants using both traditional treatment methods and more modern alternatives (membrane filtration, UV radiation). In some cases, indicator organisms (e.g. bacteriophages and coliforms) were not detected although adenoviruses were present. Several reports of this phenomenon are discussed next.

While more research has been conducted regarding the survivability in wastewater treatment, there are a few reports available by van Heerden et al. (2003,

2005), Alibinana-Gimenez et al. (2009), and Dong et al. (2010) documenting its persistence during drinking water treatment processes [37-40]. The research conducted by these authors highlights the potential for adenovirus to cycle through the environment and population, as river systems are commonly used both for waste water effluent discharge and drinking water intake (directly or through groundwater) [41, 42]. These studies also highlight the deficiency of using indicator organisms as a measure of microbial water quality, especially when viruses are of concern. Both research groups find the treatment processes adequately eliminate indicator organisms yet still contain infectious adenoviruses.

2.5.1. Survival in drinking water treatment plants

Adenovirus was twice found to persist to a degree (5.32% samples positive) to the final effluent of a South African treatment plant meeting WHO specifications for treatment processes, influent quality, and presence of indicator organisms [39, 40]. The treatment plant in these cases utilized six stages: coagulation using slaked lime; flocculation; sedimentation; carbonation; filtration and chlorination. In their 2003 study, van Heerden et al. detected infectious adenoviruses in 13/102 raw water and 9/204 treated drinking water samples collected over the course of a year [40]. Cell culture was used to amplify infectious viruses, and nested PCR was used to detect adenovirus in the cell culture systems, guaranteeing that all detections represented active viruses. In 2005 van Heerden et al. reported the detection, concentration, and serotypes of the adenovirus present at what is presumably the same water treatment plant [39]. Infectious adenovirus was detected in 10/45 raw water samples at concentrations ranging from $<1.2 \times 10^{-5}$ to 4.24×10^{-2} genomes/L. In the treated drinking water samples, 10/188 were positive for

infectious adenovirus at concentrations of $<1.5 \times 10^{-6}$ to 5.25×10^{-3} genomes/L. The serotypes detected were mostly (70%) types 40 and 41 with one type 2 and two D species also present. In a more recent study, Dong et al. (2010) report detecting infectious adenovirus using integrated cell culture (ICC)-nested PCR in 4/11 finished (post chlorination) samples taken from three drinking water treatment plants in New Zealand that utilize surface water as a source [38].

The studies above highlight the resistance of adenovirus to drinking water treatment processes. This same resistance is also reported to occur during wastewater treatment. This resistance leads to the contamination of water systems that are ultimately relied on for drinking water, allowing adenovirus to cycle through people and the environment. These results highlight the problem adenovirus poses for water treatment, and support the notion that an improved disinfection strategy is necessary. Photocatalytic oxidation may prove to be a better method for inactivation of resistant adenoviruses in drinking water

2.5.2. Survival in wastewater treatment plants

Along with showing resistance to full scale drinking water treatment processes, adenoviruses were found to survive similar wastewater disinfection treatments in several studies. These studies are included to further emphasize that adenoviruses are a serious problem in the environment, and support the development of photocatalysis as an alternative disinfection method or strategy of overcoming the limitations of UV_{254} and combined-chlorine based disinfection methods.

Adenovirus has been documented to survive after final chlorination at 3 different activated sludge plants in Melbourne, Australia; Pisa, Italy; and the City of Oak Creek, Wisconsin. Since secondary treatment is commonly used throughout the world, it is reasonable to say that adenovirus contaminated wastewater is regularly combined with drinking water sources. The following paragraphs will briefly highlight the studies documenting adenovirus survival in during secondary waste water treatment.

Irving and Smith (1981) reported detecting adenovirus at an average concentration of 300 infectious units (IU) /L in 5/7 samples taken from the chlorinated secondary effluent at the plant near Melbourne, Australia [43]. The average concentration in the raw water was 1,950 IU/L and 25/26 samples tested positive. This represents less than 1 log removal.

The treatment plant at Pisa, Italy was the subject of three reports by Carducci et al. [42, 44, 45]. The 2006 report aimed at correlating the occurrence of viruses (including adenovirus) in different environmental matrices (raw and treated wastewater, river water, sea water, and mussels) with the occurrence of viruses in people with gastroenteritis cases [42]. The same strain of adenovirus was detected in people and seawater, indicating that adenovirus may serve as a model for risk assessment. Regarding the efficiency of the treatment plant, 7/12 raw sewage samples and 3/12 treated samples were positive for adenovirus. This study also demonstrated that the presence / absence of indicator organisms (fecal coliforms and somatic coliphages) did not correlate with the presence of adenovirus.

In 2008 Carducci et al. again reported on the removal efficiency of adenovirus [45]. In this study all samples (n = 20 each) of the influent and effluent were positive for adenovirus. QPCR was used to quantify the adenovirus concentration present at the inlet and effluent, and the authors report an average 2 log reduction in viral genomes detected. The resulting effluent concentrations ranged from ~10^1-10^4 genomes/L. The 2009 report by these authors again reported 100% of influent and effluent samples were positive for adenovirus, with the treatment reducing the viral titer by an average of 2.1 log [44]. This study also reported on the serotypes detected. Most belonged to serotype 2 while one type 31 and one type 45 were also detected. The prevalence of serotype 2 (along with its plaquing ability) makes it a good choice for laboratory disinfection studies.

Along with analyzing samples from an activated sludge plant, Rodriguez et al. (2008) reported on virus detection in a high-rate enhanced flocculation and UV sterilization treatment process at a wastewater plant in the City of Oak Creek, Wisconsin [46]. In this study, infectious adenovirus were detected using cell culture assays in 2/11 samples of chlorinated secondary effluent and 1/9 samples of UV disinfected water treated with the high-rate enhanced flocculation process.

The ability of adenovirus to persist despite conventional wastewater and drinking water treatment processes underscores the need for an improved treatment method for virus inactivation. The next section reviews the efficacy of several disinfectants against adenoviruses as studied at the bench scale. The documented resistance of adenovirus to several of the studied methods reveals the need for a new disinfection strategy for viruses, which may be met by photocatalytic oxidation treatment methods.

2.5.3. Inactivation of adenoviruses at the bench scale: kinetics and mechanisms

The existing bench scale studies indicate that adenoviruses are highly resistant to many alternative disinfection methods that are increasingly used for to limit DBP formation that occurs with disinfection. The inactivation mechanism of adenovirus is primarily attributed to protein damage for all but two disinfection methods, UV_{254} irradiation, which is not very effective and acts through genetic damage, and coagulation – flocculation, a physical removal process. Photocatalytic oxidation is expected to damage proteins and may prove to be highly effective at inactivating adenoviruses, however there are no reports on this topic. Several reports have been published on the inactivation of adenovirus by both traditional and alternative disinfection methods. A brief review of the studies available on adenovirus disinfection by various methods is given next.

2.5.3.1. Coagulation – flocculation

Abbaszadegan et al. (2008) evaluated ferric chloride (0-40 mg/L) + polydialyldimethyl ammonium chloride (0.4 mg/L) for removal of adenovirus serotype 4 by coagulation – flocculation in a jar test apparatus [47]. In this study, the virus was spiked at $1x10^6$ 50 % tissue culture infective dose / mL ($TCID_{50}$/mL) into raw drinking water from a treatment plant (pH 8, turbidity 0.2 NTU, alkalinity 210 mg/L as $CaCO_3$). The maximum removal of adenovirus, 1.4 log, was observed with a dose of 40 mg/L ferric chloride. This is much less than the 4 log inactivation of viruses mandated by the USEPA for drinking water plants. Physical processes like this are typically not relied upon to provide high (> 4 log) inactivation of viruses.

2.5.3.2. Free chlorine

Free chlorine is the most efficient for inactivating adenoviruses when compared to the inactivation of other microorganisms at the same concentration x time (CT) value [48]. However, its use is being limited due to its potential to form DBPs [3]. Page et al. (2010) report free chlorine inactivates adenovirus 2 by inhibiting internal proteins that regulate its lifecycle rather than damaging the capsid/receptor proteins or genome [12]. This protein damage may be key to the rapid inactivation kinetics provided by chlorine. Free chlorine has long been known to provide high (> 4 log) inactivation of adenovirus. In 1956 Clarke et al. showed adenovirus serotype 3 required a CT of 0.027-0.067 (mg*min)/L for 99.8% inactivation, which generally agrees with more recent reports [49]. CT values required to achieve 4 Log inactivation under various reaction conditions are reported to fall between 0.06-2.6 (mg Cl_2*min)/L [49-53]. The USEPA recommends a CT of 3 (mg Cl_2*min)/L to achieve 4 log inactivation of all viruses [54].

While highly effective, free chlorine is not without its limitations. It was reported to lose its efficacy of adenovirus inactivation as pH increases and temperature decreases [52, 53]. The inactivation kinetics were also found to vary in different source waters, although rates were still relatively high [51]. Page et al. (2009) also observed pH and temperature dependence on adenovirus serotype 2 inactivation [52]. They characterized the inactivation kinetics as three parallel reaction pathways which are dominant in specific pH ranges. Their pathway 1, hypothesized to be reactions of HOCl with surface moieties, is dominant at pH<8.1 and is temperature sensitive. This pathway produces the rapid initial drop in infectivity but fails to completely inactivate the virus, which is governed by slower processes, pathways 2 and 3. These pathways are hypothesized to be

associated with additional conformation changes or damage due to secondary oxidizing species (e.g. thiol oxidation by chloramines formed by HOCl and amine groups) [52]. However, this 3 pathway hypothesis was ruled out in their subsequent mechanistic [12].

Other parameters besides pH and temperature can also affect the efficacy of free chlorine (and other methods). Virus aggregation was found to increase the required CT values by up to 31 and 2.8 orders of magnitude for feline calcivirus and poliovirus-1, respectively [53]. This is significant as viruses are likely present as aggregates or associated with particles in the environment and require higher than recommended CT values for adequate disinfection [53, 55]. This may explain why adenovirus has been found to survive chlorination in some degree in several drinking and waste water treatment plants, as is discussed in sections 2.5.1 and 2.5.22.5.1. Changes in temperature and pH, virus aggregation, and particle shielding are likely to reduce the efficiency of TiO_2 photocatalytic oxidation as well.

2.5.3.3. Monochloramine

Combined chlorine, particularly monochloramine, is an alternative to chlorine disinfection for use when the formation of disinfection byproducts is a concern. Similar to free chlorine, monochloramine inactivates adenoviruses by inhibiting early lifecycle events, although it is not clear if this is due to protein or genetic damage, which both occur [4]. In general, adenovirus is highly resistant to monochloramine, although the published reaction kinetic data is not very consistent. The redox potential of monochloramine is much less than free chlorine (450 vs. 700 mV, respectively) which may explain its inefficiency [56]. Most studies do not report achieving 4-log

inactivation, and reaction rates are slower at lower temperatures. For example, Baxter et al. (2007) report 2.5-log inactivation of adenovirus types 5 and 41 at an exposure of 340 (mg*min)/L at 5˚C and pH 8.5 [50]. Shin and Lee (2010) report that much higher doses are necessary; they observed 2-log inactivation by a dose of 2,500 (mg*min)/L at 5˚C and pH 8.0 [57]. The reaction rate increases with increasing temperature and decreasing pH but relatively high CT values are still required. Sirikanchana et al. (2008) report a 4-log inactivation of adenovirus type 2 from an exposure of 240 (mg*min)/L at 10˚C and pH 6 [58].

The high CT values required to achieve moderate disinfection levels of adenovirus make monochloramine a poor choice for disinfection when viruses are of concern. The EPA recommends a CT of 712 (mg*min)/L for 3 log removal of all viruses vs. 72 (mg*min)/L for bacteria (E. coli) [48]. Since monochloramine is capable of damaging adenovirus proteins as chlorine can, the question arises as to why there is such a large difference in the efficacy of these oxidizing disinfectants. It is possible that the damage sites are different, or monochloramine is less effective due to its lower oxidation potential. Photocatalytic oxidation using TiO_2 produces highly oxidizing HO• that may rapidly damage adenovirus proteins and lead to effective inactivation.

2.5.3.4. Chlorine dioxide

One study is available on the disinfection of adenoviruses by chlorine dioxide (ClO_2) [59]. Using adenovirus type 40, the maximum CT required for 4-log inactivation under the conditions tested was 1.59 mg*min/L. This is much less than that recommended by the EPA in the disinfection guidance manual for 4-log inactivation of

viruses (33.5 mg*min/L). Like free chlorine and monochloramine, the inactivation kinetics is highly dependent on the solution conditions, namely pH and temperature. ClO_2 has a high oxidation potential, and oxidation occurs in a very specific manner [48]. This specificity may explain why adenovirus is rapidly inactivated, but feline calcivirus is much more resistant to ClO_2 disinfection [59]. Regardless, this study demonstrates that highly oxidizing species, which are capable of damaging proteins, rapidly inactivate adenoviruses. The ROS produced by TiO_2 and other photocatalysts may therefore be highly effective for adenovirus disinfection.

2.5.3.5. UV irradiation

UV radiation is attractive as an alternative disinfection method since most organisms are highly susceptible and it is not known to form any disinfection byproducts. However, adenovirus is highly resistant to UV radiation, particularly low pressure (LP) 254 nm "germicidal" rays. This resistance is due to the ability of adenovirus to utilize host cell enzymes for repair of genetic damage, which is the mechanism of LP UV inactivation [5]. Because of this resistance, the USEPA has specified a fluence of 186 mJ/cm^2 for 4-log inactivation of viruses from drinking water [2]. Several literature reports are available demonstrating 4-log inactivation of adenovirus serotypes 2, 4, 5, 40, and 41from a UV_{254} fluence of 80-226 mJ/cm^2 [60-65]. The discrepancy in fluence requirements is mainly due to the different serotypes used in the studies. The high fluence requirement for adenovirus inactivation translates into a higher energy usage and treatment cost.

Significant improvement in the UV inactivation kinetics is obtained by using polychromatic (medium pressure, MP) UV sources. For example, Linden et al (2007) observed 4-log inactivation of adenovirus type 40 from an MP fluence of 30 mJ/cm^2 [66]. Eischeid et al. (2009) showed 4-log removal of adenovirus type 2 with an MP fluence of only 23 mJ/cm^2 [60]. The improved inactivation by MP UV is attributed to damage to outer capsid and inner core proteins by the longer UV wavelengths present in the MP UV emission spectrum [10].

The results of the MP UV studies suggest that application of a photocatalyst to UV disinfection systems can also improve the adenovirus inactivation efficiency. Clearly protein damage plays a dominant role in the inactivation of this pathogen. The ROS produced by photocatalysts would accelerate protein damage and thus the inactivation kinetics of UV disinfection processes.

2.5.3.6. UV irradiation + chemical residual

More information on the inactivation of adenoviruses through both genetic and protein damage mechanisms can be obtained in studies of disinfection by UV irradiation followed by chemical residual. A downside to UV radiation is that no disinfecting residual remains in the distribution system. Free chlorine or monochloramine are commonly used to provide a residual after UV treatment. These chemicals have been investigated in conjunction with UV radiation for adenovirus inactivation to determine if a synergism occurs and if they can provide adequate disinfection. These studies are interesting since they combine disinfection processes which act through different

mechanisms, i.e. genetic damage for LP UV and protein damage for free chlorine, monochloramine, and MP UV.

Ballester and Malley (2004) demonstrated >4-log inactivation of adenovirus type 2 from a UV_{254} dose (40 mJ/cm^2) and subsequent chlorination (3 mg/L total, 0.33 mg/L free) in water containing 0.77 mg/L ammonia for 15 minutes [67]. They also observed inactivation was greater when chlorination followed UV radiation rather than vice versa, which provides some evidence for a synergism. This gives support to the hypothesis that including a photocatalyst in existing UV_{254} disinfection processes could greatly enhance the virus inactivation efficiency by introducing a new inactivation mechanism: protein damage. A study using monochloramine does not show as promising a result.

Baxter et al. (2007) specifically investigated if adenovirus type 2 was more susceptible to preformed monochloramine after UV_{254} irradiation [50]. They found irradiated and non- irradiated viruses were disinfected at the same rate, suggesting no synergism occurs, however monochloramine may not damage proteins to as great extent as free chlorine due to its lower oxidation potential. Shin and Lee (2010) investigated both UV_{254} and polychromatic UV along with monochloramine for adenovirus type 2 disinfection [57]. Like Baxter et al. (2007), they did not observe increased susceptibility of the virus to monochloramine after UV exposure (either source). An interesting result in Baxter et al. (2007) is that they demonstrated > 4-log inactivation of adenovirus type 2 from sequential UV_{254} (45 mJ/cm^2) and monochloramine addition (CT = 50 mg * min / L), while the individual processes required 190 mJ/cm^2 (which is unusually high) or a CT of 125 mg * min / L. Baxter et al. (2007) do not point out that the dosage requirements to reach 4-log inactivation for each method when combined are less than half that required

when applied individually. This then also supports the hypothesis that including a photocatalyst in existing UV disinfection processes could greatly enhance the virus inactivation efficiency.

The results of the bench scale adenovirus disinfection studies for all treatment methods reveal that there exists much room for improving the disinfection of these viruses in drinking water. While free chlorine is effective, it's use is limited due to DBP formation. Adenoviruses are highly resistant to alternatives monochloramine and UV_{254} as compared to other microorganisms, indicating the need for more disinfection strategies. MP UV irradiation is promising, and including a photocatalyst in the process could further increase the efficiency. These studies also show that protein damage is the most effective mechanism for adenovirus inactivation. Since photocatalytic oxidation is expected to readily damage adenovirus proteins, this technology may prove highly efficient for adenovirus inactivation.

2.5.3.7. Ozone

Two studies are available on the disinfection of adenoviruses by ozone. Under the conditions tested by Thurston-Enriquez et al. (2005), the highest CT value required for 4-log inactivation of adenovirus type 40 was 0.6 mg*min/L [13]. This value is less than that recommended by the EPA, 1.2 mg*min/L for viruses, as given in the disinfection guidance manual. With its high oxidation potential, ozone is capable of damaging virus proteins. Murray et al. (2008) showed major capsid damage to adenovirus type 2 after disinfection with ozone [11]. In this study, TEM imaging showed the capsids of treated virions were broken open while untreated remained intact. The fact

that ozone, a ROS, rapidly inactivates adenovirus and causes significant damage to virus proteins lends credence to the hypothesis that ROS generated by photocatalysts may be highly effective for adenovirus disinfection.

2.6. Photocatalytic oxidation as alternative treatment method for virus inactivation

The reactive oxygen species generated by photocatalysts are highly reactive and capable of damaging proteins. On account of this, photocatalytic oxidation may be highly effective for inactivating viruses in water. Several different photocatalysts exist, however TiO_2 is by far the most studied. Fullerene based materials are also receiving increased attention. The following sections review information on both these photocatalysts.

2.6.1. Titanium dioxide based photocatalytic oxidation

Titanium dioxide is an attractive photocatalyst for water treatment as it is resistant to corrosion and non-toxic when ingested [68]. Its ability to degrade organic contaminants and inactivate both viruses and bacteria has been demonstrated, although the information on virus inactivation is limited. Several reports demonstrate virus inactivation by TiO_2 and TiO_2 based materials. Many questions still remain regarding the photocatalytic inactivation of viruses that must be answered before photocatalytic oxidation may be relied upon as a treatment method. First, it is not known how adenovirus, which is resistant to many disinfection methods and has a complex structure, responds to photocatalytic inactivation. Second, it is also not known (for any virus)

whether damage to protein or genetic materials is primarily responsible for virus inactivation. The inactivation method may be different for different viruses, especially for viruses with simple structures containing RNA (e.g. MS2, noroviruses) vs. viruses with complex structure containing DNA (e.g. adenoviruses).

Thirdly, while it has been shown that HO• is primarily responsible for MS2 inactivation [69, 70], it is not known if different ROS have a greater role in inactivating other viruses. Other studies have demonstrated singlet oxygen inactivates MS2 by oxidation in a site specific manner [69, 71] when HO• is not present / insignificant. Of the studies available on virus inactivation kinetics, it is clear that the inactivation rates must increase before photocatalysis is a viable virus disinfection option, yet little research has been conducted on improving catalyst reactivity for virus inactivation. Improvements to catalyst reactivity may be accomplished by increasing ROS production and/or increasing substrate adsorption, however the relative importance of these parameters is not known.

2.6.1.1. TiO_2 mechanism of action

The basic mechanism of TiO_2 photoactivation and reactive oxygen species (ROS) generation is well known [72]. Upon adsorbing a photon of energy equal to or greater than the material bandgap, an electron is promoted from the valence to the conduction band. The typical fate of the excited electron is recombination with the electron hole; however, the charges may migrate to the material surface where they directly engage in redox reactions with solution components, or first become trapped and then engage in redox reactions. This scheme is presented in Figure 2-2.

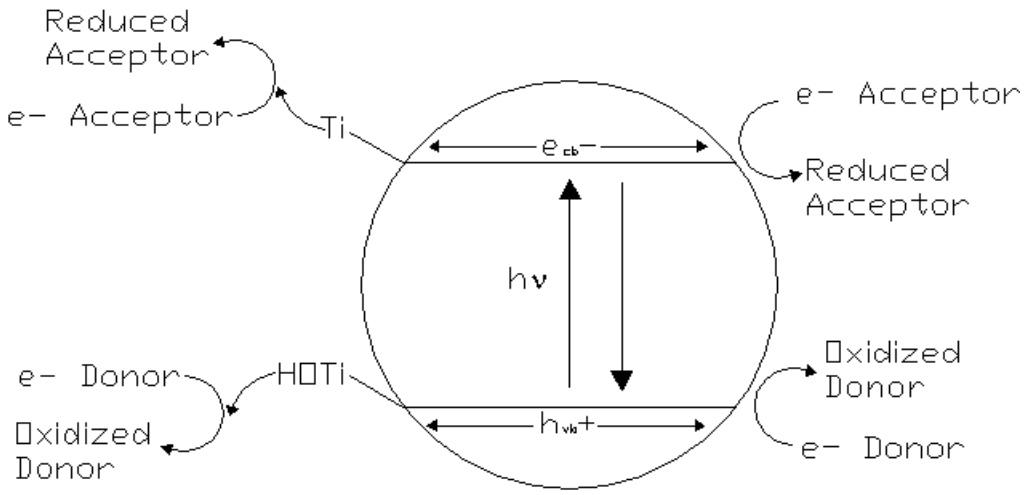

Figure 2-2 - Mechanism of charge generation and transfer in TiO_2 photocatalytic oxidation. Adapted from [60]

ROS species may be formed through both reductive and oxidative pathways. In a typical environmental application of TiO_2 photocatalytic oxidation, oxygen is present to readily accept exited electrons. Adsorbed oxygen is first reduced to superoxide anion ($O_2^{\bullet-}$), from which hydroperoxyl radical ($HO_2^{\bullet}$), hydrogen peroxide (H_2O_2), and hydroxyl free radical (HO•) are subsequently produced as detailed in reactions (R1) – (R11). [73].

$$O_2 + e_{cb}^- \rightarrow O_2^{\bullet-} \quad \text{(R1)}$$

$$O_2^{\bullet-} + H^+ \rightarrow HO_2^{\bullet} \quad \text{(R2)}$$

$$HO_2^{\bullet} + HO_2^{\bullet} \rightarrow H_2O_2 + O_2 \quad \text{(R3)}$$

$$O_2^{\bullet-} + HO_2^{\bullet} \rightarrow HO_2^- + O_2 \quad \text{(R4)}$$

$$HO_2^- + H^+ \rightarrow H_2O_2 \quad \text{(R5)}$$

$$O_2^{\bullet-} + H_2O_2 \rightarrow HO^{\bullet} + OH^- + O_2 \quad \text{(R6)}$$

$$H_2O_2 + e^- \rightarrow {}^{\bullet}H_2O_2 \quad \text{(R7)}$$

$$O_2^- + {}^{\bullet}H_2O_2 \rightarrow HO^{\bullet} + OH^- + O_2 \quad \text{(R8)}$$

$$H_2O_2 + 2e^- + 2H^+ \rightarrow 2H_2O \quad \text{(R9)}$$

$$H_2O_2 + 2h^+ \rightarrow H^+ + O_2 \quad \text{(R10)}$$

$$H_2O_2 + h\nu \rightarrow 2HO^{\bullet} \quad \text{(R11)}$$

The holes vacated by the excited electrons in TiO_2 are another source of ROS. Holes are capable of directly oxidizing adsorbed compounds, or becoming trapped as Ti-HO•. Holes can also oxidize H_2O and OH^- to form HO•. The HO• can either remain adsorbed on the TiO_2 surface or migrate into the bulk solution and oxidize other solution components [72]. HO• has the highest oxidizing potential of the ROS formed, and is generally considered the primary ROS reactant in photocatalytic systems.

Table 2-1 lists the oxidation potentials (vs. SHE, pH7) of relevant ROS.

Table 2-1 - Potentials of various redox pairs vs. SHE at pH 7 [68]

Redox Pair	Potential (V)
Conduction Band e^-	-0.52
O_2 / $O_2^{\bullet-}$	-0.28
H_2O_2 / H_2O	+1.35
O_3 / H_2O	+2.07
HO• / H_2O	+ 2.27
TiO_2 Valence Band Hole*	+2.53

*value varies depending on crystal structure

2.6.1.2. ROS responsible for TiO_2 based virus inactivation

Studies on the ROS responsible for virus inactivation by TiO_2 have only investigated the response of bacteriophage MS2. It is possible other viruses behave differently. The first report of virus inactivation by TiO_2 by Sjorgen and Sierka (1993) demonstrated that MS2 can be inactivated by 1 g/L suspended P25 TiO_2 [70]. In their study 2 μM ferrous sulfate was added as an enhancer of HO• production, resulting in a marked increase in MS2 inactivation (3 log vs. 1 log inactivation after 10 minutes irradiation). This result provided evidence that HO• is at least partly responsible for the antiviral activity of the material. Likewise, Cho et al. (2005) demonstrated ~2 log removal of MS2 after 180 minutes of UV-A irradiation using suspended P25 TiO_2 as the catalyst [74]. They were able to show that HO• was primarily responsible for the antiviral activity by employing methanol and tert-butanol as scavengers for HO•. Similar to Sjorgen and Sierka (1993), Cho et al. (2005) employed Fe^{2+} as an enhancer of HO• production, which resulted in increased MS2 inactivation, further indicating HO• is primarily responsible.

2.6.1.3. Assessing oxidative damage to protein and genetic material

Only the potential for photocatalytic oxidation to degrade both virus protein and genetic material has been demonstrated. It is not known whether protein damage is responsible and sufficient for inactivation, or if damage to genetic material is necessary. It is also not known what level or type of protein damage is required for inactivation. As a potent oxidizing agent, HO• is likely to attack the virus capsid, envelope (if present), and genetic material. Sufficient degradation of the capsid may prevent the virus from

infecting cells, while sufficient genetic damage may prevent replication within infected cells. Since the genetic material is protected within the capsid, it is likely the capsid is first degraded sufficiently before genetic damage occurs.

Kashige et al. (2001) synthesized a thin film of anatase and applied it for inactivation of phage PL-1 [75]. While their material was shown to be effective, it took ~27 hours of UV-A irradiation to produce 4-$\log_{10}$ inactivation. The kinetics was slowed in the presence of bovine serum albumin, suggesting that protein (capsid) damage is the mechanism of inactivation. However this evidence is extremely weak, as it does not show the albumin is specifically degraded or reacts with ROS. It is possible albumin merely blocks TiO_2 active sites. DNA damage was also shown to occur by analyzing treated virus DNA using agarose gel electrophoresis. DNA from treated viruses smeared along the length of the gel indicating fragmented DNA, while DNA from the controls formed a tight band. Smearing suggests random damage to the DNA rather than specific fragmentation. No conclusions may be drawn from their work other than TiO_2 can damage genetic material and extra protein in the reaction medium slows the kinetics.

Other authors have provided evidence that proteins and genetic material are both targeted by TiO_2. Zan et al. (2007) demonstrated that irradiated TiO_2 (liquid suspension and dry film) can degrade hepatitis B virus surface antigen (HBsAg) [76]. Xu et al. (2007) confirmed the degradation of HBsAG and also showed that irradiated TiO_2 is capable of degrading RNA and casein [77]. While Kashige et al., Zan et al., and Xu et al. provide evidence that TiO_2 degrades both protein and genetic material, neither study is specific enough to identify if either general capsid oxidation or oxidation of specific

proteins is primarily responsible for virus inactivation. It is also not clear if inactivation occurs before damage to genetic material begins.

There is evidence to suggest that ROS damage to virus capsids occurs in a site specific manner. Damage to capsid proteins was identified as the mechanism of MS2 inactivation in a study of oxidation by singlet oxygen and UV_{254}. Wigginton et al. (2010) used mass spectroscopy (MS) to specifically identify the 4 exact protein damage sites caused by oxidation [71]. While HO• has a higher oxidation potential and thus reactivity than singlet oxygen, there is some evidence that it may react at specific amino acid residues in proteins and short peptides.

Hawkins and Davies (1998) used electron paramagnetic resonance (EPR) spectroscopy and computer simulation to demonstrate preferential peptide cleavage at alanine and glycine resides (at the α-carbon), while side chain attack was more common when residues containing larger side chains (valine, leucine) [78]. They attributed this to the inability of the α-carbon radicals formed at residues with large side chains to form a planar configuration on account of hindrance of the side chains with the protein backbones. This in turn prevents maximal delocalization of the unpaired electron. Jones et al. (2007) developed a protocol to specifically cleave peptides using irradiated TiO_2 [79]. They observed repeatable cleavage at proline residues, while proteins with no proline residues were not cleaved. They offer no explanation for the specificity of cleavage at proline other than references to other (inconclusive) studies. The studies on specific protein cleavage sites do not dismiss that additional protein oxidation occurs. Oxidation that does not result in cleavage may still lead to virus inactivation, as observed by Wigginton et al. (2010) [71].

2.6.1.4. Effect of catalyst reactive oxygen species (ROS) production

Increasing catalyst ROS production is one strategy to improve the virus inactivation kinetics. This strategy is most important when mass transfer of viruses is not limiting. In their studies of MS2 inactivation by TiO_2, both Sjorgen and Sierka (1993) and Cho et al. (2005) show inactivation increases in the presence of a HO• production enhancer (ferrous sulfate) [70, 74]. Sato and Taya (2006) varied the anatase : rutile ratio of their catalyst to affect the quantum yield and MS2 adsorption quantity to the catalyst [80]. Although they did not measure ROS production, they relied on modeling to conclude that increased ROS production was responsible for the observed enhanced inactivation kinetics produced by one of their materials (70:30 anatase : rutile TiO_2). While Sato and Taya (2006) controlled for differing virus adsorption quantities to the materials in their calculations, their conclusions are not solid without corresponding ROS production measurements. Other studies suggest virus adsorption is a major factor in controlling the virus inactivation kinetics.

2.6.1.5. Effect of solution conditions and virus adsorption

Solution chemistry directly affects the adsorptive dynamics of photocatalytic systems. Although long range ROS such as H_2O_2 can be generated by TiO_2, viruses adsorbed to the catalyst will experience the highest ROS concentrations and be inactivated more quickly than those in the solution bulk. The presence of ionizable surface residues on the virus and solution chemistry are both important factors governing the interaction between the virus and catalyst.

In studying the effect of various ionic species on MS2 inactivation by suspended P25 TiO_2, Koizumi and Taya (2002) found that the inactivation rate was proportional to the adsorption quantity of MS2 on TiO_2 [81]. NO_3^-, SO_4^{2-}, K^+, PO_4^{3-} and Ca^{2+} each lowered the adsorption quantity of MS2 and reduced the inactivation rate when present at 100 mM, while Cl^-, Br^-, and Na^+ did not significantly affect the amount adsorbed or the inactivation rate. In a separate study, Koizumi and Taya (2002) varied the pH of the reaction solution and again observed that the MS2 inactivation rate by suspended P25 TiO_2 was proportional to the adsorption quantity, which varied with the pH as a result of electrostatic interactions [25]. While these studies demonstrate the importance of virus adsorption on the photocatalytic inactivation kinetics, they do not fully characterize the phenomenon. They also do not account for the potential of different ROS production rates under different solution conditions. Measuring ROS production and modeling both adsorption and photocatalytic inactivation processes are required to fully understand the inactivation mechanisms.

2.6.1.6. Virus adsorption and kinetic photocatalytic inactivation models

Adsorption and reaction modeling are important to understand the dependence of virus inactivation kinetics on the various system parameters (virus concentration, light intensity, catalyst concentration / surface area, water quality). This knowledge is then used to understand the relative importance of the different processes involved: adsorption, ROS generation, surface and bulk reactions, and desorption of inactivated viruses. There is no information on the effect of initial virus concentration and adsorption quantity over large (6 orders of magnitude) differences in values, which could occur during actual treatment applications. One study exists on virus inactivation by

TiO_2 that predicts changing kinetics with changes in catalyst ROS production and virus adsorption quantity.

Sato and Taya (2006) discussed the kinetics of virus inactivation by TiO_2 and shed some light on this system [80]. They observed pseudo first order kinetics for virus inactivation, as is demonstrated in other virus inactivation studies [25, 70, 74, 81]. However, they varied the anatase : rutile ratio of their catalyst to affect the quantum yield and MS2 adsorption quantity to the catalyst. They derived (Equation 2-1) the apparent deactivation rate constant (k', s^{-1}) to be a function of the ROS concentration (C_{ox}, kg m^{-3}) and total (active + inactive) quantity of virus adsorbed to the photocatalyst (q_T, PFU kg^{-1}). The rate constant is also a function of the inherent or true rate constant (k_{true}, m^3 mol^{-1} s^{-1}), TiO_2 concentration (C_T, kg m^{-3}), the concentration of ROS, (C_{ox}, (kg m^{-3}) and titer of active virus (N_T, PFU m^{-3}). They assumed adsorption equilibrium between the viruses and catalyst, that only adsorbed viruses are inactivated, that adsorption follows the Freundlich isotherm (Equation 2-3), that the inactivation reaction is second order with respect to the ROS and virus concentrations, and that active and inactive viruses have the same adsorption affinity. Their analysis showed that

Equation 2-1

$$k' = \frac{k_{true} C_T}{N_T} C_{ox} q_T \quad .$$

In the above equation C_{ox} is related to the quantum yield of the catalyst, light intensity, irradiated reactor area, ROS extinction rate, and catalyst volume. By keeping

these parameters constant, they could compare k'/q_T values for disinfection of MS2 by different nanomaterials to compare the values of C_{ox} and identify catalysts that demonstrate enhanced ROS production. They reported a change in the quantum yield and adsorption capacity of TiO_2 by adjusting the percentages of anatase and rutile phases mixed in the reaction system. While adsorption (q_T) of the virus was highest when 100% anatase was used ($q_T = 7.6 \times 10^{13}$ PFU kg^{-1}, $k' = 1.8 \times 10^{-2}$ s^{-1}), the inactivation rate constant (k') was the highest with 70% anatase ($q_T = 3.8 \times 10^{13}$ PFU kg^{-1}, $k' = 5.1 \times 10^{-2}$ s^{-1}). The enhanced inactivation rate was attributed to improved electron transfer through anatase-rutile contact points, although the ROS production was not measured for the different catalysts to confirm this result [80].

Sato and Taya's (2006) study is a good example of how modeling the photocatalytic reaction can provide information on the relative importance of adsorption and ROS production. While their analysis is specific for viruses, more modeling work has been conducted using simpler compounds as the contaminant in the reaction system. These models may also be used to obtain information of the effects of photocatalytic system parameters.

The general consensus regarding photocatalytic reactions is that the species of interest (contaminant) is first adsorbed to the photocatalyst upon which it is subsequently degraded. While some ROS (e.g. H_2O_2) have long lifetimes, the more potent ROS (e.g. HO•, $^1O_2$) have short lifetimes (micro to nano seconds) and only exist at significant concentration near the catalyst surface. Therefore both the rates of adsorption and reaction must be considered, in kinetic models of the reaction system. Common adsorption and reaction models are given in the subsections below. These models are

developed for describing photocatalytic degradation of chemical contaminants. It is unclear whether they apply to microbial pathogens such as viruses, which are particles much larger than dissolved chemical species.

Adsorption models

The Langmuir isotherm is commonly applied to model substrate adsorption to photocatalysts. This model assumes that adsorption occurs via reversible chemisorption to only one adsorption site per molecule, that only a monolayer forms and that adsorbed molecules do not interact (i.e. energy of adsorbed species is the same and not affected by adsorbates present at other sites) [82]. At equilibrium, the fractional surface coverage of a species on an adsorbent (θ) is given by Equation 2-2, where C_e is the equilibrium solution concentration of the species and K is the Langmuir adsorption constant.

Equation 2-2

$$\theta = \frac{KC_e}{1 + KC_e}$$

Another commonly used adsorption model is the Freundlich isotherm. This model applies to materials than contain a population of sites having different adsorption energies. Each site however obeys the assumptions of the Langmuir model, and the Freundlich isotherm can be derived by adding up the Langmuir adsorption isotherms of the individual sites. This model may be more applicable to the virus-TiO_2 system when modified TiO_2 is used where multiple species are present on the catalyst surface (e.g.

TiOH, SiOH). The Freundlich ishotherm is given as Equation 2-3, where K_f and n are Freundlich model parameters.

Equation 2-3

$$q_{eq} = K_f C_e^{1/n}$$

Kinetic photocatalytic reaction models

The Langmuir-Hinshelwood (L-H) kinetic model is frequently employed to describe the data obtained in various photocatalytic degradation studies [72, 83-85]. The model's applicability in these studies makes it a good starting point for analyzing the virus-TiO_2 system. In the L-H model, all reactant species are adsorbed and in equilibrium with the surface before reacting (i.e. species react in chemisorbed state) and adsorption equilibrium is instantaneous [82]. By assuming that the system is at steady state, that the product formation step is rate limiting, that the product is weakly adsorbed, and one (of two) reactant is present in excess, the unimolecular form of the L-H model (

Equation 2-4) may be written as [82]:

Equation 2-4

$$r_0 = k\theta = \frac{kKC_e}{1 + KC_e}$$

In photocatalytic oxidation, the [HO•] is typically considered to be present at much higher concentrations than the other reactant, and this form is commonly used to model data [85]. It should be noted that *k* is an apparent rate constant in this sense, as it is related to the concentration of ROS (namely HO•) through the catalyst concentration and light intensity [82, 85]. When these parameters are held constant, *k* may be considered "true."

To determine the rate and adsorption constants, a plot of r_o^{-1} vs C_o^{-1} is generated where the slope is equal to $(kK)^{-1}$ and the intercept is equal to k^{-1}. Numerical methods can also be used to fit the data directly. This model has been modified to account for other adsorbing species (C_i) which may interfere with the compound of interest, as shown in

Equation 2-5 [82]. Other species competing for adsorption could be substances from the solution matrix or simply the reaction products if they adsorb significantly. This can be avoided by using ultrapure water and initial reaction rate data, where the product concentration is very low and can be neglected.

Equation 2-5

$$r = k\theta = \frac{kK_LC}{1+K_LC+\sum_1^n K_iC_i}$$

The fact that the Langmuir-Hinshelwood equation frequently fits experimental data well is not sufficient evidence to conclude that the underlying assumptions are valid. It is important to restate that according to the L-H mechanism, reaction occurs subsequent

to adsorption. In 1990 Turchi and Ollis investigated the mechanisms possible for HO• attack on organic substrates, considering reactions on the surface, in the fluid, and via a Rideal mechanism (reactant from solution reacts with adsorbed reactant directly) [86]. The derived rate equations all had forms similar to the L-H equation, yet the respective parameters differed in their fundamental meanings. It is therefore erroneous to assume that the L-H mechanism applies to a particular system when the only evidence is that the data fits the L-H equation. The investigation of the underlying mechanism of substrate degradation by TiO_2 still continues.

Ollis revisited this issue in a 2005 publication in an attempt to clarify the underlying reaction mechanism [87]. His analysis was prompted by reports in the literature evidence of *k* and *K* values (unimolecular L-H equation,

Equation 2-4) changing with the light irradiance. By developing a pseudo-steady state analysis method, Ollis determined that both the apparent photocatalytic rate constant, *k*, and the apparent adsorption equilibrium constant, K^{app}_{LH}, depend on light intensity (*I*) through the formation of HO• (Equation 2-6 and

Equation 2-7). K^{app}_{diss} in this equation is the apparent disassociation equilibrium constant, k_{+1} the rate constant for adsorption, k_{-1} the rate constant for disassociation, and *n* an equation parameter.

Equation 2-6

$$k_{LH} = k_{true}(HO\cdot)$$

Equation 2-7

$$K_{diss}^{app} = \frac{1}{K_{LH}^{app}} = \frac{k_{-1} + \alpha I^n}{k_{+1}}$$

In explaining these equations, Ollis hypothesized that reactant adsorption/desorption equilibrium is not established during illumination since the high reactivity of active sites causes continuous displacement of the adsorbed reactant concentration from the coverage corresponding to the equilibrium surface concentrations under dark conditions [87]. This "slow step" approximation depends on light intensity only through the apparent rate constant, k_{LH}. The assumption by Ollis of continuous reactant displacement from the catalyst may not be true when the contaminant is large and complex (e.g. viruses), since they require repeated and prolonged ROS attack to completely mineralize.

One of the literature reports prompting Ollis to develop the pseudo-steady state analysis method for photocatalytic oxidation was published by Emeline et al. (2000) [88]. In this study Emeline et al. observed that the parameters k_{LH} and K_{LH} for phenol oxidation by TiO_2 varied with the light intensity. In 2005, Emeline et al. responded to the pseudo-steady state analysis proposed by Ollis with an alternative mechanism to explain their data reported in 2000 [83]. Namely, they propose a reaction step for the photo-induced inactivation of excited surface states to account for the recombination of trapped charges through surface active centers. Assuming that photodesorption is the major pathway

responsible for the drop in surface coverage of the reactant (otherwise the analysis leads to the L-H equation), Emeline et al. writes a reaction rate equivalent to:

Equation 2-8

$$\frac{dC}{dt} = \frac{\alpha\rho C}{\beta\rho+\gamma C} \quad .$$

In the above equation, ρ is the photon flow, C is the reactant concentration, and α, β, and γ are empirical constants independent of light irradiance and concentration. This equation is the same form as the L-H model. This rate form accounts for the observed dependence of k_{LH} and K_{LH} on the light irradiance. Emeline et al. proposed that this mechanism was more realistic than that proposed by Ollis for two reasons [83]. The first issue is regarding Ollis' assumption of steady state applying to the surface coverage of the reactant molecules without providing evidence besides the observed kinetics. Secondly, at low concentrations of the reactant molecule, steady state could not be applied to the reaction steps proposed by Emeline et al.

The mechanistic analyses conducted by Ollis and Emeline et al. are based on the degradation of relatively simple substrates. Viruses in contrast are complex, large structures that may behave differently during photoreactions. They are not the ideal substrate for probing the fundamental mechanisms of TiO_2 photocatalytic oxidation.

While the debate over the exact mechanisms underlying the photocatalytic oxidation continues, several research groups have applied this technology for inactivating

viruses despite the lack of clarity concerning the exact mechanism. It is clear however that increasing virus adsorption and/or catalyst ROS production are strategies for improving the efficiency of virus inactivation by TiO_2.

2.6.1.7. Modified TiO_2 catalysts for enhanced virus inactivation

There are several potential routes for improving the efficiency of virus inactivation by TiO_2. Ultimately, these methods either increase the ROS production of the catalyst, alter the activation energy to that corresponding to visible light wavelengths, or increase the adsorption of target contaminants. Various metals, such as Ag, Pt, Pd, Au, Fe, Mg, V, Cr, Mn, and Ni, have been identified to increase contaminant degradation [89-92]. Other elements and compounds, such as N, carbon nanotubes, and silica, have been shown to provide a benefit [93-95]. Of the thousands of studies published on improving TiO_2 reactivity for contaminant degradation, only two exist seeking to improve its virus inactivation potential.

Sato and Taya (2006) varied the anatase : rutile ratio of their TiO_2 and found 70: 30 produced the fastest virus inactivation kinetics (2.5 times faster than 100% anatase and 5 times faster than 100% rutile) [80]. Improving (or enabling) ROS production at visible light wavelengths is another motivation for modifying TiO_2. Li et al. (2008) synthesized palladium doped TiO_2 fibers and applied it for inactivating MS2 [96]. They produced over 99.7% inactivation (by adsorption and photocatlaysis combined) under visible light irradiation and confirmed the production of HO• formation under visible light using electron paramagnetic resonance spectroscopy.

These two studies demonstrate improvements may be made to TiO_2 for virus inactivation, but there is no information on whether the other successful improvement strategies identified in the multitude of studies of simple contaminant degradation will also improve the inactivation of viruses. In selecting a method for improving the virus inactivation kinetics, it is important to consider the stability and toxicity of the species used for modifying TiO_2.

Silver and silica are two species that hold promise for enhancing virus inactivation by TiO_2. Silver is known to be antimicrobial itself and is not generally a concern in water systems when present at levels below 0.1 mg/L [2]. Thus limited leaching of silver from Ag/TiO_2 should not pose a problem. Silica is non-toxic, stable and has improved TiO_2 activity in some instances.

Modifications with Silver

Metal doping is thought to enhance photocatalytic oxidation by trapping excited electrons and preventing charge recombination (Figure 2-3) [97-100]. Electron trapping can occur if the dopant has a lower Fermi level than the excited electron. Silver in particular has been shown to enhance the photocatalytic efficiency of TiO_2 for both contaminant degradation and bacterial inactivation [73, 92, 101-110]. However, there is limited information on the antiviral capabilities of this material [111]. Along with facilitating charge separation, silver is thought to enhance TiO_2 photocatalytic oxidation by providing more surface area for adsorption and directly interacting bacteria [112, 113]. However, one study demonstrating the enhanced activity of nAg/TiO_2 found that silver did not increase the surface area according to BET analysis [73].

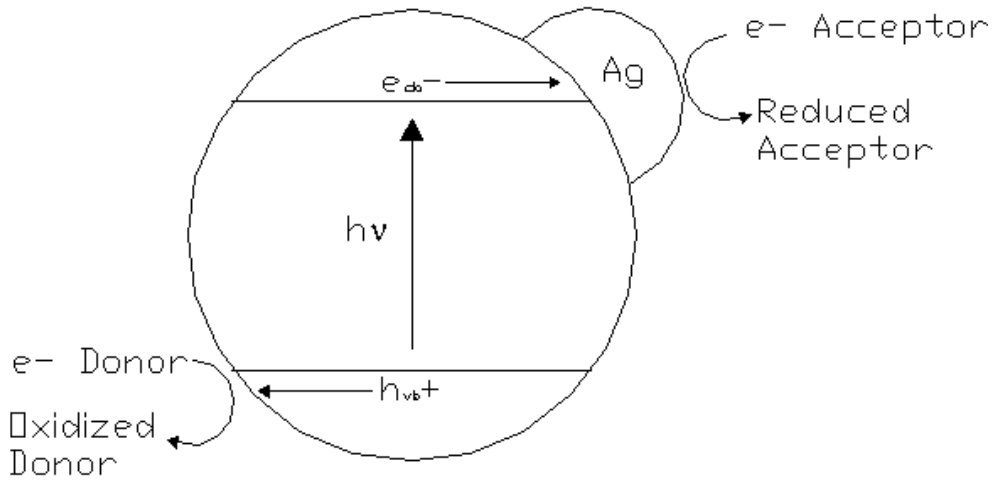

Figure 2-3 - Electron capture by a noble metal on TiO_2 surface. Adapted from Iliev et al. [99].

Another reason to choose silver to improve the virus inactivation kinetics is that silver ions and nanoparticles have been shown to have antimicrobial properties themselves. Silver ions bind to the thiol groups of cysteine residues in microbial enzymes, hindering their functions, as well as producing damaging ROS, even without UV irradiation [114]. Silver ions have also been shown to damage bacterial cell membranes and inhibit DNA replication [115]. Silver nanoparticles have been shown to bind to external glycoproteins on HIV-1 viruses, inhibiting their infective mechanism [116]. A study by Morones et al. (2005) suggested that three mechanisms are involved in the antibacterial action of silver nanoparticles against gram negative bacteria [117]. The first mechanism is particles from 1-10nm bind to the cell membrane and disrupt its

function. The second is particles enter the cell and disrupt the functions of sulfur and phosphorous containing compounds. The third is particles release silver ions which have been shown to have antimicrobial activities.

Utilizing silver to enhance the antimicrobial action of TiO_2 photocatalytic oxidation allows several different inactivation mechanisms to work in concert. Therefore, it is possible that a synergism occurs between silver and TiO_2 when silver doped titanium dioxide (nAg/TiO_2) is used for inactivating microorganisms under UV radiation. While dissolution of silver may pose a challenge in implementing this technology, the reducing power of activated TiO_2 may aid in keeping the metal in its zero valent state. This in turn may limit the effect of silver ions on microorganisms.

The optimum silver content for enhancing TiO_2 photocatalytic oxidation has been suggested in several studies. One study examining the simultaneous photochemical reduction of Ag^+ onto Degussa P25 TiO_2 and degradation of sucrose and salicylic acid found that 2 atomic % of Ag was the optimum silver loading after testing a range of 0.5-20 atomic % Ag [73]. Two other studies that synthesized both TiO_2 and nAg/TiO_2 via the sol-gel route found that 5 atomic % of Ag was the optimum silver loading after testing a range of 0-10 atomic % Ag for Rhodamine B dye degradation [108] and 0-5 atomic % Ag for Rhodamine 6G dye degradation [107].

Multiple explanations have been given for an optimum silver content on TiO_2 [73]. High silver contents can decrease the amount of light reaching the TiO_2 surface and reducing the generation of excited electrons and holes [118]. When applied above the optimum loading mass, the deposited silver can also act as recombination centers by

capturing holes [112]. Smaller silver particles also may capture holes more readily than larger deposits, making them unavailable for oxidizing other solution components [112].

Modification with silica

Like silver, silica can also be used to enhance TiO_2 for photocatalytic oxidation, however the improvement mechanisms are different. Silica is typically used in TiO_2 photocatalytic oxidation either as a physical support structure or as a chemical dopant dispersed within the TiO_2 lattice and thus affecting the fundamental properties of the material. In the reports available on the topic, silica is incorporated into the TiO_2 lattice during its synthesis according to varying formulations of the sol-gel technique. Several studies are available where silica addition improved the photocatalytic activity of TiO_2 [93, 119-121]. Improvements in photocatalytic activity in these studies are attributed to bandgap changes, the generation of acid sites, and increased adsorption.

Bandgap changes (widening) are a result of the quantum size effect and interface interactions [93]. The presence of silicon during TiO_2 synthesis inhibits crystallite size [93], and smaller TiO_2 nanoparticles are known to have wider bandgaps which result in reduced electron-hole recombination [122]. The incorporation of silica into the TiO_2 lattice also results in the formation of surface acid sites that increase the binding of HO^- and subsequent production of HO•. Other studies attribute enhanced substrate adsorption to SiO_2 as increasing the photoreaction [119, 120].

2.6.1.8. Effectiveness of TiO_2 against pathogenic viruses

To determine the suitability of photocatalytic oxidation as a treatment option for personal or municipal use, its efficacy needs to be shown against a wide variety of

viruses, including actual pathogenic viruses. There are a few reports detailing the inactivation of some pathogenic viruses in water that suggest photocatalytic oxidation may be an effective treatment option, but no one has reported using adenovirus, a pathogen of particular concern. The viruses used in these studies, poliovirus and murine norovirus, are highly susceptible to UV_{254} disinfection, requiring only 21.7 and 26.9 mJ/cm^2 for 4 log inactivation, respectively [8, 9]. These viruses are also very similar to bacteriophage MS2, a commonly studied surrogate of relatively simple structure. The question of how highly UV_{254} resistant viruses that are significantly different in structure than MS2 (e.g. adenoviruses) behave during photocatalysis is a critical question that must be answered before photocatalytic oxidation can be relied on to provide adequate disinfection.

Watts et al. (1995) demonstrated poliovirus inactivation in water by anatase TiO_2 [9]. In this study 3 log inactivation of poliovirus was demonstrated using 250 mg/L suspended anatase TiO_2 irradiated with UV-A lights for 1 hr. In a study of inactivation of murine norovirus, 10 mg/L suspended P25 TiO_2 (in PBS) did not enhance the inactivation by 25 mJ/cm^2 UV_{254} irradiation (3.6 vs. 3.3 log reduction) [8]. However, high phosphate concentrations are known to inhibit TiO_2, making PBS a poor choice for the reaction medium in this study. Also, for viruses highly susceptible to UV_{254} disinfection, the addition of a photocatalyst may not provide any benefit, or may even slow the inactivation due to shielding [123]. Since adenovirus is the "limiting factor" in setting UV_{254} fluence requirements [2], and protein oxidation may be key to adenovirus inactivation (section 2.5), the addition of a photocatalyst is expected to reduce the

required treatment times in UV disinfection. Shielding may also be avoided by applying a photocatalyst as a thin film coating the reactor surface or another substrate.

The inactivation of a more complex virus, avian influenza, has been studied in air in a preliminary investigation [124]. This study achieved 2-3 $\log_{10}$ inactivation of the virus in a photocatalytic air purification device. While the results from studies in air and water are not directly comparable, the demonstrated inactivation of influenza reveals that photocatalysis is effective against more complex viruses. These studies provide more evidence that photocatalytic oxidation may be a viable option for inactivating pathogenic viruses in drinking water, however much more information is needed regarding the susceptibility of different virus strains, especially adenovirus.

2.6.1.9. Pilot studies of TiO_2 based virus disinfection systems

After demonstrating its efficacy against pathogenic viruses, photocatalytic oxidation must eventually be shown to be viable at the pilot scale prior to full scale implementation. One pilot scale study exists by Gerrity et al. 2008, which demonstrates that photocatalytic oxidation may be a viable option for inactivating viruses in drinking water [123], however the kinetics need to be improved to make this option attractive. In this study the different bacteriophages tested (MS2, PRD1, phi-X174, and fr) showed different inactivation behaviors, which brings to light the lack of knowledge of how virus structure leads to differences in photocatalytic inactivation kinetics. Selected properties of the viruses (and adenoviruses for comparison) are shown in Table 2-2.

The pilot scale study by Gerrity et al. (2008), conducted using a commercial Photo-Cat Lab treatment system (Purifics), revealed that UV-C induced DNA damage

was responsible for viral inactivation at low TiO_2 concentrations, but that photocatalytic oxidation was responsible at high (400 mg/L) concentrations [123]. At 400 mg/L TiO_2 and a UV dosage (34 mJ/cm^2), PRD1 was inactivated the most (2.6 log) and MS2 the least (1.8 log).

Table 2-2 - Properties of various bacteriophages and human adenoviruses

Virus	Size (nm)	Isoelectric Point	Genetic Structure	Genome Length (nt)
MS2	24 - 27	3.5 - 3.9	ssRNA	3,569
PRD-1	62	3.0 - 4.2	dsDNA	14,927
phi-X174	23	6.6	ssDNA	5,386
fr	23	8.9 - 9.0	ssRNA	3,575
Adenoviruses	70 - 100	undetermined	dsDNA	30,000 - 40,000

The inactivation of PRD1 by photocatalytic oxidation was comparable to the inactivation by UV-C alone, while MS2 was inactivated to a lesser degree than by UV-C alone. The differences in inactivation were hypothesized to be a result of differences in capsid surface densities of alanine, proline, and glycine residues, which were cited to be preferential targets for HO• attack [78, 79] (section 2.6.1.3). PRD1 has the highest surface density of these residues and MS2 the lowest [123]. However, these studies on HO• cleavage specificity do not rule out protein changes due to minor oxidations (i.e. no cleavage), which may also lead to virus inactivation [71]. More information is needed on how virus structure leads to different inactivation behavior during photocatalytic oxidation.

2.6.2. Fullerene Based Photocatalytic Oxidation

Since fullerene has been discovered, it has received considerable attention for its unique properties. One disadvantage of using C_{60} as a photocatalyst is its potential to degrade over time, whereas TiO_2 is highly stable. Exposure of C_{60} to UV irradiation causes oxidation and the introduction of surface oxygen groups to the particle surface [125]. While research on this material has shown its activity is not reduced after 5 irradiation cycles (total 10 minutes) [126], further research is needed using more relevant timescales (i.e. days) and disinfection cycles to determine a realistic lifetime expectancy of this material.

2.6.2.1. C_{60} mechanism of action

The photactivity in water of C_{60} is dependent on the effective dispersion of the particles. When C_{60} forms aggregates, singlet oxygen ($^1O_2$) and superoxide anion ($O_2^{\bullet-}$) are undetectable due to self-quenching and triplet-triplet annihilation [127]. The pathway of ROS production by irradiated C_{60} is shown in Figure 2-4. When irradiated in water in the presence of oxygen, C_{60} forms singlet oxygen with a quantum efficiency of 0.76 [128]. When a suitable electron donor is present, $C_{60}^{\bullet-}$ is formed which transfers an electron to O_2, forming $O_2^{\bullet-}$ which can further react to form HO•. The adsorption spectra of C_{60} extends to 620 nm, which allows for excitation using visible light [128]. This is highly desirable for water treatment applications, as solar irradiance can be used to drive the treatment process resulting in limited energy usage and decreased infrastructure costs.

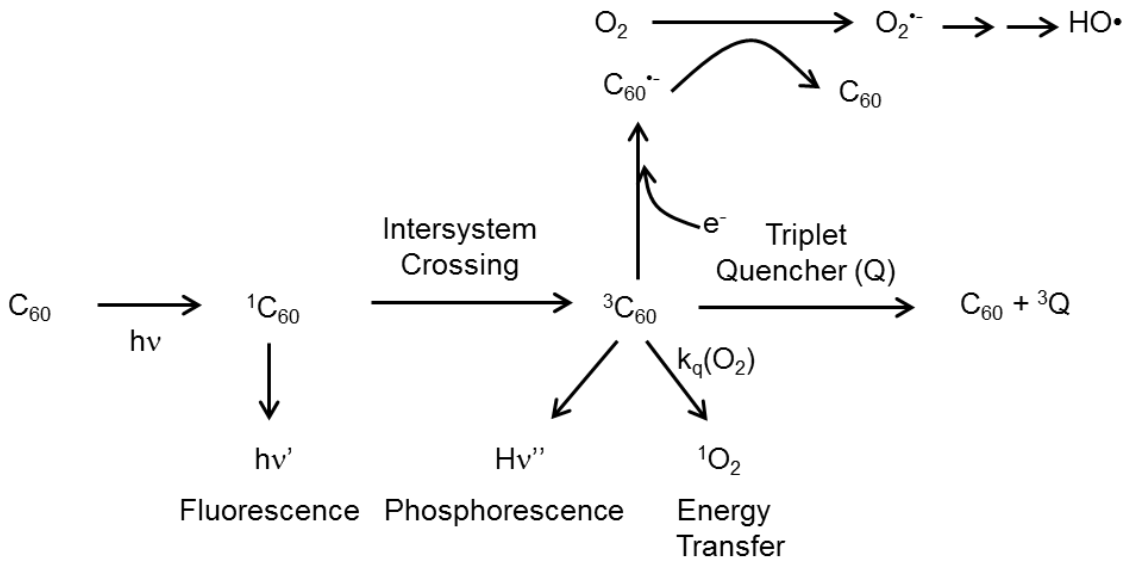

Figure 2-4 – ROS generation by irradiated C_{60}. Adapted from [128, 129].

2.6.2.2. Modified C_{60} catalysts for enhanced activity

The hydrophobic nature of pristine C_{60} causes severe aggregation in aqueous media, which effectively eliminates ROS production by the material [130]. Several surface modifications have been developed to prevent aggregation and maintain photoactivity. Examples of such modifications include the attachment of terminal carboxyl, quaternary amine, and hydroxyl groups [131]. Characterization of these materials show that aggregation is not eliminated, but $^1O_2$ is still efficiently produced, possibly due to the functionalities separating C_{60} enough to prevent triplet-triplet quenching [131]. Hexakis amino-C_{60} performed the best of all materials developed by Lee et al (2009) [131].

One problematic issue in using nanomaterials for water treatment is preventing the nanomaterials from entering the finished water supply and becoming a contaminant

themselves. Lee et al. (2010) developed a method of attaching C_{60} amino-fullerenes to relatively large silica beads, which may easily be retained in water treatment systems [126]. Immobilization of the catalyst particles improved their reactivity, which was likely due to further decreased aggregation [126].

2.6.2.3. ROS responsible for virus inactivation by C_{60}

As shown in Figure 2-4, several ROS can be formed from irradiated C_{60}, including $^1O_2$, $O_2^{\bullet-}$, and HO•. Lee et al. (2009) applied their modified C_{60} catalysts (section 2.6.2.2) for MS2 inactivation in the presence of various ROS scavengers [131]. $^1O_2$ was found to be the primary ROS responsible for inactivation of MS2, as scavengers for $O_2^{\bullet-}$ and HO• had no effect on the inactivation rate. When a scavenger for $^1O_2$ was used, the inactivation profile was unchanged as compared to inactivation that occurred in the dark (due to interaction with quaternary amines).

2.6.2.4. Viral protein damage caused by irradiated C_{60}

In general viruses may be inactivated through damage to their proteins and/or genomes. For adenoviruses, protein damage may be the pathway leading to the most rapid inactivation (section 2.5.3). In a study of MS2 inactivation by hexakis amino-fullerene, Cho et al. (2010) found the quantity of oxidized capsid proteins increased with the irradiation time [69]. This protein oxidation is the likely mechanism of inactivation for MS2. This result suggests C_{60} based photocatalytic oxidation may be highly effective for inactivation of adenoviruses.

2.7. Evaluation of reactive oxygen species production by photocatalysts

Protein (capsid) and nucleic acid damage are known to occur during TiO_2 photocatalytic oxidation as a result of oxidation (section 2.6.1.3). However, the degree of damage required to completely inactivate any virus by photocatalytic oxidation is unknown. It is possible that slight damage to the capsid alters its shape enough to prevent infection for some viruses, or significant cleavage of capsid proteins and internal enzymes / genetic material may be necessary to inactivate others. For example, HO• is capable of cleaving proteins [78, 79] while singlet oxygen can inactivate MS2 with minor oxidation of specific amino acid residues [71]. Different viruses may also behave differently based on their structure.

2.7.1. Methods for detecting reactive oxygen species production

ROS and HO• in particular are generally believed to be responsible for virus inactivation by TiO_2 [70, 74]. Measuring the ROS production of different catalysts helps identify their suitability for virus inactivation. ROS may be detected directly using electron paramagnetic resonance (EPR) spectroscopy or by chemical methods using reagents that react to individual ROS with high specificity. Several reagents are available for measuring HO•. Terephthalate has been used for decades in studies of radical formation in radio- and sono- chemical systems [132, 133]. The detection principle is based on the formation of stable fluorescent 2-hydroxyterephthalic acid from the reaction of terephthalic acid with HO•, as shown in Reaction 12.

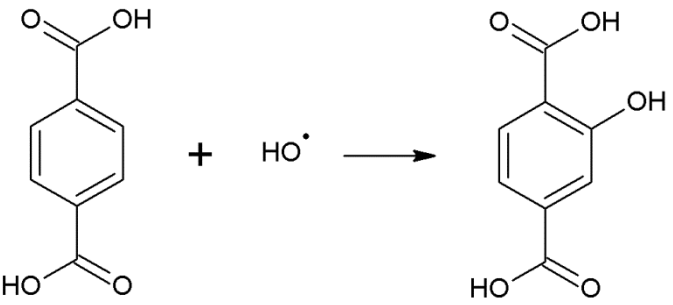

Terephthalic Acid 2-hydroxyterephthalic Acid (R12)

Utilizing chemical methods for measurement of ROS requires careful consideration of the specificity and yield of a particular reagent. While terephthalate has high specificity for HO•, the yield of 2-hydroxyterephthalate is only 35% of the HO• yield [132, 133]. Two possibilities exist to explain the reduced yield [132]. First, HO• may add to the *iso* position of the carboxylate groups, forming a non-fluorescent product. Secondly, when HO• has added to the *ortho* position, oxygen may cause further oxidation yielding a non-fluorescent phenol. Despite this, the terephthalate method is a useful tool to compare HO• production by different catalyst.

Ishibashi et al. (2000) first demonstrated the application of terephthalate for measuring HO• by TiO_2 and revealed several conditions that must be met to perform a successful analysis [134]. It is possible that electron holes may directly oxidize terephthalate producing the fluorescent product. This can be avoided by keeping the substrate concentration low (10^{-3}-10^{-4} M). However, too low a concentration will result in a reduction of sensitivity as the HO• decays before it can react. In balancing the above concerns, Ishibashi et al. (2000) found 4 x 10^{-4} M terephthalate was optimum for testing

TiO_2 films [134]. The measured fluorescent intensity of their reaction solution revealed zero order kinetics, which can be interpreted to be the HO•˙ production rate.

After the study by Ishibashi et al. (2000), several other authors have reported using this method [135-137]. While they all use low concentrations of terephthalate in alkaline solution, the concentrations of suspended TiO_2 used vary from 25 – 3,333 mg/L. Eremia et al. (2008) investigated several parameters on the reaction, including catalyst concentration, and determined that 25 mg/L was optimum in terms of measuring HO• production (for P25 TiO_2) [135]. Another interesting observation was made by Kohtani et al. (2008) [136]. After observing the generation of 2-hydroxyterephthalate following zero order kinetics, the concentration increase eventually ceased and began to decrease substantially, indicating that the product was further degraded to non-fluorescent compounds. When using this method, samples must be taken at appropriate times to avoid the loss of fluorescent product.

Along with terephthalate, other reagents are available for measuring HO•. For example, *para*-chlorobenzoic acid is often used as a probe in studies of HO• production by ozone [138, 139]. However, there are no reports available detailing its use as a probe in photocatalytic reactions. This makes it inconvenient to use at this point for screening catalysts. Alternate detection methods, such spin trapping (e.g. with 5,5-dimethyl-pyrroline N-oxide, DMPO) and electron paramagnetic resonance (EPR) spectroscopy measurements are useful for detecting the types of radicals generated by a catalyst, but provide less quantitative results than other methods.

2.8. Surrogate pathogens in disinfection studies

The result from Gerrity et al. (2008) that bacteriophage PRD1 (dsDNA) is most susceptible to photocatalytic oxidation gives further hope for the application of this technology for adenovirus removal [123]. PRD1 closely resembles adenovirus in structure and even function, which is remarkable considering they have such different hosts. The major capsid protein of PRD1 (P3) is nearly identical to the major capsid protein of adenovirus (HEX) in both individual and lattice structure, and a pentameric protein with a protruding infective spike is present at the lattice vertices, as in adenoviruses [140]. It is possible that adenovirus is also highly susceptible to photocatalytic oxidation based on these results. However, as reviewed above in section 2.6, most photocatalytic oxidation studies report using MS2 as a surrogate pathogen.

Bacteriophage MS2 (ATCC 15597-B1) is commonly used as a surrogate pathogen due to its similarity to many waterborne pathogenic viruses [24-26, 81] and the simplicity of its propagation and enumeration. MS2 has been found to be comparable or more resistant to chlorine and chloramines than Hepatitis A virus [27] and Poliovirus [29], and more resistant to UV disinfection than other bacteriophages [28]. Gerrity et al. (2008) found MS2 the most resistant to inactivation by TiO_2 as compared to three other bacteriophages (PRD1, phi-X174, and fr) [123]. Hence, using MS2 as a surrogate pathogen provides conservative assessment on treatment efficiency.

MS2 is markedly different in structure and function than the actual target pathogen, adenovirus (section 2.4). MS2 is a small (~25 nm) icosahedral ssRNA virus that contains only two protein types: coat (structural, 180 copies) and A (infective, single

copy). In contrast, adenovirus is large (~90 nm) with dsDNA and 13 different protein types, including 12 copies of the infective protein. While MS2 has proved to be a suitable indicator in studies of other disinfectants, it is not known if this simple virus is suitable for use a surrogate in photocatalytic disinfection studies.

2.9. Conclusions of Literature Review

The information currently available indicates a need for improved virus inactivation technology in drinking and waste water treatment systems. Adenoviruses are ubiquitous in the environment, are resistant to many disinfection techniques, and have emerged as a pathogen of concern. There is clearly room for improving the disinfection of adenovirus (and other viruses). The disinfection methods displaying the highest efficiency of adenovirus inactivation are highly oxidizing and have been demonstrated to or have the potential to damage viral proteins. Photocatalytic oxidation using a high efficiency photocatalyst is an alternative disinfection technology that holds promise for virus inactivation. Photocatalysts produce highly oxidizing ROS which are capable of damaging proteins. However, there are no published reports on the susceptibility of adenovirus to this disinfection method. Also, the required treatment time for adequate virus inactivation by photocatalytic oxidation must be decreased for this technology to be fully viable. This may be accomplished by modifying catalysts to increase ROS production, increase substrate adsorption, and improve catalyst solubility / dispersion stability. Understanding the mechanism of virus inactivation by photocatalytic oxidation may also be useful for designing treatment systems with improved efficiency.

Chapter 3

Virus inactivation by silver doped titanium dioxide nanoparticles for drinking water treatment[1]

[1] Published manuscript: Liga, M. V., E. L. Bryant, V. L. Colvin, and Q. Li (2011). Virus inactivation by silver doped titanium dioxide nanoparticles for drinking water treatment. *Water Research* (45): p. 535-544.

Keywords: Drinking Water, Nanotechnology, Photocatalysis, Silver, Titanium Dioxide, Virus

3.1. Introduction

The removal of viruses and other pathogens from drinking water (and the environment in general) is important for the maintenance of the health and well-being of

society. Pathogenic viruses such as adenovirus, norovirus, rotavirus, and hepatitis A commonly occur in both surface and ground water sources [16, 19, 141] and must be effectively inactivated to provide safe water. In the United States just between 2003 and 2005 there were four reported waterborne disease outbreaks attributed to viruses in drinking water affecting 282 people [21, 22]. The USEPA requires treatment systems capable of providing 4 log (99.99%) removal of viruses for all surface water sources and groundwater sources with a history of contamination or other deficiencies [2, 23].

Traditional chlorine disinfection, while highly effective for viral inactivation, produces harmful disinfection byproducts (DBPs) when organic compounds are present in the water. This has prompted stricter regulations concerning the acceptable levels of these compounds [3]. Although UV disinfection has not been found to form DBPs [6], some viruses such as adenoviruses are highly resistant to UV disinfection [5]. As a result, the USEPA has increased the UV fluence requirements for 4 log removal of viruses from 40 mJ/cm^2 to 186 mJ/cm^2 [2]. The new high fluence requirement significantly increases the energy demand, which translates into a higher treatment cost.

The employment of a highly efficient photocatalyst for advanced oxidation could potentially enable effective virus inactivation in drinking water as chlorine can while limiting the formation of DBPs [6, 7, 142]. It would also require less energy than UV disinfection. Therefore, photocatalytic oxidation is being actively researched as an alternative water disinfection method [143, 144]. A highly efficient photocatalyst could also be utilized for air treatment or as an antimicrobial coating.

3.1.1. Titanium dioxide photocatalysis

Titanium dioxide is an attractive photocatalyst for water treatment as it is resistant to corrosion and non-toxic when ingested [68]. The basic mechanism of TiO_2 photoactivation and reactive oxygen species (ROS) generation is well known [72].

There are currently a few commercial treatment systems that utilize TiO_2 photocatalysis (e.g. Wallenius AOT®, Purifics®). However their usage is not wide spread. One major reason for the limited application is the slow reaction kinetics as a consequence of charge recombination, which consumes the activated electrons and holes.

The antibacterial properties of TiO_2 have been well documented [9, 74, 105, 145-147] and are attributed to the generation of ROS, especially hydroxyl free radicals (HO•) and hydrogen peroxide (H_2O_2) [146]. While fewer studies have investigated the antiviral properties of TiO_2, its potential for inactivating viruses has been demonstrated [9, 25, 74, 81, 148]. However, the inactivation rates obtained in most of these studies were extremely low. For example, Cho, et al. (2005) demonstrated only ~1 log removal of MS2 after 2 hours of irradiation using P25 TiO_2 suspended at 1 g/L [74]. The inactivation kinetics needs to be greatly improved in order to provide efficient drinking water disinfection.

Metal doping has been used to enhance TiO_2 photocatalysis by trapping excited electrons to prevent charge recombination [97-100]. Electron trapping can occur if the dopant has a lower Fermi level than the excited electron. Several metals including Fe, Mo, Ru, Os, Re, V, Rh, Au, Pt, and Ag have been shown to enhance TiO_2 performance. Silver in particular has been shown to enhance the photocatalytic efficiency of TiO_2 for

both organic contaminant degradation and bacterial inactivation [73, 92, 105, 107, 108, 110]. Tran et al. (2006) showed selective enhancement by silver, which increased degradation rates for short chain carboxylic acids but not for alcohols or aromatics [149]. Silver coatings above the optimum amount can also decrease the photocatalytic activity [112, 113]. However, there is limited information on its impact on the antiviral capabilities of TiO_2 [111]. In addition to facilitating charge separation, silver is thought to enhance TiO_2 photocatalysis by directly interacting with microorganisms and providing more surface area for adsorption [113, 150], although Vamathevan et al. (2002) found no increase in BET surface area after silver doping [73]. Silver ions and nanoparticles have been shown to have antimicrobial properties themselves through a variety of mechanisms [115-117], which could also aid in bacterial or viral inactivation.

Utilizing silver in conjunction with TiO_2 photocatalysis could potentially allow several different inactivation mechanisms to work in concert. Therefore, it is possible that a synergism occurs between silver and TiO_2 when silver doped titanium dioxide is used for inactivating microorganisms under UV radiation. The study reported here demonstrated that silver doping TiO_2 greatly enhanced the photocatalytic inactivation of viruses primarily by increasing HO• production in addition to slightly increasing virus adsorption.

3.2. Materials and methods

3.2.1. Synthesis and characterization of nano-silver doped TiO_2 (nAg/TiO_2)

nAg/TiO_2 was prepared by depositing nano-sized silver islands via photochemical reduction of silver nitrate (Alfa Aesar) onto two commercially available TiO_2: Aeroxide TiO_2 P 25 (denoted hereafter P25 TiO_2, Degussa) and Anatase TiO_2 (denoted hereafter $AATiO_2$, Alfa Aesar; CAS: 1317-70-0). A solution containing oxalic acid (Sigma-Aldrich, anhydrous 99%) as a sacrificial electron donor, TiO_2, and silver nitrate (Sigma-Aldrich, 99.9999%) was stirred for two hours at pH 1 under ambient light at room temperature while purged with nitrogen gas. The solution was then irradiated with a germicidal UV lamp for one day and the product purified by washing with excessive water four times [99]. The concentration of silver nitrate used in the reaction solution was varied to achieve 4, 8, and 10 wt %; oxalic acid was added at a 25:1 acid to silver molar ratio. The $AATiO_2$ was doped using 10% $AgNO_3$ in solution. The doped particles were then dried and stored under vacuum in dark.

Samples were prepared for TEM and XPS analysis by applying a drop of a $nAgTiO_2$ suspension to a Silicon Monoxide/Formvar grid (Ted Pella; 01829) or a silicon wafer coated with gold (~ 68 nm). The grid was then used to analyze the sample in a JEOL 2100 field emission gun transmission electron microscope (JEM 2100F TEM) at 200KV. The silicon wafer was used for x-ray photoelectron spectroscope (PHI Quantera XPS).

The actual silver content of the nAg/TiO_2 nanoparticles was determined by acid digestion and subsequent analysis of silver concentration using inductively coupled

plasma-optical emission spectroscopy (ICP-OES, PerkinElmer Optima 4300 DV). Aliquots of 0.01 g nAg/TiO_2 nanoparticles were mixed with 5 mL of 50% HNO_3, briefly bath sonicated, refluxed for 4 hours and diluted to 50 mL with ultrapure water. The resulting suspensions were centrifuged and the supernatants filtered through a 0.22 μm-pore-size syringe filter. The filtrates were then analyzed by ICP-OES to determine the silver concentration.

3.2.2. Model virus

Bacteriophage MS2 (ATCC 15597-B1) was used as a model virus in this study due to its similarity to many water borne pathogenic viruses [24-26] and the simplicity of its propagation and enumeration. MS2 has been found to be comparable or more resistant to chlorine and chloramines than Hepatitis A virus and Poliovirus, and more resistant to UV disinfection than other bacteriophages [27-29]. Hence, using MS2 as a virus surrogate provides conservative assessment on treatment efficiency.

The virus stock solution used in the disinfection procedures was obtained by infecting an incubation of the *E. coli* host (ATCC 15597) with a liquid MS2 suspension. The mixture was mixed with a molten LB-Lennox (Fisher) medium containing 0.7 % Bacto™ agar (Difco Laboratories) and poured over a Petri dish containing solid LB-Lennox media. After incubating overnight at 37°C, sterile 0.1 M bicarbonate (Fisher) buffer was added to the plate which was gently rocked for 3 hours. The solution was withdrawn from the plate, centrifuged, and the supernatant filtered through a 0.22 μM-pore-size PES syringe filter. The virus suspension contained ~$7x10^9$ plaque forming units per milliliter (PFU/mL) and was stored at 4 °C before use.

MS2 samples were enumerated according to the double agar layer method [151]. Samples were analyzed either immediately or stored at 4 °C in dark and analyzed within 24 hr. No change in viral titers was found within 24 hr. of storage in the presence or absence of the nanomaterials. To determine if the presence of nanoparticles interfered with virus enumeration, parallel samples containing nanoparticles were enumerated directly or after centrifugation at 10,900 G for 15 minutes to remove the nanoparticles. No significant difference was found between the two methods. Therefore, all data reported hereafter were obtained from direct enumeration of the samples without removing the nanoparticles. Control tests consisted of enumerating buffer solution to ensure that viral contamination was not present in any of the reagents.

3.2.3. Virus inactivation experiments

All materials that came in contact with the virus solutions, media, and reagents were sterilized by autoclaving, filtering, or purchased sterile. Nanoparticle suspensions were freshly prepared in ultrapure water and were bath sonicated for 30-45 minutes to ensure good dispersion before each experiment. Particle size and zeta potential of each suspension was analyzed by dynamic light scattering (DLS) using a Zen 3600 Zetasizer (Malvern Instruments, Worcestershire, UK) to determine if differences in particle size and thus surface area were responsible for any observed differences in viral inactivation.

3.2.3.1. Dark inactivation of viruses

Dark inactivation of viruses was assessed using undoped P25 TiO_2 and nAg/TiO_2 synthesized with P25 and 10 wt. % $AgNO_3$. A suspension of ~$7x10^7$ PFU/mL MS2 was made in ultrapure water to which sonicated nAg/TiO_2 or P25 TiO_2 nanoparticles were

added. The suspension was then stirred for up to 10 minutes in the dark, and sampled at different times for virus enumeration. The virus/nanoparticle mixtures were subsequently kept in dark at 4 °C for 24 hours before enumerated again. The effect of leached silver was investigated by removing the catalyst particles from suspension after sonication by centrifugation and filtration. The resulting solution was added to an MS2 suspension, which was sampled periodically for the active MS2 titer.

3.2.3.2. Photocatalytic virus inactivation

The photocatalytic viral inactivation experiments were carried out in a pre-stabilized Luzchem LZC-4V photoreactor (Luzchem Research, Inc., Ottawa, ON Canada) fitted with four 8W UV-A (315-400 nm) lamps with peak emission at 350 nm (Hitachi). The total light intensity used in all experiments was 2.5 mW/cm^2 as determined by a UV radiometer (Control Company, Friendswood, TX) with a NIST traceable 350 nm photosensor.

Reactions were housed in sealed 25 mL Pyrex Erlenmeyer flasks. Sterile ultrapure water was combined with the MS2 stock solution and catalyst suspensions or leached Ag^+ solutions to achieve a final concentration of ~$7x10^7$ PFU/mL MS2 and 100 mg/L TiO_2 or nAg/TiO_2. The volume of leached Ag^+ solution added was the same as that used with particles in suspension. The mixture was stirred for one minute in the dark, after which a sample was taken representing the initial virus concentration after adsorption. The reaction flask was then placed in the reactor and 1 mL samples were taken at 30 second intervals. All samples were immediately enumerated or covered and refrigerated at 4 °C to prevent further inactivation while waiting to be processed.

To investigate the role of HO• in MS2 inactivation, reactions were carried out in the presence of two HO• scavengers, methanol (99.9%, Fisher spectranalyzed) or *tert*-butanol (Fisher, ACS Certified) at concentrations from 30 to 400 mM. Control experiments were performed by mixing MS2 in the corresponding alcohol solution for 10 minutes to account for any inactivation due to the alcohol. Samples were immediately diluted into 0.1 M bicarbonate buffer.

3.3. Results and discussion

3.3.1. nAg/TiO_2 characterization

The color of the dried nAg/TiO_2 nanoparticles varied from light brown to reddish brown. The degree of surface oxidation of the silver is likely responsible for the differences in color.

3.3.2. Silver content

The amount of silver captured by the TiO_2 varied with both the $AgNO_3$ concentration and the base TiO_2 material used. The P25 TiO_2 based nAg/TiO_2 made with 10, 8, and 4 wt. % $AgNO_3$ had final Ag contents of 5.95, 4.36, and 2.46 wt. %. The $AATiO_2$ based nAg/TiO_2 made with 10 wt. % $AgNO_3$ had a final Ag content of 3.94 wt. %. The nAg/TiO_2 materials are hereafter designated by the final nAg content and base TiO_2 material (e.g. 5.95%nAg/P25TiO_2). Silver deposition was more efficient at higher $AgNO_3$ concentrations. Deposition onto P25 was notably greater than that on the $AATiO_2$: 90% of the Ag added was coated onto P25 while only 59% onto the $AATiO_2$

when 10% $AgNO_3$ was applied. The lower doping efficiency of $AATiO_2$ is attributed to its limited photoactivity.

3.3.3. TEM and XPS analysis

Figure 3-1 presents representative TEM images of the Ag doped and undoped P25 samples. Silver islands of ~ 2-4 nm in diameter were found on the TiO_2 nanoparticles (~ 10-50 nm), although they were not apparent on all crystallites. No silver deposits were observed on any TiO_2 particles not treated with silver.

XPS analyses showed similar results for all samples. Figure 3-2 presents the XPS spectra for the 5.95%nAg/P25TiO_2 as an example. O 1s spectra (e.g., Figure 3-2 a) of all samples showed a major peak with a broad shoulder in the area for metal oxides (528 – 531 eV). The presence of the shoulder indicates the presence of multiple metal oxides, i.e., titanium dioxide and silver oxide. The Ag 3d spectra (e.g., Figure 3-2 b) confirm the presence of silver oxide (peak range 367.3-368.0). This may be due to silver adsorbing on the TiO_2 surface at oxygen sites or the oxidation of the surface of the deposited silver.

3.3.4. Dispersed particle size

Mean hydrodynamic diameters of all photocatalyst suspensions in ultrapure water are presented in Figure 3-3. The sizes of P25 TiO_2, AA TiO_2, and 3.94%nAg/$AATiO_2$ stayed constant for at least 25 min, suggesting that these suspensions were stable during the virus inactivation experiments (~ 5 minutes). All the P25 based nAg/TiO_2 materials, however, formed large aggregates and settled out gradually. The aggregation of the silver doped samples was consistent with the measured changes in zeta potential: -9.1 to -

9.3 mV versus -38.7 mV for P25. The sizes presented in Figure 3-3 for these materials are the average of data obtained in the first 5 minutes concurrent with the inactivation procedure.

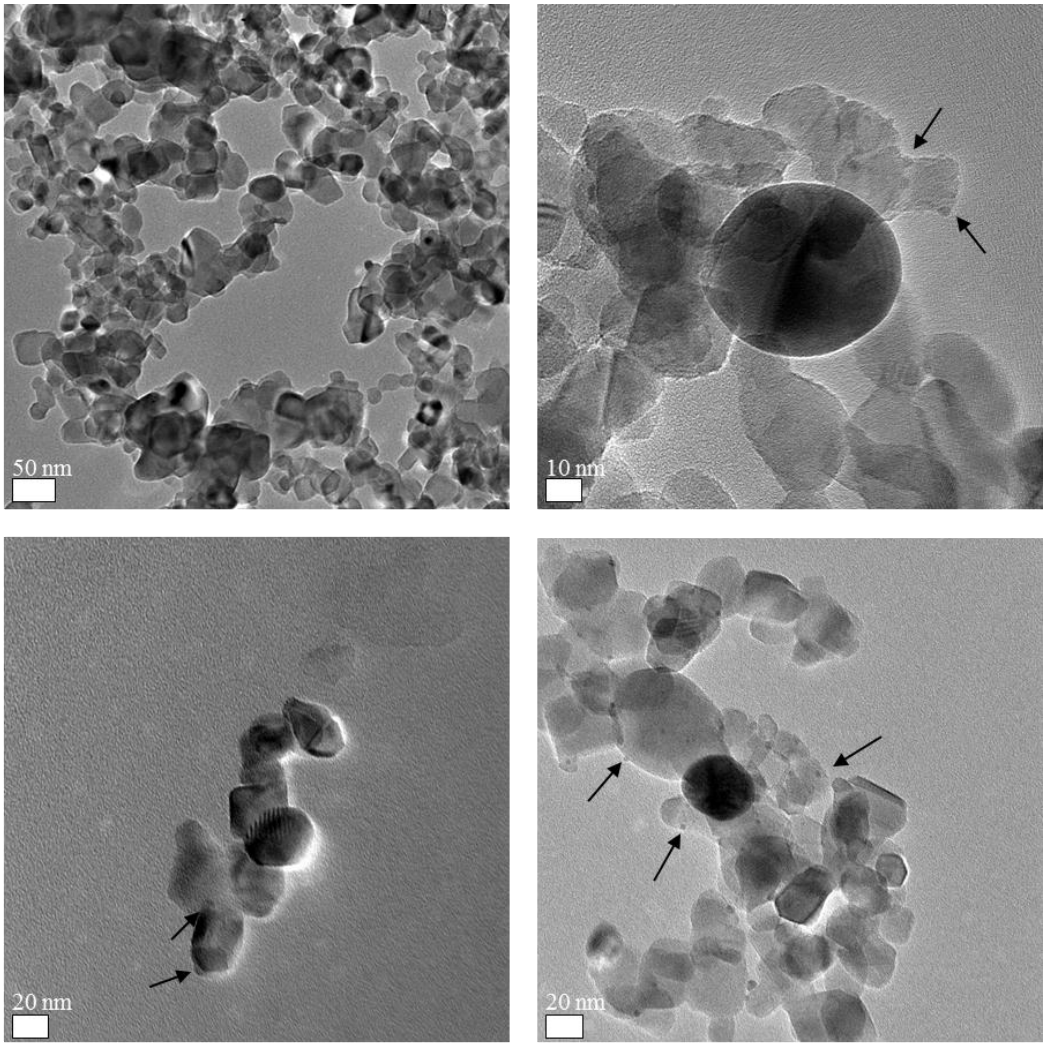

Figure 3-1 - TEM images of nAg/P25TiO_2 with silver particles (~ 2-4 nm dia.) indicated by arrows. Silver particles are visible on all doped samples, although they are not apparent on all TiO_2 crystallites (10-50 nm dia.). Top left undoped P25 (50 nm scale), top right 5.95% Ag (10 nm scale), bottom left 4.36% Ag (20 nm scale), bottom right 2.46% Ag (20 nm scale).

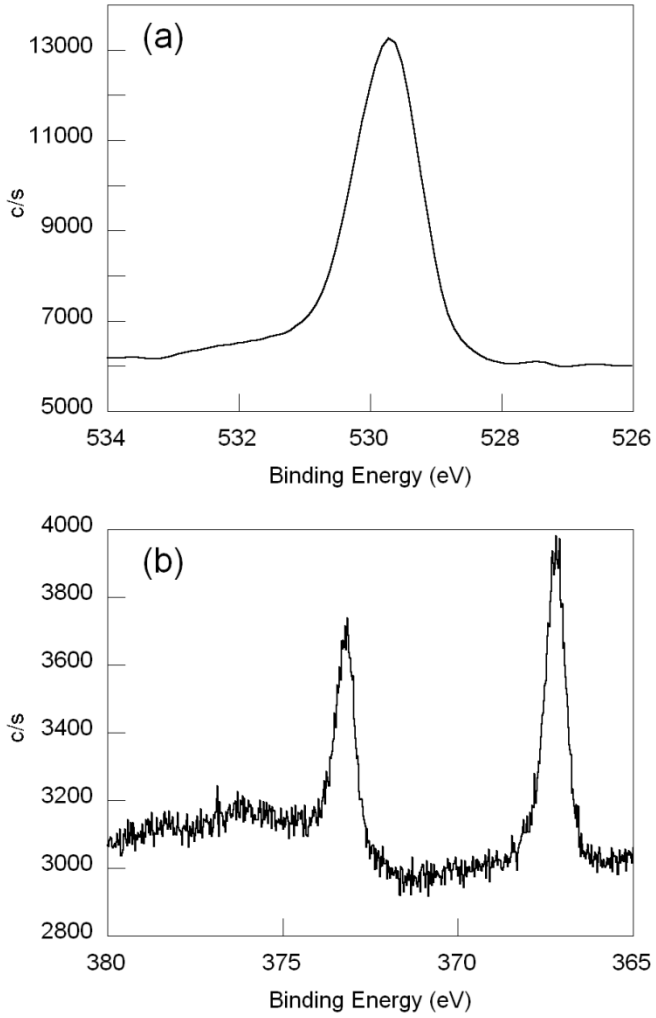

Figure 3-2 - Typical X-ray photoelectron spectra of (a) O 1s, which reveals the presence of multiple metal oxides through the observed peak shoulder and (b) Ag 3d, with peak between 367.3 and 368 eV which corresponds to silver oxide. Spectra shown for 5.95%nAg/P25TiO$_2$.

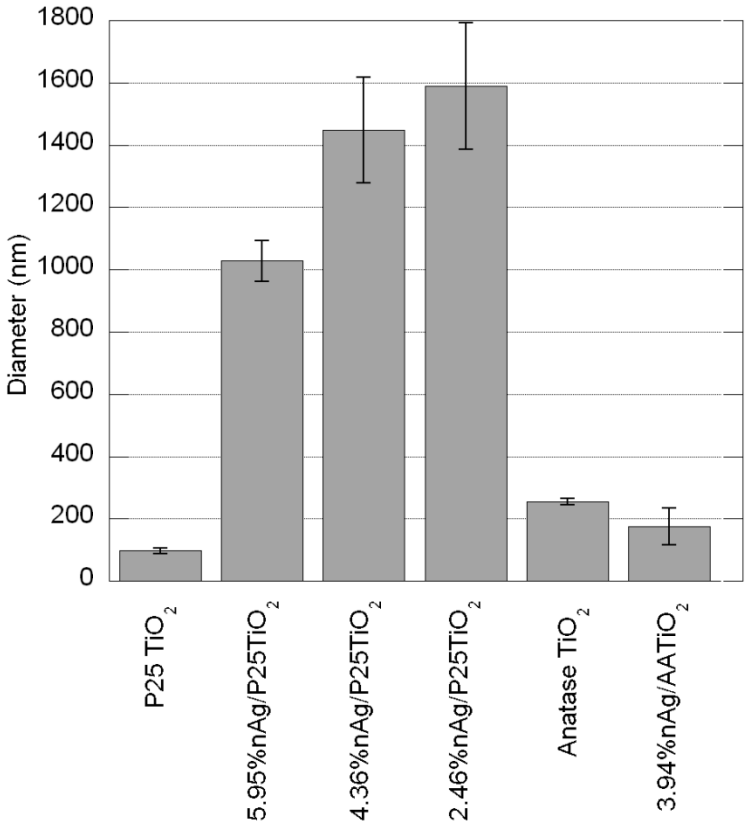

Figure 3-3 - Dispersed particle diameters of nanoparticles used for virus inactivation as measured by DLS. Silver doping P25 TiO_2 was found to decrease the stability of the suspended particles, resulting in the observed aggregation.

3.3.5. MS2 dark inactivation

Inactivation and removal of MS2 by the photocatalysts in dark (referred to as dark inactivation hereafter) is attributed to adsorption to the photocatalyst particles and inactivation by Ag^+ released from nAg/TiO_2. Figure 3-4 shows the total dark removal after 10 minutes of exposure to P25 and $5.95\%nAg/P25TiO_2$. Leached Ag^+ was responsible for 37% (0.2 log) MS2 inactivation, with most inactivation occurring during the first 1 minute of exposure. When enumerated with catalyst particles in suspension, a

total of 75% (0.6 log) removal was observed with 5.95%nAg/P25TiO_2. After accounting for the effect of leached Ag^+ (37% removal), the 5.95%nAg/TiO_2 removed 38% (0.2 log) of the MS2 by adsorption, 12% more than that adsorbed by undoped P25, which inactivated 26% (0.13 log) of the MS2. The majority of dark inactivation occurred during the first minute of exposure. Therefore, the MS2 concentration measured after 1 min. of dark contact in each photocatalytic inactivation experiment was used as the initial concentration for analysis of the photocatalytic inactivation data.

The increased adsorptive removal by nAg/TiO_2 may be explained by interactions of viral surface amino acids with silver. Silver has a high affinity for sulfur moieties, and there are 183 cysteine residues exposed on the MS2 capsid surface [152-154]. Carboxyl groups on the amino acids are also known to interact with silver [155]. The minimum difference between virus titers with nanoparticles in suspension and nanoparticle free centrifuge supernatant (Figure 3-4) suggests that adsorption of MS2 to the nAg/TiO_2 or undoped TiO_2 surface either inactivates these viruses or sterically inhibits access of the MS2 A protein to the *E. coli* pili, where infection occurs. The limited additional removal observed after centrifugation of samples is attributed to the interception of MS2 by the catalyst particles during centrifugation.

The mixtures of the MS2 and the P25 TiO_2 or 5.95%nAg/P25TiO_2 were further kept in dark at 4 °C for 24 hours and re-enumerated to assess the potential dark inactivation of stored samples. Negligible change in virus titer was observed during the 24 hour period for either materials (data not shown), suggesting that further inactivation was absent in dark.

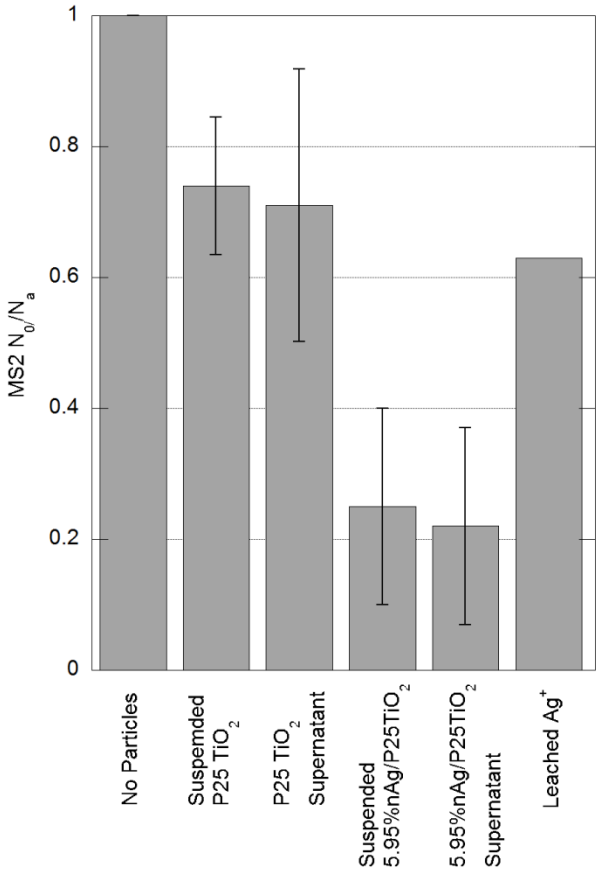

Figure 3-4 - Removal of MS2 by P25 TiO_2, 5.95%nAg/P25TiO_2, and leached Ag^+ from 5.95%nAg/P25TiO_2 after 10 min of contact in dark. TiO_2 and nAg/TiO_2 samples were enumerated both with particles in suspension and after their removal by centrifugation (data marked "supernatant") to determine if adsorbed viruses remained infective. The limited difference in virus titers between solutions with particles suspended and removed suggests that MS2 is inactivated upon adsorption to the catalysts. After accounting for the effect of leached Ag^+, the 5.95%nAg/P25TiO_2 removed 38% (75-37%) MS2 by adsorption as compared to only 26% by P25 TiO_2. N_a is the titer of viruses before particle addition. N_0 is the virus titer after dark stirring.

3.3.6. Photocatalytic MS2 inactivation

The inactivation of MS2 by the different nanomaterials and UV-A alone is shown in Figure 3-5. The plain P25 TiO_2 achieved 1.6 log inactivation of MS2 in 2 min. while UV-A irradiation alone showed negligible MS2 removal within the same time period (Figure 3-5 a), showing that the inactivation in the presence of P25 TiO_2 is attributed to photocatalytic oxidation. Silver doping significantly enhanced MS2 inactivation by P25 TiO_2 and the inactivation rate increased with silver content. The enhanced inactivation was also observed with the Ag doped $AATiO_2$ (Figure 3-5 b), even though $AATiO_2$ showed minimum inactivation.

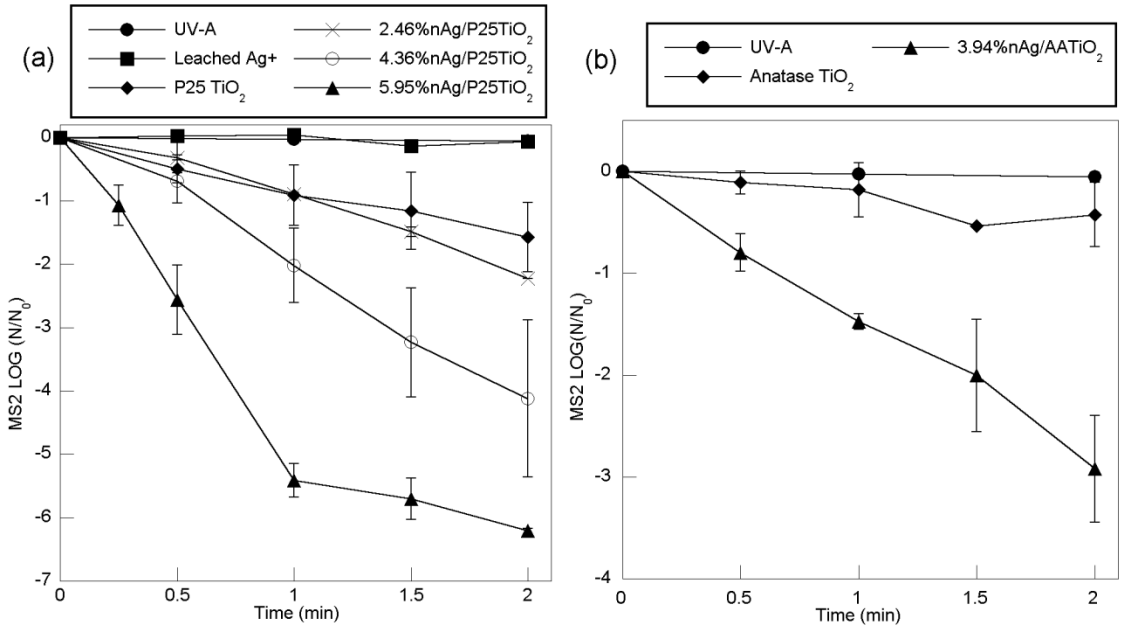

Figure 3-5 - MS2 Inactivation by (a) UV-A alone and Ag^+, P25 TiO_2, 2.46%nAg/P25TiO_2, 4.36%nAg/P25TiO_2, and 5.95%nAg/P25TiO_2 under UV-A irradiation, and by (b) UV-A alone and, $AATiO_2$, 3.94%nAg/$AATiO_2$ under UV-A irradiation. The inactivation rate was found to increase along with the silver content on P25 TiO_2 up to the maximum amount tested (5.95%). 3.94% nAg on anatase TiO_2 also dramatically increased the inactivation rate.

The photocatalytic inactivation kinetics data could be described by the Chick-Watson model (Equation 3-1), where k' is the rate constant (s^{-1}) and N_0 and N are the titer of active viruses at time zero and t (s). Here, the virus titer after dark adsorption equilibrium was used as N_0.

Equation 3-1

$$\text{Log}\,(N/N_0) = -k't$$

The inactivation rate constants obtained from fitting the kinetics data with the Chick-Watson model are shown in Table 3-1. The silver doping increased the reaction rate constant by up to 584% as compared to the base TiO_2. The inactivation rate was found to increase with the silver content on P25 TiO_2, with rate constants of 0.089, 0.035, 0.017 and 0.013 s^{-1}, for the materials with 5.95, 4.36, 2.46 and 0 % silver, respectively. The inactivation rate constant for 3.94%nAg/AATiO_2 (0.024 s^{-1}) showed a 5 fold increase from the plain AATiO_2 (0.004 s^{-1}); it also outperformed P25 TiO_2 and 2.46%nAg/P25TiO_2, even though the P25 TiO_2 inactivated MS2 ~3.2 times faster than the AATiO_2. While silver was found to be beneficial when doped onto P25 TiO_2, the increased aggregate size may have offset some enhancement in photoactivity. Also shown in Table 3-1 is the time required for each nanomaterial to achieve 4 log removal of MS2. With 5.95 wt. % nAg loading on P25, 4 log removal of MS2 could be obtained in 45 seconds, making it feasible to achieve virus removal from drinking water using a small photoreactor or to improve removal of UV resistant viruses of existing UV reactors.

Table 3-1 - Actual silver contents on nAg/TiO_2 particles and first order rate constants for MS2 inactivation

Material	Rate Constant (s^{-1})	R^2	Time Required to Achieve 4 Log Removal (min) [a]
P25 TiO_2	0.013	0.91	5.1
2.46%nAg/P25TiO_2	0.017	0.99	3.9
4.36%nAg/P25TiO_2	0.035	0.97	1.9
5.95%nAg/P25TiO_2	0.089[b]	0.99	0.75
AA TiO_2	0.004	0.98	16.7
3.94%nAg/AATiO_2	0.024	0.99	2.8

[a]Times greater than 2 min obtained by projecting kinetic data

[b]Rate for first 60 seconds of inactivation

Experiments using solutions containing leached Ag^+ resulted in no notable photocatalytic inactivation. These results suggest that the enhanced inactivation was due to the increase in the photocatalytic activity of TiO_2 instead of the antimicrobial property of nAg. Two mechanisms may be responsible for such enhancement: increased MS2 adsorption and greater ROS generation. MS2 inactivation has been shown to be directly proportional to the amount adsorbed to the TiO_2 surface [25, 81]. Increased adsorption as demonstrated in Figure 3-4 may enhance the inactivation rate by placing the virus in close proximity to newly generated HO• (both surface bound and bulk) and may increase direct hole oxidation. In addition, silver doping has been proposed to facilitate charge separation in TiO_2 resulting in more efficient ROS generation and consequently greater MS2 inactivation.

MS2 inactivation by 5.95%nAg/P25TiO_2 shows a tailing effect after 60 seconds (5.4 log removal), when the inactivation rate constant decreased from 0.089 to 0.013 s^{-1}.

This was not observed when MS2 was inactivated by the other materials. This is likely due to the presence of the large number of inactivated viruses and their remnants, which compete with infective viruses for adsorption sites and ROS, since 99.9996% of the MS2 had been inactivated after 60 seconds.

3.3.6.1. Effects of HO• scavengers

As discussed above, one potential mechanism for the enhanced virus inactivation of nAg/TiO_2 is higher HO• production rate. To test this mechanism, methanol and *tert*-butanol were employed to elucidate the role of Ag doping in HO• production and MS2 inactivation. Alcohols, especially methanol and *t*-butanol, are known HO• scavengers. Methanol was reported to scavenge both surface bound and bulk HO•, as well as holes [74]. While *t*-butanol has been shown to competitively adsorb to TiO_2 [156], research has demonstrated that it does not scavenge all surface bound HO• [157]. Using methanol and *t*-butanol as HO• scavengers, Cho et al. (2005) showed that bulk HO• was responsible for the inactivation of MS2 by TiO_2 [74]. Singlet oxygen and superoxide anion were also found to inactivate MS2 in a study using fullerol as the photocatalyst [158].

Experiments were performed using P25 TiO_2 (Figure 3-6 a, Figure 3-6 b) and 5.95%nAg/P25TiO_2 (Figure 3-6 c, Figure 3-6 d) at different methanol or *t*-butanol concentrations. Both methanol and *t*-butanol completely stopped inactivation of MS2 by the plain P25 TiO_2 at 400 mM and considerably slowed the reaction at 200 mM. P25 TiO_2 showed higher sensitivity to *t*-butanol, as 30 and 100 mM *t*-butanol both decreased the inactivation rate while the same concentrations of methanol had no effect.

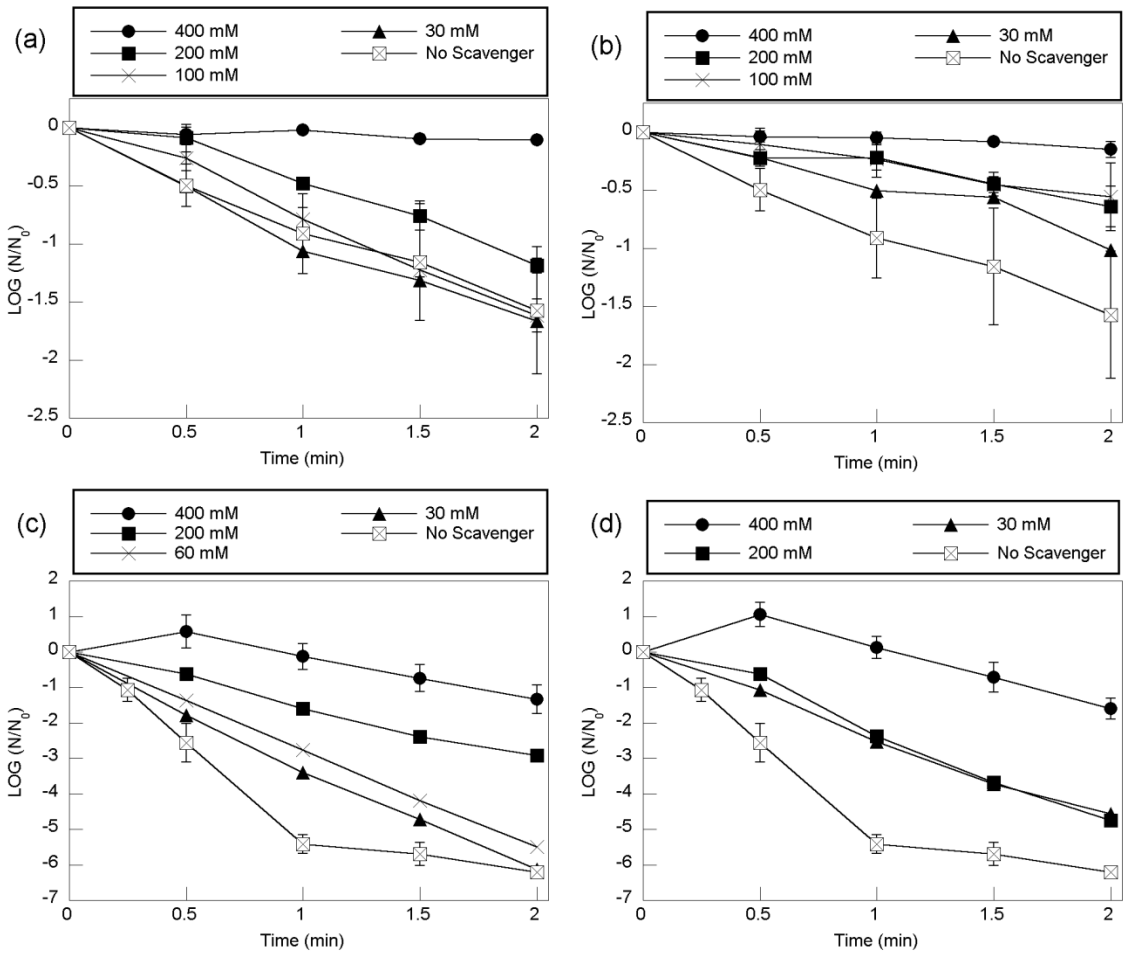

Figure 3-6 - MS2 inactivation in the presence of HO• scavengers methanol and t-butanol. (a) P25 TiO_2 with methanol; (b) P25 TiO_2 with t-butanol; (c) 5.95%nAg/P25TiO_2 with methanol; (d) 5.95%nAg/P25TiO_2 with t-BuOH. The inactivation rate was found to decrease in a concentration dependent manner when either alcohol was applied. When present at 400 mM, both alcohols completely stopped MS2 inactivation by P25 TiO_2 while inactivation still occurred by 5.95%nAg/P25TiO_2, but to a much lesser degree than the case when no HO• scavenger is applied. Dark inactivation of MS2 by 5.95%nAg/P25TiO_2 was enhanced when either alcohol was present at 400 mM, but the effect was reversed after 30 seconds of irradiation corresponding to the apparent initial rise in active virus titer.

Control experiments using methanol or *t*-butanol in the absence of any photocatalyst did not show any decrease in virus titer for methanol or *t*-butanol

concentrations up to 400 mM. These results suggest that HO• is primarily responsible for MS2 inactivation by P25 TiO_2. Although singlet oxygen and superoxide anions are also produced by TiO_2 [72], they did not seem to cause notable MS2 inactivation in our study. Because there was no significant difference in reaction rates when either methanol or *t*-butanol was used at 400 mM and the inactivation rate was more sensitive to low *t*-butanol concentrations, the data suggests that bulk HO• plays a more important role than surface bound HO· in MS2 inactivation. This observation agrees with the conclusion by Cho et al. (2005) [74].

Both alcohols also reduced the inactivation rate of MS2 by 5.95%nAg/P25TiO_2, but to a much less extent. With 400 mM methanol or *t*-butanol, 1.3 and 1.6 log of MS2 inactivation was achieved, respectively, suggesting that silver doping increases HO• production and consequently MS2 inactivation. When nAg/TiO_2 was used with 400 mM of either alcohol, the amount of viruses removed by dark stirring was greater than that observed without added alcohol (90-98%, data not shown). The active virus titer increased after 30 seconds of irradiation compared to that before UV exposure. Since the depression of initial virus concentration was not observed with undoped P25 TiO_2, this effect is attributed to the interaction of the alcohol with the silver and the subsequent changes in viral adsorption capacity. Any increased adsorption of alcohol to silver/silver oxide as compared to TiO_2 could change the electrostatic and/or hydrophilic properties of the catalyst, resulting in changes to its adsorptive capacity. From 30 seconds to 2 minutes, the MS2 was slowly inactivated. The inactivation rate by nAg/TiO_2 was observed to be influenced by both alcohols in a concentration dependent manner, confirming the role of HO• in MS inactivation.

3.4. Conclusion

This study demonstrated that silver doping TiO_2 nanoparticles is an effective way to increase TiO_2 photocatalytic activity for virus inactivation. Silver doping enhances photocatalytic inactivation of viruses primarily by increasing HO• production, although increased virus adsorption to silver sites and leaching of antimicrobial Ag^+ also contribute to virus removal. The fast virus inactivation kinetics of the nAg/TiO_2 materials demonstrated in our study suggest that effective virus inactivation can be achieved using a small photoreactor and photocatalytic disinfection of drinking water at both point of use and municipality scales could be a potential application of the nAg/TiO_2 materials. Further research is needed to address issues such as photocatalyst fouling, impact of water quality, loss of silver, and need for catalyst regeneration to ensure the sustainability of the technology. Very importantly, the retention of the nAg/TiO_2 materials in the treatment system is critical. This can be achieved by using a hybrid photoreactor/membrane system, where the photocatalyst is retained by a membrane unit down-stream of the photoreactor and recirculated, or by applying the photocatalyst as a coating on surfaces inside a photoreactor. Because UVA is a significant component of the solar irradiation that reaches earth surface, coating transparent piping or shallow open channels with the photocatalyst at sunny locations could also be a low-cost solution to drinking water disinfection. Ag/TiO_2 may also be activated by visible light through the silver surface plasmon resonance, however it is not clear how the catalyst will behave under both UV and visible radiation [107, 113].

3.5. Acknowledgements

This work was supported by the Center for Biological and Environmental Nanotechnology at Rice University (NSF Award EEC-0647452). Laboratory work was assisted by Zoltan Krudy.

Chapter 4

Silica decorated TiO_2 for virus inactivation in drinking water – Green synthesis method and mechanisms of enhanced inactivation kinetics[2]

[2] Manuscript in preparation for submission to the journal *Environmental Science and Technology*

Michael V. Liga[†‖], Samuel J. Maguire-Boyle[‡], Huma R. Jafry[‡$], Andrew R. Barron[‡$∂]*, and Qilin Li[†‖]*

[†]Department of Civil and Environmental Engineering, [‡]Department of Chemistry, [$]Department of Mechanical Engineering and Materials Science, and [‖]the Center for Biological and Environmental Nanotechnology, Rice University, Houston, Texas 77005, USA. [∂]College of Engineering, Swansea University, Singleton Park, Swansea SA2 8PP, Wales UK.

4.1. Introduction

Much of the world lacks reliable access to safe drinking water, and even highly developed nations face serious challenges in ensuring safe water supply. A major challenge in drinking water disinfection is the presence of resistant microbial pathogens. Viruses commonly occur in drinking water sources, [16, 20], and certain types (e.g. adenoviruses, rotaviruses) are recalcitrant to several traditional and alternative disinfection techniques, such as monochloramination and UV_{254} irradiation [5, 58, 159]. While free chlorine is generally highly effective for virus inactivation, its use is limited due to the potential to form toxic disinfection byproducts (DBPs). Alternative disinfection methods that effectively inactivate viruses without significant DBP formation are greatly needed.

Titanium dioxide (TiO_2) based photocatalysis continues to gain attention as an alternative method for chemical contaminant degradation as well as for disinfection. It has been shown to be competitive with other advanced oxidation processes (AOPs) and can be combined with them for improved performance (e.g. $UV/TiO_2/H_2O_2$, $UV/TiO_2/O_3$) [160-162]. Several studies are available demonstrating the antimicrobial activity of TiO_2. The inactivation is usually attributed to oxidation by reactive oxygen species (ROS), with the best results obtained when the microorganisms are in direct contact with the catalyst [163]. However, slow reaction kinetics is a major factor limiting the application of this technology in water and wastewater disinfection. Modifications to the catalyst, such as doping or depositing metals in or on TiO_2, can improve the catalyst efficiency by increasing ROS production (Figure 3-6) or improving contaminant adsorption to the catalyst [99, 164]. For water treatment, it is important that the material

conjugated with TiO_2 also be stable and nontoxic. Silica (SiO_2) is one such material that we have identified for improving virus inactivation kinetics of TiO_2 (Appendix A).

Silica is typically used in TiO_2 photocatalysis as either a physical support or as a dopant dispersed within the TiO_2 lattice and thus affecting the fundamental properties of the material. In previous studies on silica/silicon – titania composite catalysts, improvement to the catalyst efficiency is attributed to bandgap changes, the generation of surface acid sites, and increased adsorption [93, 119-121]. In these studies Si is incorporated into the TiO_2 lattice during its synthesis using the sol-gel technique. In a previous study, we developed simple procedures to chemically (through surface doping that results in formation of Ti-O-Si bonds) and physically (through direct deposition of SiO_2 nanoparticles) modify TiO_2 nanoparticle surface. Such modifications greatly improved the photocatalytic inactivation kinetics of bacteriophage MS2, a commonly used surrogate for waterborne pathogenic viruses, by up to 300% (Appendix A). Because these synthesis procedures produce only surface deposits of SiO_2 on TiO_2, the role of SiO_2 in the photocatalytic activity of TiO_2 is hypothesized to be different from those found in SiO_2-TiO_2 materials reported in previous studies. Additionally, SiO_2 present as a physical deposit improved MS2 inactivation, suggesting that the mere presence of SiO_2 on the TiO_2 surface results in enhancement, and a chemical linkage is not required. However, it was not clear what role such surface deposits of silica played in enhancing virus inactivation kinetics.

In this study we report the synthesis of composite SiO_2-TiO_2 nanomaterials using a simple, low-cost and green process, and their efficiency for inactivating MS2 bacteriophage. The effects of SiO_2 modification on MS2 adsorption, dark inactivation,

and hydroxyl radical (HO•) production were investigated to elucidate the role of SiO_2 in photocatalytic inactivation of MS2.

4.2. Experimental methods

4.2.1. Materials and equipment

P25 Aeroxide® TiO_2 (avg. size 25 nm, 70:30 anatase:rutile, BET 50 m^2/g, referred to as P25 hereafter) obtained from Evonik Degussa Corporation (Parsippany, NJ) was used as the benchmark TiO_2 photocatalyst. Fumed silica (Aerosil®,) was obtained from Sigma-Aldrich (St. Louis, MO). According to the vendor, the primary SiO_2 particles are 14 nm in diameter with 40-60% of particles fused in branched chains of 0.1 – 0.2 μm long, and the BET surface area is 200 m^2/g. Terephthalic acid (99% purity) was obtained from Acros Organics (Geel, Belgium). Ultrapure water was generated by a Barnstead E-Pure® system (Thermo Scientific, Waltham, MA).

Bacteriophage MS2 (ATCC 15597-B1) and *E. coli* (ATCC 15597) were obtained from the ATCC (Manassas, VA**).** MS2 propagation and enumeration was carried out as described previously (Appendix A). The virus stock was purified in an ultrafiltration cell fitted with a regenerated cellulose membrane (Millipore, Billerica, MA) with a nominal molecular weight limit of 10 kDa until salt and dissolved organics were reduced by 99.99%, and a final virus titer of 1.5×10^{11} PFU/mL was reached. The pH of the ultrapure water used for washing was adjusted to 7.0 with NaOH to ensure optimal survival of MS2 during storage at 4 °C [165].

4.2.2. SiO_2-TiO_2 synthesis and characterization

SiO_2-TiO_2 nanocomposite materials were prepared using P25 and fumed silica. Three synthesis methods were evaluated. In the first two methods, SiO_2 (2.5 – 20 wt %) was attached to TiO_2 through a condensation reaction by refluxing the TiO_2-SiO_2 mixture in toluene and through physisorption by stirring the mixture in toluene. Details of the synthesis procedures and characterization of materials prepared by these two methods can be found in Appendix A. In the third method, 100 mg TiO_2 and 2.5 - 10 mg fumed silica were stirred in 40 mL DI water at ambient conditions for 24 hours. The resulting materials were vacuum filtered using 0.2 μm PTFE membranes (Cole-Parmer, Vernon Hills, IL), dried in a vacuum desiccator for 24 hours and stored at room temperature in the dark. Samples are named according to the SiO_2 weight percentage used and the reaction conditions. For example, 5%SiO_2-TiO_2-tr denotes a sample containing 5 wt% SiO_2 made by toluene reflux (-tr), while ending in –ts or –w denotes samples made by stirring in toluene (ts) or water (w).

XPS analyses were done using a PHI Quantera XPS instrument (Chanhassen, MN). The particle size, morphology and electrophoretic mobility of the nanoparticles dispersed in water were characterized by dynamic light scattering (DLS), TEM, and phase analysis light scattering (PALS), respectively. Suspensions of photocatalysts in ultrapure water (pH 5.5) were prepared immediately prior to testing using an ultrasonic processor fitted with a cup-horn operated at 100W for 15 minutes. The same protocol was followed for all experiments. For TEM analysis, the suspension was drop cast onto 300 mesh carbon coated, formvar removed copper TEM grids (Ted Pella, Redding, CA). Excess liquid was removed and the grids were allowed to dry in darkness for 3 hrs. TEM

imaging was performed on a Jeol 1230 high contrast TEM (Peabody, MA) at 120 kV and a Jeol 2100 FE-TEM at 200 kV. DLS and PALS analyses were performed using a Zen 3600 Zetasizer (Malvern Instruments, Worcestershire, UK) at 25 °C; three measurements were made for each sample.

4.2.3. Virus adsorption and dark inactivation assays

Since contaminant adsorption to the catalyst is an important factor in the photocatalytic process, adsorption and subsequent dark inactivation of MS2 to the catalysts was measured over a wide range of applied MS2 (N_a = 10^4 – 10^{10} PFU/mL) and photocatalyst concentrations (1 – 102.6 mg/L). The freshly prepared photocatalyst suspension was added to a virus suspension of known titer in unbuffered ultrapure water (pH 5.5) and stirred in the dark for 10 minutes to reach adsorption equilibrium. Dark inactivation of MS2 was determined by directly enumerating active virus titers in the suspension samples, i.e., with catalyst particles present (N_0). N_0 measures infective viruses in the aqueous phase as well as those adsorbed on the catalyst particles but still infective. MS2 adsorption to the catalyst was determined by removing the photocatalyst from the suspension via centrifugation at 10,900 G for 10 min., and enumerating virus titers in the supernatant (N_s). To determine whether the adsorbed viruses were inactivated, 3% Bacto™ beef extract (pH 9.5, Becton Dickenson and Company, Franklin Lakes, NJ) was used to release adsorbed MS2 from the photocatalyst surface [55], and the resulting suspension was analyzed for active MS2 titer before and after centrifugation.

4.2.4. Photocatalytic virus inactivation

Photocatalytic inactivation experiments were performed in a LZC-4V photoreactor (Luzchem Research Inc. Ottawa, Canada) equipped with varying numbers of UVA bulbs (8W, peak emission at 350 nm, Hitachi) to achieve desirable irradiation intensity (1.2 or 2.5 mW/cm^2). Light bulbs were placed only on the opposing sides of the reaction flask and pre-lit for stabilization before experiments. The total irradiation intensity was measured using a UV radiometer with a 350 nm NIST traceable sensor (Control Company, Friendswood, TX). A built-in stirring plate at the center of the reactor provided mixing during the experiments and an exhaust fan circulated ambient air through the reactor to provide O_2 and control the temperature (25 ± 1 °C).

In each experiment, a newly prepared photocatalyst suspension was combined in a Pyrex Erlenmeyer flask with ultrapure water (pH 5.5) and an aliquot of virus stock. The resulting 20 mL suspension had a catalyst concentration of 97.5 mg/L as TiO_2 for all experiments and a virus titer of 10^4 - 10^{10} PFU/mL. The mixture was stirred for 10 min. in the dark and sampled directly to quantify dark inactivation and post-centrifugation to quantify adsorption. The flask was then placed in the photoreactor with preset irradiation intensity, and timed samples were taken for MS2 titer measurement.

4.2.5. Reactive oxygen species (ROS) measurement

As HO• is the primary ROS responsible for photocatalytic virus inactivation by TiO_2, the effect of SiO_2 modification on HO• production was investigated. HO• was measured using terephthalic acid as the scavenger [134, 135]. The reaction mixture contained 0.1 mM terphthalic acid, 25 mg/L (as TiO_2) photocatalyst and 1 mM NaOH.

The mixture was placed in the photoreactor with 2.5 mW/cm^2 light intensity and timed samples were taken from the irradiated suspension. The samples were centrifuged at 10,900 G for 15 minutes and the supernatants were filtered through a 0.45 μm PES syringe filters (Whatman, Maidstone, UK). The fluorescent intensity of the reaction product, 2-hydroxyterepthalic acid, was measured at 424 nm in a quartz cuvette using an f-2500 fluorescence spectrophotometer (Hitachi, Tokyo, Japan) with 315 nm excitation.

4.3. Results and discussion

4.3.1. Catalyst characterization

XPS analysis was used to determine the elemental composition of the composite catalysts (Table 4-1). The Si2p spectrum clearly shows the presence of silica (SiO_2). The percentages of Si determined from XPS analysis are higher than the weight percentages used in synthesizing the materials because the modification happens only on the TiO_2 surface.

Table 4-1 - Elemental composition of catalyst materials based on XPS analyses.

Material	Atomic Percentages			Mass Percentages	
	Ti	O	Si	Si	SiO_2
P25 TiO_2	32.1%	67.9%	0.0%	0.0%	0.0%
2.5% SiO_2-TiO_2-ts	26.7%	69.0%	4.3%	4.8%	10.3%
2.5% SiO_2-TiO_2-tr	26.0%	69.7%	4.3%	4.9%	10.4%
2.5% SiO_2-TiO_2-w	25.4%	72.2%	2.5%	2.8%	6.0%
5% SiO_2-TiO_2-w	23.8%	69.9%	6.4%	7.4%	15.8%
7% SiO_2-TiO_2-w	23.6%	69.6%	7.0%	8.0%	17.1%
10% SiO_2-TiO_2-w	24.2%	68.8%	7.1%	8.1%	17.3%
Silica	0.0%	68.2%	31.9%	45.1%	96.4%

Figure 4-1 presents TEM images of the varoius composite materials synthesized in this study as well as the fume silica particles used (Figure 4-1 A). High resolution (HR)-TEM analysis of the 2.5%SiO_2-TiO_2-tr material shows small SiO_2 islands deposited on the surface of the P25 (Figure 4-1 B). This synthesis method forms Si-O-Ti bonds at the SiO_2/TiO_2 interface (Appendix A). The HC-TEM images of SiO_2-TiO_2 prepared in water (Figure 4-1 C-D) reveal silica particles/clusters attached to TiO_2. This is in contrast with the –toluene samples, where no silica particles were apparent (Appendix A).

Dispersion of catalyst particles in water is an important factor in photocatalytic processes for water treatment as it determines the surface area available for contaminant adsorption. Modification with SiO_2 by mixing in water significantly reduced the dispersitivity of the catalyst particles in water. The number mean particle hydrodynamic diameter of materials increased from 117 nm to 177 - 913 nm depending on the percentage of SiO_2 added (Figure 4-2 A). This is attributed to the attachment of silica particles/aggregates as well as heteroaggregation induced by SiO_2. As shown in Figure 4-2 B, SiO_2 and TiO_2 are oppositely charged at the pH tested; simultaneous hetero- (between TiO_2 and SiO_2) and homo- (TiO_2-TiO_2 and SiO_2-SiO_2) aggregation leads to complex behaviors in particles size and electrophoretic mobility of the SiO_2-TiO_2 materials.

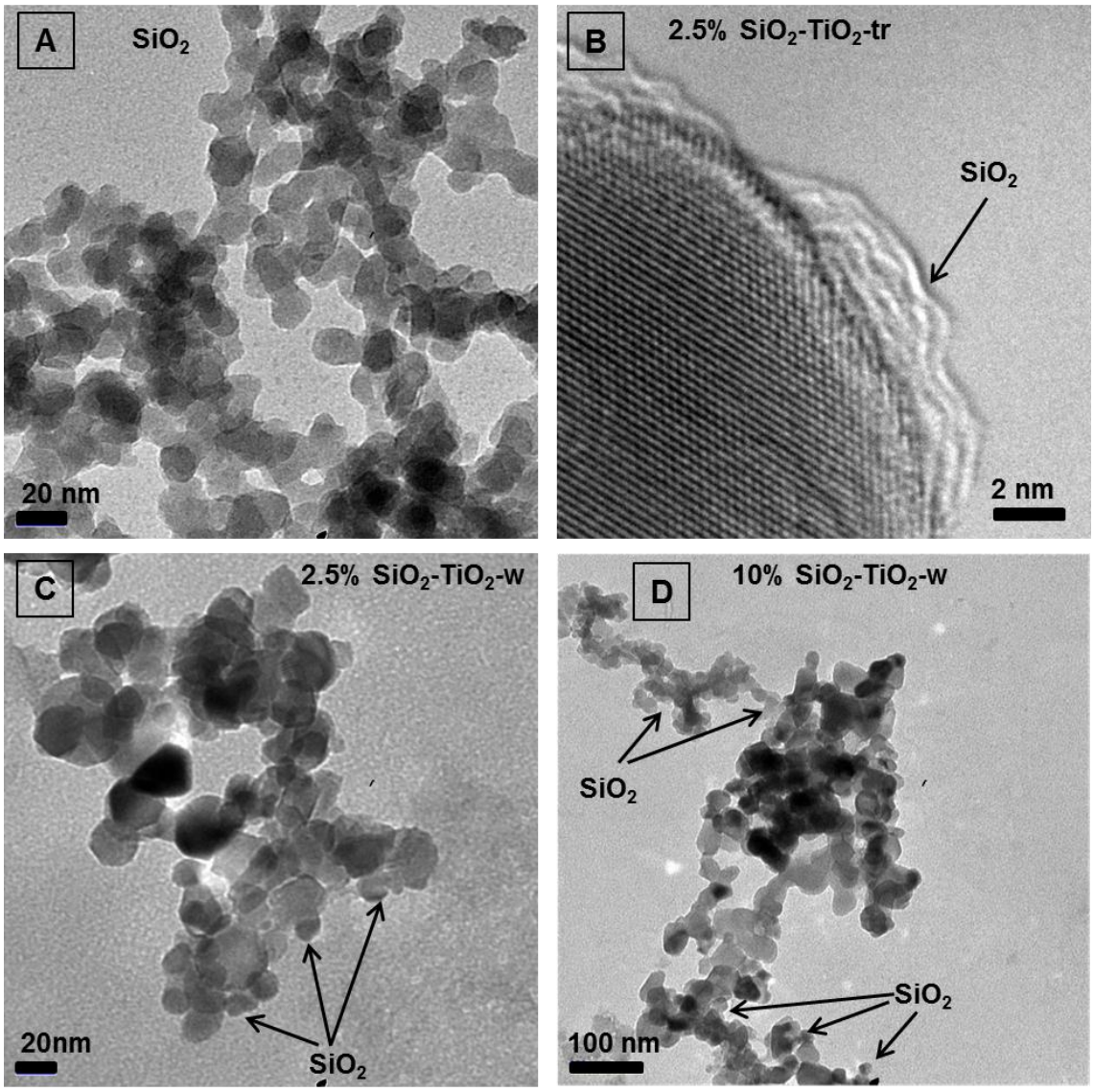

Figure 4-1 - (A) HC-TEM image of fumed silica particles. (B) HR-TEM image of 2.5% SiO_2-TiO_2-tr shows small islands of SiO_2 present on the particle surface. (C-D) HC-TEM images of SiO_2-TiO_2-w materials showing silica present as individual particles and aggregates attached to TiO_2 particles.

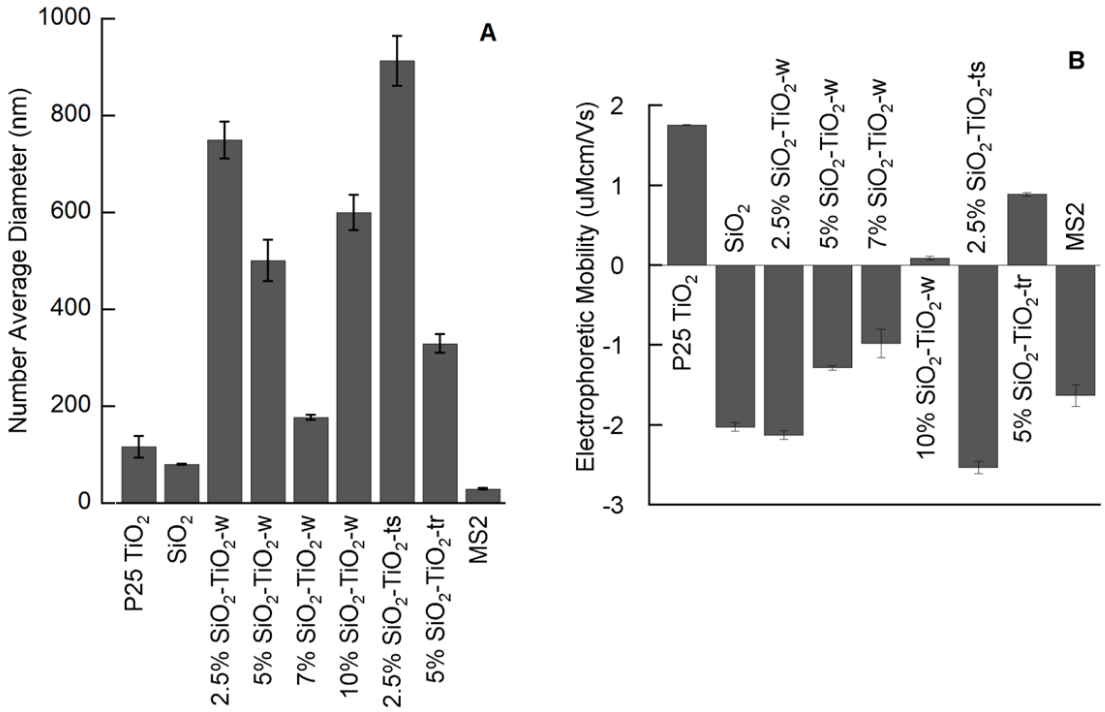

Figure 4-2 - (A) Average particle diameters of nanomaterials and MS2 in ultrapure water at pH 5.5 and (B) electrophoretic mobilities of nanomaterials and MS2 in 1 mM NaCl at pH 5.5.

4.3.2. Photocatalytic inactivation of MS2 by SiO_2-TiO_2 materials prepared by different methods

The dark and photocatalytic MS2 inactivation efficiencies of the SiO_2-TiO_2 photocatalysts made by the three different methods were evaluated using non-purified MS2. Dark inactivation by all three types of SiO_2-TiO_2 materials was improved to a similar degree compared to unmodified P25 (N_0/N_a = 0.31-0.57 vs. 0.88) (Figure 4-3). With UVA, all SiO_2-TiO_2 materials exhibited significantly enhanced photocatalytic MS2 inactivation (Figure 4-4). The optimum content of SiO_2 used during the synthesis of

SiO_2-TiO_2-tr is 5% (Figure 4-5). Both the 2.5% and 5% SiO_2-TiO_2-w samples outperform those made using toluene. This may be partly due to better dispersion of TiO_2 in water versus toluene, which results in more even distribution of SiO_2 on TiO_2 particles. The water synthesis procedure is attractive as it requires little energy input and neither uses nor produces hazardous compounds.

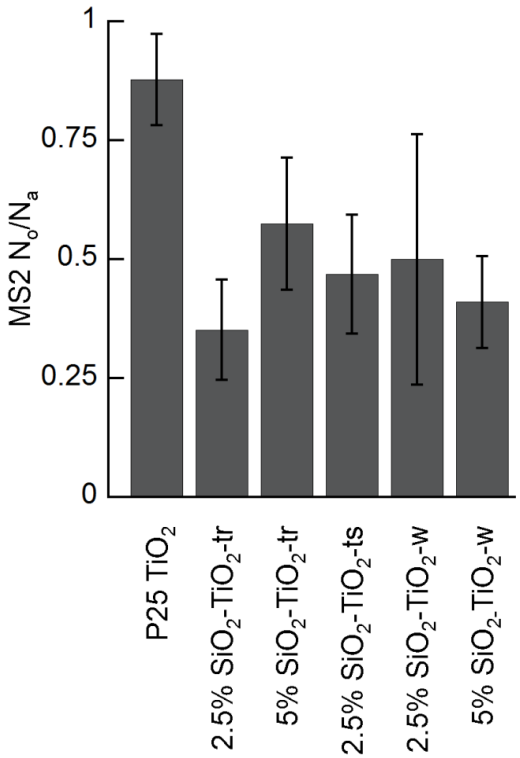

Figure 4-3 - Inactivation of MS2 in the dark by nanomaterials. Virus stock used is not purified of dissolved salts and organic compounds.

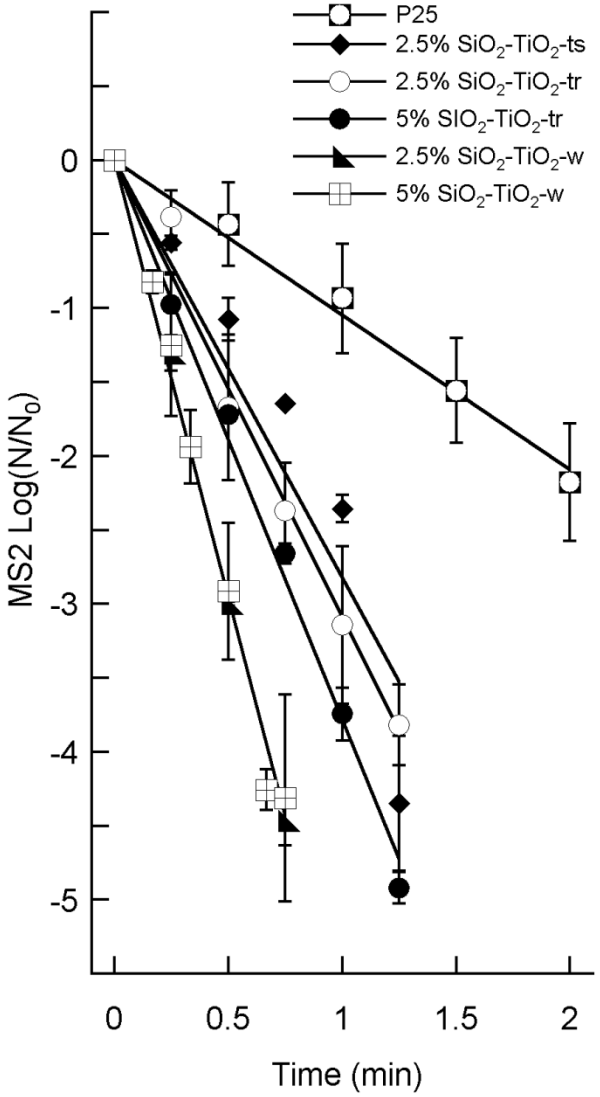

Figure 4-4 - Photocatalytic inactivation of unpurified MS2 . The applied MS2 concentration (N_a) was 3 x10^7 PFU/mL; N_0 is the active titer (PFU/mL) mesured with particles in suspension after dark stirring; UV-A irradiance was 2.5 mW/cm^2.

It is noted that impurities in the virus suspension significantly reduce adsorption and slow the photocatalytic inactivation kinetics of MS2. At an applied MS2 concentration of 10^7 PFU/mL, the pseudo first order rate constant *k'* (Eq. 1) and adsorptive removal are an order of magnitude lower than the values obtained using purified viruses (Table 4-2). All data discussed hereafter were obtained using purified MS2.

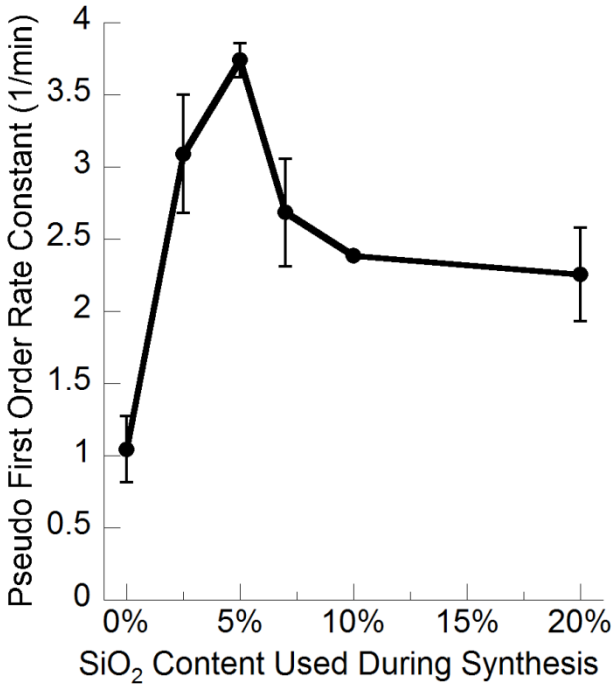

Figure 4-5 - Values of the pseudo first order rate constants produced by TiO_2-SiO_2-tr materials synthesized using different amounts of SiO_2. 5% SiO_2 is the optimum content. Data obtained using 2 x 10^7 PFU/mL MS2 (unpurified) and 2.5 mW/cm^2 UVA irradiation.

Table 4-2 - Survival ratio of MS2 in the supernatant after dark stirring and the corresponding pseudo first order rate constant, *k'*, of the irradiated suspensions. N_s is virus titer in solution supernatant. N_a is applied virus titer.

	P25 TiO_2		5%SiO_2-TiO_2-w	
Applied [MS2] PFU/mL	Adsorption -Log (N_s/N_a)	k' (sec^{-1})	Adsorption -Log (N_s/N_a)	k' (sec^{-1})
$(1.9 \pm 0.9) \times 10^4$	2.3	0.20 ± 0.01		
$(1.4 \pm 0.4) \times 10^5$	2.3	0.17 ± 0.04		
$(2.0 \pm 1.0) \times 10^6$	2.3	0.22 ± 0.05	6.5	0.92
$(2.8 \pm 0.4) \times 10^7$	1.7 ± 0.21	0.24 ± 0.01	7.4	0.69 ± 0.23
$(2.6 \pm 0.7) \times 10^8$	1.5 ± 017	0.14 ± 0.01	6.3 ± 2.3	0.39 ± 0.11
$(2.8 \pm 1.4) \times 10^9$	0.055 ± 0.037	0.022 ± 0.01	0.91 ± 0.34	0.062 ± 0.006
$(3.7 \pm 0.7) \times 10^7$ unpurified*	0.16 ± 0.14	0.015 ± 0.006	1.1	0.098 ± 0.011

*data obtained using unpurified MS2 stock and reactor irradiance of 2.5 mW/cm^2. All other data obtained using ultrafiltration purified MS2 stock and reactor irradiance of 1.2 mW/cm^2.

4.3.3. SiO_2-TiO_2-w catalysts show enhanced virus adsorption and dark and photocatalytic inactivation

Figure 4-6 A compares the dark inactivation and adsorption of purified MS2 by P25 and the SiO_2-TiO_2-w catalysts with different SiO_2 content. The SiO_2-TiO_2-w catalysts showed a large increase in adsorption and dark inactivation of MS2 compared to P25, by up to 623 and 745% for adsorption and dark inactivation, respectively. A large fraction of MS2 adsorbed on the SiO_2-TiO_2-w catalysts was not inactivated. The increased adsorption cannot be explained by changes in catalyst surface area or bulk electrostatic interaction as both SiO_2 and MS2 are negatively charged at the pH tested. Although the silica nanoparticles have a greater specific surface area (200 ± 25 m^2/g), its contribution to surface area increase (30% with 10% SiO_2) cannot account for the large increase in adsorption. Moreover, all SiO_2-TiO_2-w catalysts have larger aggregate sizes

and hence less accessible surface area than P25 in the test solution (Figure 4-2 A). More discussion on adsorption is provided later.

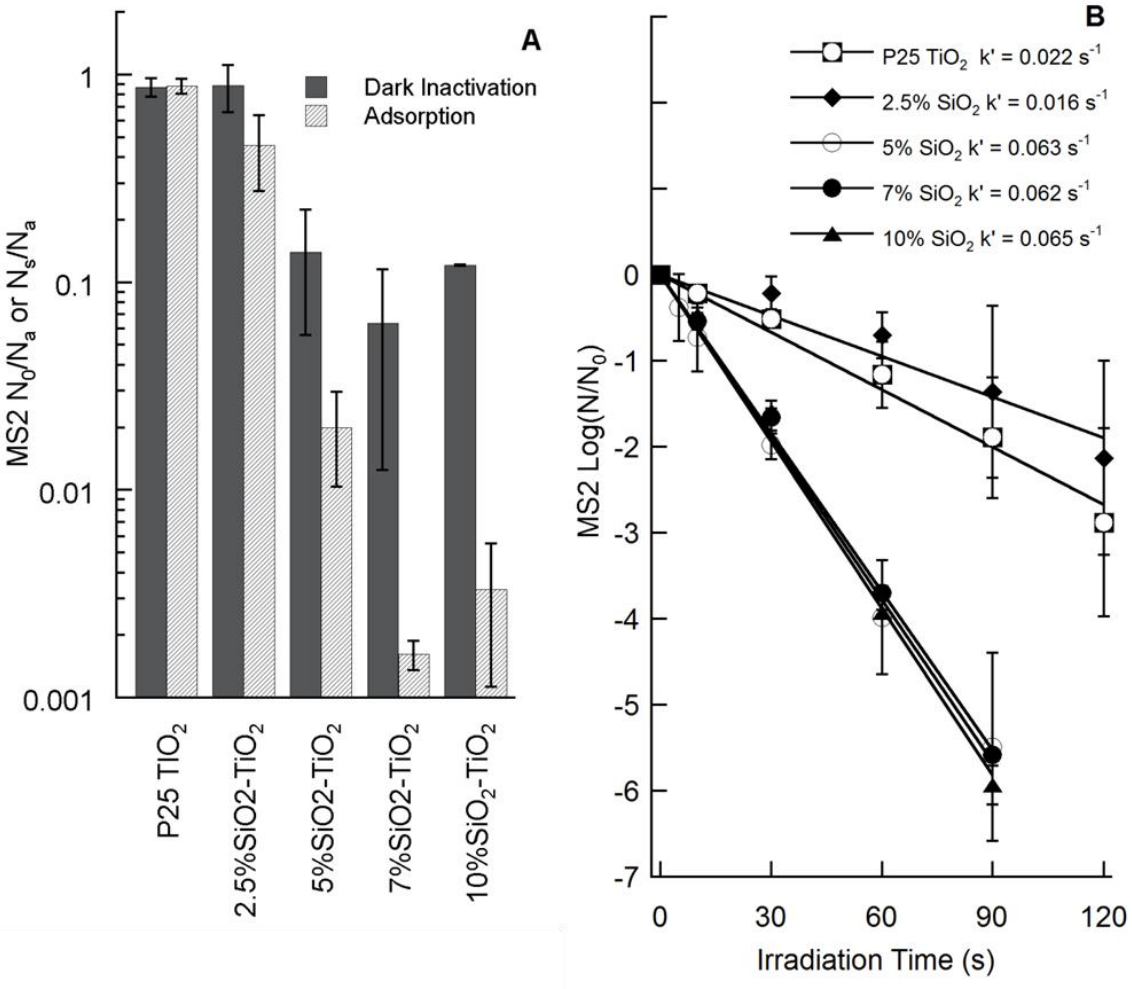

Figure 4-6 - Comparison of MS2 dark inactivation and adsorption (A) and photocatalytic inactivation (B) by P25 and SiO_2-TiO_2-w catalysts. Applied MS2 concentration N_a = 1-2 x 10^9 PFU/mL. Catalyst dosage = 97.5 mg/L as TiO_2, Light intensity = 1.2 mW/cm^2.

When added at 5-10%, SiO_2 greatly improved the photocatalytic inactivation kinetics of MS2, (Figure 4-6 B). It is noted that SiO_2 alone did not inactivate MS2 either

in the presence or absence of UV light (data not shown). Therefore, these results suggest that the presence of SiO_2 improves the photocatalytic MS2 inactivation activity by TiO_2. A lower SiO_2 content of 2.5%, however, showed decreased MS2 inactivation kinetics compared to P25 under these conditions. This is in contrast to the results obtained using unpurified viruses at an initial titer of 3 x 10^7 PFU/mL, where 2.5% Si improved the kinetics, a discrepancy that may be due to differences in initial virus titer and hence the impact of adsorption.

Photocatalytic inactivation kinetics of MS2 by both the P25 and the SiO_2-TiO_2-w materials can be well described by the Chick-Watson model (Equation 4-1):

Equation 4-1

$$Log\left({}^{N}/_{N_0}\right) = -k't$$

Here N_0 is the active titer of viruses in solution (including those adsorbed) after dark stirring, N is the active titer at time t, and k' is the pseudo first order rate constant (s^{-1}). The rate constant for 7%SiO_2-TiO_2-w is 270% of that for P25 (0.062 vs. 0.022 s^{-1}). This is comparable to the improvement achieved using SiO_2-TiO_2 catalysts prepared in toluene (Appendix A).

Photocatalytic inactivation kinetics of microorganisms is largely determined by adsorption of the microorganisms on the photocatalyst surface and the rate of ROS production [163]. HO• is considered the main ROS responsible for inactivation of MS2 by TiO_2, as shown in Figure 3-6 and by [74]. Figure 4-7 compares HO• production by

P25 TiO_2 and two SiO_2-TiO_2-w samples with 2.5 and 5% SiO_2. Surprisingly, the presence of SiO_2 at 5 and 2.5% actually reduced HO• production by a factor of 1.6 and 2.1 respectively. It suggests that this SiO_2 modification method does not enhance charge separation or improve oxidation/reduction at the catalyst surface, as is hypothesized when SiO_2 is incorporated into the TiO_2 lattice [93, 121]. It is likely that deposits of SiO_2 on the TiO_2 surface block migration of electrons/holes to the surface, and hence reduce HO• production. With the 2.5%SiO_2-TiO_2-w, the reduction in HO• production outweighs the effect of increased MS2 adsorption, resulting in decreased MS2 photocatalytic inactivation kinetics (Figure 4-6 B). At higher SiO_2 content, the effect of MS2 adsorption becomes more prominent, leading to higher photocatalytic efficiency toward MS2 inactivation.

It is hypothesized that the silica outcroppings observed in the TEM images (Figure 4-1) may serve as favorable adsorption sites for MS2 adsorption, which brings virus particles within close proximity to high HO• concentration and hence improves photocatalytic virus inactivation.

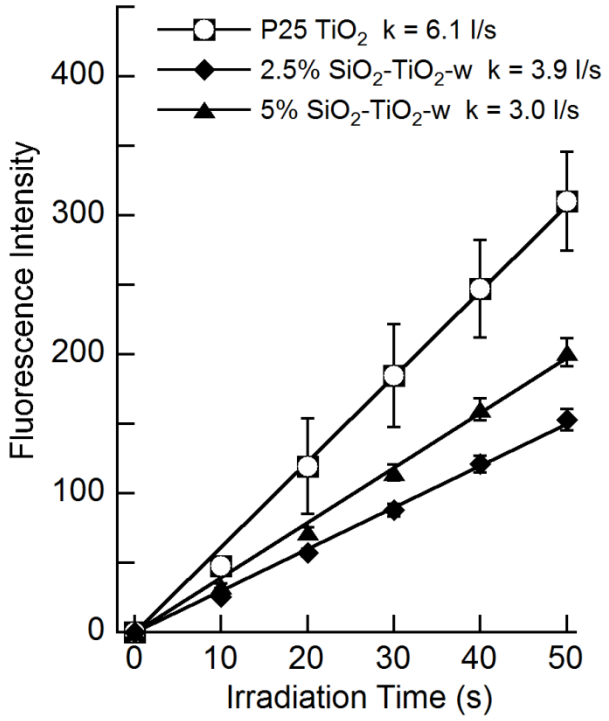

Figure 4-7 - Hydroxyl free radical production monitored by formation of fluorescent 2-hydroxyterephthalic acid.

4.3.4. MS2 adsorption on P25 and SiO_2-TiO_2-w

Considering the importance of adsorption to photocatalytic inactivation of MS2, the adsorptive properties of the SiO_2-TiO_2-w catalysts and the base P25 TiO_2 were further characterized. Varying concentrations of MS2 and catalysts were stirred together in the dark to achieve adsorption equilibrium and sampled both with particles in suspension to determine dark inactivation, and after centrifugal removal of the catalyst to determine the amount of MS2 adsorbed. To help understand the role of adsorption in dark inactivation, 3% beef extract (pH 9.5) was used to desorb MS2 from the catalyst before re-measuring the titer.

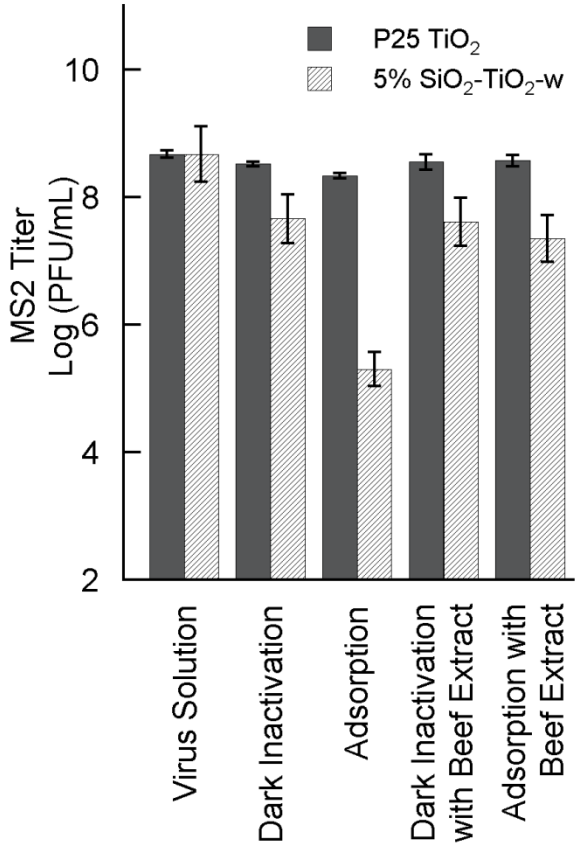

Figure 4-8 - Dark inactivation and adsorption of MS2 (N_a = 4.7 x 10^8 PFU/mL) by P25 TiO_2 and 5%SiO_2-TiO_2-w. Catalyst dosage = 20 mg/L as TiO_2.

Figure 4-8 shows that 5%SiO_2-TiO_2-w achieved 1 log MS2 inactivation in dark, while there was negligible dark inactivation by P25. After centrifugation, the titer of MS2 exposed to 5%SiO_2-TiO_2-w decreased by another 2 log, while the virus exposed to P25 only showed a 0.2 log additional removal. This indicates that silica modification greatly increases the virus adsorptive capacity of the catalyst, and a significant fraction of the adsorbed MS2 is inactivated. The mechanism of such dark inactivation is unclear. Control experiments using fumed silica alone showed no loss of active titer before and

after centrifugation (data not shown), suggesting that contact with SiO_2 alone does not account for the dark inactivation observed.

When beef extract was applied to a pre-stirred suspension of catalyst and viruses, there was no difference in titer when particles were in suspension or removed by centrifugation, indicating that all the active viruses were desorbed from the catalyst. The active titer measured after beef extract treatment was also the same as that determined in the presence of the catalyst without the beef extract, suggesting that the dark inactivation was irreversible and due to true inactivation of the viruses and not due to catalyst particles physically blocking viruses from contacting with host cells. It is possible that the SiO_2 (negatively charged) and TiO_2 (positively charged) interface creates favorable adsorption sites for MS2 due to the charge heterogeneity of MS2 protein capsid [154]; strong adsorption at these interfaces leads to irreversible changes in MS2 capsid conformation that prevents host infection [166]. There was a larger fraction of MS2 whose infectivity was not affected by adsorption as indicated by the large difference between the active titers before and after removal of the SiO_2-TiO_2 catalyst as well as the active titer measured after application of the beef extract. These results suggest that the SiO_2-TiO_2-w catalysts contain both high and low affinity adsorption sites. The high levels of virus adsorption and inactivation resulting from exposure to SiO_2-TiO_2-w makes this material a good candidate for disinfection in the absence of irradiation.

Because adsorption plays such an important role in the photocatalytic inactivation of MS2, MS2 adsorption isotherm experiments were performed to further investigate MS2 adsorption behaviors of the photocatalysts. The results are presented in Figure 4-9. Since the MS2 concentration applied ranged over 7 orders of magnitude, the data was fit

with isotherm models by minimizing the weighted least square (Equation 4-2), where *Weighted* SS_{resid} is the sum of weighted residual squares, y_n is the measured value, and y_{calc} is the model calculated value [167, 168]. Among the isotherm models tested, the data fit the best with the Langmuir model (Equation 4-3) for both P25 and SiO2-TiO_2-w samples (Figure 4-9).

Equation 4-2

$$Weighted\ SS_{resid} = \sum_{n=1}^{N} \frac{1}{y_n^{\,2}} (y_n - y_{calc})^2$$

Equation 4-3

$$q_{eq} = q_{\max} \frac{KN_s}{1 + KN_s} \quad .$$

Here, K is the Langmuir adsorption constant (mL/PFU), N_s the active titer in the aqueous phase at equilibrium (PFU/mL), q_{eq} the equilibrium adsorption density (PFU/g), and q_{max} the maximum adsorption density (PFU/g). The adsorption isotherms clearly show adsorption saturation for both catalysts at high MS2 concentrations. To our knowledge, this is the first demonstration of MS2 adsorption on TiO_2 following the Langmuir isotherm. Koizumi and Taya (2002) reported a power function relationship between MS2 q_{eq} on P25 and the total number of viruses in the system for $10^2 – 10^6$ PFU/mL, and developed an adsorption model based on the Freundlich isotherm [25]. In our study, the Freundlich isotherm (data not shown) fits the data well at low N_s, but could not adequately model the saturation at high N_s. Adsorption of MS2 to activated carbon

has previously been found to follow the Langmuir (Equation 4-3) and Freundlich (Equation 2-3) isotherms [169].

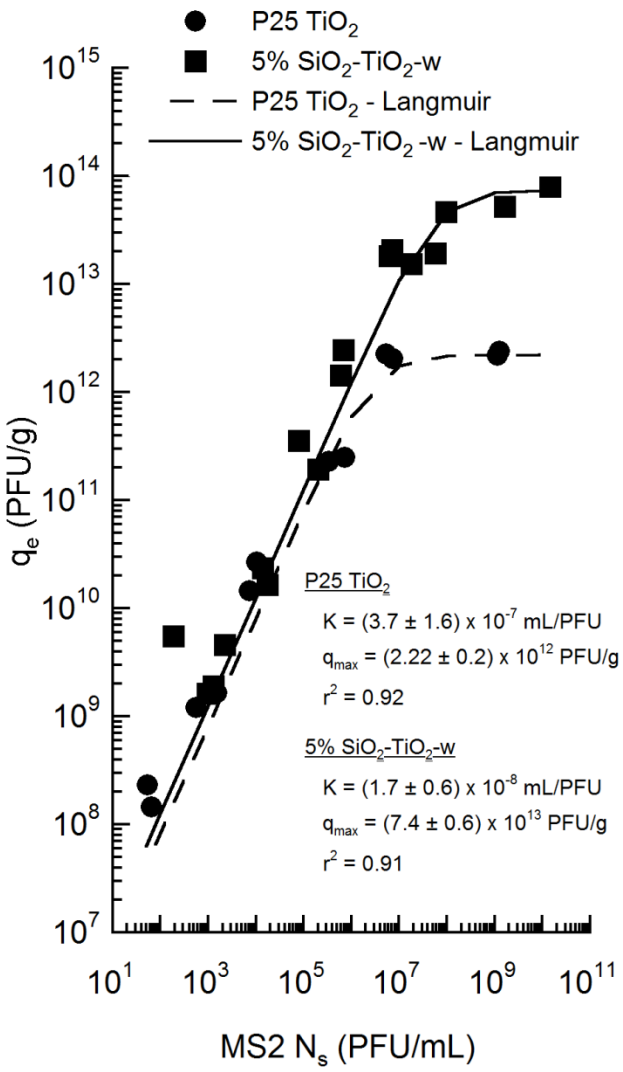

Figure 4-9 - Adsorption isotherms and Langmuir model fits for MS2 adsorption by P25 TiO_2 and 5% SiO_2-TiO_2-w. For P25 TiO_2 K = (3.7 ± 1.6) x 10^{-7} mL/PFU, q_{max} = (2.22 ± 0.2) x 10^{12} PFU/g, r^2 = 0.92. For 5% SiO_2-TiO_2 K = (1.7 ± 1.6) x 10^{-8} mL/PFU, q_{max} = (7.40 ± 0.2) x 10^{13} PFU/g, r^2 = 0.91. The maximum adsorption density of the Among the isotherm models tested, the data fit the best with the Langmuir model (Equation 4-3) for both P25 and SiO_2-TiO_2-w samples (Figure 4-9):

Figure 4-9 reveals that the 5% SiO_2-TiO_2-w has a maximum adsorption density ([7.4 ± 0.6] x 10^{13}) 37 times that of P25 ([2.2 ± 0.2] x 10^{12} PFU/g), although its adsorption affinity is lower (K = [1.7 ± 0.6] x 10^{-8} vs. [3.7 ± 1.6] x 10^{-7} mL/PFU), consistent with the overall electrostatic repulsion between MS2 and SiO_2. The net effect is an increase in adsorption, especially at high MS2 concentrations. The mechanism responsible for the increased adsorption is unknown and is the subject of further study.

4.3.5. Photocatalytic reaction kinetics and effect of initial viral concentration

Since the viral load may fluctuate greatly in drinking water sources, it is important to understand how photocatalytic treatment systems respond to changes in virus concentration. However, no photocatalytic inactivation kinetic data has been published for virus concentrations varied over several orders of magnitude, as may occur in natural waters. Previous studies typically model photocatalytic inactivation of viruses by TiO_2 using pseudo-first order kinetics (e.g., Chick-Watson) models (Equation 4-1) [70, 80, 81] based on either the aqueous phase or aqueous + adsorbed concentration of viruses without considering the adsorption quantity. Koizumi and Taya (2002) developed equations for MS2 photocatalytic inactivation rate and pseudo first order rate constant as a function of the concentration and adsorption of the virus to the catalyst based on a Freundlich isotherm, although they did not publish any data to support their model [25].

The Langmuir-Hinshelwood (L-H) model (Equation 4-4) considers photocatalytic reactions of contaminants adsorbed on the catalyst surface following a Langmuir isotherm, and is commonly used to model photocatalytic degradation of chemical

contaminants [82, 83]. In addition to determining its suitability as a model for photocatalytic virus inactivation, the L-H model was used in our study to investigate the relative contribution of adsorption and photocatalytic reaction to the overall virus inactivation at various initial concentrations. The initial photocatalytic inactivation rate was calculated using data obtained within the first 2-10 seconds of irradiation. The L-H model (Equation 4-4) was used to fit the data using the weighed least squares method (Equation 4-2), where r is the initial reaction rate (PFU/ g^{-1}-s^{-1}), k is the inherent reaction rate constant (sec^{-1}), and the other parameters as defined in Equation 4-3. The K values used for fitting the L-H equation to the data were those determined for the Langmuir isotherm fitting (Figure 4-9).

Equation 4-4

$$r = q_{\max} \frac{kKN_s}{1 + KN_s}$$

As shown in Figure 4-10, both catalysts display saturation kinetics, consistent with the Langmuir adsorption isotherm (Figure 4-9). The data obtained with P25 conforms reasonably to the L-H model over the entire concentration range tested. The data obtained with 5%SiO_2-TiO_2-w is skewed greatly at low N_s due to (nearly) complete adsorption. The three lowest N_s were excluded from the model fitting. These results suggest that photocatalytic inactivation of MS2 primarily occurs on the catalyst surface. The intrinsic reaction rate constant k is lower for 5%SiO_2-TiO_2 (0.043 ± 0.007) than P25 (0.15 ± 0.03 s^{-1}). This is consistent with the reduced production of HO• (Figure 4-7) as ROS production is the main factor determining k.

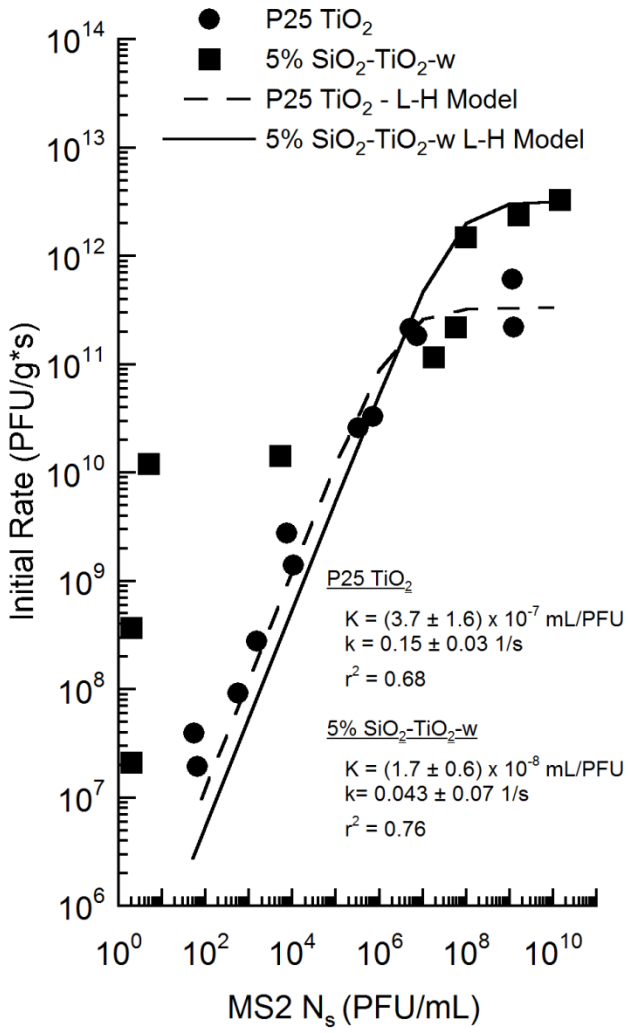

Figure 4-10 - Initial MS2 inactivation rate as a function of virus concentration in solution can be described by the Langmuir-Hinshelwood model. For P25 TiO_2 K = (3.7 ± 1.6) x 10^{-7} mL/PFU, k = 0.15 ± 0.03 s^{-1}, r^2 = 0.68. For 5%SiO_2-TiO_2 K = (1.7 ± 1.6) x 10^{-8} mL/PFU, k = 0.043 ± 0.09 s^{-1} r^2 = 0.76. [catalyst] = 97.5 mg/L as TiO_2, Light intensity = 1.2 mW/cm^2.

The initial inactivation rate by 5%SiO_2-TiO_2, however, is notably higher over the whole concentration range tested, showing the important role of adsorption on MS2 photocatalytic inactivation. The maximum initial reaction rate is an order of magnitude

higher for 5%SiO_2-TiO_2 than P25 TiO_2 (3.2×10^{12} vs. 3.3×10^{11} PFU/g), consistent with the high q_{max} of 5%SiO_2-TiO_2. This shows that increasing contaminant adsorption to the catalyst is equally, if not more, effective for enhancing photocatalytic treatment as compared to improving catalyst reactivity. Strategies for increasing contaminant adsorption to catalysts should be developed further. A catalyst with both improved absorptive and reactive properties would greatly improve the viability of photocatalytic oxidation as a water treatment option.

The MS2 inactivation data obtained over different MS2 concentrations revealed that the pseudo first order rate constant *k'* is not a good parameter for evaluating photocatalysts as it is only constant within a limited contaminant concentration range, i.e., the linear range of the Langmuir adsorption isotherm. This concentration range changes with catalyst type and dosage. For 97.5 mg/L P25 TiO_2, *k'* is constant for initial MS2 concentrations of 10^4-10^8 PFU/mL. At 10^9 PFU/mL, *k'* becomes more than an order of magnitude lower (Table 4-2), which corresponds to the plateau predicted by the Langmuir adsorption isotherm and the L-H model (Figure 4-9 and Figure 4-10) due to adsorption saturation. The effects of virus concentration on the reaction kinetics also makes it difficult to compare results reported in different studies, where virus concentration may differ along with catalyst particle size, solution conditions, etc. A robust virus inactivation kinetic model is needed.

The large and abrupt drop in reaction kinetics at high virus concentrations poses a challenge for the design and operation of photocatalytic treatment systems. Spikes in virus (or other contaminant) loadings in source water could overwhelm the treatment system, resulting in inadequately treated water. Photocatalytic UV reactor validation

protocols need to be developed to account for the effect of catalyst surface saturation and water constituents.

4.4. Acknowledgements

This work was supported by the US Navy (contract N61331-08-G0001), Center for Biological and Environmental Nanotechnology at Rice University (NSF Award EEC-0647452), the Robert A. Welch Foundation, and the University of Wales through the Prince of Wales Visiting Innovator Program (A.R.B). We thank Professor Benito Mariñas of the University of Illinois at Urbana-Champaign for advice on virus purification before experimentation, and Xiaolei Qu at Rice University for the XPS analysis.

Chapter 5

Kinetics of Human Adenovirus Disinfection by Titanium Dioxide Nanoparticles for Drinking Water Treatment[3]

[3] Manuscript in preparation for submission to the journal *Water Research*

Michael V. Liga and Qilin Li*

Department of Civil and Environmental Engineering, Rice University, 6100 Main St., Houston, TX 77005, United States

Key Words: Drinking Water, TiO_2, Photocatalysis, Adenovirus, Disinfection

5.1. Introduction

The increased regulation of disinfection byproducts (DBPs) in drinking water has caused new issues in water quality and safety. Specifically, utilities increasingly rely on alternative disinfection technologies that are less prone to form DBPs (e.g. UV_{254}, chloramines); however, some viruses are highly resistant to these methods. Adenoviruses in particular have become a concern, as they require a high (186 mJ/cm_2) UV_{254} fluence for 4-log_{10} inactivation credit [2] and are poorly inactivated by monochloramine [5, 57, 58].

Adenovirses are large (~90 nm), relatively complex dsDNA viruses that cause wide ranging symptoms depending on the serotype present. They contain 13 different protein types, with the receptor protein (fibre) being present in 12 copies, which provides a level of redundancy in infection capability in the event of minor capsid damage [30]. In contrast, a common surrogate virus in water disinfection studies, bacteriophage MS2, is a small (~25 nm), relatively simple ssRNA virus that contains only 2 protein types and only one copy of the infective (A) protein [33].

Studies of adenovirus disinfection in drinking water reveal that disinfectants causing damage to the viral proteins leads to more efficient inactivation. Free chlorine, which is highly effective but suffers from DBP formation, damages proteins responsible for governing early lifecycle events after the virus infects a cell [12]. Monochloramine is much less effective than free chlorine. Although it is not clear if monochlaramine primarily inactivates adenoviruses by causing protein or genetic damage [4], the oxidation potential of monochloramine is less than free chlorine, which may reduce its

ability to damage proteins. Polychromatic MP UV irradiation damages adenoviral proteins, and is much more efficient than UV_{254}, which only damages the viral genome [10]. Ozone is also highly effective against adenovirus and causes severe damage to the virus capsid [11, 13]. Since disinfectants which oxidatively damage adenoviral proteins are the most effective, photocatalytic oxidation may be a useful method for inactivating adenoviruses in drinking water. However, there are no published studies investigating this possibility for adenovirus.

Titanium dioxide (TiO_2) based photocatalysis is an attractive process for application to drinking water treatment since TiO_2 is stable and non-toxic when ingested [68] and generates highly reactive hydroxyl radicals (HO•) [72]. HO• is primarily responsible for the inactivation of MS2 by TiO_2, as shown in Figure 3-6 and by [70, 74]. Inactivation is most efficient when the solution conditions promote adsorption of the virus to the catalyst [25, 81], where the concentration of HO• is highest. Since TiO_2 is activated with UV irradiation, it has the potential to be used in combination with UV disinfection methods to improve the virus inactivation kinetics. Solar irradiation may be used to activate TiO_2 as well since it partially consists of UV-A irradiation, and catalyst modifications can be made to shift the TiO_2 adsorption spectra to the visible range to improve reactivity under sunlight [90, 170].

In this study the effectiveness of TiO_2 photocatalytic oxidation against human adenovirus serotype 2 is investigated. Several parameters affecting the reaction kinetics which are important to consider in designing a treatment system, such as light intensity, catalyst concentration, and virus adsorption quantity, are studied herein. The resulting

kinetics are modeled and compared to those obtained when inactivating bacteriophage MS2.

5.2. Materials and methods

5.2.1. Materials

P25 Aeroxide® TiO_2 (avg. size 25 nm, 70:30 anatase:rutile, BET 50 m^2/g, referred to as P25 TiO_2 hereafter) obtained from Evonik Degussa Corporation (Parsippany, NJ) was used as the TiO_2 photocatalyst. P25 was suspended in unbuffered ultrapure water (pH 5.5) and dispersed using an ultrasonic processor fitted with a cuphorn operated at 100W for 15 minutes immediately prior to all experiments. Ultrapure water was generated by a MilliQ Direct 3 (Millipore, Billerica, MA) fitted with a Biopack filter for pyrogen removal. All glassware and reusable materials for tissue culture work were depyrogenated either by heating at 190 °C overnight or soaking in 0.5 M HNO_3 overnight followed by rinsing in pyrogen-free water. All items used in the propagation, assay, and testing of the viruses was purchased sterile or sterilized by autoclave or 0.22 μm PES membrane filters (Millipore).

5.2.2. Virus propagation, purification, and assay.

The procedures used for virus propagation and assay were taken from multiple sources [52, 171-173]. Human adenovirus serotype 2 (AdV2) (ATCC VR-186) and A549 human lung carcinoma cells (ATCC CCL-185) were obtained from the ATCC (Manassas, VA). A549 cells were grown in Ham's F-12k medium (Sigma Aldrich, St. Louis, MO) supplemented with 10% FBS (Hyclone, Logan, UT), 100,000 units/L

penicillin (Sigma Aldrich), 10 mg/L streptomycin (Sigma Aldrich), 0.25 mg/L Amphotericin B (Sigma Aldrich), and 2.5 g/L $NaHCO_3$. Cells were propagated by seedeing at 8 x 10^3 cells/cm^2 in T75 flasks, incubating at 37 °C in humidified air containing 5% CO_2, and subculturing every 3 days. Cells were received at passage 82 and not used beyond passage 97. T75 flasks were used for virus propagation and T25 flasks were used for plaque assays after being seeded at 1.4 x 10^4 cells/cm^2 and incubating 40 hours, when monolayers were approximately 80% confluent.

AdV2 were propagated by inoculating DPBS rinsed monolayers with viruses in 2 mL serum free F-12k at an MOI of 200 and incubating for 90 minutes, with flasks being rocked at 15 minute intervals. The inoculate was withdrawn and infected cells were incubated in F-12k containing 2% FBS, 100,000 units/L penicillin, 10 mg/L streptomycin, 0.25 mg/L Amphotericin B, and 2.5 g/L $NaHCO_3$for 3 days, when cytopathic effect was complete. The flasks were subject to two cycles of freeze-thaw and the fluids recovered and centrifuged at 170 G for 10 minutes to remove large cellular debris. The supernatant was then passed through a 0.45 micron pore size PES syringe filter to further remove cellular debris and virus aggregates. The virus solution was then purified of dissolved salts and organics by washing with 1mM $NaHCO_3$ in an ultrafiltration cell fitted with a 100 kDa nominal molecular weight limit regenerated cellulose acetate membrane (Millipore) until 99.999% removal was achieved. The final virus solution contained 2 x 10^9 PFU/mL and was aliquoted and stored at -80 °C. Virus plaque assays were conducted by inoculating DPBS rinsed monolayers with virus samples in 200 or 800 microliters serum-free F-12k media containing 1.5 g/L $NaHCO_3$ for 90 minutes, with flasks being rocked at 10-15 minute intervals. The inoculates were

withdrawn and the monolayers overlaid with F-12k medium supplemented with 2% FBS, 50,000 units/L penicillin, 5 mg/L streptomycin, 0.25 mg/L Amphotericin B, 25 mM $MgCl_2$, 1.5 % Bacto™ Agar (Becton Dickenson and Company, Franklin Lakes, NJ) and 2.5 g/L $NaHCO_3$ at 45 °C. Flasks were given 15 minutes for the media to solidify before being inverted and incubated for 7 days at 37 °C in humidified air containing 5% CO_2. The monolayers were then stained for 2 hours with 5 mg/mL thiazolyl blue tetrazolium (MTT, Sigma Aldrich) [171] and virus plaques counted.

Bacteriophage MS2 (ATCC 15597-B1) and *E. coli* (ATCC 15597) were obtained from the ATCC. MS2 propagation and enumeration was carried out as described previously (Appendix A). The virus stock was purified to remove salts and dissolved organics by washing with ultrapure water in an ultrafiltration cell fitted with a regenerated cellulose membrane (Millipore, Billerica, MA) with a nominal molecular weight limit of 10 kDa. Ultrafiltration was performed until salt and dissolved organics were reduced by 99.99% and a final virus titer of 1.5×10^{11} PFU/mL was reached. The pH of the ultrapure water used for washing was adjusted to 7.0 with NaOH to ensure optimal survival of MS2 during storage at 4 °C [165].

5.2.3. Virus Adsorption and dark inactivation experiments

Contaminant adsorption to the catalyst particles is one factor that can significantly influence the reaction kinetics. Adsorption may also cause inactivation in the absence of light. Adsorption and dark inactivation assays were designed for each virus to determine if differences in adsorption are responsible for differences in photocatalytic reaction kinetics between MS2 and AdV2, and to quantify inactivation that occurs in the dark.

Ultrapure water, $NaHCO_3$, and virus stock were combined in a Pyrex® Erlenmeyer flask to achieve 2 x 10^7 PFU/mL AdV2 or MS2 and 1 mM $NaHCO_3$. This was sampled to measure the baseline virus concentration and to serve as the positive control before adding P25 to a final concentration of 200 mg/L. The solution was stirred in the dark at room temperature for 20 minutes and sampled. To determine dark inactivation, samples were enumerated directly with particles in suspension to quantify active viruses in both solution and adsorbed phases, and compared with the initial titer before catalyst addition. To measure the quantity of viruses adsorbed to the catalyst, samples were first centrifuged at 6000 G for 10 min to remove catalyst particles and adsorbed viruses enumerating the supernatant and comparing the titer to the baseline virus titer. Experiments were conducted in triplicate and all samples were taken in triplicate.

The PFU/mL values determined from all flasks were averaged for each condition and the pooled standard deviations calculated and converted to 95% confidence intervals. Before enumeration, AdV2 samples were serially diluted in serum-free F-12k media containing 1.5 g/L $NaHCO_3$ and MS2 samples were serially diluted in 100 mM $NaHCO_3$. The inoculate volume used when titering AdV2 samples was 200 microliters. Catalyst free virus suspensions were centrifuged at 6000 G for 10 min to ensure settling of the viruses by centrifugation was not a factor when measuring adsorption quantity. Negative controls consisting of enumerating virus-free F-12k solution (AdV2) or virus-free 100 mM $NaHCO_3$ (MS2) were conducted for each experiment. Controls for A549 cell viability under exposure of TiO_2 were conducted by inoculating cells with virus-free F-12k solution containing 40 mg/L TiO_2 (highest exposure) and treating the flasks in the same manner as when enumerating virus samples. The flasks were monitored using

phase contrast microscopy over the 7 day incubation period and viability stained to determine if survival was effected and if TiO_2 could cause cellular lysis zones. No differences were observed between these flasks and the negative control flasks.

5.2.4. Virus photocatalytic inactivation experiments

Photocatalytic inactivation experiments were performed in a LZC-4V photoreactor (Luzchem Research Inc. Ottawa, Canada) equipped with 2, 4, or 6 UVA bulbs (8W, peak emission at 350 nm, Hitachi) to achieve desirable irradiation intensity (1.5, 3.0 or 4.0 mW/cm^2). Light bulbs were placed only on the opposing sides of the reaction flask and pre-lit for intensity and temperature stabilization before experiments. The total irradiation intensity was measured using a UV radiometer with a 350 nm NIST traceable sensor (Control Company, Friendswood, TX). Temperature was measured using a NIST traceable digital thermometer (Control Company) and was 23.9 ± 0.2 °C at 1.5 mW/cm^2 light intensity, 25.4 ± 0.4 °C at 3 mW/cm^2, and 27.2 ± 0.5 °C at 4 mW/cm^2. A built-in stirring plate at the center of the reactor provided mixing during the experiments and an exhaust fan circulated ambient air through the reactor to provide O_2 and stabilize the temperature.

The reaction conditions used in the photocatalytic inactivation assays are the same as in the adsorption and dark inactivation assays, except the P25 concentration used was either 50, 200, or 400 mg/L. After the viruses and catalyst stirred in the dark for 20 minutes, a sample was taken to quantify the active virus titer before the start of irradiation. The flasks were then irradiated and samples taken at timed intervals for serial dilution and titering. All samples were measured with catalyst particles in suspension.

Experiments were conducted in triplicate and all samples were taken in triplicate. The inoculate volume used when titering AdV2 samples was 800 microliters. The PFU/mL values determined from all flasks were averaged for each time point and the pooled standard deviations calculated and converted to 95% confidence intervals. Positive and negative controls were conducted with each experiment as described in the dark inactivation and adsorption experiment methods.

5.3. Results and discussion

5.3.1. Comparison of adenovirus and MS2 inactivation kinetics

MS2 is commonly used as a surrogate viral pathogen in water disinfection studies due to its ease of propagation and assay, similarity in size and structure to some pathogenic viruses, and resistance to various disinfection techniques [24-29]. For comparative purposes and to determine if MS2 is a suitable surrogate for adenovirus in photocatalytic oxidation disinfection studies, both MS2 and AdV2 were treated with irradiated TiO_2 under the same conditions. The results, shown in Figure 5-1, reveal that AdV2 is much more resistant than MS2 to photocatalytic oxidation.

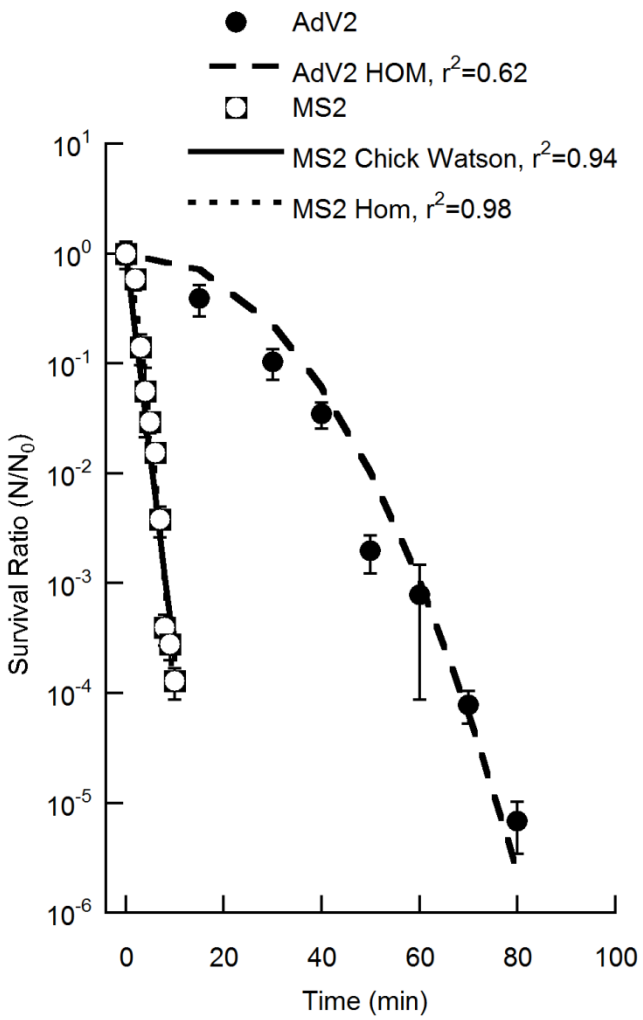

Figure 5-1 - Photocatalytic inactivation kinetics in of AdV2 compared to MS2 using 50 mg/L P25 and 1.5 mW/cm^2 UV-A irradiation. AdV2 displays a strong initial shoulder in the kinetics which can be described by the Hom model with *n* = 1.20, *m* = 2.21, *k* = 3.16 x 10^{-6} mg^{-n} L^n min^{-m}, and C = 50 mg/L. MS2 is inactivated more rapidly than AdV2 and the kinetics display a very slight shoulder that can be fit well using the Chick Watson model with *k'* = 0.37 1/min or the Hom model with *n* = 1.9, *m* = 1.4, *k* = 1.2 x 10^{-4} mg^{-n} L^n min^{-m}, and C = 50 mg/L.

AdV2 took a much greater time to reach 4-log$_{10}$ inactivation than MS2 (70 vs. 10 min.) when using 50 mg/L P25 TiO_2 irradiated with 1.5 mW/cm^2 UV-A irradiation. It is likely that the differences in capsid structure are responsible for the differences in

susceptibility to photocatalytic oxidation. MS2 contains only one infective site that either needs to be damaged itself or obscured by damaged / misshapen coat proteins to render the virus non-infective [33, 174]. In contrast, AdV2 contains 12 infective sites (fibre) that protrude prominently from the capsid surface [30]. Assuming the other capsid proteins (hexon, penton) retain adequate integrity during disinfection, all 12 fibre proteins must be damaged to render the virus non-infective.

The kinetics of AdV2 and MS2 inactivation by TiO_2 also take a different form. The AdV2 kinetics display a strong initial shoulder and are described well by the Hom model (Equation 5-1) [175], where N (PFU/mL) is the virus titer at irradiation time t (min), N_0 (PFU/mL) is the initial virus titer after dark stirring with catalyst, k ($mg^{-n}\ L^{n}\ min^{-m}$) is the rate constant, C (mg/L) is the TiO_2 concentration, and n and m are unit less parameters. In contrast, the MS2 kinetics displays a very slight initial shoulder and is described well by both the Chick-Watson model (Equation 5-2), where k' is the pseudo first order rate constant (min^{-1}) and the other parameters are the same as in Equation 5-1, and by the Hom Model with n = 1.9, m = 1.4, k = 1.2 x 10^{-4} $mg^{-n}\ L^{n}\ min^{-m}$, and C = 50 mg/ L. The different kinetic forms suggest that different mechanisms may be responsible for inactivation of the viruses, or that MS2 requires much less damage before inactivation occurs.

Equation 5-1

$$Log\ {}^{N}/_{N_0} = -kC^{n}t^{m}$$

Equation 5-2

$$Log\ {}^{N}/_{N_0} = -k't$$

The shoulder present in the AdV2 data is evidence that multiple sites may require damage before inactivation can occur [175]. This is likely due to the multiple infective sites present on AdV2. An initial delay in the inactivation kinetics is commonly observed in the inactivation of bacteria by TiO_2, where multiple ROS attacks are required before the cell membrane is breached and rapid inactivation occurs [145, 176, 177]. Another possibility explaining the shoulder effect is demand for HO• by bicarbonate in the reaction mixture [178]. This is less likely, however, since the magnitude of the effect should be similar when using MS2. Ultimately the large differences in inactivation behavior between MS2 and AdV2 imply that another surrogate virus may be more suitable for evaluating photocatalytic treatment systems for adenovirus inactivation. Identifying another surrogate is not within the scope of this study; however, AdV2 is used directly here to evaluate the efficacy of P25 TiO_2 for inactivation of adenoviruses.

5.3.2. Adsorption and dark inactivation of adenovirus and MS2 by TiO_2

The fraction of viruses adsorbed to the catalyst is an important parameter which affects the photocatalytic inactivation kinetics [25]. The concentration of ROS is highest at the catalyst surface, and adsorbed viruses will be more rapidly oxidized than those in the solution bulk. Both dark inactivation and adsorption were assayed to determine if differences in these values could explain any differences in the photocatalytic inactivation kinetics between AdV2 and MS2. Figure 5-2 shows there was no dark

inactivation for either virus, and only limited adsorptive removal occurred with adenovirus (N_0/N_a = 0.71). Control tests consisting of centrifuging TiO_2 – free virus suspensions at 6,000 G did not result in significant reduction of virus titer (data not shown), indicating that the removal of AdV2 was solely due to adsorption to TiO_2. These results suggest that adenoviruses will be damaged more rapidly than MS2 when irradiating the suspensions.

For AdV2 the survival ratio for dark inactivation is 1.2, signifying an increase in titer. During the course of experimentation, samples containing TiO_2 consistently titered higher than TiO_2 – free virus samples. It is hypothesized that particle associated viruses settle onto cellular monolayers and infect cells more rapidly than by diffusion during the inoculation procedure. TiO_2-free solutions rely solely on diffusion of viruses within the inoculate to contact cells. Diffusion alone may take longer than the 90 minute inoculate time for all viruses to contact the cellular monolayer, especially considering the low diffusivity of adenoviruses [179]. The inoculate titer used for assaying dark inactivation was decreased to 200 microliters (vs. 800 microliters for assay of photocatalytic inactivation) to minimize this effect. For MS2, the apparent small increase in titer observed when measuring dark inactivation and adsorption is attributed to experimental variability and error.

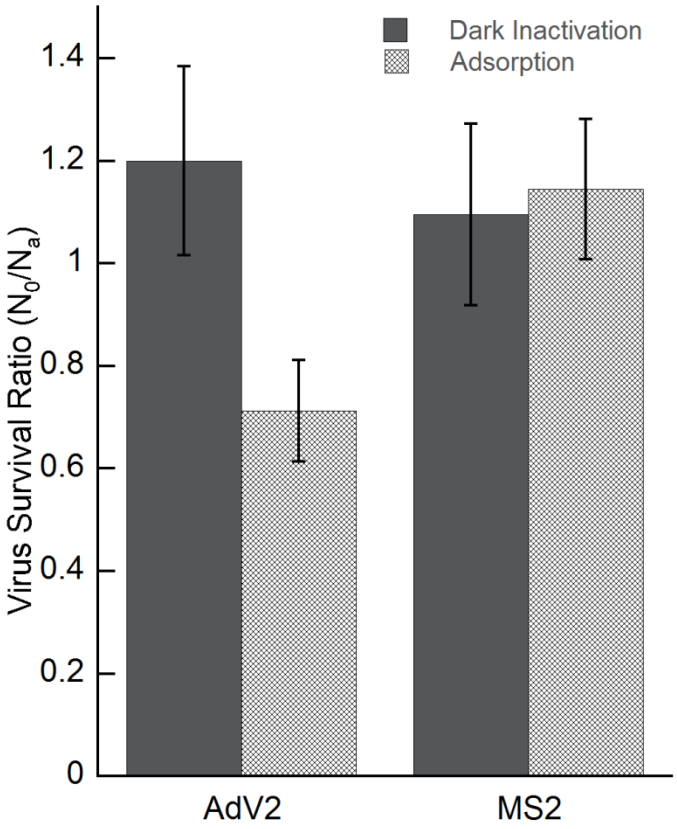

Figure 5-2 - Dark inactivation and adsorption of MS2 and AdV2 to 200 mg/L P25 under dark condition. No dark inactivation occurs for either virus. 29% of AdV2 are adsorbed while no MS2 is adsorbed to P25 under these conditions. N_a is applied virus concentration. N_o is virus concentration after dark stirring either with particles in suspension (dark inactivation) or in the solution supernatant (adsorption).

5.3.3. Effect of TiO_2 concentration on adenovirus inactivation kinetics

The concentration of catalyst is an important parameter in photocatalytic systems. Typically, the rate of reaction increases with catalyst concentration until the optical density of the solution increases to a point where the light cannot penetrate through the entire reaction mixture [180]. Increasing the catalyst concentration allows for increased

HO• production, which may then increase the inactivation rate of viruses. Figure 5-3 shows the AdV2 inactivation kinetics produced by 50, 200, and 400 mg/L TiO_2 under 1.5 mW/cm^2 UV-A irradiation. As is typically the case, the inactivation rate increases with increasing catalyst concentration to the highest amount tested, 400 mg/L. This is in contrast to one study which found the MS2 inactivation rate begins to plateau at 50 mg/L P25 TiO_2 and does not significantly increase at concentrations past 100 mg/L [25]. The discrepancy may be due to the different reactor systems employed in this study. The optimum TiO_2 concentration is highly dependent on reactor configuration, and can be as high as 2.5 g/L or as low as 0.2 g/L [180].

The data in Figure 5-3 is modeled using the Hom equation, keeping all parameters constant (k = 3.16 x 10^{-6}, n = 1.20, m = 2.21) and only changing the value of the concentration, C (mg/L). The model fits the data best for 200 mg/L TiO_2 (r^2 = 0.91), however tends to slightly underestimate (<0.5 log_{10}) the inactivation during the shoulder region when using 50 mg/L (r^2 = 0.62) and 400 mg/L (r^2 = 0.74) TiO_2. While not ideal, underestimation is more conservative when using models to predict inactivation of pathogenic organisms.

A primary motivation of this work is to reduce the UV energy required to achieve adequate disinfection of viruses in drinking water treatment. When using 400 mg/L TiO_2, 1,960 mJ/cm^2 UV-A irradiation is required to achieve 4-log_{10} inactivation. This is approximately an order of magnitude higher than the UV_{254} fluence required (120 – 200 mJ/cm^2) to reach 4-log_{10} inactivation of adenoviruses during conventional UV disinfection [5].

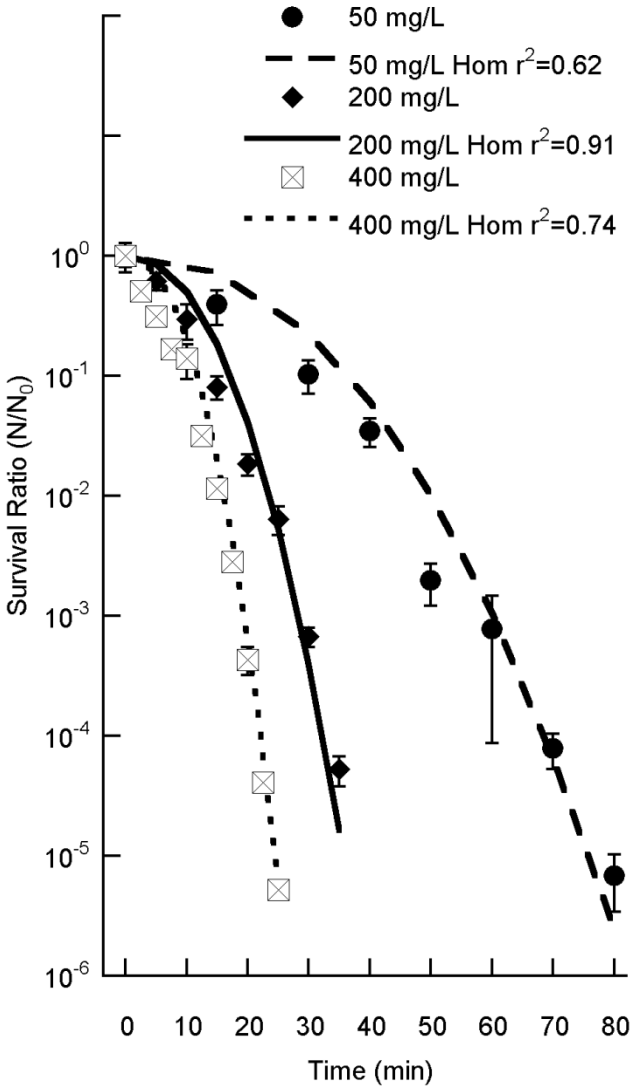

Figure 5-3 - Effect of P25 concentration on the photocatalytic inactivation kinetics of AdV2. The kinetics change in a dose dependent manner and can be described using the Hom model with n = 1.20, m = 2.21, k = 3.16 x 10^{-6}, and the Concentration, C, given in mg/L.

While increasing the catalyst concentration further may reduce the discrepancy, it is not likely this strategy can fully bridge the gap. Using the maximum optimum TiO_2 concentration of 2.5 g/L reported in prior studies [180], a fluence of 750 mJ/cm^2 is

required to achieve 4-$\log_{10}$ inactivation as predicted by the Hom model with parameters determined in our study. Other strategies are required to improve the virus inactivation kinetics, such as increasing the production of HO• (Chapter 3) or increasing adsorption of the viruses to the catalyst (Chapter 4).

5.3.4. Effect of light intensity on adenovirus inactivation kinetics

Increasing the light intensity can increase photocatalytic reaction kinetics, although typically not the total fluence required to achieve a certain treatment level. In studies of chemical contaminant degradation, the photocatalytic reaction rate increases linearly with the radiation intensity at low intensity, increases with the square root of intensity at intermediate intensities, and is a constant after reaching a certain threshold intensity [88]. Too high of an intensity may even reduce the reaction rate, as it promotes recombination of excited electrons and holes on the catalyst [72]. To gauge the response of AdV2 photocatalytic inactivation to increasing light intensities, the kinetics were measured using 200 mg/L TiO_2 under 1.5, 3.0 and 4.0 mW/cm^2 UV-A intensity. The results, shown in Figure 5-4, reveal that the kinetics increases with the intensity.

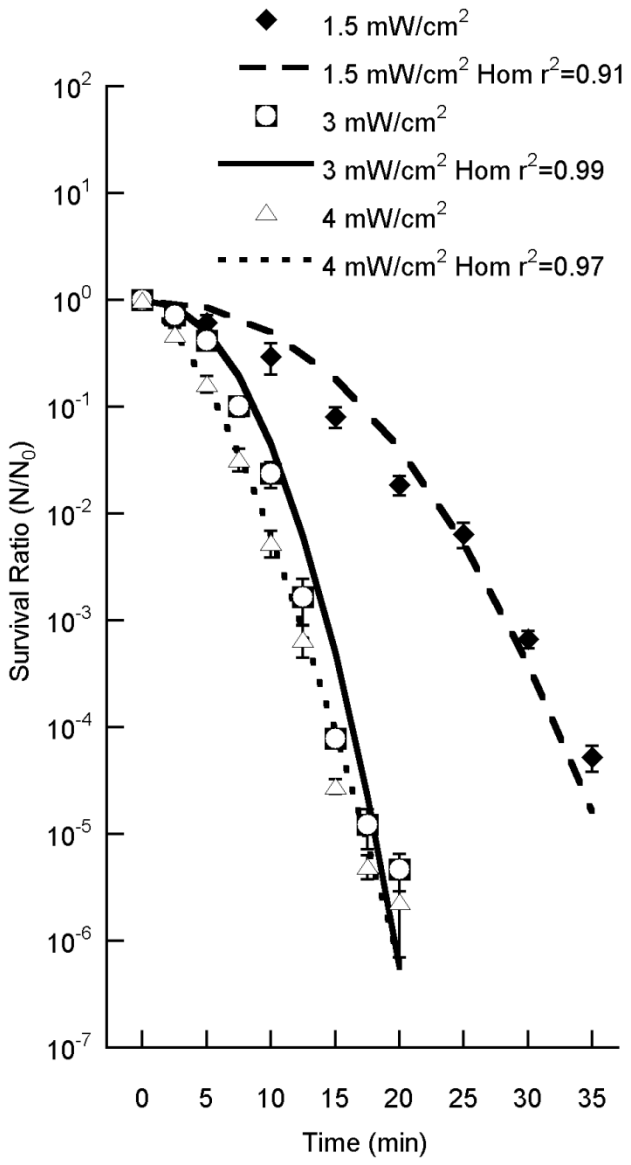

Figure 5-4 - Effect of light intensity on photocatalytic inactivation kinetics of AdV2 by 200 mg/L P25. The inactivation rate increases up to 4 mW/cm^2, the highest tested, although diminishing returns are obtained after 3 mW/cm^2. The Hom model fits the data for 1.5 and 3 mW/cm^2 with n = 1.20 and m = 2.21. For 4 mW/cm^2 m = 1.49 is used to account for the diminished shoulder observed in the kinetics. The value of k is adjusted to fit each data set.

The Hom model was fit to the data in Figure 5-4 by changing the value of *k* for the different light intensities since the rate constant is a function of the amount of reactive oxygen species produced. The values of Hom equation parameters and fluence required for 4-$\log_{10}$ inactivation are listed in Table 5-1. The values of *n*, *m*, and *C* were kept the same, except in the case of 4.0 mW/cm^2, where the value of *m* needed to be decreased to fit the data well. The degree of shoulder (or tailing) is governed by the value of *m* in the Hom model. It is clear from the data the shoulder effect is diminished at 4.0 mW/cm^2, necessitating the reduction of the *m* value in the model fit. It is possible that some minor capsid damage occurs under exposure to UV-A irradiation, and this is more pronounced at high intensities. It may then require less HO• attack to inactivate the viruses, which manifests as a change in the inactivation kinetic form.

Table 5-1 - Parameters used to fit Hom model to AdV2 photocatalytic inactivation data obtained under different light intensities and fluence required to achieve 4-$\log_{10}$ inactivation.

I (mW/cm^2)	k x 10^{-5}	n	m	I*t for 4-$\log_{10}$ inactivation (mJ/cm^2)
1.5	0.316	1.20	2.21	2,960
3.0	1.42	1.20	2.21	2,730
4.0	12.2	1.20	1.49	3,370

The fluence required to achieve 4-$\log_{10}$ inactivation is approximately the same when using 1.5 and 3.0 mW/cm^2 irradiation (2,730 – 2,960 mJ/cm^2). However at 4.0 mW/cm^2, the required fluence is greater (3,370 mJ/cm^2). This indicates that 1.5 and 3.0 mW/cm^2 intensities fall into the low intensity regime, where the reaction rate is proportional to the intensity. At 4.0 mW/cm^2, the system is moving into the intermediate intensity regime, where the reaction rate is proportional to the square root of the light intensity and system efficiency is decreasing. The results obtained at 1.5 and 3.0 mW/cm^2 are consistent with previous work, where the MS2 inactivation rate by P25 TiO_2 increased linearly with irradiation intensity up to the maximum tested, 2.2 mW/cm^2 [25]. The UV-A intensities used in our study are well within the range found in natural sunlight, although the intensity in sunlight varies according to location, season, and time of day [181]. Solar driven photocatalytic oxidation may be a viable treatment option until advanced catalysts with improved efficiency can be developed.

5.4. Conclusions

TiO_2 based photocatalytic oxidation can inactivate human adenovirus in a reasonable time, however the energy required is still greater than UV-C disinfection methods. Utilizing solar irradiation is necessary to make photocatalytic oxidation with a suspended photocatalyst a viable alternative from an energy usage standpoint. Using an immobilized catalyst on an UV-C reactor surface may show improved inactivation kinetics compared to UV-C alone, and is the subject of future research. The development of new catalysts with greater efficiency will also aid in improving the viability of this technology.

The differences in inactivation kinetics between AdV2 and MS2 suggest that differences in virus structure are responsible for the varying susceptibility to photocatalytic oxidation. Further research is warranted to determine the mechanisms responsible for inactivation of these viruses and provide insight to the viral characteristics responsible for increased resistance to photocatalytic oxidation. The relative increased resistance of adenovirus may be due to the multiple infective sites on the capsid, position of the infective sites relative to other capsid proteins, stability of the capsid after minor oxidation, and the viruses ability to use host DNA repair enzymes to repair damage to its dsDNA genome after infection [5, 30].

The increasing global population is expected to further strain supplies of both clean water and energy. There exists the need to more efficiently utilize existing resources and develop new sources of clean water and energy. Photocatalytic oxidation technologies have the potential to improve the outlook in both of these resources as we progress into a future world with increased demand driven by increased population and prosperity.

5.5. Acknowledgements

We have copious gratitude for Benito Mariñas and Martin Page at UIUC for providing training on propagation and assay of adenoviruses. MS2 kinetic inactivation data was obtained by Nina Hwang.

Chapter 6

Inactivation of human adenovirus by modified photocatalytic nanomaterials[4]

[4] Manuscript in preparation for submission to the journal *Water Research*

Michael Liga[a], Yuri Mackeyev[b], Huma R. Jafry[c], Erika L. Bryant[b], Lon J. Wilson[b], Vicki L. Colvin[b], Andrew R. Barron[b,c], and Qilin Li[a*]

[a] Department of Civil and Environmental Engineering,

[b] Department of Chemistry

[c] Department of Mechanical Engineering and Materials Science

Rice University, 6100 Main St., Houston, TX 77005, United States

Key Words: virus disinfection, advanced oxidation, TiO_2, silver, silica, fullerene, water

6.1. Introduction

Advanced oxidation processes for water treatment continue to gain increased attention in the research community, and are increasingly being implemented in municipal / industrial water treatment systems [182]. The systems currently employed typically rely on either ozone or UV/H_2O_2 technologies. Another potential option is advanced oxidation using a photocatalyst (e.g. TiO_2, fullerene) in conjunction with UV or visible light irradiation. A major limitation blocking the implementation of photocatalytic oxidation is slow reaction kinetics and poor efficiency of contaminant degradation or microbial inactivation. On account of this, much research has been conducted on using solar irradiation to drive the photocatalytic system to negate the high energy cost required [170]. Another strategy for improving the efficiency of photocatalytic oxidation is to modify the catalyst materials for increased activity. Two general strategies are available to accomplish this: 1. Increase reactive oxygen species (ROS) production for a given light input and 2. Increase the adsorption affinity of target compounds to the catalyst surface, where ROS concentrations are highest.

One application that photocatalytic oxidation may be particularly suitable for is the inactivation of UV_{254} resistant viruses, such as adenovirus. Adenoviruses with damaged genomes (e.g. by UV_{254}) are still capable of infecting cells where they utilize host cell DNA repair enzymes to repair their damaged viral DNA and competently replicate [5]. A review of various disinfectants against adenoviruses reveals that disinfection methods which cause protein damage, such as chlorine, MP UV, and ozone, are the most effective for rapid adenovirus inactivation [10-13]. Photocatalytic oxidation generates highly reactive ROS, such as hydroxyl free radical (HO•) and singlet oxygen

($^1O_2$), which are known to damage proteins [69, 78, 79]. On account of this, photocatalytic oxidation may be highly effective for inactivation of adenoviruses. In Chapter 5 it was revealed that human adenovirus type 2 (AdV2) can be inactivated by P25 TiO_2 based photocatalytic oxidation in a reasonable time, however the kinetics must be improved before this technology can compete with UV_{254} methods.

Modifying TiO_2 with silver increases the inactivation kinetics of bacteriophage MS2 by improving the production of HO• (Chapter 3). Modifying TiO_2 with surface deposits of silica improves the kinetics of MS2 inactivation by increasing the adsorption of the virus to the catalyst (Appendix A, Chapter 4). These catalyst modification strategies may also be effective at improving the kinetics of adenovirus inactivation. While the virucidal activity of TiO_2 is primarily due to the generation of HO• (Figure 3-6) [74], other ROS, such as $^1O_2$, are known to inactivate viruses [69, 71, 126, 131]. Recently, an amine functionalized C_{60} catalyst was developed which generates $^1O_2$, forms a stable suspension in water, and is effective at inactivating MS2 [69, 126, 131]. This material is also activated by visible rather than UV light, which makes it attractive for solar disinfection systems.

The objectives of this study are to determine if silver or silica modified TiO_2 improve the inactivation of AdV2 compared to neat TiO_2. The efficacy of amine functionalized C_{60} for AdV2 inactivation is also investigated and compared to TiO_2 based materials.

6.2. Materials and methods

P25 Aeroxide® TiO_2 (avg. size 25 nm, 70:30 anatase:rutile, BET 50 m^2/g, referred to as P25 TiO_2 hereafter) obtained from Evonik Degussa Corporation (Parsippany, NJ) was used as the base TiO_2 photocatalyst. All nanomaterials were suspended in unbuffered ultrapure water (pH 5.5) and dispersed using an ultrasonic processor fitted with a cuphorn operated at 100W for 15 minutes immediately prior to all experiments. Human adenovirus serotype 2 (AdV2) (ATCC VR-186) and A549 human lung carcinoma cells (ATCC CCL-185) were obtained from the ATCC (Manassas, VA). AdV2 was propagated, purified, and enumerated as previously described (Chapter 5). Bacteriophage MS2 (ATCC 15597-B1) and *E. coli* (ATCC 15597) were obtained from the ATCC (Manassas, VA**).** MS2 propagation, purification, and enumeration were carried out as described previously (Chapter 5). Ultrapure water was generated by a MilliQ Direct 3 (Millipore) fitted with a Biopack filter for pyrogen removal. All glassware and reusable materials for tissue culture work were depyrogenated either by heating at 190 °C overnight or soaking in 0.5 M HNO_3 overnight followed by rinsing in pyrogen-free water. All items used in the propagation, assay, and testing of the viruses was purchased sterile or sterilized by autoclave or 0.22 μm PES membrane filters (Millipore, Billerica, MA).

6.2.1. Modified TiO_2 nanomaterials

The silver modified material is the same used for MS2 inactivation containing 5.95% silver (5.95%nAg/TiO_2) (Chapter 3). Briefly, the nAg/TiO_2 was synthesized by a photochemical reduction method using P25 TiO_2, $AgNO_3$, and oxalic acid under UV

irradiation. The material was stored in the dark and under vacuum to prevent further oxidation. It was dispersed and irradiated for 20 hours to recover photocatalytic activity prior to using in virus inactivation studies. The silica modified material is the same used for MS2 inactivation in Chapter 4. The material used here for AdV2 inactivation was made by the water synthesis method using 5% SiO_2 (5%SiO_2-TiO_2-w) and was stored sealed in a vial in the dark.

6.2.2. Amine functionalized C_{60}

Cationic hexakis C_{60} derivative with amine functionality [$C_{60}(CR_2)_6$, R = $CO_2(CH_2)_2NH_3^+Cl^-$] (Figure 6-1, hereafter referred to as amino-C_{60}) was synthesized as described previously but without immobilization onto silica [126]. The material was stored as a powder at -20 °C in the dark.

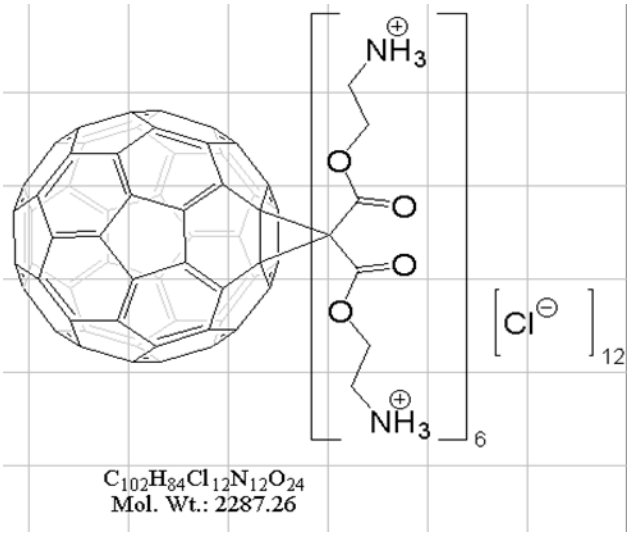

Figure 6-1 – Structure of hexakis amino-C_{60}

6.2.3. Dark inactivation and adsorption of viruses by nanomaterials

The degree of adsorption of the viruses to the catalyst particles is an important parameter which may affect the photocatalytic inactivation kinetics. Adsorption may also lead to inactivation without irradiation. Both adsorption and dark inactivation of AdV2 and MS2 were assayed by combining viruses (final 2 x 10^7 PFU/mL) and ultrapure water containing 1 mM $NaHCO_3$ at pH 7.8 in a Pyrex® Erlenmeyer flask. The virus solution was sampled to quantify the virus concentration before particle addition and serve as a positive control. Nanoparticles were then added to a final concentration of 200 mg/L as TiO_2 for either nAg/TiO_2, SiO_2-TiO_2, or neat P25 TiO_2, or 20 μM (45.7 mg/L) amino-C_{60}. The virus – nanomaterial mixtures were stirred in the dark at room temperature for 20 minutes before being sampled. Samples were taken and enumerated directly with particles to quantify dark inactivation. To quantify adsorption (TiO_2 based materials only), samples were first centrifuged at 6,000 G for 10 minutes before enumerating the supernatant.

Positive and negative controls were carried out during each experiment. Control tests for A549 cell viability in the presence of nanomaterials were conducted by inoculating cellular monolayers with serum free F-12k solution containing 20 mg/l as TiO_2 of nAg/TiO_2, 5%SiO_2-TiO_2, or neat P25 TiO_2 or 2 μM amino-fullerene, the highest concentrations cells were exposed to when inoculated with samples from virus inactivation tests. The inoculation and subsequent incubation of the flasks was undertaken exactly the same as when titering virus samples. Cells were monitored by phase contrast light microscopy during the incubation period and viability stained after 7 days to check for excessive loss of viability. To further ensure that any reduction in viral

titer was not due the death of virus-infected host cells by the nanomaterials, virus stock solution was diluted in serum free F-12k (for AdV2) or 100 mM $NaHCO_3$ (for MS2) containing 20 mg/l as TiO_2 of nAg/TiO_2, $5\%SiO_2$-TiO_2, or neat P25 TiO_2 or 2 μM amino-fullerene. The resulting solution was used to inoculate cells and the resulting titer compared to the positive controls.

6.2.4. Virus photocatalytic inactivation experiments

Photocatalytic inactivation experiments were performed in a LZC-4V photoreactor (Luzchem Research Inc. Ottawa, Canada). The reactor was equipped with either 2 or 4 UVA bulbs (8W, peak emission at 350 nm, Hitachi) for tests with TiO_2 based nanomaterials and with 6 fluorescent visible light bulbs (8W, cool white, 91% emission between 400-700 nm, Sylvania) for tests with amino-fullerene. The UVA irradiation intensity of 1.5 mW/cm^2 (2 bulbs) or 3.0 mW/cm^2 (4 bulbs) was measured using a UV radiometer with a 350 nm NIST traceable sensor (Control Company, Friendswood, TX). A visible light intensity of 51,490 lux, which converts to 15.2 mW/cm^2 [183], was measured using a digital lux meter (Reliability Direct, League City, TX). Light bulbs were placed only on the opposing sides of the reaction flask and pre-lit for intensity and temperature stabilization before experiments. Temperature was measured using a NIST traceable digital thermometer (Control Company) and was 23.9 ± 0.2 °C (2 bulbs) or 25.4 ± 0.4 °C (4 bulbs) when using UVA bulbs, and 26.2 ± 0.34 °C when using visible bulbs. A built-in stirring plate at the center of the reactor provided mixing during the experiments and an exhaust fan circulated ambient air through the reactor to provide O_2 and stabilize the temperature.

The solution conditions used when testing photocatalytic inactivation were the same as those used during tests of adsorption and dark inactivation. After viruses and catalyst particles were stirred for 20 minutes in the dark, a sample was taken to quantify the active virus titer before irradiation but after any dark inactivation. The flasks were then irradiated and timed samples taken for enumeration of active viruses. All samples were measured with catalyst particles in suspension.

6.3. Results and discussion

6.3.1. Adenovirus inactivation by nAg/TiO_2

The adsorption / dark inactivation and photocatalytic inactivation of AdV2 by nAg/TiO_2 were tested using 200 mg/L as TiO_2 catalysts and 3.0 mW/cm^2 UV-A irradiation. Dark inactivation was quantified by enumerating viruses with catalyst particles remaining in solution. Adsorption was assayed by centrifuging catalyst particles from the reaction suspension before enumerating the supernatant. Silver modification of TiO_2 improved the adsorption and dark inactivation (Figure 6-2) and initial photocatalytic inactivation (Figure 6-3) of AdV2. In the dark, 29% of the virus was inactivated and 83% adsorbed by nAg/TiO_2, vs. no dark inactivation and 29% adsorption for neat TiO_2. The inactivation by nAg/TiO_2 is likely due to silver ions released from the catalyst and not adsorption, since the multiple fibre proteins on adenovirus should not all be occluded when a virion is adsorbed. With MS2, a large fraction of MS2 dark inactivation was due to leached silver ions, however adsorption caused further inactivation of MS2 (Figure 3-4). The apparent increase in AdV2 titer (Figure 6-2) when using P25 may be due to

increased infection efficiency of particle associated viruses during the inoculation period, as discussed in Chapter 5.

Since MS2 contains one infective site, it is possible that adsorption prevents access of the site to host *E. coli* pili, where infection occurs. In contrast, AdV2 contains 12 infective sites distributed across the capsid, some of which will remain exposed after adsorption of the virus to the catalyst particles. When using neat TiO_2, no dark inactivation is observed despite 29% adsorption of viruses to the catalyst. This leads to the conclusion that the dark inactivation is due to leached silver. The large increase in adsorption of AdV2 to nAg/TiO_2 vs. neat TiO_2 is likely due to interactions of the virus proteins with the silver particles. Silver interacts strongly with sulfer (i.e. cysteine) and carboxyl groups [155]. The fibre protein of AdV2 contains an appreciable quantity of cysteine, making it a prime target for interaction with silver [184]. Control tests revealed the presence of nAg/TiO_2 or P25 TiO_2 in the inoculate did not reduce the formation of viral plaques, and all adsorption / inactivation of the viruses can be attributed to interaction of the viruses with the catalyst.

The photocatalytic inactivation of AdV2 by nAg/TiO_2 follows a different kinetic profile than neat TiO_2 (Figure 6-3). The most rapid inactivation occurs during the first two minutes where 95% of the viruses inactivated, after which the rate diminishes and follows a first order profile. The time to 4-$\log_{10}$ inactivation is the same for nAg/TiO_2 and neat TiO_2.

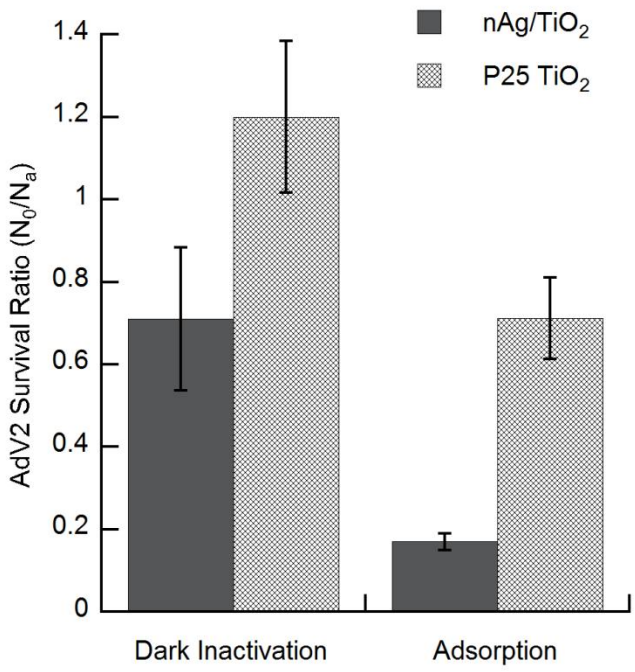

Figure 6-2 - Dark inactivation and adsorption of AdV2 to nAg/TiO_2 compared to P25 TiO_2. AdV2 was stirred in the dark for 20 minutes and the titer (N_0) compared to the titer of viruses before catalyst addition (N_a). nAg/TiO_2 improves both the dark inactivation (N_0/N_a = 0.71) and adsorption (N_0/N_a = 0.17) as compared to P25 TiO_2. [catalyst] = 200 mg/L as TiO_2, Applied [AdV2] = N_a = 2 x 10^7 PFU/mL.

The Hom kinetic model (Equation 6-1) fits the data well for both catalyst types, where N (PFU/mL) is the virus titer at irradiation time t (min), N_0 (PFU/mL) is the initial virus titer after dark stirring with catalyst, k ($mg^{-n} L^n min^{-m}$) is the rate constant, C (mg/L) is the catalyst concentration, and n and m are unit less parameters [175]. The m value is less than 1 (0.7) for the nAg/TiO_2 data, which produces the tailing effect. For neat TiO_2, the m value is greater than 1 (2.2), which produces the shoulder effect. The presence of a shoulder can be attributed to either a requirement for multiple sites on the virus to come in contact with the disinfectant (ROS) before inactivation occurs or to demand from solution species (i.e. HCO_3^-) [175, 178]. Since AdV2 contains multiple infective sites, it

is possible that both repeated ROS attacks and demand from HCO_3^- contribute to the shoulder present in the inactivation kinetics.

Equation 6-1

$$Log\ {}^{N}/_{N_0} = -kC^n t^m$$

It is possible that the rapid initial inactivation and tailing observed with nAg/TiO_2 is due to the strong adsorption of the viruses to the catalyst coupled with the greater HO• production by this material. The high adsorption quantity puts most of the viruses in close proximity to the generated ROS, causing rapid inactivation. With the higher HO• production rate by nAg/TiO_2, the multiple attacks by HO• to cause inactivation may occur at the same time or sufficiently quick enough to eliminate the shoulder effect. The tailing may be due to inactivated viruses not desorbing quickly, which then react with the newly generated ROS before they can react with active viruses remaining in solution, which manifests as a decrease in the inactivation rate.

6.3.2. Adenovirus and bacteriophage MS2 inactivation by SiO_2-TiO_2

The mechanism through which surface deposits of SiO_2 improve the virus inactivation kinetics of TiO_2 is by greatly increasing the absorbance of viruses to the catalyst, where the concentration of ROS is highest (vs. the solution bulk) (Chapter 4). This mechanism was elucidated in tests of MS2 adsorption / photocatalytic inactivation in

ultrapure water at pH 5.5. During reactions with AdV2, TiO_2 aggregates strongly under this condition shortly after irradiation begins.

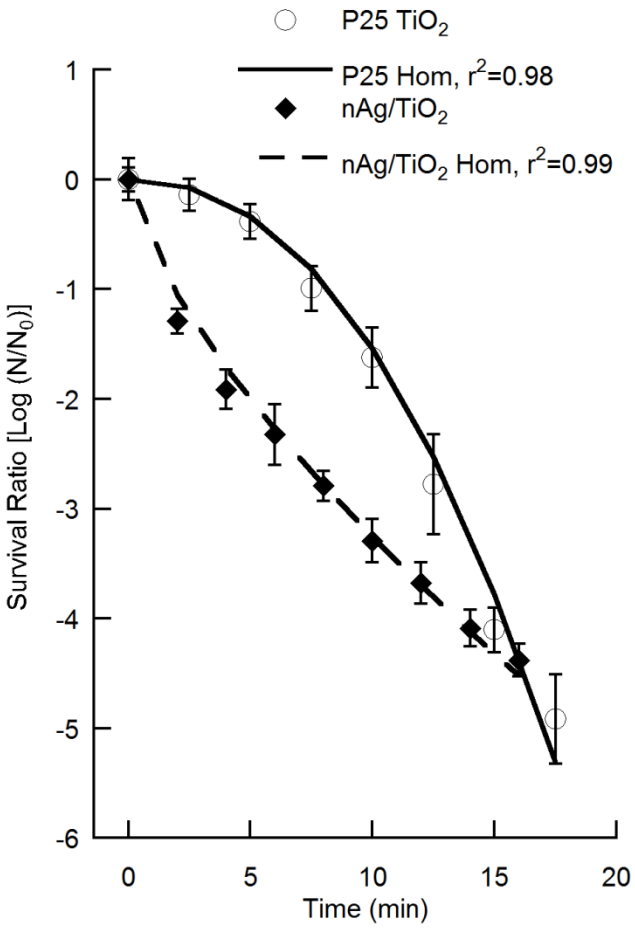

Figure 6-3 - Photocatalytic inactivation kinetics of AdV2 by nAg/TiO_2 compared to P25 TiO_2. The kinetics produced by nAg/TiO_2 are most rapid initially and display a slight tailing profile. The Hom model fits the data well with C = 200 mg L^{-1}, k = 5.3 x 10^{-6} mg^{-n} L^n min^{-m}, n = 2.2 and m = 0.7. The kinetics produced by P25 TiO_2 display a shoulder profile followed by rapid inactivation. The Hom model fits this data with C = 200 mg L^{-1}, k = 1.6 x 10^{-5} mg^{-n} L^n min^{-m}, n = 1.2 and m = 2.2. The time to 4-log_{10} inactivation is the same for both catalysts, 15 minutes. [catalyst] = 200 mg/L as TiO_2, UV-A intensity = 3.0 mW/cm^2. N_0 is the active virus titer after viruses and catalyst are stirred in the dark for 20 minutes. Applied [AdV2] = N_a = 2 x 10^7 PFU/mL.

The particles were stable at higher pH (7.8) when using 1 mM $NaHCO_3$ buffer in ultrapure water, and all AdV2 reactions were undertaken in this condition. Since solution conditions affect the adsorption of viruses to TiO_2 [25, 81], MS2 was re-tested in 1 mM $NaHCO_3$ solution as well to determine if SiO_2 enhances adsorption and the rate of photocatalytic inactivation under these conditions.

Figure 6-4 shows the adsorption and dark inactivation of both viruses using 200 mg/L as TiO_2 catalysts. SiO_2-TiO_2 displays vastly improved adsorption (97% vs. 0 % adsorbed) when using MS2 in these conditions. However, AdV2 adsorption is only slightly improved (44% vs. 29% adsorbed). The same trend occurred when testing dark inactivation. SiO_2-TiO_2 inactivated (or sterically prevented virus-host interaction of) 97% of the MS2 vs. 0% with neat TiO_2. With AdV2 no dark inactivation occurred with either material. The mechanism responsible for improving the adsorption of MS2 is still unclear. Previously we found that SiO_2 alone did not adsorb or inactivate MS2, suggesting that the improved adsorption / dark inactivation is due to virus interaction at the interface of SiO_2 and TiO_2 particles. Since AdV2 is much larger than MS2 (90 nm vs. 27 nm diameter), AdV2 particles may not have access to as many SiO_2 : TiO_2 particle interface points as MS2 does, which may explain the lack of improvement in adsorption / dark inactivation of AdV2. Differences in surface amino acid residues between the viruses may also be responsible for the differences in adsorption / dark inactivation by SiO_2-TiO_2. Control tests revealed the presence SiO_2-TiO_2 or P25 TiO_2 in the inoculate did not reduce the formation of viral plaques, and all adsorption / inactivation of the viruses can be attributed to interaction of the viruses with the catalyst.

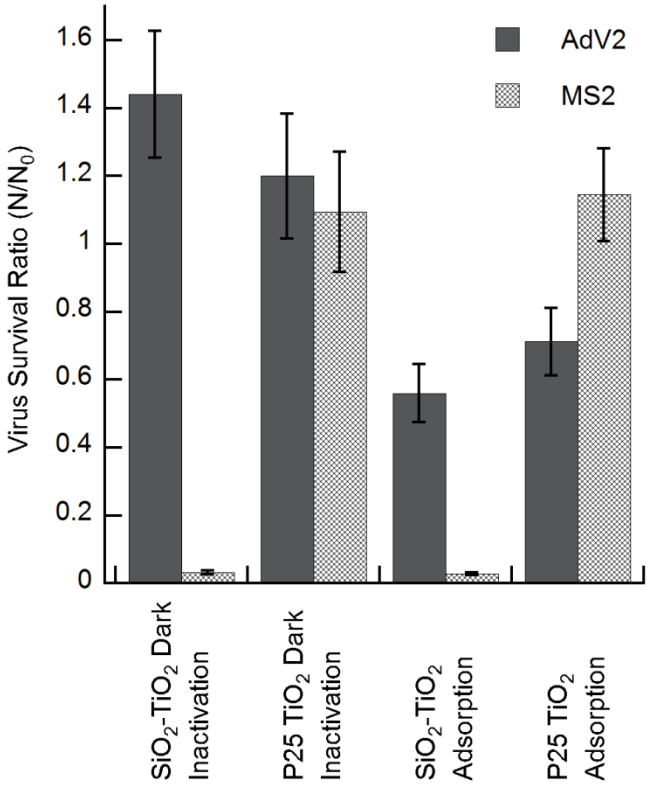

Figure 6-4 - Dark inactivation and adsorption of AdV2 and MS2 by SiO_2-TiO_2 compared to P25 TiO_2. Viruses were stirred in the dark for 20 minutes and the titer (N_0) compared to the titer of viruses before catalyst addition (N_a). SiO_2-TiO_2 greatly improves the dark inactivation (N_0/N_a = 0.032) and adsorption (N_0/N_a = 0.028) of MS2. The adsorption of AdV2 is slightly improved (N_0/N_a = 0.56 vs. 0.71), but neither SiO_2-TiO_2 or P25 TiO_2 produce any dark inactivation. [catalyst] = 200 mg/L as TiO_2, Applied [AdV2] and [MS2] = N_a = 2 x 10^7 PFU/mL.

The photocatalytic inactivation kinetics of MS2 and AdV2 were tested using 50 mg/L as TiO_2 catalysts and 1.2 mW/cm^2 UV-A irradiation. The effect of SiO_2 modification produces different results for the different viruses (Figure 6-5). SiO_2 modification improves the kinetics for MS2 but not AdV2. 4-$\log_{10}$ inactivation of MS2

occurs in 5 minutes with SiO_2-TiO_2 vs. 10 minutes with neat TiO_2. With AdV2, it takes 50 minutes achieve 4-log_{10} inactivation with SiO_2-TiO_2 vs. 33 minutes for neat TiO_2. The lack of improvement in AdV2 inactivation kinetics by SiO_2-TiO_2 is expected since adsorption is only slightly improved. In Chapter 4 we found that SiO_2 modification decreases the production of HO• by TiO_2, and that the improvement of MS2 inactivation kinetics is solely due to the orders of magnitude increase in adsorption of MS2 to the catalyst particles which places the viruses in a region of high ROS concentration as compared to the solution bulk. The inactivation kinetics of MS2 and AdV2 by SiO_2-TiO_2 also take a different form. The MS2 kinetics are best described (r^2 = 0.99) by the Chick-Watson (first-order) model (Figure 6-3), which is essentially the Hom model with $n = m = 1$ and k' is the pseudo-first order rate constant (min^{-1}). The AdV2 kinetics display a strong shoulder effect and are best described by the Hom model (r^2 = 0.98). With neat TiO_2, the MS2 inactivation kinetics display a slight shoulder, and can be described by the 1st order model (r^2 = 0.94) or the Hom model (r^2 = 0.98). The AdV2 kinetics display a strong shoulder and is best described by the Hom model (r^2 = 0.99).

Equation 6-2

$$Log\, {}^{N}/_{N_0} = -k't$$

With MS2, the minor shoulder present when using neat TiO_2 could be due to demand from HCO_3^- in the solution bulk, where inactivation occurs under the conditions tested, or due to the relatively smaller ROS concentration in the solution bulk vs. the high concentration at the catalyst surface. When using SiO_2-TiO_2, the high adsorption

quantity of MS2 places most viruses in close proximity to newly generated ROS that can react with virus proteins before being scavenged in the solution bulk. Since the ROS concentration is higher at the catalyst surface, the multiple ROS attacks which may be required to cause inactivation of MS2 could occur at the same or nearly the same time, rather than occurring over a longer timescale as may occur in the solution bulk. Since AdV2 contains multiple infective sites, it likely requires more ROS attacks to be inactivated than MS2 requires. It is possible that the increased number of ROS attacks, the relatively lower ROS concentration in the solution bulk, and demand from HCO_3^- contribute to the shoulder present in the AdV2 inactivation kinetics.

6.3.3. Adenovirus and bacteriophage MS2 inactivation by amino-C_{60}

Hexakis amino-C_{60} has previously proven effective for inactivating bacteriophage MS2 under visible irradiation in 10 mM phosphate buffer at pH 7.0 [69, 126, 131]. The inactivation observed in these studies is primarily attributed to $^1O_2$ production. One study observed significant (1.4-$\log_{10}$ in 9 minutes) inactivation under dark conditions using 50 micromolar hexakis amino-C_{60} [131]; however, another study found no inactivation occurred in the dark when using 15 micromolar hexakis amino-C_{60} [69]. In our study MS2 and AdV2 inactivation was assayed using 20 micromolar (45.7 mg/L) hexakis amino-C_{60} in 1 mM $NaHCO_3$ at pH 7.8. Figure 6-6 shows the survival ratio of these viruses after stirring in the dark for 20 minutes. 1.8-$\log_{10}$ inactivation MS2 occurred from this treatment; however, no loss of AdV2 viability was observed. The dark inactivation of MS2 is likely due to interaction of the positive charged quaternary amines on C_{60} with negatively charged viral proteins.

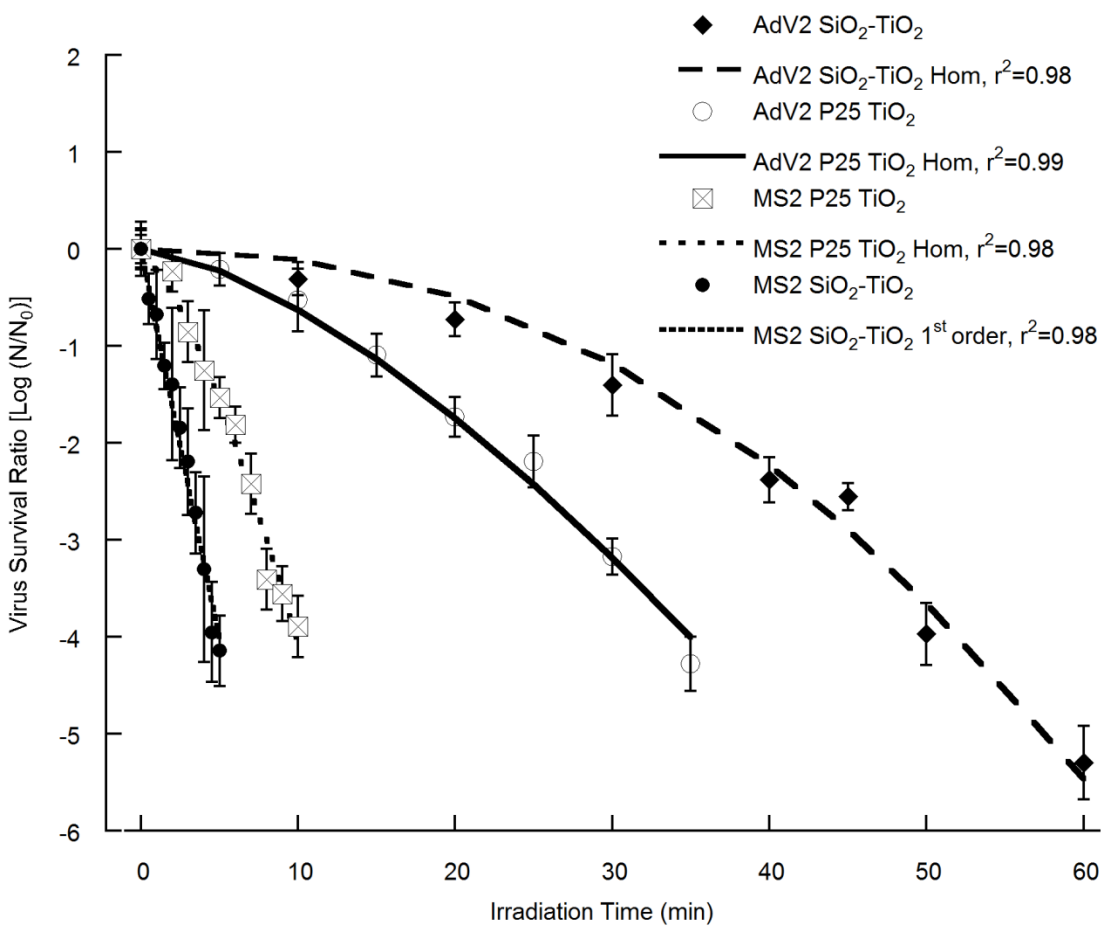

Figure 6-5 - Photocatalytic inactivation kinetics of AdV2 and MS2 by SiO_2-TiO_2 compared to P25 TiO_2. SiO_2-TiO_2 inactivates MS2 approximately 2 times faster than P25 TiO_2, providing 4-log_{10} inactivation in 5 minutes vs. 10 minutes. The MS2 inactivaiton kinetics produced by SiO_2-TiO_2 are best fit by a first order model (k' = 0.81), while the kinetics produced by P25 TiO_2 are best fit with the Hom model with C = 50 mg L^{-1}, k = 1.2 x 10^{-4} mg^{-n} L^n min^{-m}, n = 1.9 and m = 1.4. SiO_2-TiO_2 reduces the rate of AdV2 inactivation, with 4-log_{10} inactivation occurring in 50 minutes compared to 35 minutes for P25. The AdV2 kinetic profiles from both catalysts show a pronounced shoulder region and are fit well with the Hom model. For SiO_2-TiO_2 C = 200 mg L^{-1}, k = 1.1 x 10^{-6} mg^{-n} L^n min^{-m}, n = 1.2 and m = 2.2. For P25 TiO_2 C = 200 mg L^{-1}, k = 2.0 x 10^{-6} mg^{-n} L^n min^{-m}, n = 1.7 and m = 1.5. When using MS2 the [catalyst] = 50 mg/L as TiO_2. When using AdV2 the [catalyst] = 200 mg/L as TiO_2. UV-A intensity = 1.5 mW/cm^2. N_0 is the active virus titer after viruses and catalyst are stirred in the dark for 20 minutes. Applied [AdV2] = [MS2] = N_a = 2 x 10^7 PFU/mL.

The reason for the dark inactivation discrepancy between [69], [131], and our study is unknown. The lack of AdV2 inactivation in the dark is in line with a study of germicidal agents against adenovirus serotype 8, which displayed strong resistance to disinfection with alkyl (50% C14, 40% C12, 10% C16) dimethyl benzyl ammonium chloride [185]. Control tests revealed the presence amino-C_{60} in the inoculate did not reduce the formation of viral plaques, and all inactivation of the viruses can be attributed to interaction of the viruses with the catalyst.

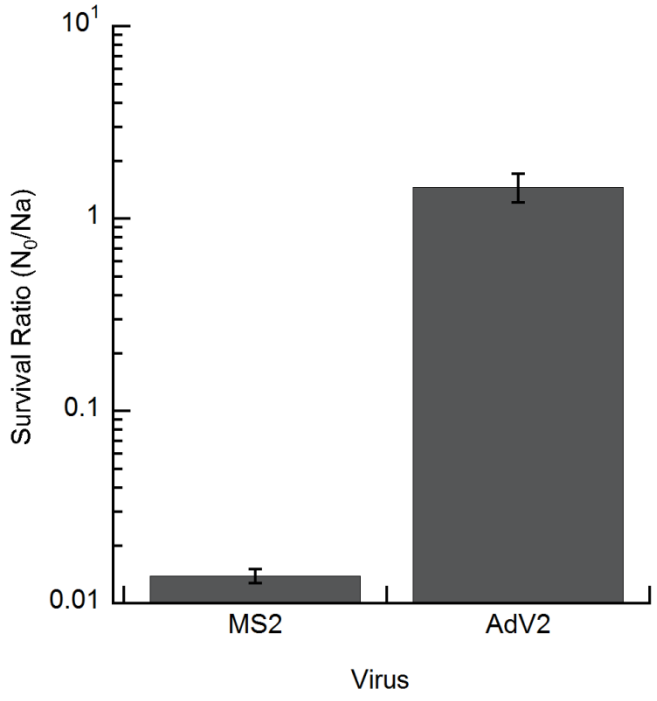

Figure 6-6 - Dark inactivation of MS2 and AdV2 by hexakis amino-C_{60}. Viruses were stirred in the dark for 20 minutes and the titer (N_0) compared to the titer of viruses before catalyst addition (N_a). MS2 was strongly inactivated (N_0/N_a) = 0.014 while no inactivation of AdV2 occurred. [amino-C_{60}] = 20 micromolar = 45.7 mg/L, applied [AdV2] = [MS2] = N_a = 2 x 10^7 PFU/mL.

Amino-C_{60} proved highly effective for inactivating both MS2 and AdV2 under visible light irradiation. Figure 6-7 shows the inactivation kinetic profile for both viruses with survival data normalized to the active virus titer after the 20 minute dark stirring period. MS2 is inactivated very rapidly and is fit well using a pseudo first order model (Equation 6-2) with $k' = -12.6\ min^{-1}$ ($r^2 = 0.99$). While not inactivated nearly as quickly as MS2, AdV2 is inactivated relatively quickly compared to TiO_2 based materials. 4-log_{10} inactivation is achieved after 6 minutes irradiation. The kinetics show a slight tailing effect, and are best described using the Hom model with $C = 45.7\ mg\ L^{-1}$, $k = 2.6 \times 10^{-4}$ ($mg^{-n}\ L^{n}\ min^{-m}$), $n = 2.2$, and $m = 0.71$ ($r^2 = 0.99$).

In Chapter 5, the fastest time to 4-log_{10} inactivation determined experimentally with P25 TiO_2 is 14 minutes (200 mg/L P25 TiO_2 in 1 mM $NaHCO_3$ at pH 7.8 under 4 mW/cm^2 UV-A), and is 8 minutes as estimated from kinetic parameters assuming an optimum TiO_2 concentration of 2.5 g/L under the same conditions. It is likely that the kinetics produced by hexakis amino-C_{60} could be further increased to achieve 4-log_{10} inactivation of AdV2 faster than 6 minutes. Previously, increased kinetics both with MS2 inactivation and furfuryl alcohol degradation were observed up to a maximum tested amino-C_{60} concentration of 20 micromolar (concentration used in our study) [69]. It is likely that the kinetics will further increase as the amino-C_{60} concentration is increased past 20 micromolar. Although the optimum concentration is unknown, 50 micromolar amino-C_{60} has produced rapid inactivation of MS2 in another study [131]. Because these two studies utilize different reactor configurations and light sources, it is not possible to directly compare the results to determine if 50 micromolar improved the kinetics over 20 micromolar amino-C_{60}.

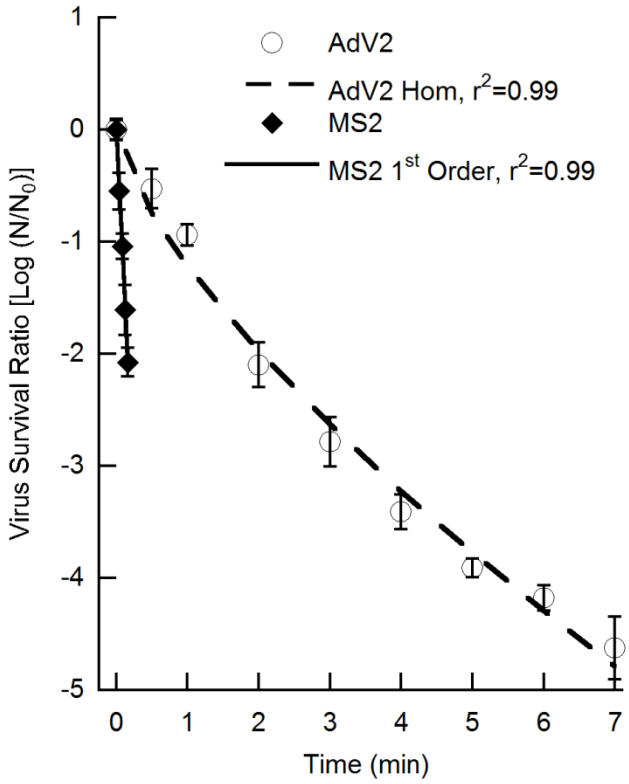

Figure 6-7 - Photocatalytic inactivation of AdV2 and MS2 by hexakis amino-C_{60}. Amino-C_{60} is highly effective for both viruses. 4-$\log_{10}$ inactivation of AdV2 occurs in 5.5 minutes and 2-$\log_{10}$ inactivation of MS2 occurs in 7.5 seconds. The AdV2 kinetics display a slight tailing profile, and are fit using the Hom model with C = 45.7 mg L^{-1}, k = 2.6 x 10^{-4} mg^{-n} L^{n} min^{-m}, n = 2.2 and m = 0.7. The MS2 kinetics display no shoulder or tailing, and are fit using a first order model with k' = 12.6. N_0 is the active virus titer after viruses and catalyst are stirred in the dark for 20 minutes. Applied [AdV2] = [MS2] = N_a = 2 x 10^7 PFU/mL.

The photocatalytic MS2 inactivation kinetics produced in our study is much faster than those previously reported [69, 126, 131]. This is likely due to the higher light intensity and reactor configuration used in our study, and our choice of using 1 mM

$NaHCO_3$ as the reaction medium rather than 10 mM phosphate buffer, which causes aggregation of the particles [131]. Aggregation of C_{60} is known to inhibit the production of $^1O_2$, although the effect is less pronounced in the functionalized materials [130, 131]. The light intensity used in our study, 51,490 lux, is equivalent to 15.2 mW/cm^2 radiation from 400-700 nm for cool white fluorescent bulbs [183]. 91% of the bulb emission falls within this spectral range, 45% is in the region of 380 – 550 nm, and 5.1% in the UV region (manufacturer specification). The absorbance spectra of hexakis amino-C_{60} is strong in the UV region and extends into the visible region up to ~550 nm [131]. For the light bulbs used in our study, the intensity up to 550 nm is 6.8 mW/cm^2 (380 – 550 nm) plus 0.78 mW/cm^2 (UV) based on manufacturer specification. While no UV cutoff filter was used in our study, it was previously shown that visible wavelengths provide the majority (84%) of the photocatalytic activity of hexakis amino-C_{60} when irradiated by fluorescent bulbs [69]. While the visible and UV irradiance reaching the earth from the sun varies according to location and time of year, the light intensity used in our study is representative of the intensity form solar irradiation on a sunny day.

6.4. Conclusions

The rapid inactivation of AdV2 by amino-C_{60} under visible light supports the use of this catalyst in solar disinfection systems, where limited external energy inputs (e.g. mixing, pumping) are required. This nanomaterial can be immobilized on silica beads to enable catalyst recycling and prevent exposure of water consumers to catalyst particles while still retaining its high photoactivity [126]. TiO_2 based catalyst materials have been given much attention for water disinfection since they generate HO•, which has a much

higher oxidation potential than $^1O_2$ and may cause more damage to microorganisms. However, the extent of damage may be less important than the damage location. Studies of bacteriophage MS2 inactivation by $^1O_2$ demonstrate that inactivation is caused by oxidation of a single residue on the virus coat proteins (180 copies/virion) [33, 71]. One disadvantage of amino-C_{60} is its potential to degrade over time, whereas TiO_2 is highly stable. Exposure of C_{60} to UV irradiation causes oxidation and the introduction of surface oxygen groups to the particle surface [125]. While research on this material has shown its activity is not reduced after 5 irradiation cycles (total 10 minutes) [126], further research is needed using more relevant timescales (i.e. days) and disinfection cycles to determine a realistic lifetime expectancy of this material.

The AdV2 inactivation kinetics produced by the modified TiO_2 nanomaterials is disappointing considering the improvement in MS2 inactivation kinetics observed in Appendix A, Chapter 3, and Chapter 4. Two important points may be taken from the results. First, catalyst modifications may need to be designed specifically for the pathogen of interest. A "one size fits all" approach may not be a suitable tactic. Second, MS2 is not a suitable surrogate virus for use in photocatalytic disinfection studies. This study and the results shown in Chapter 5 show that MS2 is much more susceptible to both TiO_2 based materials and amino-C_{60} than AdV2. The high energy input required to achieve 4-$\log_{10}$ inactivation of AdV_2 by TiO_2 makes it unable to compete with UV_{254} disinfection. Regardless, highly stable TiO_2 based materials still remain a good option for solar disinfection of water. Solar disinfection of water continues to gain attention [170], especially for application in developing countries where energy costs are preclusive to adequate water treatment. Our results demonstrate that AdV2 inactivation

by TiO_2 occurs in a reasonable time under environmentally relevant UV-A irradiation intensities, and this material still holds promise for enabling effective solar based disinfection of water.

Chapter 7

Inactivation mechanism of adenovirus type 2 and bacteriophage MS2 by TiO_2 – based photocatalytic oxidation[5]

[5] Manuscript in preparation for submission to the journal *Applied and Environmental Microbiology*

Michael V. Liga[a], Jacques M. Mathieu[a], Yizhi J. Tao[b], and Qilin Li[a,*]

[a] Department of Civil and Environmental Engineering, Rice University, 6100 Main St., Houston, TX 77005, United States

[b] Department of Biochemistry and Cell Biology, Rice University, 6100 Main St., Houston, TX 77005, United States

Key Words: Virus, Disinfection, TiO_2, Protein, DNA, Inactivation Mechanism

7.1. Introduction

The effective disinfection of viruses in drinking water remains a challenge, especially due to the increased reliance on disinfection methods which limit the formation of disinfection byproducts (e.g. UV_{254}, monochloramine). Adenoviruses (AdV) in particular have emerged as a contaminant of concern as they are resistant to disinfection with UV_{254} and monochloramine [5, 58]. Studies of the inactivation mechanisms of AdV reveal that those disinfectants which cause damage to viral proteins (e.g. free chlorine, MP UV, ozone) result in the most rapid AdV inactivation kinetics. Free chlorine damages AdV proteins that govern lifecycle events [12]. MP UV causes damage to a wide range of AdV proteins [10]. Ozonation breaks open AdV capsids [11]. In light of this, we hypothesize that photocatalytic oxidation may be highly effective for adenovirus inactivation.

TiO_2 based photocatalytic oxidation generates reactive oxygen species (ROS), most notably hydroxyl radical (HO•). TiO_2 and HO• are known to damage proteins through both cleavage and side chain oxidations [78, 79]. This leads to our hypothesis that photocatalytic oxidation may be a good alternative disinfection methods for AdV. TiO_2 is a candidate for use as a photocatalyst due to its stability, safety when ingested, and well understood reactivity [68, 72]. However, there is very limited information on the mechanism of virus inactivation by TiO_2 based photocatalytic oxidation.

Kashige et al. (2001) synthesized a thin film of anatase and applied it for inactivation of phage PL-1 [75]. The inactivation kinetics was slowed in the presence of bovine serum albumin, suggesting that protein (capsid) damage is a mechanism of

inactivation. However this evidence is extremely weak, as it does not show the albumin is specifically degraded or reacts with ROS. It is possible albumin merely blocks TiO_2 active sites or competes with viruses for ROS. Kashige et al. (2001) also showed DNA damage occurs from treating viruses with TiO_2. No conclusions on the specific inactivation mechanism may be drawn from their work other than TiO_2 can damage genetic material and extra protein in the reaction medium slows the kinetics.

Other authors have provided evidence that proteins and genetic material are both targeted by TiO_2. Zan et al. (2007) demonstrated that irradiated TiO_2 (liquid suspension and dry film) can degrade hepatitis B virus surface antigen (HBsAg) [76]. Xu et al. (2007) confirmed the degradation of HBsAG and also showed that irradiated TiO_2 is capable of degrading free RNA and casein protein [77]. While Kashige et al. 2001, Zan et al. 2007, and Xu et al. 2007 provide evidence that TiO_2 degrades both protein and genetic material, neither study is specific enough to identify if virus inactivation occurs through damage to viral proteins or viral genetic material. Different viruses may be inactivated through different mechanisms, and the results of these studies may not correlate to the mechanism of AdV inactivation by TiO_2.

In this study we investigate the inactivation mechanisms of adenovirus type 2 (AdV2) and bacteriophage MS2 by P25 TiO_2. Adenoviruses are much more complex than other water-borne viruses, which may lead to their resistance to many disinfection methods. In contrast, bacteriophage MS2, which is commonly used as a surrogate in disinfection studies due to its similarity to other water-borne viruses [24-26] and relative resistance to some disinfection methods [27-29] is relatively simple when compared to adenoviruses.

AdV is different from most waterborne pathogenic viruses in that its genome is dsDNA rather than RNA. This enables the virus to utilize the DNA repair enzymes present in host cells to repair damage to its own genome (e.g. from UV_{254} disinfection) thus increasing its resistance to disinfectants which act through genetic damage [5]. The genome is relatively large, containing 30-40 kb [30]. The 51 human serotypes are known to infect the pulmonary, gastrointestinal, and ocular body systems. Along with the gastrointestinal strains (AdV 40 and 41), the respiratory strains may be transmitted through the fecal-oral route as well through pulmonary secretions [5]. Respiratory serotypes (e.g. type 2) have been identified in the environment and are as much a concern as the enteric serotypes [20].

The AdV structure is rather large and complex when compared to other waterborne viruses and common surrogate pathogens, such as MS2. The virus size varies with the serotype, but is generally stated to be 70-100 nm in diameter [31]. There are 3 major capsid proteins (Hexon, Penton base, Fibre), 4 minor capsid associated proteins (IIIa, VI, VIII, IX), 5 DNA associated core proteins (V, VII, Mu Terminal protein, IVa2) and 1 core protease [30]. The capsid proteins are the most likely target for photocatalytic oxidation since they should come into contact with ROS first. The Fibre protein is responsible for infection, and damage to it may render the virions non-infective. Damage to hexons may directly inactivate the virions or enable easy access for ROS to enter the core and damage the core proteins and/or DNA.

Bacteriophage MS2 is a relatively small (~25 nm in diameter) virus containing positive-sense ssRNA that is 3,569 nucleotides long [33]. The capsid forms an icosahedral shape and consists of 2 proteins: coat (180 copies) and A (1 copy) [33]. The

A protein, also denoted the maturation protein, interacts with host cells (F+ E. coli) by attaching to the bacterial pilus, after which the virus injects its genome and A protein into the cell [33, 34]. The A protein is attached to the genome at both the 5' and 3' ends [35]. While it is known that the A protein is exposed to the capsid surface [34], the exact location is unknown, although it is hypothesized to be at a vertex of the icosahedron [36]. During photocatalytic oxidation of MS2, the virus may be inactivated by damaging the A protein and preventing interaction with host cells or inhibiting lifecycle processes after the A protein enters the host. Damage to the coat proteins can expose the RNA to damaging ROS or change the capsid conformation and preventing the A protein from interacting with bacterial pili.

The primary objective of this study is to determine if protein damage is responsible for AdV inactivation and therefore identify the suitability of photocatalytic oxidation for disinfection of AdV. We investigate the inactivation mechanisms of both AdV2 and MS2 to determine how differences in virus structure and function lead to differences in inactivation mechanisms and inactivation kinetics. SDS-PAGE is used to assay for damage to viral proteins [10], and PCR analysis is used for assaying damage to AdV2 genomes [60, 186]. The observed damage to proteins and DNA is correlated with inactivation data to elucidate the inactivation mechanisms.

7.2. Materials and methods

7.2.1. Materials

P25 Aeroxide® TiO_2 (avg. size 25 nm, 70:30 anatase:rutile, BET 50 m^2/g, referred to as TiO_2 hereafter) obtained from Evonik Degussa Corporation (Parsippany, NJ) was used as the photocatalyst. TiO_2 was suspended in unbuffered ultrapure water (pH 5.5) and dispersed using an ultrasonic processor fitted with a cuphorn operated at 100W for 15 minutes immediately prior to all inactivation experiments. Human adenovirus serotype 2 (AdV2) (ATCC VR-186) and A549 human lung carcinoma cells (ATCC CCL-185) were obtained from the ATCC (Manassas, VA). Bacteriophage MS2 (ATCC 15597-B1) and E. coli (ATCC 15597) were obtained from the ATCC. Ultrapure water was generated by a MilliQ Direct 3 (Millipore) fitted with a Biopack filter for pyrogen removal. All glassware and reusable materials for tissue culture work were depyrogenated either by heating at 190 °C overnight or soaking in 0.5 M HNO_3 overnight followed by rinsing in pyrogen-free water. Plastic items were depyrogenated using PyroCLEAN™ (ALerCHEK™, Inc., Springvale, Maine). All items used in the propagation, assay, and testing of the viruses were purchased sterile or sterilized by autoclave or 0.22 μm PES membrane filters (Millipore, Billerica, MA).

7.2.2. Virus propagation, assay, and purification

AdV2 and MS2 propagation and assay were carried out as described in section 5.2.2. All samples were assayed for active titer with particles in suspension (if applicable). After ultrafiltration and concentration of the crude virus isolates, sucrose density gradient ultracentrifugation was used to obtain highly purified virus stocks [187].

20 – 80% step sucrose gradients were laid by hand in 10% concentration intervals into 32.4 mL polyallomer ultracentrifuge tubes (Beckman Coulter) and allowed to equilibrate overnight at 4 °C. An aliquot of virus stock was added to each tube which was immediately placed in a SW-32Ti rotor (Beckman Coulter) and spun in an Optima L-80XP ultracentrifuge (Beckamn Coulter) at 80,000 G and 4 °C for 3 hours (AdV2) or 5 hours (MS2). To remove sucrose from solution, the recovered bands containing viruses were washed in an ultrafiltration cell fitted either with a PES 300 kDa NMWL (Millipore) membrane (AdV2) or regenerated cellulose 10 kDA NMWL (Millipore) membrane (MS2) using 1 mM $NaHCO_3$ (AdV2) or pH 7 ultrapure water (MS2). AdV2 was aliquoted into cryovials and stored at -80 °C. MS2 was stored at 4 °C. The final purified virus stocks measured 3.4 x 10^9 PFU/mL (AdV2) and 5.6 x 10^{12} PFU/mL (MS2).

7.2.3. Virus inactivation experiments

Virus inactivation experiments were designed to yield enough protein for analysis by SDS-PAGE and enough genetic material for analysis by PCR. In general, the concentration of viruses used in the reaction was set relatively high (2 x 10^8 PFU/mL for AdV2, 6 x 10^{11} PFU/mL for MS2), and the concentration of TiO_2 kept relatively low (50 mg/L) to prevent adsorptive losses. Viruses, ultrapure water, and $NaHCO_3$ (AdV2 only, final 1 mM) were combined in a Pyrex® Erlenmeyer flask, stirred briefly, and sampled to establish the baseline virus titer and serve as positive control. TiO_2 was added and the mixtures stirred under dark condition for 20 minutes to allow for adsorption equilibrium to occur. The flasks were then placed in a photoreactor (Luzchem) fitted with 4 UV-A bulbs (8W, peak emission 350 nm, Hitachi) on opposing sides of the reactor and timed samples taken for enumeration and/or analysis by SDS-PAGE and PCR. The

UV-A intensity in the reactor measured 3 mW/cm^2 and the temperature was 25.4 ± 0.4 °C.

7.2.4. Sodium dodecyl sulfate polyacrylamide gel electrophoresis (SDS-PAGE)

Virus samples from inactivation experiments were taken in 3.5 mL volumes and centrifuged at 6,000 G for 10 minutes to remove TiO_2. 3 mL supernatant was recovered from each sample and spiked with either bovine serum albumin (BSA, Sigma-Aldrich), carbonic anhydrase (CA, Sigma-Aldrich) or DNase I (LongLife™, G-Biosciences) as an internal standard. Where noted, the recovered 3 mL supernatants were untreated or treated with 0.1 – 0.2% SDS, 1-5% Na-deoxycholate, 0.1% Tween-20, or 113.3 units of DNase I (1.5 hour incubation). The virus solutions were concentrated by a factor of ~10 using centrifugal ultrafiltration units with 10 kDa NWML regenerated cellulose membranes (Amicon® Ultra-4, Millipore). The recovered concentrates were then mixed with 4X Laemmli sample buffer (Bio Rad) containing β-mercaptoethanol (Bio Rad) and denatured in boiling water for 4 minutes. The samples were immediately cooled on ice and analyzed or stored at -20 °C for later analysis. SDS-PAGE runs were conducted using 4-20% gradient 10 x 8 cm Precise tris-glycine gels (Pierce Protein Products) ran at 150 V in a Mini-PROTEAN® gel tank (Bio Rad) filled with tris/glycine/SDS running buffer (Bio Rad).

Gels were stained with Sypro® Ruby Protein Gel Stain (Invitrogen) using the rapid protocol recommended by the manufacturer. Protein bands were visualized using a Fluorchem™ 5500 (Alpha Innotech) imaging system and analyzed using Alpha View SA 3.3.0 software (Cell Biosciences, Inc.). Two independent inactivation experiments were

conducted for protein analysis and samples from each experiment were run by SDS-PAGE three times. The band densities from each run were adjusted based on the intensity of the internal standard and were normalized to the corresponding band densities of non-irradiated (dark stirred) samples. The normalized values were then averaged and the 95% confidence intervals of the data determined. For correlation of band density values with virus survival data, band density values from each experiment and SDS-PAGE run were averaged together.

7.2.5. Polymerase chain reaction (PCR)

Virus samples from inactivation experiments were taken in 1.1 mL volumes and centrifuged at 6,000 G for 10 minutes to remove TiO_2. 1 mL supernatant was recovered from each sample and incubated with 110 units DNase I at room temperature for 1.5 hours. The solution was then concentrated as done for samples prepared for SDS-PAGE analysis. Virus solutions which were treated with DNase or untreated were also made and analyzed to determine if DNase caused DNA damage. The samples were heated at 65 °C for 10 minutes to inactivate the DNase before extracting the DNA.

AdV2 DNA was extracted using a QIAamp MinElute Virus Spin Kit (Qiagen) according to the manufacturer's protocol without the addition of carrier RNA. DNA concentrations were measured by fluorescence spectroscopy (ex. 497 nm, em. 520 nm) on a Tecan Infinite F500 plate reader using SYBR Green dye and serial dilutions of λ Mix Marker 19 (Fermentas) as a standard. Adenovirus DNA concentrations for each treatment were normalized and used as template for real-time quantitative PCR (RT-qPCR) on an ABI 7500 system. Each 25 µl PCR reaction consisted of 12.5 µl of Power

SYBR Green PCR Master Mix, 1.25 µL of forward primer, 1.25 µL of reverse primer, 0.5 ng of template DNA, and nuclease-free molecular grade water. The primer sequence used for amplification was the same used by [60]. PCR reaction conditions were as follows: 50 °C for 2 minutes, an initial activation step of 95 °C for 10 minutes, and 40 repetitions of denaturation (95 °C for 15 seconds), annealing (56 °C for 30 seconds), and elongation (72 °C for 90 seconds). Fluorescent measurements were taken at the end of each elongation step (total 40). The data was analyzed using Applied Biosystems 7500 System SDS v1.2 software. RT-qPCR products from dark stirred and 15 minute irradiated samples were analyzed using agarose gel electrophoresis to ensure proper amplification. SYBR Safe DNA gel stain was added directly to a 1% agarose gel prior to solidification. DNA bands were visualized under UV illumination. PCR product sizes were determined through comparison with a standard 500 bp DNA ladder (Fermentas). Products formed a single, sharp band of the appropriate size, 1 kb.

Two independent inactivation experiments were conducted for DNA analysis and samples from each experiment were run in duplicate by PCR two times. A sample of untreated virus stock containing 0.05 ng DNA and a sample of PCR reaction solution without template DNA were run with all virus samples as controls. Cycle 24 was chosen for analysis of DNA damage, where the amplification curve was just below the top of the exponential phase for each sample and the greatest difference between the non-template control and virus sample signals was observed. The background intensity value (non-template control) was subtracted from the intensity value for each sample. Samples from each experiment and PCR replicate were analyzed by normalizing the signal intensity to the signal intensity from the non-irradiated samples (dark stirred) that corresponded to the

same inactivation experiment and PCR replicate. The normalized values were used to calculate the lesions/kb for each experiment and PCR replicate [186], which were then averaged and the 95% confidence interval determined. For correlation of DNA damage with virus survival data, the raw fluorescent intensity values for all experiments and PCR replicates were averaged together.

7.3. Results and discussion

7.3.1. Virus inactivation kinetics

Virus inactivation experiments conducted for assaying protein damage of AdV2 and MS2 were designed to yield enough protein for analysis by SDS-PAGE and enough genetic material for analysis by PCR. In general, the concentration of viruses used in the reaction was set relatively high (2×10^8 PFU/mL for AdV2, 6×10^{11} PFU/mL for MS2), and the concentration of TiO_2 kept relatively low (50 mg/L) to prevent adsorptive losses. Viruses were assayed with catalyst particles in suspension, but particles were removed before performing biochemical assays in order to prevent interferences. The inactivation kinetics of AdV2 and bacteriophage MS2 are shown in Figure 7-1.

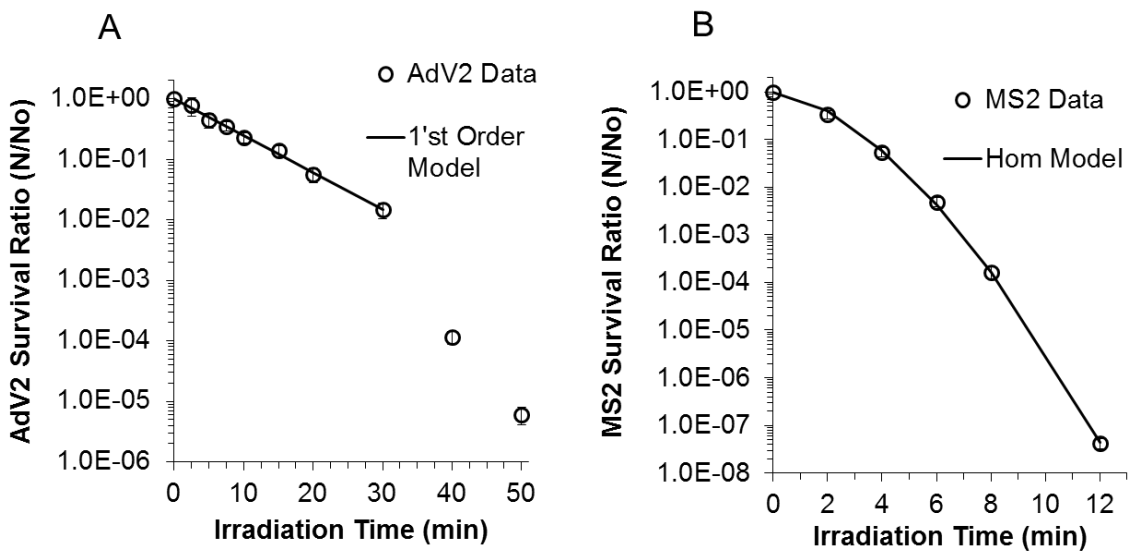

Figure 7-1 - Inactivation kinetics of AdV2 and MS2 under conditions used for assaying protein and genetic damage. AdV2 kinetics follow a 1st order profile for the first 30 min. (k_N = 0.141, R^2 = 0.99). MS2 data is best described using the Hom model with C = 50 mg L^{-1}, k = 1.94 x 10^{-4} mg^{-n} L^n min^{-m}, n = 1.66, m = 1.64 (R^2 = 0.99). Applied AdV2 = 2 x 10^8 PFU/mL, Applied MS2 = 6 x 10^{11} PFU/mL, [TiO_2] = 50 mg/L, UV-A intensity = 3 mW/cm^2, pH 7.8 1 mM $NaHCO_3$ (AdV2) or pH 5.5 ultrapure water (MS2).

Equation 7-1

$$Log\, {}^{N}/_{N_0} = -kC^n t^m$$

Consistent with the results of Chapter 5, the inactivation kinetics of AdV2 are much slower than MS2. Although in the present study MS2 inactivation was not conducted in 1 mM bicarbonate which may scavenge some HO• and slow inactivation, the kinetics are comparable to our previous study where 4-log_{10} inactivation occurred in 10 minutes with 50 mg/L P25 TiO_2, 1.5 mW/cm^2 UV-A, pH 7.8 1 mM $NaHCO_3$. Thus,

the difference in kinetics observed in Figure 7-1 is not due to the $NaHCO_3$ present in the AdV2 reaction mixture. Both the AdV2 and MS2 display an initial lag in the kinetics. The AdV2 kinetics display a 1st order profile (Equation 7-2, $k_N = 0.141$ min^{-1}, $R^2 = 0.99$) up to 30 minutes (2-$\log_{10}$) inactivation, after which the kinetics abruptly become more rapid. The shoulder in the MS2 kinetics displays a smoother profile and the inactivation rate gradually increases with time. The MS2 kinetic profile is best described ($R^2 = 0.99$) using the Hom Model (Equation 7-1) [175] with $C = 50$ mg L^{-1}, $k = 1.94 \times 10^{-4}$ mg^{-n} L^{n} min^{-m}, $n = 1.66$, $m = 1.64$. The presence of the initial lag in kinetics for both AdV2 and MS2 is most likely due to multiple ROS attacks required for inactivation [175] and/or saturation of the catalyst particles due to the high virus titers used in the reaction solution (Chapter 4). Assays for protein and genetic damage are conducted for each virus to determine the mechanism responsible for the vast difference in inactivation kinetics between AdV2 and MS2.

7.3.2. Assays for adenovirus protein damage caused by photocatalytic oxidation

SDS-PAGE is used to assay damage of viral proteins, similar to that described by [10]. While this technique is not sensitive enough to identify minor oxidations which may lead to virus inactivation [71], it can give an indication to which proteins are more susceptible to major damage (i.e. cleavage, cross linking). When proteins suffer major damage, their migration in the protein gel is altered which results in a reduction in the protein band intensity (at normal position). Therefore, a reduction in intensity of a specific protein band after inactivation is an indication that the specific protein has undergone extensive damage. Protein bands were identified based on their molecular weight and descriptions available in the literature [187-192].

Initial SDS-PAGE analysis of inactivated AdV2 showed that samples treated with photocatalytic oxidation were severely aggregated, even after denaturation in SDS – βME sample buffer (Figure 7-2). Viruses that had been stirred with TiO_2 but not irradiated did not display aggregation. Core proteins (V and VII) did not aggregate, indicating that capsid proteins primarily comprise the aggregated protein fraction. The dark stir (un-irradiated) sample was ran at 1/2 and 1/10 volume to show which proteins produced a linear signal over 1 order of magnitude. Only protein II (hexon) is present in sufficient quantity.

One possibility explaining the observed aggregation of capsid proteins is protein oxidative induced cross-linking [193]. If two or more hexon subunits (109 kDa each) are crosslinked, the combined molecular weight would place the band at the very top of the gel / bottom of the sample well, depending on the number of connected subunits. Such crosslinking could disrupt the release of DNA from the capsid into the host cell nucleus, effectively resulting in inactivation. A second possibility explaining the aggregation is that oxidation changes the conformation of the capsid proteins. This may cause internal hydrophobic amino acid residues to face the outer surface, which may then form strong interactions with the hydrophobic residues on other proteins / peptides [194]. To test this possibility, virus samples were pre-treated with detergents (SDS, Na-deoxycholate, or Tween-20) to disrupt hydrophobic interactions before concentration and denaturation with SDS-PAGE sample buffer [190, 195]. Detergent pre-treatment did not reduce the observed aggregation (data not shown), indicating that conformation change induced hydrophobic interaction is not responsible.

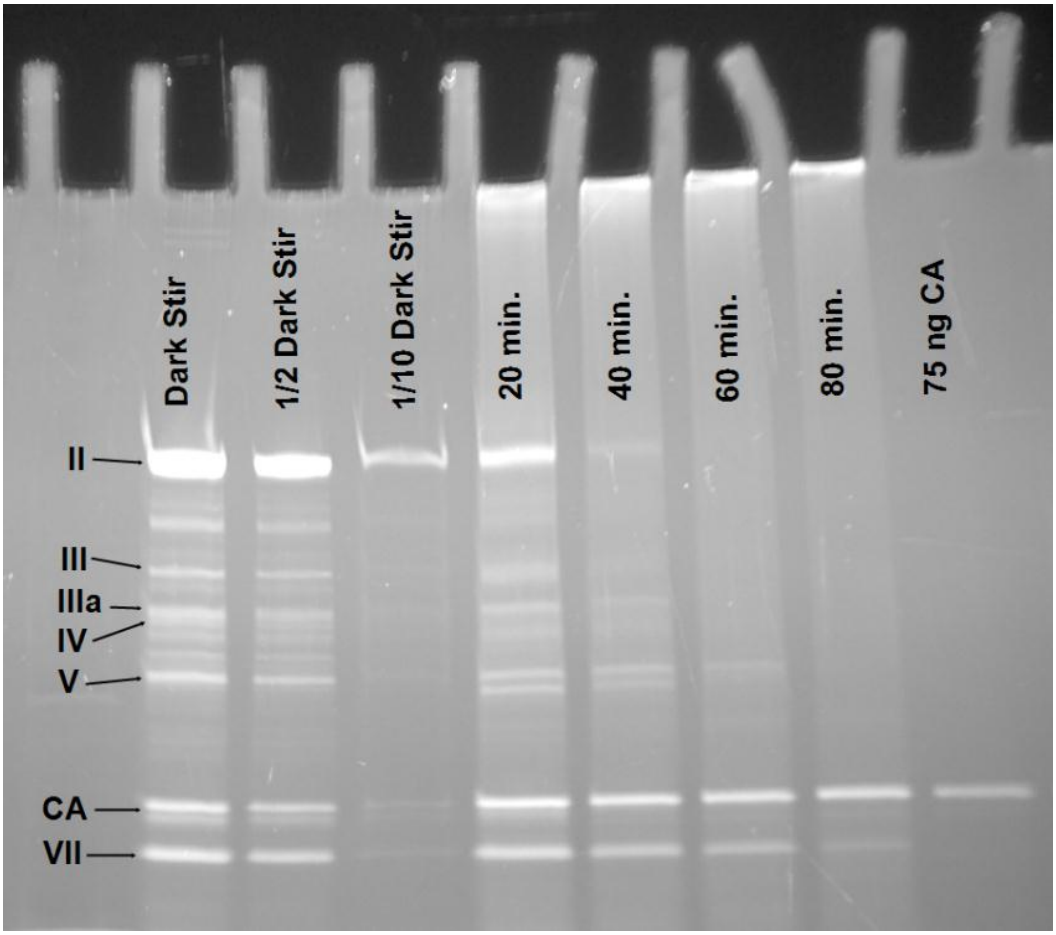

Figure 7-2 - Protein gel of AdV2 treated by photocatalytic oxidation. Severe aggregation is observed in irradiated samples (20 – 80 min.), as a large fraction of the protein remains at the bottom of the sample well and streaking is present throughout the lanes. The dark stir (un-irradiated) sample was ran at 1/2 and 1/10 dilution to verify linear signal over 1-order of magnitude. AdV2 proteins II – VII were identified. CA (carbonic anhydrase) is used as an internal standard.

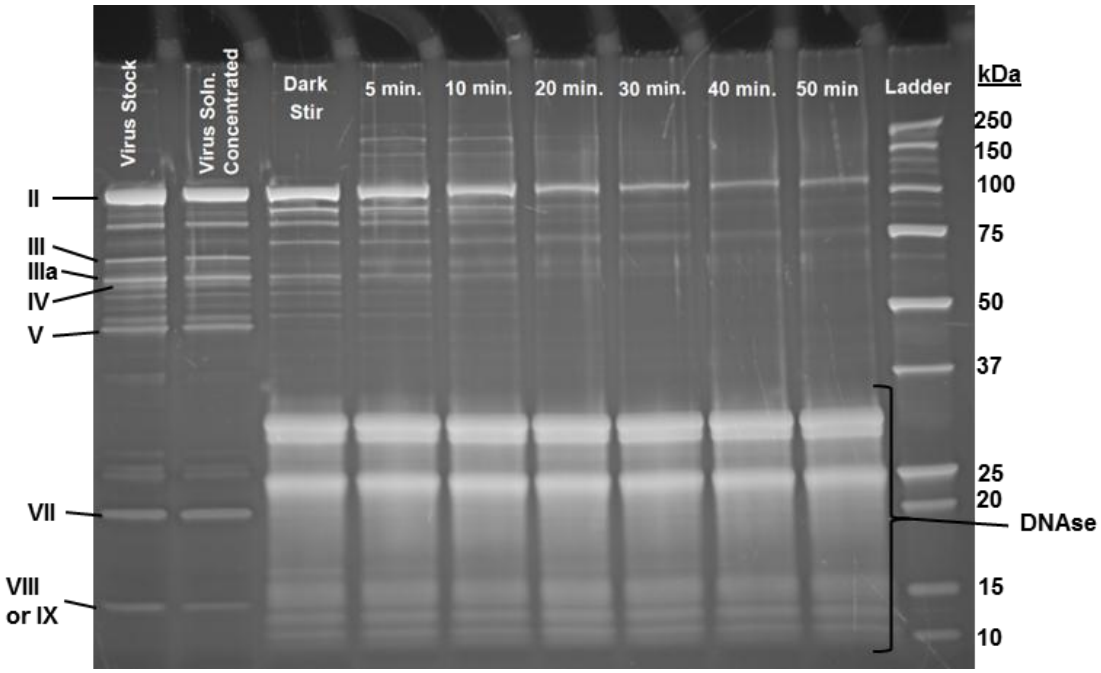

Figure 7-3 - Protein gel of AdV2 treated by photocatalytic oxidation when samples are incubated with DNase before denaturation with SDS-PAGE sample buffer. No aggregation is apparent in the sample wells. Faint bands of higher molecular weight than normal AdV2 proteins are apparent in the lanes ran with 5 and 10 min. treated viruses. A decrease in hexon band intensity is apparent over all treatment times. DNase causes severe interference with lower molecular weight proteins, and the upper DNase band is used as the internal standard.

A third possibility explaining the observed aggregation of capsid proteins after photocatalytic oxidation is crosslinking between viral DNA released from broken capsids and capsid proteins. Even small amounts of DNA are known to cross-link adenoviral particles, resulting in aggregation [190]. To test this possibility, virus samples were incubated with DNase to digest free DNA and eliminate the possible crosslinking between DNA and proteins / peptides. The results, shown in Figure 7-3, reveal that aggregation is eliminated after treatment with DNase, indicating that the observed aggregation (Figure 7-2) is due to protein crosslinking with released DNA. This provides

strong evidence that photocatalytic oxidation breaks open AdV2 capsids and exposes the internal DNA. Damage to virus capsids of this severity is likely to cause inactivation. Since virus stock, concentrated virus solution, and virus samples which had only been dark stirred with TiO_2, but not irradiated, did not aggregate (Figure 7-2), it is not possible that any DNA remaining in the virus stock, that the concentration procedure, or that some interaction with non-irradiated TiO_2 particles caused the aggregation. Therefore, photocatalytic oxidation breaks the AdV2 capsids open, releasing DNA. This result is consistent with a study of ozone disinfection of adenovirus that showed the capsids break open during the disinfection process [11].

Some oxidation induced crosslinking of proteins is apparent in Figure 7-3. The lanes corresponding to 5 and 10 minute treated samples reveal some higher molecular weight proteins are formed at approximately 150 and 200 kDa. This is likely due to crosslinking between hexon (II) subunits (109 kDa each) with themselves or with penton base (III) subunits (63 kDa each) or protein IIIa (63 kDa). Crosslinking in this manner could lead to inactivation of the viruses if it disrupts attachment to host cells or disrupts transfer of the viral genome to the host cell nucleus.

As shown in Figure 7-2 and Figure 7-3, only protein II (hexon), the major capsid protein, is present in a concentration high enough to produce a signal over 1-order of magnitude. Overloading the gel with sample to increase the band densities of other AdV2 proteins resulted in interferences from the DNase solution at higher molecular weights and from extraneous proteins remaining in the purified virus stock. As such, only the band density values for hexon were measured for analysis. Figure 7-4 shows the hexon band density decreases with a 1^{st} order profile (Equation 7-3, $k_H = 0.038$, $R^2 =$

0.97), similar to the AdV2 inactivation kinetics for the first 30 minutes of inactivation (Figure 7-1). After 50 minutes of irradiation, only 13% of the hexon band density remains. Hexon is the major adenovirus capsid protein. Severe damage to this protein would break open the capsid structure causing release of DNA, as is apparent from elimination of aggregation after incubation of samples with DNase (Figure 7-3).

Eischeid and Linden (2011) used SDS-PAGE to identify protein damage to AdV2 after MP UV irradiation [10]. Their study shows significant damage to hexon (and other) proteins, but only after MP UV doses (186 – 300 mJ/cm^2) far exceeding those required to produce 5-log$_{10}$ inactivation (40 mJ/cm^2). While SDS-PAGE methods are not capable of identifying minor oxidations which may lead to inactivation [71] and which likely occur from MP UV irradiation (due to the high inactivation efficiency), our data shows photocatalytic oxidation produces more major (i.e. cleavage) hexon protein damage for a given virus inactivation level. Apparently, such severe damage does not lead to an increased level of AdV2 inactivation. Eischeid and Linden's (2011) study showed damage also occurred to AdV2 fibre (IV) and core proteins, which are responsible for host interactions and regulating lifecycle processes, respectively [10]. AdV2 may be more susceptible to minor damage of these proteins, which we were unable to assay for, as discussed above. It is possible that these proteins are relatively resistant to photocatalytic oxidation, either through their amino acid profile or location in the virions, and therefore AdV2 inactivation by photocatalytic oxidation requires significant hexon damage to occur. An examination of the AdV2 cell infection process reveals that hexon proteins are destabilized after entry into cells in order to enable release of genomic material into the cell nucleus [189]. Oxidative damage to hexons could disrupt their

conformation and destabilize them, but may not lead to inactivation since destabilization is normal for cellular infection to proceed. Significant damage to the capsid structure may be required to expose core proteins and/or DNA to ROS before inactivation occurs.

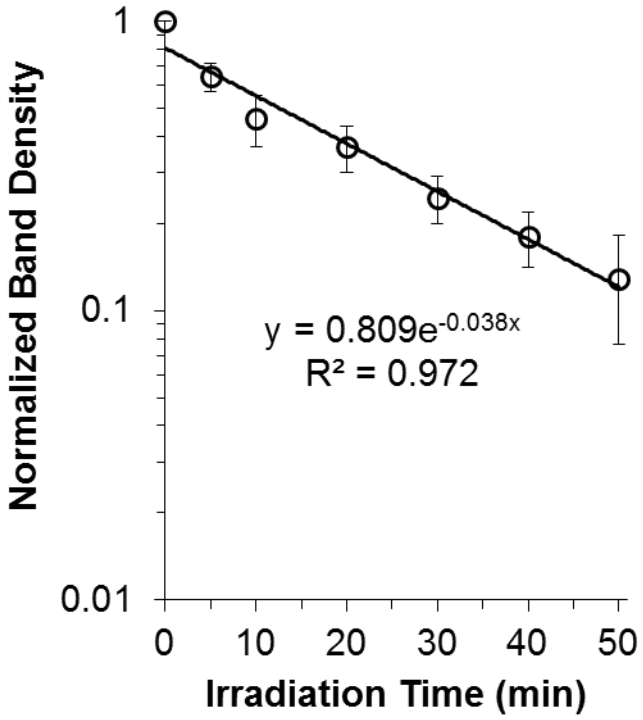

Figure 7-4 - Reduction in AdV2 hexon (protein II) band density with increasing treatment time. Decrease in band density follows a first order profile.

Since both AdV2 survival and hexon band density decrease according to 1st order profiles (Equation 7-2 and Equation 7-3), a relation can be formulated (Equation 7-4) which relates the survival with the hexon band density. In these equations N is the virus titer (PFU/mL) at time, t (min), N_0 is the initial virus titer, H is the hexon band density at t, H_0 is the initial hexon band density, k_N (min^{-1}) is the 1st order rate constant for AdV2 survival, and k_H (min^{-1}) is the 1st order rate constant for hexon band density. Figure 7-5

shows a plot of *H/N* data values vs. time and a plot of Equation 7-4 ("model") using the 1st order rate constants for survival and hexon density shown in Figure 7-1 A and Figure 7-4, respectively. Equation 4 fits the data well ($R^2 = 0.88$), indicating a strong relationship between hexon band density and virus survival. The data can also be plotted directly against each other (Figure 7-6) to further show that AdV2 survival is directly related to the hexon band density during photocatalytic oxidation. These analyses provide strong evidence that photocatalytic oxidation inactivates AdV2 through damage to the virion capsids.

Equation 7-2

$$N = N_0 e^{-k_N t}$$

Equation 7-3

$$H = H_0 e^{-k_H t}$$

Equation 7-4

$$\frac{H}{N} = \frac{H_0}{N_0} e^{-(k_H - k_N)t}$$

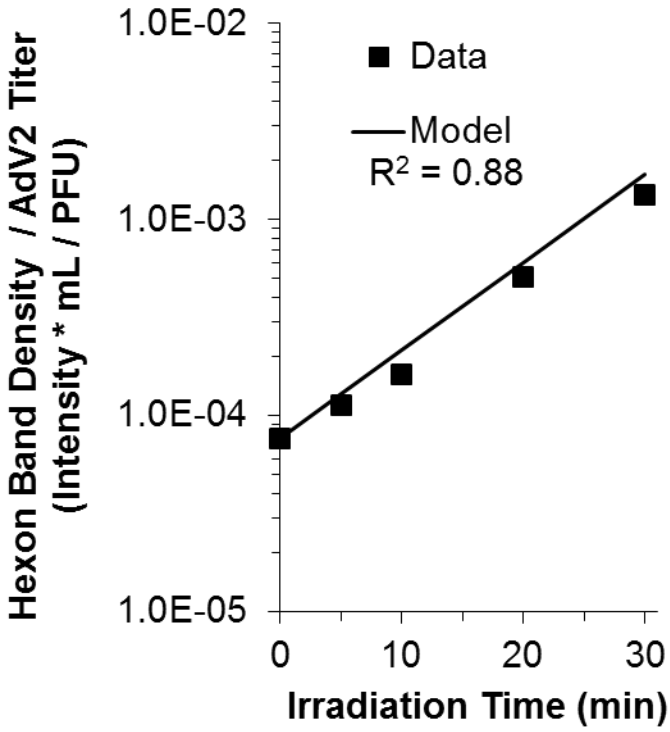

Figure 7-5 - Plot of relationship between AdV2 survival and hexon band density (Equation 7-4 – "model") as a function of time.

7.3.1. Assays for damage to adenovirus DNA

The reaction conditions used to assay for genetic damage of AdV2 are the same as those used for assaying protein damage. Since the protein damage assays reveal that viral capsids break open and release DNA when photocatalytically oxidized, we only analyzed samples within the first 15 minutes of irradiation (~ 1 $\log_{10}$ inactivation) since the DNA available for analysis decreases as more capsids break. In addition, samples were treated with DNase to remove free DNA from solution before DNA extraction was carried out. DNA released from capsids into solution is likely subject to increased oxidation and would skew the results to show increased DNA damage with treatment time if this

fraction of were included in the assay. Treatment with DNase ensures that the DNA analyzed only corresponds to intact virions, which may or may not be inactivated.

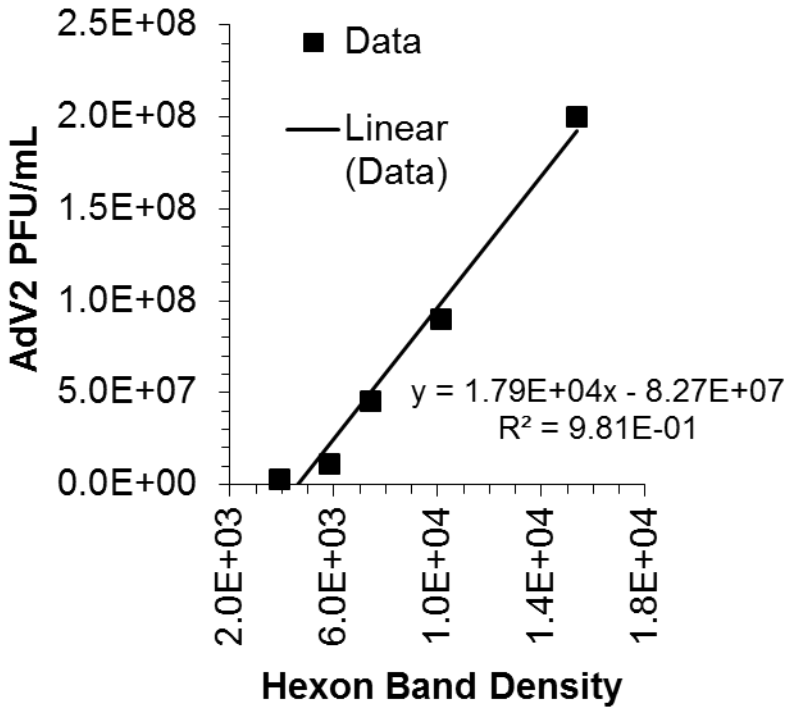

Figure 7-6 - Plot of AdV2 titer vs. hexon band density show a linear relationship between the two variables.

Equal amounts of DNA (0.5 ng) from each sample were analyzed by real-time PCR. The fluorescent intensity values at cycle 24 were chosen for analysis. The amplification curves for all samples (and 1/10 and 10x DNA content controls) were near the top of the exponential phase at this cycle and intensity signals were maximized against background. The lesions per kilobase (kb) of the strands were calculated as shown in Equation 7-5 [186]. Here *I* is the background corrected signal intensity measured for

each sample well and I_0 is the background corrected signal intensity measured for virus samples stirred with TiO_2 under dark condition.

Equation 7-5

$$lesions/kilobase = \frac{-\ln\left(\frac{I}{I_0}\right)}{Amplicon\ Length\ (kb)}$$

Figure 7-7 shows the DNA lesions per kilobase (kb) of AdV2 genomes as a function of irradiation time. The lesions/kb are calculated for each PCR run from each independent inactivation experiment, and the results averaged and 95% confidence intervals determined from the data. The lesions increase most rapidly during the first 2.5 minutes of irradiation, and then slowly increase to 1.4 lesions/kb at 15 minutes irradiation time, corresponding to 86% inactivation. Eischeid et al. (2009) performed a similar analysis for the UV inactivation of AdV2 [60]. In their study, ~99% inactivation corresponded to a DNA damage of 1.4 lesions/kb when using UV_{254} irradiation, which only causes genetic damage. Based on DNA damage alone, we should observe greater inactivation than 86%. Since our study shows a 60% reduction in hexon protein (Figure 7-4) along with 1.4 lesions/kb at 86% inactivation, it is likely that the DNA results are skewed despite DNase treatment, as inactivation should be higher. It is possible that a fraction of virions have breaks in the capsid structure smaller than 4 nm in diameter, the approximate minimum size of DNase (33kDa) [196]. These breaks could allow easy access for ROS to enter the capsid and cause severe DNA damage past that required for

inactivation, but prevent DNase from removing this material before PCR analysis. The consequence of this would be an increase in the measured DNA damage. Equation 7-5 was also derived assuming an equal distribution of genetic damage [186], which may not hold in this system since capsids exist in fractured and unfractured states and may be prone to differing levels of DNA damage.

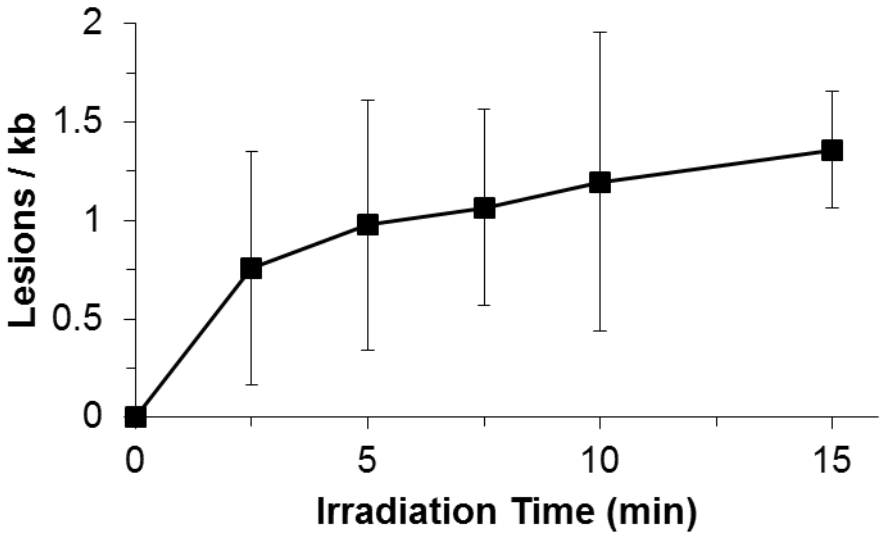

Figure 7-7 - AdV2 DNA lesions/kb as a function of irradiation time as determined by PCR assay.

Despite the likelihood of the DNA damage data being skewed, the correlation between AdV2 titer and the raw amplified DNA fluorescence values at PCR cycle 24 were analyzed using Figure 7-8. The plot of AdV2 titer vs. amplified DNA fluorescence values is bet fit using a logarithmic function, indicating survival decreases more rapidly

with a decreasing amount of DNA damage at longer irradiation times. While this weakens the possibility that AdV2 inactivation is solely due to genetic damage during photocatalytic oxidation, we cannot rule out that DNA damage plays an important role in the process. Indeed, it may be that inactivation proceeds by first breaching the capsid structure through damage to hexons followed by damage to the DNA and core regulatory proteins by ROS. This inactivation mechanism is shown in Figure 7-9. Damage to both core proteins and DNA may produce faster inactivation than damage to DNA alone, which may explain the logarithmic relationship observed in Figure 7-8.

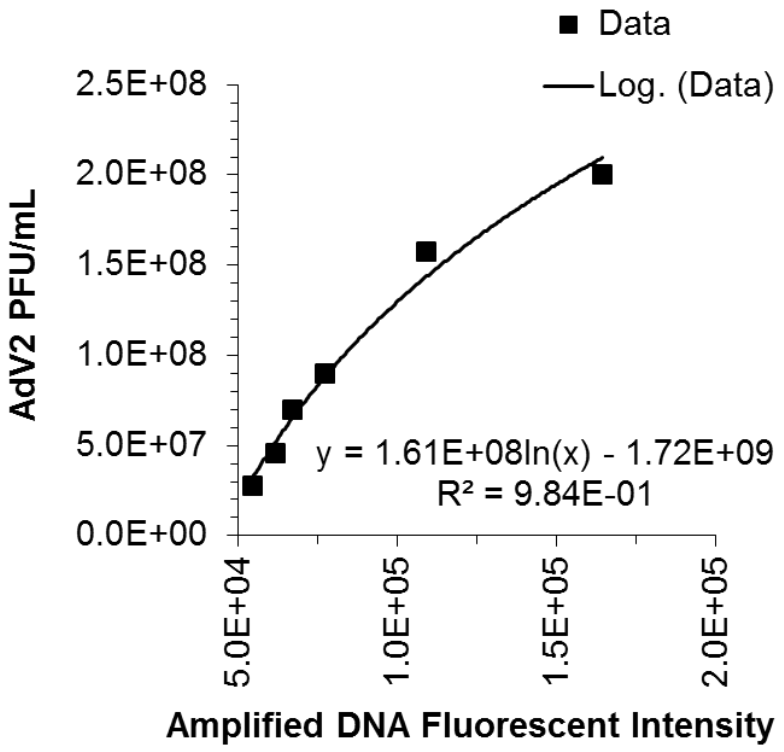

Figure 7-8 - Plot of AdV2 titer vs. amplified DNA fluorescent intensity at PCR cycle 24. The data are best fit using a logarithmic function, indicating reduced sensitivity of survival to decreasing amounts of undamaged DNA in photocatalytically oxidized virus samples.

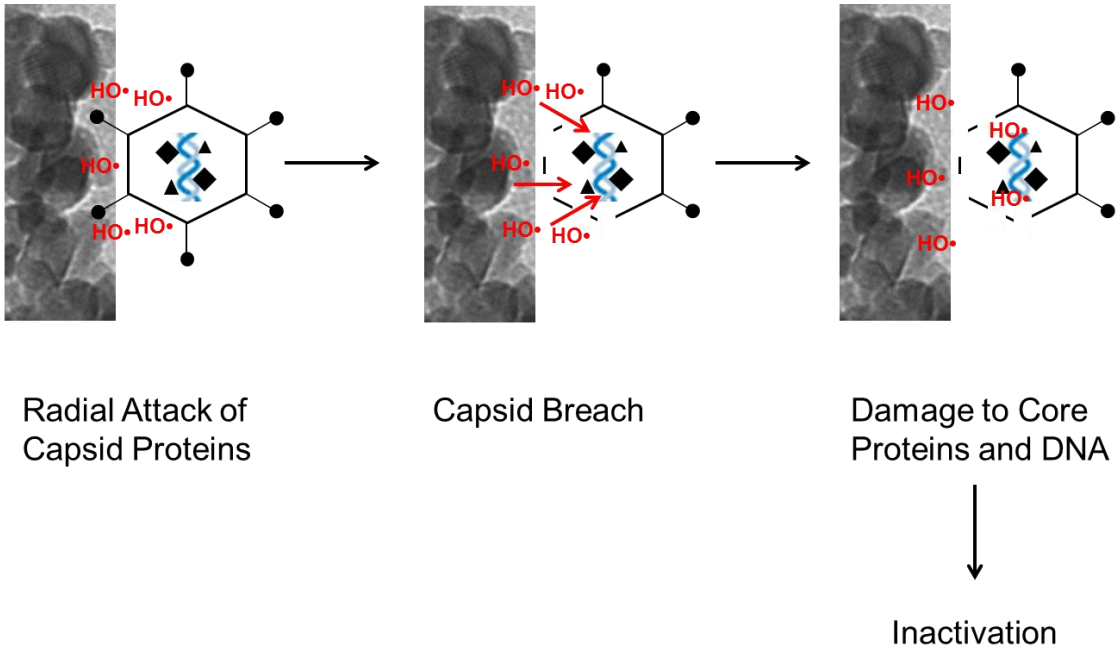

Figure 7-9 – Proposed inactivation mechanism of AdV2 by TiO_2 photocatalytic oxidation.

7.3.2. Assays for MS2 protein damage caused by photocatalytic oxidation

The inactivation kinetics of MS2 are much faster than AdV2 (Figure 7-1), suggesting that inactivation of MS2 occurs through a different mechanism than AdV2. Figure 7-10 shows protein gels used to assay damage to the two proteins present in MS2: coat and A. Due to the differences in content of these proteins in each virion, and to the presence of low molecular weight extraneous proteins in the purified virus stock, separate gels were ran using different amounts of sample to analyze the coat and A proteins separately. Figure 7-10 A, used for analysis of A proteins, was ran using 10 times the sample volume as Figure 7-10 B, which was used for analysis of coat proteins. Taken together, both gels show at least 1 order of magnitude signal range for the A protein. A

plot of the A and coat protein band density values corrected by the band density values of the BSA internal standard is shown in Figure 7-11.

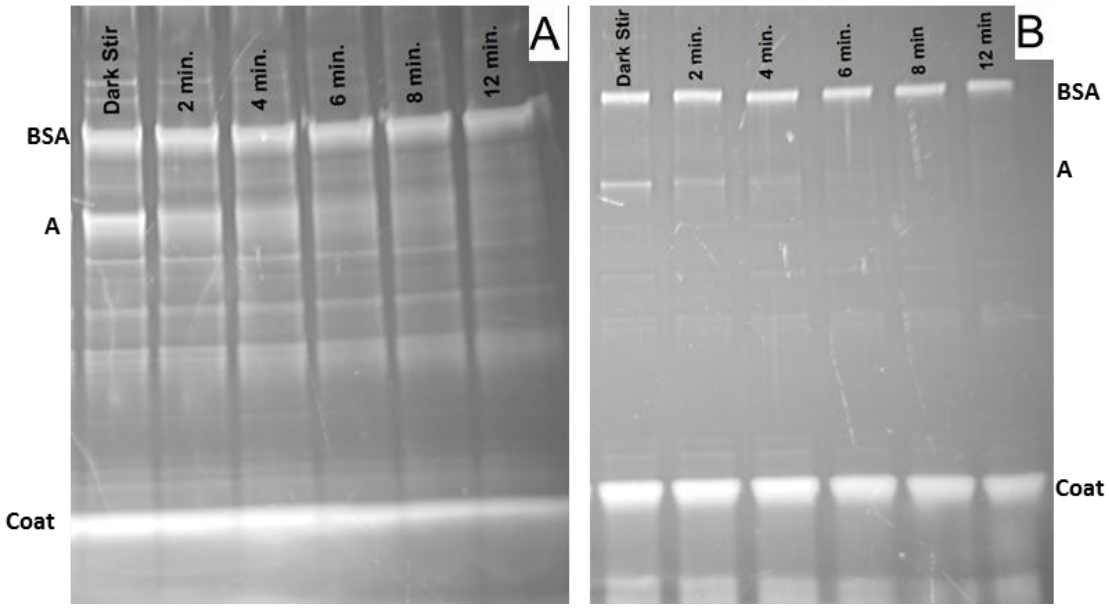

Figure 7-10 - Protein gel of MS2 treated by photocatalytic oxidation. Gel (A), used for analysis of the MS2 A protein, was ran using 10 times the sample volume as gel (B), which is used for analysis of the MS2 coat protein. The band corresponding to the A protein in (A) is rapidly reduced in density. The band corresponding to the coat protein in (B) is relatively unchanged (after accounting for differences in internal standard (BSA) density). The band corresponding to the A protein is present in both (A) and (B), confirming the protein is present in sufficient quantity to provide a signal over 1 order of magnitude.

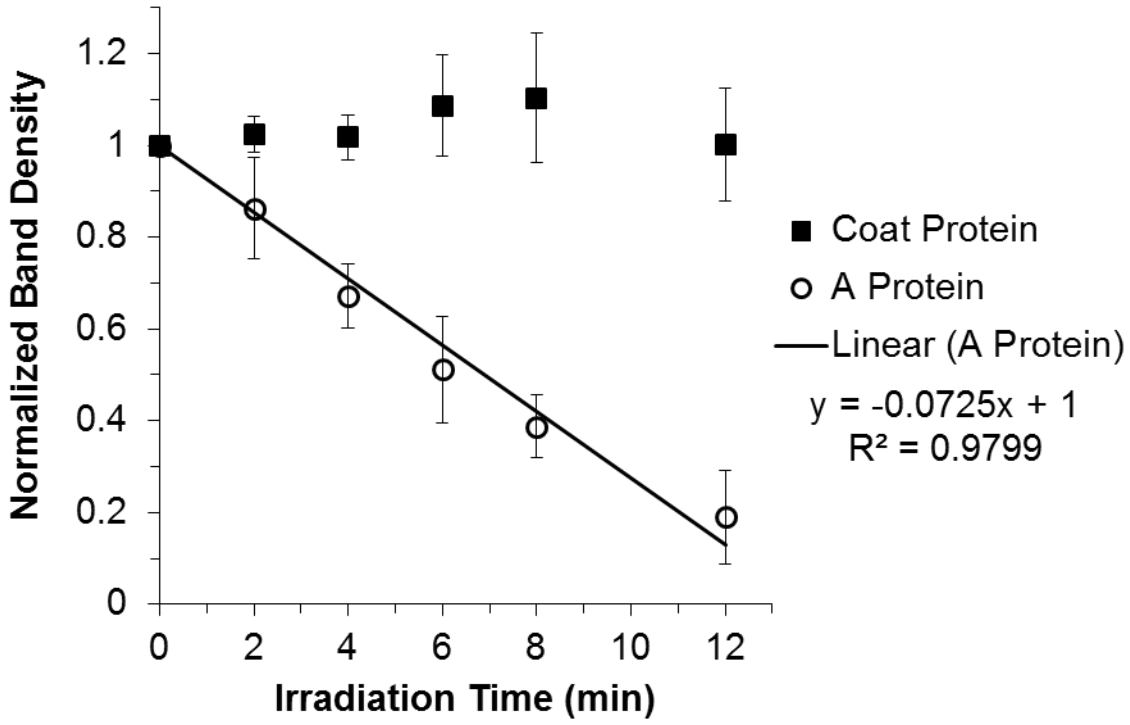

Figure 7-11 - Plot of MS2 coat and A protein band densities as a function of irradiation time shows A protein is susceptible to photocatalytic oxidation while the coat protein is not majorly damaged during the inactivation time.

As shown in Figure 7-10 and Figure 7-11, the MS2 A protein undergoes extensive damage, while the major capsid protein, coat, is unchanged (after accounting for differences in BSA density). The proposed inactivation mechanism is shown in Figure 7-12. The A protein is responsible for attachment of virions to the *E. coli* pili and is injected into the host cells along with the RNA to perform regulatory functions [33, 34]. Significant damage to the A protein could prevent MS2 virions from recognizing its host or disrupt lifecycle events after infection. Either possibility would result in inactivation. While no major (i.e. cleavage) damage was found to occur to the coat protein over the treatment time, it is possible that minor damage occurs. This minor damage may cause a

change in conformation of the coat proteins, which could then obscure the A protein and prevent it from interacting with host cells. This additional mechanism may then explain why inactivation is a (nearly) first order process while the A protein degrades according to a zero order profile. Regardless, the extreme susceptibility of the A protein to photocatalytic oxidation is the likely reason why the MS2 inactivation kinetics are much faster than the AdV2 kinetics. AdV2 apparently requires significant and extensive damage to its major capsid protein, hexon, to occur before being inactivated.

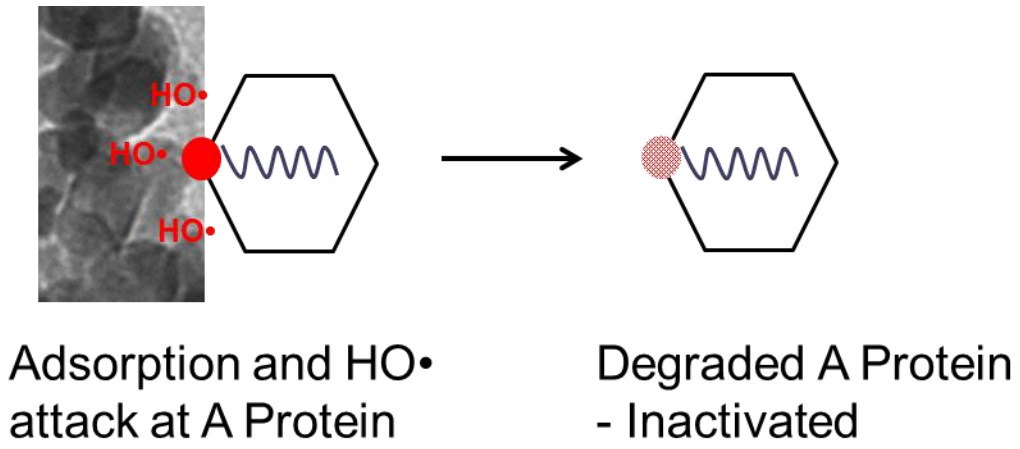

Figure 7-12 – Proposed inactivation mechanism of MS2 by TiO_2 photocatalytic oxidation.

The reason for the high susceptibility of the MS2 A protein to damage by photocatalytic oxidation is not clear. Studies of protein and peptide susceptibility to damage by TiO_2 and HO• reveal that cleavage preferentially occurs at proline, glycine, and alanine residues, and that side chain oxidations are preferential at valine and leucine residues [78, 79, 123]. Proline, glycine, and alanine comprise 20% and valine and

leucine comprise 17% of the A protein [153]. The coat protein contains a similar content of these residues; proline, glycine, and alanine comprise 23% and valine and leucine comprise 17% of the coat protein [197]. Based on the content of these proteins, the coat should be slightly more susceptible than the A protein to cleavage by photocatalytic oxidation, however no major damage to the coat protein is observed (Figure 7-10 and Figure 7-11).

It is possible that MS2 preferentially adsorbs to TiO_2 at the A protein, causing it to be exposed to a higher concentration of ROS and thus be damaged more rapidly than the rest of the capsid. There is some evidence to support this hypothesis. While the exact location of the A protein is unknown, it is known to be (partially) exposed on the capsid surface and is thought to be located at a vertex of the icosahedron [34, 36]. Since it is only present in one copy, adsorption of MS2 to TiO_2 at the A protein would prevent it from interacting with host cells through a steric mechanism. In Chapter 3, we observed that the same quantity of MS2 adsorbed to TiO_2 was also inactivated under dark condition, supporting the hypothesis that the MS2 A protein preferentially adsorbs to TiO_2. A study of amino acid adsorption to TiO_2 reveals that the acidic amino acids, aspartatic acid and glutamic acid, formed ordered layers on TiO_2, while amino acids without acidic side chains showed little adsorption affinity [198]. 16.5% of the MS2 A protein is comprised of these residues, while they comprise 19.9 % of the coat protein [153, 197]. Therefore, differences in the content of these residues cannot be used to explain the possibility that the MS2 A protein preferentially adsorbs to TiO_2. Further study is warranted to determine why the A protein is so susceptible to photocatalytic

oxidation, as it may provide insight into the types of proteins (and therefore pathogens) most susceptible to disinfection by photocatalytic oxidation.

7.4. Conclusions

This study has elucidated the mechanisms responsible for the inactivation of AdV2 and bacteriophage MS2 by photocatalytic oxidation. AdV2 is inactivated relatively slowly and requires significant damage to the general capsid structure for inactivation to occur. MS2 is inactivated relatively quickly, as its protein which interacts with host cells is preferentially and rapidly degraded. The differences in kinetics and mechanisms of inactivation of AdV2 and MS2 call into question the suitability of using MS2 as a surrogate pathogenic virus in photocatalytic oxidation disinfection studies. It also calls for further study of why the MS2 protein is so susceptible to degradation. The protein characteristics responsible for this susceptibility may provide insight to the microorganisms that are most susceptible to inactivation by photocatalytic oxidation.

It was initially hypothesized that photocatalytic oxidation would be highly effective for adenovirus disinfection, since studies of other disinfectants (free chlorine, MP UV, ozone) revealed that those causing protein damage lead to the most rapid inactivation [10-13, 60]. Our study shows that AdV2 requires major damage to the capsid hexon proteins before inactivation occurs by photocatalytic oxidation. It is possible that damaging other proteins, which govern virus – host interactions or regulate lifecycle events, is more effective for rapid adenovirus disinfection. Free chlorine damages proteins which govern lifecycle events [12] and MP UV damages both of these protein classes [10], which may explain the high efficiency of these processes. It is not

known if ozone causes other damages besides breaking open adenovirus capsids [11]. Assuming ozone acts solely through hexon damage, the inactivation kinetics may be much faster due to the much higher concentration of ozone used during disinfection than the concentration of ROS produced by TiO_2. Enhancing the ROS production of TiO_2 through catalyst modifications may overcome this limitation and make photocatalytic oxidation more effective for rapid adenovirus inactivation. Despite this, the kinetics of AdV2 inactivation by TiO_2 proceed rapidly enough to develop solar based disinfection systems for cheap and effective water treatment, as shown in Chapter 5. Further study is warranted on the mechanism of AdV2 inactivation by photocatalysts which primarily produce singlet oxygen (e.g. fullerene based materials) vs. those which primarily produce HO• (e.g. TiO_2), since singlet oxygen has been shown to be effective for inactivating AdV2 (Chapter 6).

Chapter 8

Conclusions

Photocatalytic oxidation continues to gain attention as an alternative water treatment process for a wide variety of contaminants, including viruses. Adenoviruses in particular pose a threat to the water supply due to their resistance to other alternative disinfection methods (e.g. UV_{254}, monochloramine). Photocatalytic oxidation is a good candidate adenovirus inactivation, as photocatalysts produce ROS capable of damaging proteins, and the most effective adenovirus disinfectants act through damaging proteins. To make photocatalytic oxidation competitive with other disinfection processes, the catalyst efficiency needs to be increased. In addition, the susceptibility of adenoviruses to this technology and mechanism of inactivation need to be understood to gauge the suitability of photocatalytic oxidation.

Two modifications were developed to improve the virus inactivation kinetics by TiO_2: silver and silica modifications. These modifications enhance the kinetics through different mechanisms. Silver increases the production of HO• and increases virus

adsorption to a small degree, while silica acts solely through a dramatic increase of virus adsorption to the composite catalyst. As reported in the literature, the typical strategy for improving catalyst efficiency is focused around improving ROS production. However, the results obtained with SiO_2-TiO_2 indicate that improving contaminant adsorption to the catalyst is just as an important strategy as improving ROS production. The improvement to the virus inactivation kinetics observed with nAg/TiO_2 and SiO_2-TiO_2 bring photocatalytic oxidation closer to being a viable option for water disinfection. Ultimately, a composite catalyst displaying both improved ROS production and significantly enhanced adsorption properties will be the most effective.

When using P25 TiO_2, the AdV2 inactivation kinetics was much slower than the MS2 inactivation kinetics. Despite this, AdV2 is inactivated in a reasonable time. The silver and silica modifications, which were developed using bacteriophage MS2 as a surrogate, affected AdV2 differently. While nAg/TiO_2 initially improved the AdV2 inactivation kinetics, SiO_2-TiO_2 showed a reduced efficiency, as AdV2 adsorption was not significantly enhanced as compared to MS2. The result suggests that catalyst modifications for increased efficiency need to be developed specifically for the contaminant of concern rather than pursuing a "one size fits all" strategy. The amino-fullerene material proved highly effective for inactivating AdV2 as compared to TiO_2 based materials. This shows that $^1O_2$ is an adequate ROS for inactivating AdV2 despite its lower oxidation potential as compared to HO•. Since amino-fullerene is activated by visible light, this result improves the outlook of developing solar disinfections systems for water disinfection. Solar systems are both a "green" technology and cheap from an

energy input standpoint, making them desirable for both developed and developing communities.

The different inactivation mechanisms of AdV2 and MS2 can explain the large differences in the inactivation kinetics between these two viruses. AdV2 requires significant damage to the capsid structure and possibly further damage to core proteins and DNA before inactivation occurs. In contrast, the MS2 A protein, which interacts with host cells, is rapidly degraded by TiO_2 based photocatalytic oxidation. These results suggest that the key to rapid AdV2 inactivation may specifically through damage to regulatory core proteins rather than through general protein damage. Also, the suitability of MS2 as a surrogate pathogen in photocatalytic oxidation studies is called into question due to its extreme susceptibility to damage at the A protein. Further study on what makes the A protein so susceptible is warranted, as this may provide insight to the types of viruses (and other microorganisms) that may be efficiently disinfected by photocatalytic oxidation. The drastic differences in inactivation mechanisms and kinetics between AdV2 and MS2 implies that studies of the susceptibility of entire spectrum of water-borne viruses to photocatalytic oxidation are required before implementing this method in water treatment systems.

Along with identifying a better surrogate virus and identifying what makes the MS2 A protein so susceptible, other research is needed to further develop photocatalytic oxidation for virus disinfection in drinking water. An effective modification for TiO_2 materials which dramatically increases the adsorption of AdV2 to the catalyst needs to be found. This would enable the development of a catalyst with improved adsorptive and ROS production characteristics, which would lead to great improvement in inactivation

kinetics and a reduction in required energy input. The virus adsorption reaction kinetic modeling in Chapter 4 is a good start for describing photocatalytic treatment systems for virus inactivation; however, a better model is needed to account for the effects of catalyst fouling and competitive adsorption with inactivated viruses and other solution species. It would also be useful to identify the relative effectiveness of HO• and $^1O_2$ for virus inactivation. This requires knowledge of the ROS production rates of each catalyst, and also requires knowledge of the interaction properties of the viruses with the catalyst. Accomplishing this would help guide the further development of catalyst materials and help determine the best materials for implementation in actual treatment systems. Finally, more research is needed on the inactivation kinetics of other pathogenic viruses commonly found in source waters to identify if any are more resistant than adenoviruses. There are few studies on other pathogenic viruses. Identifying the most resistant will aid in setting minimum treatment requirements.

References

1. WHO/UNICEF-JMP, Global water supply and sanitation assessment 2000. **2000**.

2. US Environmental Protection Agency, National primary drinking water regulation: Long-term 2 enhanced surface water treatment rule; Final rule. In Federal Register (40 CFR 9,141,142): 2006a; Vol. 71:3, pp 653-786.

3. US Environmental Protection Agency, National primary drinking water regulations: Stage 2 disinfectants and disinfection byproducts rule; Final rule. In Federal Register (40 CFR 9,141,142): 2006c; Vol. 71:2, pp 387-493.

4. Sirikanchana, K.; Shisler, J. L.; Marinas, B. J., Effect of exposure to UV-C irradiation and monochloramine on adenovirus serotype 2 early protein expression and DNA replication. *Applied and Environmental Microbiology* **2008,** *74*, (12), 3774-3782.

5. Yates, M. V.; Malley, J.; Rochelle, P.; Hoffman, R., Effect of adenovirus resistance on UV disinfection requirements: A report on the state of adenovirus science. *American Water Works Association Journal* **2006,** *98*, (6), 93-106.

6. Liberti, L.; Notarnicola, M.; Petruzzelli, D., Advanced treatment for municipal wastewater reuse in agriculture. UV disinfection: parasite removal and by-product formation. *Desalination* **2003,** *152*, (1-3), 315-324.

7. Richardson, S. D.; Thruston, A. D.; Collette, T. W.; Patterson, K. S.; Lykins, B. W.; Ireland, J. C., Identification of TiO_2/UV disinfection byproducts in drinking water. *Environmental Science & Technology* **1996,** *30*, (11), 3327-3334.

8. Lee, J.; Zoh, K.; Ko, G., Inactivation and UV disinfection of murine norovirus with TiO_2 under various environmental conditions. *Applied and Environmental Microbiology* **2008,** *74*, (7), 2111-2117.

9. Watts, R. J.; Kong, S. H.; Orr, M. P.; Miller, G. C.; Henry, B. E., Photocatalytic inactivation of coliform bacteria and viruses in secondary waste-water effluent. *Water Research* **1995,** *29*, (1), 95-100.

10. Eischeid, A. C.; Linden, K. G., Molecular Indications of protein damage in adenoviruses after UV disinfection. *Applied and Environmental Microbiology* **2011,** *77*, (3), 1145-1147.

11. Murray, B. K.; Ohmine, S.; Tomer, D. P.; Jensen, K. J.; Johnson, F. B.; Kirsi, J. J.; Robison, R. A.; O'Neill, K. L., Virion disruption by ozone-mediated reactive oxygen species. *Journal of Virological Methods* **2008,** *153*, (1), 74-77.

12. Page, M. A.; Shisler, J. L.; Marinas, B. J., Mechanistic aspects of adenovirus serotype 2 inactivation with free chlorine. *Applied and Environmental Microbiology* **2010,** *76*, (9), 2946-2954.

13. Thurston-Enriquez, J. A.; Haas, C. N.; Jacangelo, J.; Gerba, C. P., Inactivation of enteric adenovirus and feline calicivirus by ozone. *Water Research* **2005,** *39*, (15), 3650-3656.

14. Charles, K. J.; Shore, J.; Sellwood, J.; Laverick, M.; Hart, A.; Pedley, S., Assessment of the stability of human viruses and coliphage in groundwater by PCR and infectivity methods. *Journal of Applied Microbiology* **2009,** *106*, (6), 1827-1837.

15. Keswick, B. H.; Gerba, C. P., Viruses in groundwater. *Environmental Science & Technology* **1980,** *14*, (11), 1290-1297.

16. Abbaszadegan, M.; Lechevallier, M.; Gerba, C., Occurrence of viruses in US groundwaters. *Journal American Water Works Association* **2003,** *95*, (9), 107-120.

17. Futch, J. C.; Griffin, D. W.; Lipp, E. K., Human enteric viruses in groundwater indicate offshore transport of human sewage to coral reefs of the upper Florida Keys. *Environmental Microbiology* **2010,** *12*, (4), 964-974.

18. Johnson, T. B.; McKay, L. D.; Layton, A. C.; Jones, S. W.; Johnson, G. C.; Cashdollar, J. L.; Dahling, D. R.; Villegas, L. F.; Fout, G. S.; Williams, D. E.; Sayler, G., Viruses and bacteria in karst and fractured rock aquifers in East Tennessee, USA. *Ground Water* **2011,** *49*, (1), 98-110.

19. Hamza, I. A.; Jurzik, L.; Stang, A.; Sure, K.; Uberla, K.; Wilhelm, M., Detection of human viruses in rivers of a densly-populated area in Germany using a virus adsorption elution method optimized for PCR analyses. *Water Research* **2009,** *43*, (10), 2657-2668.

20. Jiang, S. C., Human adenoviruses in water: Occurrence and health implications: A critical review. *Environmental Science & Technology* **2006,** *40*, (23), 7132-7140.

21. US Centers for Disease Control and Prevention, Surveillance for waterborne disease and outbreaks associated with drinking water and water not intended for drinking - United States, 2003—2004. In Morbidity and Mortality Weekly Report Surveillance Summaries: 2006; Vol. 55(SS12), pp 31-58.

22. US Centers for Disease Control and Prevention, Surveillance for waterborne disease and outbreaks associated with drinking water and water not intended for drinking --- United States, 2005--2006. In Morbidity and Mortality Weekly Report Surveillance Summaries: 2008; Vol. 57(SS09), pp 39-62.

23. US Environmental Protection Agency, National primary drinking water regulations: Ground water rule; Final rule. In Federal Register (40 CFR 9,141,142): 2006b; Vol. 71:216, pp 65574-65659.

24. Butkus, M. A.; Labare, M. P.; Starke, J. A.; Moon, K.; Talbot, M., Use of aqueous silver to enhance inactivation of coliphage MS-2 by UV disinfection. *Applied and Environmental Microbiology* **2004,** *70*, (5), 2848-2853.

25. Koizumi, Y.; Taya, M., Kinetic evaluation of biocidal activity of titanium dioxide against phage MS2 considering interaction between the phage and photocatalyst particles. *Biochemical Engineering Journal* **2002,** *12*, (2), 107-116.

26. Mackey, E. D.; Hargy, T. M.; Wright, H. B.; Malley, J. P.; Cushing, R. S., Comparing Cryptosporidium and MS2 bioassays - implications for UV reactor validation. *Journal American Water Works Association* **2002,** *94*, (2), 62-69.

27. Sobsey, M. D.; Fuji, T.; Shields, P. A., Inactivation of hepatitis A virus and model viruses in water by free chlorine and monochloramine. *Water Science and Technology* **1988,** *20*, (11-12), 385-391.

28. Sommer, R.; Pribil, W.; Appelt, S.; Gehringer, P.; Eschweiler, H.; Leth, H.; Cabaj, A.; Haider, T., Inactivation of bacteriophages in water by means of non-ionizing (UV-253.7 nm) and ionizing (gamma) radiation: A comparative approach. *Water Research* **2001,** *35*, (13), 3109-3116.

29. Tree, J. A.; Adams, M. R.; Lees, D. N., Chlorination of indicator bacteria and viruses in primary sewage effluent. *Applied and Environmental Microbiology* **2003,** *69*, (4), 2038-2043.

30. Russell, W. C., Adenoviruses: update on structure and function. *Journal of General Virology* **2009,** *90*, 1-20.

31. Horne, R. W.; Bonner, S.; Waterson, A. P.; Wildy, P., The icosahedral form of an adenovirus. *Journal of Molecular Biology* **1959,** *1*, 84-86.

32. Knipe, D. M.; Howley, P. M., *Fields Virology*. Lippincott Williams & Wilkins: Philadelphia, PA, 2006.

33. Valegard, K.; Liljas, L.; Fridborg, K.; Unge, T., The 3-dimensional structure of the bacterial-virus MS2. *Nature* **1990,** *345*, (6270), 36-41.

34. Curtiss, L. K.; Krueger, R. G., Localization of coliphage MS2 A-protein. *Journal of Virology* **1974,** *14*, (3), 503-508.

35. Shiba, T.; Suzuki, Y., Localization of a prtoein in the RNA-A complex of phage MS2. *Biochimica et Biophysica Acta* **1981,** *654*, 249-255.

36. O'Callaghan, R.; Bradley, R.; Paranchych, W., Controlled alterations in the physical and biological properties of R17 bacteriophage induced by guanidine hydrochloride. *Virology* **1973,** *54*, (2), 476-494.

37. Albinana-Gimenez, N.; Miagostovich, M. P.; Calqua, B.; Huguet, J. M.; Matia, L.; Girones, R., Analysis of adenoviruses and polyomaviruses quantified by qPCR as indicators of water quality in source and drinking-water treatment plants. *Water Research* **2009,** *43,* (7), 2011-2019.

38. Dong, Y.; Kim, J.; Lewis, G. D., Evaluation of methodology for detection of human adenoviruses in wastewater, drinking water, stream water and recreational waters. *Journal of Applied Microbiology* **2010,** *108,* (3), 800-809.

39. van Heerden, J.; Ehlers, M. M.; Heim, A.; Grabow, W. O. K., Prevalence, quantification and typing of adenoviruses detected in river and treated drinking water in South Africa. *Journal of Applied Microbiology* **2005a,** *99,* (2), 234-242.

40. van Heerden, J.; Ehlers, M. M.; Van Zyl, W. B.; Grabow, W. O. K., Incidence of adenoviruses in raw and treated water. *Water Research* **2003,** *37,* (15), 3704-3708.

41. van Heerden, J.; Ehlers, M. M.; Vivier, J. C.; Grabow, W. O. K., Risk assessment of adenoviruses detected in treated drinking water and recreational water. *Journal of Applied Microbiology* **2005b,** *99,* (4), 926-933.

42. Carducci, A.; Verani, M.; Battistini, R.; Pizzi, F.; Rovini, E.; Andreoli, E.; Casini, B., Epidemiological surveillance of human enteric viruses by monitoring of different environmental matrices. *Water Science and Technology* **2006,** *54,* (3), 239-244.

43. Irving, L. G.; Smith, F. A., One-year survey of enteroviruses, adenoviruses, and reoviruses isolated from effluent at an activated-sludge purification plant. *Applied and Environmental Microbiology* **1981,** *41,* (1), 51-59.

44. Carducci, A.; Battistini, R.; Rovini, E.; Verani, M., Viral removal by wastewater treatment: Monitoring of indicators and pathogens. *Food and Environmental Virology* **2009,** *1,* (2), 85-91.

45. Carducci, A.; Morici, P.; Pizzi, F.; Battistini, R.; Rovini, E.; Verani, M., Study of the viral removal efficiency in a urban wastewater treatment plant. *Water Science and Technology* **2008,** *58,* (4), 893-897.

46. Rodriguez, R. A.; Gundy, P. M.; Gerba, C. P., Comparison of BGM and PLC/PRC/5 cell lines for total culturable viral assay of treated sewage. *Applied and Environmental Microbiology* **2008,** *74,* (9), 2583-2587.

47. Abbaszadegan, M.; Monteiro, P.; Nwachuku, N.; Alum, A.; Ryu, H., Removal of adenovirus, calicivirus, and bacteriophages by conventional drinking water treatment. *Journal of Environmental Science and Health Part a-Toxic/Hazardous Substances & Environmental Engineering* **2008,** *43,* (2), 171-177.

48. US Environmental Protection Agency, Alternative Disinfectants and Oxidants Guidance Manual. In 1999.

49. Clarke, N. A.; Stevenson, R. E.; Kabler, P. W., The inactivation of purified type-3 adenovirus in water by chlorine. *American Journal of Hygiene* **1956,** *64*, (3), 314-319.

50. Baxter, C. S.; Hofmann, R.; Templeton, M. R.; Brown, M.; Andrews, R. C., Inactivation of adenovirus types 2, 5, and 41 in drinking water by UV light, free chlorine, and monochlorarnine. *Journal of Environmental Engineering-Asce* **2007,** *133*, (1), 95-103.

51. Kahler, A. M.; Cromeans, T. L.; Roberts, J. M.; Hill, V. R., Effects of source water quality on chlorine inactivation of adenovirus, coxsackievirus, echovirus, and murine norovirus. *Applied and Environmental Microbiology* **2010,** *76*, (15), 5159-5164.

52. Page, M. A.; Shisler, J. L.; Marinas, B. J., Kinetics of adenovirus type 2 inactivation with free chlorine. *Water Research* **2009,** *43*, (11), 2916-2926.

53. Thurston-Enriquez, J. A.; Haas, C. N.; Jacangelo, J.; Gerba, C. P., Chlorine inactivation of adenovirus type 40 and feline calicivirus. *Applied and Environmental Microbiology* **2003,** *69*, (7), 3979-3985.

54. Malcom Pirnie, I.; HDR Engineering, I., Guidance manual for compliance with the filtration and disinfection requirements for public water systems using surface water sources. In USEPA, Ed. 1991.

55. Gerba, C. P., Applied and theoretical aspects of virus adsoprtion to surfaces. *Advances in Applied Microbiology* **1984,** *30*, 133-168.

56. Victorin, K.; Hellström, K. G.; Rylander, R., Redox potential measurements for determining the disinfecting power of chlorinated water. *The Journal of Hygiene* **1972,** *70*, (2), 313-323.

57. Shin, G. A.; Lee, J. K., Inactivation of human adenovirus by sequential disinfection with an alternative ultraviolet technology and monochloramine. *Canadian Journal of Microbiology* **2010,** *56*, (7), 606-609.

58. Sirikanchana, K.; Shisler, J. L.; Marinas, B. J., Inactivation kinetics of adenovirus serotype 2 with monochloramine. *Water Research* **2008,** *42*, (6-7), 1467-1474.

59. Thurston-Enriquez, J. A.; Haas, C. N.; Jacangelo, J.; Gerba, C. P., Inactivation of enteric adenovirus and feline calicivirus by chlorine dioxide. *Applied and Environmental Microbiology* **2005,** *71*, (6), 3100-3105.

60. Eischeid, A. C.; Meyer, J. N.; Linden, K. G., UV disinfection of adenoviruses: Molecular indications of DNA damage efficiency. *Applied and Environmental Microbiology* **2009,** *75*, (1), 23-28.

61. Gerba, C. P.; Gramos, D. M.; Nwachuku, N., Comparative inactivation of enteroviruses and adenovirus 2 by UV light. *Applied and Environmental Microbiology* **2002,** *68*, (10), 5167-5169.

62. Gerrity, D.; Ryu, H.; Crittenden, J.; Abbaszadegan, M., UV inactivation of adenovirus type 4 measured by integrated cell culture qPCR. *Journal of Environmental Science and Health Part A-Toxic/Hazardous Substances & Environmental Engineering* **2008,** *43*, (14), 1628-1638.

63. Ko, G. P.; Cromeans, T. L.; Sobsey, M. D., UV inactivation of adenovirus type 41 measured by cell culture mRNA RT-PCR. *Water Research* **2005,** *39*, (15), 3643-3649.

64. Meng, Q. S.; Gerba, C. P., Comparative inactivation of enteric adenoviruses, poliovirus and coliphages by ultraviolet irradiation. *Water Research* **1996,** *30*, (11), 2665-2668.

65. Thurston-Enriquez, J. A.; Haas, C. N.; Jacangelo, J.; Riley, K.; Gerba, C. P., Inactivation of feline calicivirus and adenovirus type 40 by UV radiation. *Applied and Environmental Microbiology* **2003,** *69*, (1), 577-582.

66. Linden, K. G.; Thurston, J.; Schaefer, R.; Malley, J. P., Jr., Enhanced UV inactivation of adenoviruses under polychromatic UV lamps. *Applied and Environmental Microbiology* **2007,** *73*, (23), 7571-7574.

67. Ballester, N. A.; Malley, J. P., Sequential disinfection of adenovirus type 2 with UV-chlorine-chloramine. *Journal American Water Works Association* **2004,** *96*, (10), 97-103.

68. Kaneko, M.; Okura, I. E., *Photocatalysis: Science and Technology*. Springer: New York, 2002.

69. Cho, M.; Lee, J.; Mackeyev, Y.; Wilson, L. J.; Alvarez, P. J. J.; Hughes, J. B.; Kim, J. H., Visible light sensitized inactivation of MS-2 bacteriophage by a cationic amine-functionalized C_{60} derivative. *Environmental Science & Technology* **2010,** *44*, (17), 6685-6691.

70. Sjogren, J. C.; Sierka, R. A., Inactivation of phage MS2 by iron-aided titanium dioxide photocatalysis. *Applied and Environmental Microbiology* **1994,** *60*, (1), 344-347.

71. Wigginton, K. R.; Menin, L.; Montoya, J. P.; Kohn, T., Oxidation of Virus proteins during UV_{254} and singlet oxygen mediated inactivation. *Environmental Science & Technology* **2010,** *44*, (14), 5437-5443.

72. Hoffmann, M. R.; Martin, S. T.; Choi, W.; Bahnemann, D. W., Environmental application of semiconductor photocatalysis. *Chemical Reviews* **1995,** *95*, (1), 69-95.

73. Vamathevan, V.; Amal, R.; Beydoun, D.; Low, G.; McEvoy, S., Photocatalytic oxidation of organics in water using pure and silver-modified titanium dioxide particles. *Journal of Photochemistry and Photobiology A: Chemistry* **2002,** *148*, (1-3), 233-245.

74. Cho, M.; Chung, H.; Yoon, J., Different inactivation behaviors of MS-2 phage and *Escherichia coli* in TiO_2 photocatalytic disinfection. *Applied Environmental Microbiology* **2005,** *71*, (1), 270-275.

75. Kashige, N.; Kakita, Y.; Nakashima, Y.; Miake, F.; Watanabe, K., Mechanism of the photocatalytic inactivation of *Lactobacillus casei* phage PL-1 by titania thin film. *Current Microbiology* **2001,** *42*, (3), 184-189.

76. Zan, L.; Fa, W.; Peng, T.; Gong, Z. K., Photocatalysis effect of nanometer TiO_2 and TiO_2-coated ceramic plate on hepatitis B virus. *Journal of Photochemistry and Photobiology B-Biology* **2007,** *86*, (2), 165-169.

77. Xu, R. F.; Liu, X. L.; Zhang, P.; Ma, H.; Liu, G.; Xia, Z. Y., The photodestruction of virus in nano-TiO_2 suspension. *Journal of Wuhan University of Technology-Materials Science Edition* **2007,** *22*, (3), 422-425.

78. Hawkins, C. L.; Davies, M. J., EPR studies on the selectivity of hydroxyl radical attack on amino acids and peptides. *Journal of the Chemical Society-Perkin Transactions 2* **1998**, (12), 2617-2622.

79. Jones, B. J.; Vergne, M. J.; Bunk, D. M.; Locascio, L. E.; Hayes, M. A., Cleavage of peptides and proteins using light-generated radicals from titanium dioxide. *Analytical Chemistry* **2007,** *79*, (4), 1327-1332.

80. Sato, T.; Taya, M., Enhancement of phage inactivation using photocatalytic titanium dioxide particles with different crystalline structures. *Biochemical Engineering Journal* **2006,** *28*, (3), 303-308.

81. Koizumi, Y.; Taya, M., Photocatalytic inactivation rate of phage MS2 in titanium dioxide suspensions containing various ionic species. *Biotechnology Letters* **2002,** *24*, (6), 459-462.

82. Chorkendorff, I.; Niemantsverdriet, J. W., *Concepts of Modern Catalysis and Kinetics*. Second, Revised and Enlarged ed.; Wiley-VCH Verlag GmbH & Co. KGaA: Weinheim, 2007.

83. Emeline, A. V.; Ryabchuk, V. K.; Serpone, N., Dogmas and misconceptions in heterogeneous photocatalysis. Some enlightened reflections. *Journal of Physical Chemistry B* **2005,** *109*, (39), 18515-18521.

84. Ollis, D. F., Kinetic disguises in heterogeneous photocatalysis. *Topics in Catalysis* **2005,** *35*, (3-4), 217-223.

85. Wahi, R. K.; Yu, W. W.; Liu, Y. P.; Mejia, M. L.; Falkner, J. C.; Nolte, W.; Colvin, V. L., Photodegradation of Congo Red catalyzed by nanosized TiO_2. *Journal of Molecular Catalysis A-Chemical* **2005,** *242*, (1-2), 48-56.

86. Turchi, C. S.; Ollis, D. F., Photocatalytic degradation of organic-water contaminants: Mechanisms involving hydroxyl radical attack. *Journal of Catalysis* **1990,** *122*, (1), 178-192.

87. Ollis, D. F., Kinetics of liquid phase photocatalyzed reactions: An illuminating approach. *Journal of Physical Chemistry B* **2005,** *109*, (6), 2439-2444.

88. Emeline, A. V.; Ryabchuk, V.; Serpone, N., Factors affecting the efficiency of a photocatalyzed process in aqueous metal-oxide dispersions - Prospect of distinguishing between two kinetic models. *Journal of Photochemistry and Photobiology A-Chemistry* **2000,** *133*, (1-2), 89-97.

89. Adan, C.; Bahamonde, A.; Fernandez-Garcia, M.; Martinez-Arias, A., Structure and activity of nanosized iron-doped anatase TiO2 catalysts for phenol photocatalytic degradation. *Applied Catalysis B-Environmental* **2007,** *72*, (1-2), 11-17.

90. Anpo, M.; Takeuchi, M., The design and development of highly reactive titanium oxide photocatalysts operating under visible light irradiation. *Journal of Catalysis* **2003,** *216*, (1-2), 505-516.

91. Bandara, J.; Hadapangoda, C. C.; Jayasekera, W. G., TiO_2/MgO composite photocatalyst: the role of MgO in photoinduced charge carrier separation. *Applied Catalysis B-Environmental* **2004,** *50*, (2), 83-88.

92. Kondo, M. M.; Jardim, W. F., Photodegradation of chloroform and urea using Ag-loaded titanium dioxide as catalyst. *Water Research* **1991,** *25*, (7), 823-827.

93. Gao, X. T.; Wachs, I. E., Titania-silica as catalysts: molecular structural characteristics and physico-chemical properties. *Catalysis Today* **1999,** *51*, (2), 233-254.

94. Pelaez, M.; de la Cruz, A. A.; Stathatos, E.; Falaras, P.; Dionysiou, D. D., Visible light-activated N-F-codoped TiO_2 nanoparticles for the photocatalytic degradation of microcystin-LR in water. *Catalysis Today* **2009,** *144*, (1-2), 19-25.

95. Yao, Y.; Li, G.; Ciston, S.; Lueptow, R. M.; Gray, K. A., Photoreactive TiO_2/carbon nanotube composites: Synthesis and reactivity. *Environmental Science & Technology* **2008,** *42*, (13), 4952-4957.

96. Li, Q.; Page, M. A.; Marinas, B. J.; Shang, J. K., Treatment of coliphage MS2 with palladium-modified nitrogen-doped titanium oxide photocatalyst illuminated by visible light. *Environmental Science & Technology* **2008,** *42*, (16), 6148-6153.

97. Choi, W.; Termin, A.; Hoffmann, M., The role of metal ion dopants in quantum size TiO_2: Correlation between photoreactivity and charge carrier recombination dynamics. *Journal of Physical Chemistry* **1994,** *98*, 13669-13679.

98. Haick, H.; Paz, Y., Long-range effects of noble metals on the photocatalytic properties of titanium dioxide. *Journal of Physical Chemistry B* **2003,** *107*, (10), 2319-2326.

99. Iliev, V.; Tomova, D.; Bilyarska, L.; Eliyas, A.; Petrov, L., Photocatalytic properties of TiO_2 modified with platinum and silver nanoparticles in the degradation of oxalic acid in aqueous solution. *Applied Catalysis B-Environmental* **2006,** *63*, (3-4), 266-271.

100. Mu, W.; Herrmann, J. M.; Pichat, P., Room-temperature photocatalytic oxidation of liquid cyclohexane over neat and modified TiO_2. *Catalysis Letters* **1989,** *3*, (1), 73-84.

101. Cheng, Q. L.; Li, C. Z.; Pavlinek, V.; Saha, P.; Wang, H. B., Surface-modified antibacterial TiO_2/Ag^+ nanoparticles: Preparation and properties. *Applied Surface Science* **2006,** *252*, (12), 4154-4160.

102. Guin, D.; Manorama, S. V.; Latha, J. N. L.; Singh, S., Photoreduction of silver on bare and colloidal TiO_2 nanoparticles/nanotubes: Synthesis, characterization, and tested for antibacterial outcome. *Journal of Physical Chemistry C* **2007,** *111*, (36), 13393-13397.

103. Kato, S.; Hirano, Y.; Iwata, M.; Sano, T.; Takeuchi, K.; Matsuzawa, S., Photocatalytic degradation of gaseous sulfur compounds by silver-deposited titanium dioxide. *Applied Catalysis B-Environmental* **2005,** *57*, (2), 109-115.

104. Mahltig, B.; Gutmann, E.; Meyer, D. C.; Reibold, M.; Dresler, B.; Gunther, K.; Fassler, D.; Bottcher, H., Solvothermal preparation of metallized titania sols for photocatalytic and antimicrobial coatings. *Journal of Materials Chemistry* **2007,** *17*, (22), 2367-2374.

105. Page, K.; Palgrave, R. G.; Parkin, I. P.; Wilson, M.; Savin, S. L. P.; Chadwick, A. V., Titania and silver-titania composite films on glass-potent antimicrobial coatings. *Journal of Materials Chemistry* **2007,** *17*, (1), 95-104.

106. Rincon, A. G.; Pulgarin, C., Photocatalytical inactivation of *E. coli*: effect of (continuous-intermittent) light intensity and of (suspended-fixed) TiO_2 concentration. *Applied Catalysis B-Environmental* **2003,** *44*, (3), 263-284.

107. Seery, M. K.; George, R.; Floris, P.; Pillai, S. C., Silver doped titanium dioxide nanomaterials for enhanced visible light photocatalysis. *Journal of Photochemistry and Photobiology A: Chemistry* **2007,** *189*, 258-263.

108. Xin, B. F.; Jing, L. Q.; Ren, Z. Y.; Wang, B. Q.; Fu, H. G., Effects of simultaneously doped and deposited Ag on the photocatalytic activity and surface states of TiO_2. *Journal of Physical Chemistry B* **2005,** *109*, (7), 2805-2809.

109. Yuranova, T.; Rincon, A. G.; Pulgarin, C.; Laub, D.; Xantopoulos, N.; Mathieu, H. J.; Kiwi, J., Performance and characterization of Ag-cotton and Ag/TiO_2 loaded

textiles during the abatement of *E. coli*. *Journal of Photochemistry and Photobiology A-Chemistry* **2006,** *181*, (2-3), 363-369.

110. Zhang, L. Z.; Yu, J. C.; Yip, H. Y.; Li, Q.; Kwong, K. W.; Xu, A. W.; Wong, P. K., Ambient light reduction strategy to synthesize silver nanoparticles and silver-coated TiO_2 with enhanced photocatalytic and bactericidal activities. *Langmuir* **2003,** *19*, (24), 10372-10380.

111. Kim, J.-P.; Cho, I.-H.; Kim, I.-T.; Kim, C.-U.; Heo, N. H.; Suh, S.-H., Manufacturing of anti-viral inorganic materials from colloidal silver and titanium dioxide. *Revue Romaine de Chimie* **2006,** *51*, (11), 1121-1129.

112. Sclafani, A.; Mozzanega, M. N.; Pichat, P., Effects of silver deposits on the photocatalytic activity of titanium-dioxide samples for the dehydrogenation or oxidation of 2-propanol. *Journal of Photochemistry and Photobiology A-Chemistry* **1991,** *59*, (2), 181-189.

113. Sung-Suh, H. M.; Choi, J. R.; Hah, H. J.; Koo, S. M.; Bae, Y. C., Comparison of Ag deposition effects on the photocatalytic activity of nanoparticulate TiO_2 under visible and UV light irradiation. *Journal of Photochemistry and Photobiology A: Chemistry* **2004,** *163*, (1-2), 37-44.

114. Matsumura, Y.; Yoshikata, K.; Kunisaki, S.; Tsuchido, T., Mode of bactericidal action of silver zeolite and its comparison with that of silver nitrate. *Applied and Environmental Microbiology* **2003,** *69*, (7), 4278-4281.

115. Feng, Q. L.; Wu, J.; Chen, G. Q.; Cui, F. Z.; Kim, T. N.; Kim, J. O., A mechanistic study of the antibacterial effect of silver ions on *Escherichia coli* and *Staphylococcus aureus*. *Journal of Biomedical Materials Research* **2000,** *52*, (4), 662-668.

116. Elechiguerra, J. L.; Burt, J. L.; Morones, J. R.; Camacho-Bragado, A.; Gao, X.; Lara, H. H.; Yacaman, M. J., Interaction of silver nanoparticles with HIV-1. *Journal of Nanobiotechnology* **2005,** *3*, (6).

117. Morones, J. R.; Elechiguerra, J. L.; Camacho, A.; Holt, K.; Kouri, J. B.; Ramirez, J. T.; Yacaman, M. J., The bactericidal effect of silver nanoparticles. *Nanotechnology* **2005,** *16*, 2346–2353.

118. Huang, M.; Tso, E.; Datye, A. K.; Prairie, M. R.; Stange, B. M., Removal of silver in photographic processing waste by TiO_2-based photocatalysis. *Environmental Science & Technology* **1996,** *30*, (10), 3084-3088.

119. Anderson, C.; Bard, A. J., Improved photocatalyst of TiO_2/SiO_2 prepared by a sol-gel synthesis. *Journal of Physical Chemistry* **1995,** *99*, (24), 9882-9885.

120. Anderson, C.; Bard, A. J., Improved photocatalytic activity and characterization of mixed TiO_2/SiO_2 and TiO_2/Al_2O_3 materials. *Journal of Physical Chemistry B* **1997,** *101*, (14), 2611-2616.

121. Periyat, P.; Baiju, K. V.; Mukundan, P.; Pillai, P. K.; Warder, K. G. K., High temperature stable mesoporous anatase TiO_2 photocatalyst achieved by silica addition. *Applied Catalysis A-General.* **2008,** *349*, (1-2), 13-19.

122. Kormann, C.; Bahnemann, D. W.; Hoffmann, M. R., Photocatalytic production of H_2O_2 and organic peroxides in aqueous suspensions of TiO_2, ZnO, and desert sand. *Environmental Science & Technology* **1988,** *22*, (7), 798-806.

123. Gerrity, D.; Ryu, H.; Crittenden, J.; Abbaszadegan, M., Photocatalytic inactivation of viruses using titanium dioxide nanoparticles and low-pressure UV light. *Journal of Environmental Science and Health, Part A* **2008,** *43*, (11), 1261-1270.

124. Guillard, C.; Bui, T. H.; Felix, C.; Moules, V.; Lina, B.; Lejeune, P., Microbiological disinfection of water and air by photocatalysis. *Comptes Rendus Chimie* **2008,** *11*, (1-2), 107-113.

125. Hwang, Y. S.; Li, Q., Characterizing photochemical transformation of aqueous nC_{60} under environmentally relevant conditions. *Environmental Science & Technology* **2010,** *44*, (8), 3008-3013.

126. Lee, J.; Mackeyev, Y.; Cho, M.; Wilson, L. J.; Kim, J.-H.; Alvarez, P. J. J., C_{60} aminofullerene immobilized on silica as a visible-light-activated photocatalyst. *Environmental Science & Technology* **2010,** *44*, (24), 9488-9495.

127. Lee, J.; Fortner, J. D.; Hughes, J. B.; Kim, J.-H., Photochemical production of reactive oxygen species by C_{60} in the aqueous phase during UV irradiation. *Environmental Science & Technology* **2007,** *41*, (7), 2529-2535.

128. Arbogast, J. W.; Darmanyan, A. P.; Foote, C. S.; Rubin, Y.; Diederich, F. N.; Alvarez, M. M.; Anz, S. J.; Whetten, R. L., Photophysical properties of C_{60}. *Journal of Physical Chemistry* **1991,** *95*, (1), 11-12.

129. Yamakoshi, Y.; Sueyoshi, S.; Fukuhara, K.; Miyata, N., •OH and $O2^{\bullet-}$ generation in aqueous C_{60} and C_{70} solutions by photoirradiation: An EPR study. *Journal of the American Chemical Society* **1998,** *120*, (47), 12363-12364.

130. Lee, J.; Yamakoshi, Y.; Hughes, J. B.; Kim, J.-H., Mechanism of C_{60} photoreactivity in water: Fate of triplet state and radical anion and production of reactive oxygen species. *Environmental Science & Technology* **2008,** *42*, (9), 3459-3464.

131. Lee, J.; Mackeyev, Y.; Cho, M.; Li, D.; Kim, J.-H.; Wilson, L. J.; Alvarez, P. J. J., Photochemical and antimicrobial properties of novel C_{60} derivatives in aqueous systems. *Environmental Science & Technology* **2009,** *43*, (17), 6604-6610.

132. Fang, X. W.; Mark, G.; vonSonntag, C., OH radical formation by ultrasound in aqueous solutions. Part I: The chemistry underlying the terephthalate dosimeter. *Ultrasonics Sonochemistry* **1996,** *3*, (1), 57-63.

133. Matthews, R. W., The radiation-chemistry of the terephthalate dosimeter. *Radiation Research* **1980,** *83*, (1), 27-41.

134. Ishibashi, K.; Fujishima, A.; Watanabe, T.; Hashimoto, K., Detection of active oxidative species in TiO_2 photocatalysis using the fluorescence technique. *Electrochemistry Communications* **2000,** *2*, (3), 207-210.

135. Eremia, S. A. V.; Chevalier-Lucia, D.; Radu, G. L.; Marty, J. L., Optimization of hydroxyl radical formation using TiO_2 as photocatalyst by response surface methodology. *Talanta* **2008,** *77*, (2), 858-862.

136. Kohtani, S.; Yoshida, K.; Maekawa, T.; Iwase, A.; Kudo, A.; Miyabe, H.; Nakagaki, R., Loading effects of silver oxides upon generation of reactive oxygen species in semiconductor photocatalysis. *Physical Chemistry Chemical Physics* **2008,** *10*, (20), 2986-2992.

137. Xiao, Q.; Ouyang, L. L., Photocatalytic activity and hydroxyl radical formation of carbon-doped TiO_2 nanocrystalline: Effect of calcination temperature. *Chemical Engineering Journal* **2009,** *148*, (2-3), 248-253.

138. Azrague, K.; Osterhus, S. W.; Biomorgi, J. G., Degradation of pCBA by catalytic ozonation in natural water. *Water Science and Technology* **2009,** *59*, (6), 1209-1217.

139. Kao, N. H.; Su, M. C., Statistical study of instantaneous demand of para-chlorobenzoic acid as an ozone/hydroxyl radical probe compound. *Environmental Engineering Science* **2009,** *26*, (4), 791-798.

140. Benson, S. D.; Bamford, J. K. H.; Bamford, D. H.; Burnett, R. M., Viral evolution revealed by bacteriophage PRD1 and human adenovirus coat protein structures. *Cell* **1999,** *98*, (6), 825-833.

141. Wong, M.; Kumar, L.; Jenkins, T. M.; Xagoraraki, I.; Phanikumar, M. S.; Rose, J. B., Evaluation of public health risks at recreational beaches in Lake Michigan via detection of enteric viruses and a human-specific bacteriological marker. *Water Research* **2009,** *43*, (4), 1137-1149.

142. Liu, H. L.; Yang, T. C. K., Photocatalytic inactivation of *Escherichia coli* and *Lactobacillus helveticus* by ZnO and TiO_2 activated with ultraviolet light. *Process Biochemistry* **2003,** *39*, (4), 475-481.

143. Lydakis-Simantiris, N.; Riga, D.; Katsivela, E.; Mantzavinos, D.; Xekoukoulotakis, N. P., Disinfection of spring water and secondary treated municipal wastewater by TiO_2 photocatalysis. *Desalination* **2010,** *250*, (1), 351-355.

144. Sordo, C.; Van Grieken, R.; Marugan, J.; Fernandez-Ibanez, P., Solar photocatalytic disinfection with immobilised TiO_2 at pilot-plant scale. *Water Science and Technology* **2010,** *61*, (2), 507-512.

145. Benabbou, A. K.; Derriche, Z.; Felix, C.; Lejeune, P.; Guillard, C., Photocatalytic inactivation of *Escherichia coli* - Effect of concentration of TiO_2 and microorganism, nature, and intensity of UV irradiation. *Applied Catalysis B-Environmental* **2007,** *76*, (3-4), 257-263.

146. Kikuchi, Y.; Sunada, K.; Iyoda, T.; Hashimoto, K.; Fujishima, A., Photocatalytic bactericidal effect of TiO_2 thin films: Dynamic view of the active oxygen species responsible for the effect. *Journal of Photochemistry and Photobiology A: Chemistry* **1997,** *106*, 51-56.

147. Wei, C.; Lin, W. Y.; Zainal, Z.; Williams, N. E.; Zhu, K.; Kruzic, A. P.; Smith, R. L.; Rajeshwar, K., Bactericidal activity of TiO_2 photocatalysis in aqueous media: Towards a solar-assisted water disinfection system. *Environmental Science & Technology* **1994,** *28*, (5), 934-938.

148. Belháčová, L.; Krysa, J.; Geryk, J.; Jerkovsky, J., Inactivation of microorganisms in a flow-through photoreactor with an immobilized TiO_2 layer. *Journal of Chemical Technology and Biotechnology* **1999,** *74*, 149-154.

149. Tran, H.; Scott, J.; Chiang, K.; Amal, R., Clarifying the role of silver deposits on titania for the photocatalytic mineralisation of organic compounds. *Journal of Photochemistry and Photobiology A: Chemistry* **2006,** *183*, (1–2), 41-52.

150. Sclafani, A.; Mozzanega, M. N.; Herrmann, J. M., Influence of silver deposits on the photocatalytic activity of titania. *Journal of Catalysis* **1997,** *168*, (1), 117-120.

151. Adams, M. H., *Bacteriophages*. Interscience Publishers, Inc.: New York, 1959.

152. Jou, W. M.; Ysebaert, M.; Fiers, W.; Haegeman, G., Nucleotide sequence of gene coding for bacteriophage MS2 coat protein. *Nature* **1972,** *237*, (5350), 82-88.

153. Nolf, F. A.; Vandekerckhove, J. S.; Lenaerts, A. K.; Vanmontagu, M. C., Sequence of A-protein of coliphage-MS2. 1. Isolation of A-protein, determination of NH_2-terminal and COOH-terminal sequences, isolation and amino-acid sequence of tryptic peptides. *Journal of Biological Chemistry* **1977,** *252*, (21), 7752-7760.

154. Penrod, S. L.; Olson, T. M.; Grant, S. B., Deposition kinetics of two viruses in packed beds of quartz granular media. *Langmuir* **1996,** *12*, (23), 5576-5587.

155. Stewart, S.; Fredericks, P. M., Surface-enhanced Raman spectroscopy of peptides and proteins adsorbed on an electrochemically prepared silver surface. *Spectrochimica Acta Part a-Molecular and Biomolecular Spectroscopy* **1999,** *55*, (7-8), 1615-1640.

156. Sun, Y. F.; Pignatello, J. J., Evidence for a surface dual hole - radical mechanism in the TiO_2 photocatalytic oxidation of 2,4-dichlorophenoxyacetic acid. *Environmental Science & Technology* **1995,** *29*, (8), 2065-2072.

157. Kim, S.; Choi, W., Kinetics and mechanisms of photocatalytic degradation of $(CH3)_nNH4_{-n}^+$ $(0 \leq n \leq 4)$ in TiO_2 suspension: The role of OH radicals. *Environmental Science & Technology* **2002,** *36*, (9), 2019-2025.

158. Badireddy, A. R.; Hotze, E. M.; Chellam, S.; Alvarez, P.; Wiesner, M. R., Inactivation of bacteriophages via photosensitization of fullerol nanoparticles. *Environmental Science & Technology* **2007,** *41*, (18), 6627-6632.

159. Li, D.; Gu, A. Z.; He, M.; Shi, H.-C.; Yang, W., UV inactivation and resistance of rotavirus evaluated by integrated cell culture and real-time RT-PCR assay. *Water Research* **2009,** *43*, (13), 3261-3269.

160. Tizaoui, C.; Mezughi, K.; Bickley, R., Heterogeneous photocatalytic removal of the herbicide clopyralid and its comparison with UV/H_2O_2 and ozone oxidation techniques. *Desalination* **2011,** *273*, (1), 197-204.

161. Rincón, A.-G.; Pulgarin, C., Comparative evaluation of Fe^{3+} and TiO_2 photoassisted processes in solar photocatalytic disinfection of water. *Applied Catalysis B: Environmental* **2006,** *63*, (3–4), 222-231.

162. Wu, D.; You, H.; Zhang, R.; Chen, C.; Lee, D.-J., Ballast waters treatment using $UV/Ag–TiO_2 + O_3$ advanced oxidation process with Escherichia coli and Vibrio alginolyticus as indicator microorganisms. *Chemical Engineering Journal* **2011,** *174*, (2–3), 714-718.

163. Foster, H.; Ditta, I.; Varghese, S.; Steele, A., Photocatalytic disinfection using titanium dioxide: Spectrum and mechanism of antimicrobial activity. *Applied Microbiology and Biotechnology* **2011,** *90*, (6), 1847-1868.

164. Disdier, J.; Herrmann, J. M.; Pichat, P., Platinum titanium-dioxide catalysts - a photoconductivity study of electron-transfer from the ultraviolet-illuminated support to the metal and of the influence of hydrogen. *Journal of the Chemical Society-Faraday Transactions I* **1983,** *79*, 651-660.

165. Feng, Y. Y.; Ong, S. L.; Hu, J. Y.; Tan, X. L.; Ng, W. J., Effects of pH and temperature on the survival of coliphages MS2 and Qß. *Journal of Industrial Microbiology & Biotechnology* **2003,** *30*, (9), 549-552.

166. Nuanualsuwan, S.; Cliver, D. O., Capsid functions of inactivated human picornaviruses and feline calicivirus *Applied and Environmental Microbiology* **2003,** *69*, (1), 350-357.

167. Billo, J. E., *Excel for Chemists: A Comprehensive Guide, 2nd Edition*. 2 ed.; John Wiley & Sons, Inc.: New York, 2001.

168. Frontline Systems Inc. *SOLVER*.

169. Powell, T.; Brion, G. M.; Jagtoyen, M.; Derbyshire, F., Investigating the effect of carbon shape on virus adsorption. *Environmental Science & Technology* **2000,** *34*, (13), 2779-2783.

170. Malato, S.; Fernandez-Ibanez, P.; Maldonado, M. I.; Blanco, J.; Gernjak, W., Decontamination and disinfection of water by solar photocatalysis: Recent overview and trends. *Catalysis Today* **2009,** *147*, (1), 1-59.

171. Cromeans, T. L.; Lu, X. Y.; Erdman, D. D.; Humphrey, C. D.; Hill, V. R., Development of plaque assays for adenoviruses 40 and 41. *Journal of Virological Methods* **2008,** *151*, (1), 140-145.

172. Rigotto, C.; Hanley, K.; Rochelle, P. A.; De Leon, R.; Barardi, C. R. M.; Yates, M. V., Survival of adenovirus types 2 and 41 in surface and ground waters measured by a plaque assay. *Environmental Science & Technology* **2011,** *45*, (9), 4145-4150.

173. US Environmental Protection Agency, USEPA Manual of Methods for Virology. In EPA/600/4-84/013: 1987.

174. Steitz, J. A., Identification of the A protein as a structural component of bacteriophage R17. *Journal of Molecular Biology* **1968,** *33*, (3), 923-936.

175. Gyurek, L. L.; Finch, G. R., Modeling water treatment chemical disinfection kinetics. *Journal of Environmental Engineering* **1998,** *124*, (9), 783-793.

176. Hu, C.; Guo, J.; Qu, J. H.; Hu, X. X., Photocatalytic degradation of pathogenic bacteria with AgI/TiO_2 under visible light irradiation. *Langmuir* **2007,** *23*, (9), 4982-4987.

177. Marugan, J.; van Grieken, R.; Sordo, C.; Cruz, C., Kinetics of the photocatalytic disinfection of Escherichia coli suspensions. *Applied Catalysis B-Environmental* **2008,** *82*, (1-2), 27-36.

178. Tchobanoglous, G.; Burton, F. L.; Stensel, H. D., *Wastewater Engineering Treatment and Reuse, Fourth Edition*. Fourth ed.; The McGraw-Hill Companies, Inc. : New Yok, New York, 2003.

179. Curiel, D. T.; Douglas, J. T.; (Eds.), *Adenoviral Vectors for Gene Therapy*. Elsevier Inc.: 2002.

180. Herrmann, J. M., Heterogeneous photocatalysis: fundamentals and applications to the removal of various types of aqueous pollutants. *Catalysis Today* **1999,** *53*, (1), 115-129.

181. Balasaraswathy, P.; Kumar, U.; Srinivas, C. R.; Shashidharan, N., UVA and UVB in sunlight, Optimal utilization of UV rays in sunlight for phototherapy. *Indian Journal of Dermatology, Venereology and Leprology* **2002,** *68*, 198-201.

182. O'Shea, K. E.; Dionysiou, D. D., Advanced oxidation processes for water treatment. *The Journal of Physical Chemistry Letters* **2012,** *3*, (15), 2112-2113.

183. Thimijan, R. W.; Heins, R. D., Photometric, radiometric, and quantum light units of measure - A review of procedures for interconversion. *Hortscience* **1983,** *18*, (6), 818-822.

184. Boulanger, P. A.; Flamencourt, P.; Biserte, G., Isolation and coparative chemical study of structural proteins of adenoviruses 2 and 5: Hexon and fiber antigens. *European Journal of Biochemistry* **1969,** *10*, (1), 116-131.

185. Rutala, W. A.; Peacock, J. E.; Gergen, M. F.; Sobsey, M. D.; Weber, D. J., Efficacy of hospital germicides against adenovirus 8, a common cause of epidemic keratoconjunctivitis in health care facilities. *Antimicrobial Agents and Chemotherapy* **2006,** *50*, (4), 1419-1424.

186. Van Houten, B.; Cheng, S.; Chen, Y., Measuring gene-specific nucleotide excision repair in human cells using quantitative amplification of long targets from nanogram quantities of DNA. *Mutation Research/DNA Repair* **2000,** *460*, (2), 81-94.

187. Croyle, M. A.; Anderson, D. J.; Roessler, B. J.; Amidon, G. L., Development of a highly efficient purification process for recombinant adenoviral vectors for oral gene delivery. *Pharmaceutical Development and Technology* **1998,** *3*, (3), 365-372.

188. Blanche, F.; Monegier, B.; Faucher, D.; Duchesne, M.; Audhuy, F.; Barbot, A.; Bouvier, S.; Daude, G.; Dubois, H.; Guillemin, T.; Maton, L., Polypeptide composition of an adenovirus type 5 used in cancer gene therapy. *Journal of Chromatography A* **2001,** *921*, (1), 39-48.

189. Greber, U. F.; Willetts, M.; Webster, P.; Helenius, A., Stepwise dismantling of adenovirus 2 during entry into cells. *Cell* **1993,** *75*, (3), 477-486.

190. Konz, J. O.; Lee, A. L.; Lewis, J. A.; Sagar, S. L., Development of a purification process for adenovirus: Controlling virus aggregation to improve the clearance of host cell DNA. *Biotechnology Progress* **2005,** *21*, (2), 466-472.

191. van Oostrum, J.; Burnett, R. M., Molecular composition of the adenovirus type 2 virion. *Journal of Virology* **1985,** *56*, (2), 439-448.

192. D'Halluin, J. C.; Milleville, M.; Martin, G. R.; Boulanger, P., Morphogenesis of human adenovirus type 2 studied with fiber- and fiber and penton base-defective temperature-sensitive mutants. *Journal of Virology* **1980,** *33*, (1), 88-99.

193. Dunlop, R. A.; Rodgers, K. J.; Dean, R. T., Recent developments in the intracellular degradation of oxidized proteins. *Free Radical Biology and Medicine* **2002,** *33*, (7), 894-906.

194. Giulivi, C.; Pacifici, R. E.; Davies, K. J. A., Exposure of hydrophobic moieties promotes the selective degradation of hydrogen peroxide-modified hemoglobin by the multicatalytic proteinase complex, proteasome. *Archives of Biochemistry and Biophysics* **1994,** *311*, (2), 329-341.

195. Bondos, S. E.; Bicknell, A., Detection and prevention of protein aggregation before, during, and after purification. *Analytical Biochemistry* **2003,** *316*, (2), 223-231.

196. Erickson, H., Size and shape of protein molecules at the nanometer level determined by sedimentation, gel filtration, and electron microscopy. *Biological Procedures Online* **2009,** *11*, (1), 32 - 51.

197. Lin, J.-Y.; Tsung, C. M.; Fraenkel-Conrat, H., The coat protein of the RNA bacteriophage MS2. *Journal of Molecular Biology* **1967,** *24*, (1), 1-14.

198. Pászti, Z.; Guczi, L., Amino acid adsorption on hydrophilic TiO_2: A sum frequency generation vibrational spectroscopy study. *Vibrational Spectroscopy* **2009,** *50*, (1), 48-56.

Appendix A

A Simple Route to Enhanced Photocatalytic Activity of P25 Titanium Dioxide Nanoparticles by Silica Addition

HUMA R. JAFRY,[†,¶,$] MICHAEL V. LIGA,[‡,¶,$] QILIN LI,[*,‡,¶,$] AND ANDREW R. BARRON[*,†,¶,$,§,ß]

Departments of Chemistry, Civil and Environmental Engineering, and Mechanical Engineering and Materials Science, the Richard E. Smalley Institute for Nanoscale Science and Technology, and the Center for Biological and Environmental Nanotechnology, Rice University, Houston, Texas 77005, USA. Institute of Life Science, Swansea University, Singleton Park, Swansea SA2 8PP, Wales UK.

---

* Corresponding authors: e-mail: arb@rice.edu, Qilin.Li@rice.edu.

† Departments of Chemistry

‡ Civil and Environmental Engineering

§ Mechanical Engineering and Materials Science

¶ Richard E. Smalley Institute

$ Center for Biological and Environmental Nanotechnology

ß Institute of Life Science

Environmental Science & Technology

ARTICLE

pubs.acs.org/est

Simple Route to Enhanced Photocatalytic Activity of P25 Titanium Dioxide Nanoparticles by Silica Addition

Huma R. Jafry,[†,¶,∥] Michael V. Liga,[‡,¶,∥] Qilin Li,[*,‡,¶,∥] and Andrew R. Barron[*,†,¶,∥,§,⊥]

[†]Departments of Chemistry, [‡]Civil and Environmental Engineering, and [§]Mechanical Engineering and Materials Science, [¶]the Richard E. Smalley Institute for Nanoscale Science and Technology, and [∥]the Center for Biological and Environmental Nanotechnology, Rice University, Houston, Texas 77005, United States

[⊥]Institute of Life Science, Swansea University, Singleton Park, Swansea SA2 8PP, Wales U.K.

Supporting Information

ABSTRACT: Silica doped TiO_2(P25) nanoparticles are tested for its photocatalytic activity in the degradation of bacteriophage MS2. During our studies it was found that treatment of TiO_2(P25) in the glass flasks sealed with silicone grease resulted in a significant improvement in the catalytic activity of the titania. Further improvement can be made by the purposeful reaction of TiO_2(P25) with 2.5 wt % silica. This non *in situ* method of incorporating silica to TiO_2(P25) nanoparticles is tested for their role in killing of viruses, and it is found that the rate constant is three times higher to kill viruses with the addition of silica. BET measurements show no significant change/increase in the surface area of silica doped TiO_2(P25)-SiO_2, compared to the undoped TiO_2(P25). Further studies show that the addition of silica increases the adsorption of viruses onto the catalyst. There is a significant difference in the activity of the TiO_2(P25)-SiO_2 samples in the presence of methanol, supporting the notion that hydroxide radical (HO·) is responsible for the antiviral action. The TiO_2(P25)-SiO_2 either produces more HO· than non silica-doped material, or the enhanced adsorption of MS2 to the catalyst results in greater exposure to the HO·, or both mechanisms may work in concert. XPS studies suggest the formation of silica species on the surface of the TiO_2(P25), while UV−visible spectroscopy suggests that the presence of the silica results in a small increase in the measured band gap. We suggest that the enhanced catalytic activity is a result of increased adsorption and/or band bending which can occur at the interface within TiO_2(P25)-SiO_2. One result of this would be a reduction of the electron−hole recombination, the formation of a greater concentration of OH·, and hence an improved catalytic performance.

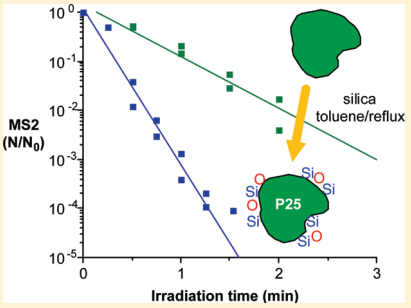

INTRODUCTION

The inadequate treatment of drinking water is currently a significant source of pathogen transmission. In 2004 the WHO estimated that point of use chlorination of drinking water could prevent 39% of the 1.58 million deaths due to diarrheal disease attributed to unsafe water supply, sanitation, and poor hygiene.[1] While chlorination has proven effective for virus inactivation in drinking water, it can form dangerous disinfection byproducts, especially in waters with high organic contents. UV disinfection processes have been increasingly utilized due to this; however, some viruses are highly resistant and particle associated viruses may be shielded from UV radiation.[2] Advanced oxidation processes, and photocatalysis in particular, are alternative disinfection strategies that may provide adequate treatment while overcoming the problems associated with traditional disinfection methods. Titania is a suitable material for use in water treatment since it is nontoxic when ingested and stable under environmental conditions.[3]

Upon excitation and charge separation, TiO_2 can generate several reactive oxygen species (ROS) in the presence of water and/or oxygen, the most significant being the hydroxyl radical (HO·),[4] which is a powerful oxidant that is typically responsible for contaminant degradation by catalyzed TiO_2.

The synthesis of TiO_2 nanoparticles is accomplished by a range of methods.[5] Among the various shapes and forms of TiO_2 nanoparticles, TiO_2(P25) is the standard commercially available material with an approximate diameter of 30 nm and an average surface area of 49 m^2/g. The powder consists of 70% anatase phase and 30% rutile phase.[6] Owing to its high surface area and mixed phase, photocatalytic studies have been performed on TiO_2(P25), including the decomposition of organic pollutants and materials.[7−9]

One limitation of TiO_2 is its high rate of charge recombination and thus reduced photocatalytic efficiency. Several dopants and supports have been studied for improving the photocatalytic efficiency of TiO_2. During a broader study on the inactivation of viruses in water systems by TiO_2, we discovered that the surface treatment of TiO_2(P25) with a range of silica sources allows for the simple enhancement of the activity of TiO_2(P25) to virus inactivation.

Received: August 11, 2010
Accepted: December 17, 2010
Revised: December 8, 2010
Published: December 31, 2010

EXPERIMENTAL METHODS

Materials and Characterization. TiO_2(P25) (Degussa), fumed silica, toluene, acetone, and $Fe(acac)_3$ (Sigma-Aldrich) were obtained from commercial sources and used without further purification. TiO_2(P25) was used without further purification as previous studies which use TiO_2(P25) or have modified TiO_2(P25) for enhanced photocatalysis have used no further purification of the as received material.[10] In this regard we wanted to ensure an equivalent comparison. Bacteriophage MS2 (ATCC 15597-B1) and *E. coli* 15597 (ATCC 15597) were originally obtained from the ATCC, LB-Lennox media and sodium bicarbonate were purchased from Fisher Scientific, and Bacto agar was purchased from Difco Laboratories. Ultrapure water was obtained from a Barnstead E-Pure system. A Luzchem LZC-4 V prewarmed photoreactor with a peak emission 350 nm was used for exposing the flasks to UV radiation for photocatalytic tests. A Fisher Scientific (06-662-65) UV radiometer with a 350 nm sensor (NIST traceable) was used. Branauer Emmett Teller (BET), X-ray photoelectron spectroscopy (XPS), and transmission electron microscopy (TEM) are performed to test for surface area, chemical make up, and structure of the nanopowder.

TiO_2(P25) Mixed with Silica via Reflux. In a typical reaction, TiO_2(P25) (100 mg, 1.25 mmol) is placed in a round-bottom flask with the appropriate amount of fumed silica (2.5 mg, 0.042 mmol, 2.5 wt.% of TiO_2(P25)). Toluene (40 mL) was added, and the powders were bath sonicated for 1 min, followed by reflux with stirring for 24 h. After cooling the sample was vacuum filtered, and the TiO_2(P25)-SiO_2 powder was collected and dispersed in acetone by bath sonication for 20 min. The mixture is vacuum filtered again and washed with copious amounts of acetone. For the purposes of NMR studies a 5 wt.% of fumed silica (20 mg) was added to the TiO_2(P25) (400 mg, 5.0 mmol) and refluxed for 24 h, following workup, the relaxation agent $Fe(acac)_3$ (4.5 mg, 0.013 mmol) is mixed with acetone (35 mL) and added. The mixture is stirred and then allowed to dry by evaporation. For the purposes of UV−vis spectroscopy two samples of TiO_2(P25)-SiO_2 are prepared with higher weight percents of silica (10 wt.% and 20 wt.% of TiO_2(P25)).

P25 Mixed with Silica via Stirring. TiO_2(P25) (100 mg, 1.25 mmol) is mixed in a round-bottom flask with fumed silica (2.5 mg, 0.042 mmol, 2.5 wt.% of TiO_2(P25)). Toluene (40 mL) was added and the powders are bath sonicated for 1 min, followed by stirring for 24 h at room temperature, after which the mixture is vacuum filtered. The TiO_2(P25)-SiO_2 powder is collected and dispersed in acetone by bath sonication for 20 min. The mixture is vacuum filtered again and washed with copious amounts of acetone.

Virus Propagation and Enumeration. Bacteriophage MS2 was used as a model pathogen in this study. The virus stock solution used in the disinfection procedures was obtained by infecting an incubation of the *E. coli* host (ATCC 15597) with a liquid MS2 suspension (ATCC 15597-B1). The mixture was combined with molten LB-Lennox (3 mL) media containing 0.7% Bacto agar and spread over a Petri dish containing solid LB-Lennox media, which was incubated overnight after solidifying. Sterile 0.1 M sodium bicarbonate (Fisher) buffer was then added to the plate that was then slowly rocked for 3 h. The buffer was withdrawn and centrifuged at 10,900 G for 15 min at 4 °C. The supernatant was withdrawn, filtered through a 0.22 μM-pore-size PES syringe filter, and stored at 4 °C in a sterile plastic centrifuge tube. The newly propagated MS2 stock measured 3×10^{10} plaque forming units per milliliter (PFU/mL) and was used without further purification.[11]

MS2 samples were serially diluted in 0.1 M $NaHCO_3$ immediately after being produced and were enumerated by the agar overlay method.[12] Following overnight incubation of the plates, the resulting plaques were counted and the corresponding PFU/mL determined. The survival ratios for each sample were determined and the results averaged from each of the tests. The kinetic data obtained from the inactivation procedures were modeled as a pseudo first order reaction conforming to Chick's Law.

Virus Inactivation Procedure. All items used for these procedures were supplied as sterile or sterilized by either autoclave or filter sterilization. Nanoparticle suspensions were freshly prepared in ultrapure water prior each test and were dispersed using an ultrasonic processor (Sonics Vibra-Cell VCX 500) with cup horn attachment set at 180 W for 30 min. Reactions were carried out in Pyrex Erlenmeyer flasks. Ultrapure water, virus stock, and particle suspension were combined in the flasks to yield a 3×10^7 PFU/mL MS2 and 100 mg/L catalyst concentrations. Methanol (99.9%, Fisher Spectranalyzed) was added to yield a final 400 mM concentration to determine the effect of scavenging HO·. After combining the virus stock and water, the flasks were stirred briefly and sampled to determine the initial virus concentration. After catalyst addition the flasks were stirred in the dark for 10 min and sampled to determine the MS2 inactivated through dark/adsorptive processes. The flasks were then placed into a prewarmed photoreactor and timed samples were taken. Four 8W UV-A bulbs (Hitachi, peak emission 350 nm) were arranged in pairs and placed on the left and right sides of the reactor. The reaction flask was placed over the internal stirring device during the reaction. A UV radiometer (Control Company, Friendswood, TX) with a 350 nm sensor (NIST traceable) was used to measure the UV intensity in the reactor prior to each test. The total intensity in the reactor measured 2.5 mW/cm^2.

RESULTS AND DISCUSSION

Using P25 Titania Refluxed in Toluene for the Deactivation of Bacteriophage. As part of our broader study to understand the role of TiO_2 in the inactivation of MS2 viruses,[13] we made some TiO_2 powders to compare the catalytic activities of the lab made TiO_2 powder and TiO_2(P25). Surprisingly, as may be seen from Figure 1, there is a marked difference in the inactivation of MS2 viruses using as received TiO_2(P25) and the sample that had been refluxed in toluene. Our prior experience with the extraction of silica (SiO_2) and low molecular weight silicon oxide species from commercial Dow Corning high vacuum silicon grease[14−16] suggested that a possible contaminant of silicon could result in the enhanced activity. XPS measurements indicated that any silicon species would be less that the detection limit, and TEM and SEM show no alteration in the morphology of the TiO_2(P25) particles. However, repeating the toluene reflux experiment using a non silicone grease (Krytox) for the glassware resulted in no significant alteration in the activity of the TiO_2(P25) (Figure 2). This suggests that the effect is due to the addition of a silicon-containing species and not the toluene reflux. Therefore, the mixing of silica from the grease with the P25 powder had pronounced effects on deactivation of viruses.

Doping TiO_2 with metal oxides (e.g., SiO_2 or ZrO_2) has been used to enhance some of the properties of titania, such as band gap, photocatalysis, surface hydrophilicity, surface acidity, quantum

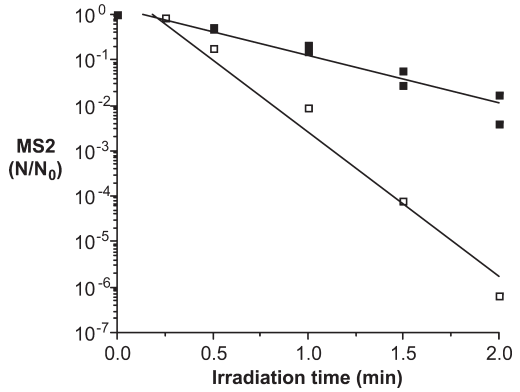

Figure 1. MS2 inactivation by untreated TiO_2(P25) (■, R^2 = 0.935) and treated by refluxing in toluene with silicone grease sealing the glass apparatus (□, R^2 = 0.971).

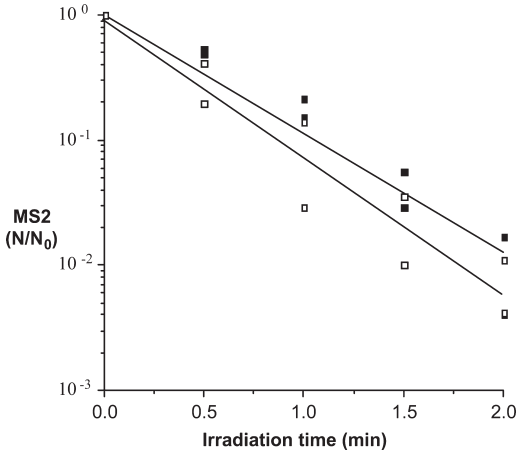

Figure 2. MS2 inactivation by untreated TiO_2(P25) (■, R^2 = 0.935) and treated by refluxing in toluene with nonsilicone (hydrocarbon-based) grease sealing the glass apparatus (□, R^2 = 0.917).

effects, and surface area. Silica doped with TiO_2 has many potential applications, and the interactions have been studied extensively in the areas of quantum-sized effects on photocatalysis and photo induced hydrophilicity.[8,17,18] Different methods of incorporation of TiO_2 doped with silica have been employed which include sol−gel synthesis, hydrosol synthesis, coprecipitation, flame hydrolysis, and physical mixing; however, in each case, the nanoparticles were made in the presence of silica, i.e., an in situ process, which helps in both doping and controlling the size of the TiO_2 nanoparticles. In contrast, the pronounced effects we have observed suggest that the activity of TiO_2(P25) can be significantly improved by a simple and scalable surface reaction with a silicon species rather than *in situ* incorporation during synthesis.

Using P25 Titania Mixed with Silica. Given the pronounced effect that the silicone grease had on TiO_2(P25) (Figure 1), we decided to incorporate fumed silica with TiO_2(P25) to test its effects on virus inactivation. Unlike previous studies[8,19−23] our approach was to physically mix a suitable silica source with as-received TiO_2(P25) nanoparticles. Previous studies[24−26] suggested that fumed silica would be an appropriate source.

Before irradiation, the viruses and catalysts are mixed for 10 min in the dark to allow for adsorption to occur. The observed inactivation of the virus during this time is attributed to adsorption. Figure 3 shows that the dark inactivation of MS2 to TiO_2(P25)-

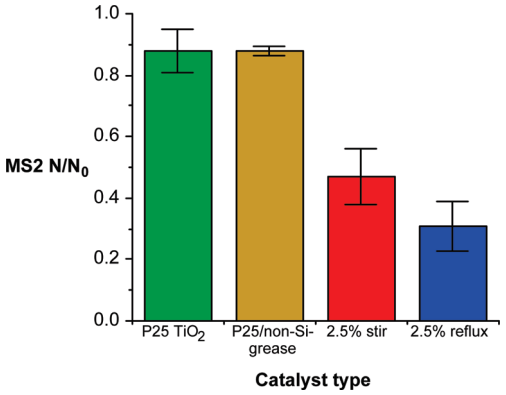

Figure 3. Adsorptive removal/dark inactivation of MS2 by TiO_2(P25) (green), TiO_2(P25) refluxing in toluene with nonsilicone grease (gold), and TiO_2(P25)-SiO_2 formed by stirring (red) or refluxing (blue).

SiO_2 is much greater than to untreated TiO_2(P25) or TiO_2(P25) refluxed in toluene (non-Si grease). Only 31% and 47% of the MS2 remained infective after the addition of the refluxed or stirred TiO_2(P25)-SiO_2, respectively. 88% of the MS2 remained infective after mixing with TiO_2(P25) that was either untreated or refluxed in toluene (non-Si grease). This suggests that the addition of silica is responsible for the enhanced adsorption and that any residual toluene remaining on the catalyst is not effecting adsorption/dark inactivation.

The photo catalytic inactivation of MS2 is significantly enhanced by the addition of silica to TiO_2(P25). The data were modeled using the Chick-Watson equation (eq 1), where N is the titer of infective viruses at time t, N_0 is the titer of infective viruses after adsorption but before irradiation, k is the pseudofirst order rate constant (min^{-1}), and t is the time in minutes

$$\mathrm{LOG}(N/N_0) = -kt \quad (1)$$

Figure 4 shows that both stirred and refluxed TiO_2(P25)-SiO_2 materials outperformed TiO_2(P25) powder. The rate constants for the stirred and refluxed TiO_2(P25)-SiO_2 materials was 2.8 and 3.1 min^{-1}, respectively, which are approximately 3 times greater than that for TiO_2(P25) (0.95 min^{-1}). The degradation results show that both TiO_2(P25)-SiO_2 (stirred) and TiO_2-(P25)-SiO_2 (refluxed) perform similarly in inactivating the viruses. The performance of the TiO_2(P25)-SiO_2 (stirred) sample being similar to the TiO_2(P25)-SiO_2 (refluxed) sample was surprising, given that there was no heat involved during the stirring which could form chemical bonds of SiO_2 with TiO_2 and lead to enhanced performance. Rate constants and correlation coefficients are shown for all materials in Table 1. UV-A radiation in the absence of catalyst did not inactivate the viruses over the time course of the experiments in this study.

The TEM images of stirred TiO_2(P25)-SiO_2 do not appear significantly changed from as-received TiO_2(P25). In a similar manner SEM images appear unchanged. Nevertheless, XPS analysis performed on these powders confirms the presence of silicon (Table 2). The slightly high oxygen ratio to silicon and titanium is possibly due to both oxygen adsorbed from air and the small percent error present with XPS. The relatively high silicon content as determined by XPS (4.3%) as compared to the amount reacted (2.5 wt %) is consistent with the surface status of the silica. XPS confirmed the formation of chemical Si−O−Ti bond for the refluxed sample. The O1s spectra of refluxed TiO_2(P25)-SiO_2 (Figure 5) show additional peaks that may be

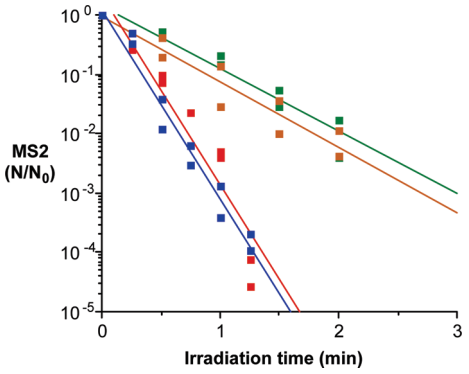

Figure 4. Photocatalytic inactivation of MS2 by TiO_2(P25) (green, R^2 = 0.935), TiO_2(P25) refluxing in toluene with nonsilicone grease (gold, R^2 = 0.917), and TiO_2(P25)-SiO_2 formed by stirring (red, R^2 = 0.907) or refluxing (blue, R^2 = 0.970).

Table 1. First Order Rate Constants for MS2 Inactivation [$Log(N/N_0) = -kt$]

material	k (min^{-1})	r^2
TiO_2(P25)	0.95	0.92
TiO_2(P25) refluxed w/Si grease	2.4	0.93
TiO_2(P25) refluxed w/non-Si grease	1.1	0.92
TiO_2(P25)-SiO_2 stirred	2.8	0.89
TiO_2(P25)-SiO_2 refluxed	3.1	0.97

Table 2. XPS Analysis

sample	Ti (%)	O (%)	Si (%)
TiO_2(P25)	32.5	67.5	-
TiO_2(P25)-SiO_2(2.5%) stirred	26.7	69.0	4.3
TiO_2(P25)-SiO_2(2.5%) refluxed w/non-Si grease	26.0	69.7	4.3

assigned to Si−O−Si and Si−O−Ti units that are not present in the as-received TiO_2(P25). The XPS results for the stirred TiO_2(P25)-SiO_2 showed the presence of Si−O−Si and Ti−O−Ti bonds, confirming no chemical bonds are formed. In addition, the ^{29}Si MAS NMR spectrum of a TiO_2(P25) sample refluxed with 5 wt % fumed silica shows a broad signal typical of silica; however, ^{29}Si NMR cannot differentiate Si−O−Si versus Si−O−Ti.

Improvement in silica-doped TiO_2 photocatalysis has been attributed to quantum confinement, increase in surface area, increase in surface acid sites, control in the grain boundary growth of the nanoparticles, and enhanced adsorption due to the presence of silica.[8,19−23] In our system, we can rule out any quantum effects as the TiO_2(P25) nanoparticles are purchased and not incorporated with silica *in situ*. We can also rule out any increase in the surface area as a result of the reaction with the fumed silica. It is clear from Table 3 that there is no significant difference in the surface area of TiO_2(P25) compared to samples of TiO_2(P25)-SiO_2, as a 25% change in the BET surface area is within the accepted error range. The TiO_2(P25)-SiO_2(2.5%) stirred sample shows a slightly higher surface area (78.79 m^2/g); however, this increase does not lead to a marked improvement or change in catalysis of TiO_2(P25)-SiO_2(2.5%) stirred sample compared to the TiO_2(P25)-SiO_2(2.5%) refluxed sample (surface area 43.95 m^2/g). Therefore, we believe that this increase in the surface area is because of the adsorbed silica onto the surface of the TiO_2(P25) nanoparticles. There are two possible

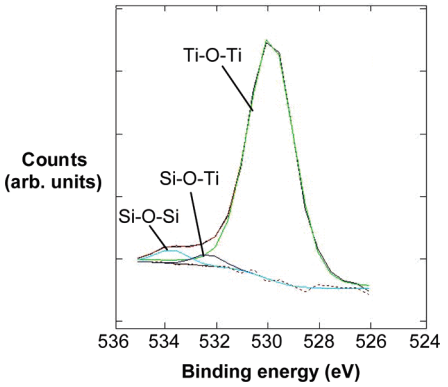

Figure 5. O1s X-ray photoelectron spectrum for TiO_2(P25)-SiO_2-(2.5%) formed by refluxing TiO_2(P25) in toluene in the presence of silica.

Table 3. BET Surface Area Measurements

sample	surface area (m^2/g)
TiO_2(P25)	49.08
SiO_2 (fumed)	239.21
TiO_2(P25)-SiO_2(2.5%) refluxed with Si grease	37.73
TiO_2(P25)-SiO_2(2.5%) refluxed without Si grease	43.94
TiO_2(P25)-SiO_2(2.5%) stirred	78.79

alternative explanations for the enhanced photocatalytic inactivation of MS2 virus by the TiO_2(P25)-SiO_2 used in this study: enhanced adsorption characteristics and/or band gap changes.

Previous studies have demonstrated that silicon-induced enhanced adsorption of substrate to TiO_2−SiO_2 hybrid particles is responsible for the increase in photocatalytic activity.[20,21] In this regard, a similar argument would suggest that the enhanced virus inactivation that we observe with the TiO_2(P25)-SiO_2 material is a result of increased exposure to reactive oxygen species on the catalyst surface resulting from the increased adsorption. Simple alcohols such as methanol are capable of scavenging hydroxyl free radical[27] and as such mostly eliminates the virucidal capability of the catalyst. As shown in Figure 6 there is a significant difference in the activity of the TiO_2(P25)-SiO_2 samples in the presence of methanol, supporting the notion that the generated HO· is responsible for the antiviral action of this material. Thus, our TiO_2(P25)-SiO_2 either produces more HO· than non silica-doped material, or the enhanced adsorption of MS2 to the catalyst results in greater exposure to the HO·, or both mechanisms may work in concert.

Silica doping of TiO_2 in this study has been found to affect the catalyst band gap. The UV−vis absorption curves for TiO_2(P25) and TiO_2(P25)-SiO_2 formed with differing amounts of fumed silica are shown in Figure 7. While it is difficult to see the blue shift between the TiO_2(P25) curve and the TiO_2(P25)-SiO_2(2.5 wt.%) and TiO_2(P25)-SiO_2(10 wt.%), Figure 7 clearly shows a curve shift for TiO_2(P25)-SiO_2(20 wt.%). The band gap energies are calculated using eq 2 and shown in Table 4. It is difficult to see the blue shift between the TiO_2(P25) curve and the TiO_2(P25)-SiO_2(2.5 wt.%) and TiO_2(P25)-SiO_2(10 wt.%); therefore, the derivative of the spectrum is analyzed, and the λ value is defined as the wavelength where the absorption peak is rising most steeply

$$E(eV) = 1239.95/\lambda(nm) \quad (2)$$

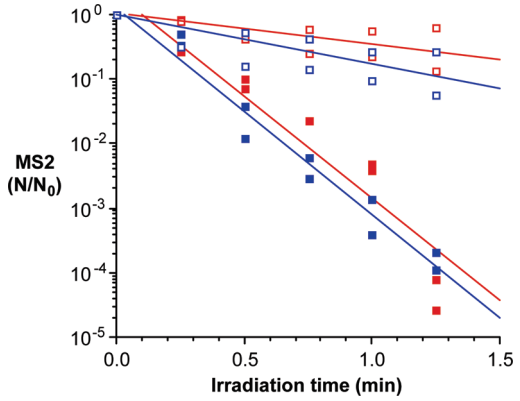

Figure 6. Photocatalytic inactivation of MS2 by TiO_2(P25)-SiO_2 formed by stirring (red solid box, R^2 = 0.907) or refluxing (blue solid box, R^2 = 0.970) as compared to the values when run in the presence of methanol, a scavenger for hydroxyl free radical (red open box, R^2 = 0.479 and blue open box, R^2 = 0.571, respectively).

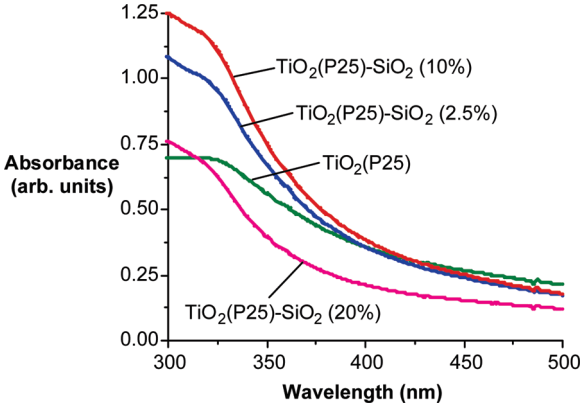

Figure 7. UV−vis absorbance curves for TiO_2(P25) (green line) and TiO_2(P25)-SiO_2 formed with 2.5% (blue line), 10% (red line), and 20% (fuchsia line) SiO_2, respectively.

Table 4. Band Gap Calculations Based on UV-vis Absorbance Spectrum

sample	calculated band gap (eV)
TiO_2(P25)	3.42
TiO_2(P25)-SiO_2(2.5%)	3.43
TiO_2(P25)-SiO_2(10%)	3.45
TiO_2(P25)-SiO_2(20%)	3.47

Anderson and Bard have suggested that the blue shift or increase in band gap energy is attributed to quantum size effects in conjunction with the interface interactions of TiO_2 formation in the presence of silica. They suggested that the presence of silica during the formation of the nanoparticles hinders the growth of the TiO_2 nanoparticle; thus, this smaller size TiO_2 nanoparticle creates a quantum effect and an increase in band gap energy.[22,23] However, since in our studies the TiO_2(P25) is preformed and the particle size is unchanged, the observed effects cannot be due to silica control over titania particle size.

An alternative mechanism was suggested in which a change in the band gap energy is caused by the lowering of the valence band and a raising of the conduction band.[20] The result would be the reduction of the electron−hole recombination when TiO_2 is illuminated with UV light. We note that in these studies the synthesis was also an *in situ* doping of silica that was thought to occur when the titania nanoparticle is formed. In the present case, the band gap energy certainly appears to be changing or slowly increasing, which would reduce the electron−hole recombination. One explanation for this band gap increase may be due to the band bending which can occur at the interface of TiO_2(P25)-SiO_2. When the SiO_2 present on the surface of TiO_2(P25) comes into contact with TiO_2(P25), a potential is created across the interface as the Fermi levels of both compounds try to equilibrate; this potential across the interface leads to band bending. This band bending may reduce the electron−hole recombination, thus allowing for efficient catalysis in our system. This effect occurs on preformed TiO_2(P25) nanoparticles that are subsequently chemically functionalized.[28,29] In our study, the slow change in band gap, along with other factors mentioned earlier, leads to an efficient photocatalysis, without having to dope TiO_2 nanoparticles *in situ* with silicon.

We have demonstrated that improved photocatalytic efficiency of commercial TiO_2(P25) for virus inactivation is achieved by the addition of fumed silica, making it unnecessary to make TiO_2−SiO_2 nanoparticles via an *in situ* process. The enhanced photocatalysis observed with the TiO_2(P25)-SiO_2 in this study is likely due to the greater adsorptive capacity of MS2 to the catalyst and/or changes in the material electronic properties, i.e., increase in band gap. The increased activity of this catalyst for virus inactivation makes it highly attractive alternative for use as a disinfectant. We finally note that our results offer an alternative view of previous "hybrid" TiO_2−SiO_2 systems.[8,19−23]

■ ASSOCIATED CONTENT

Supporting Information. SEM and TEM images, XPS for TiO_2(P25) and TiO_2(P25)-SiO_2, and ^{29}Si MAS NMR of TiO_2(P25)-SiO_2(5%). This material is available free of charge via the Internet at http://pubs.acs.org.

■ AUTHOR INFORMATION

Corresponding Author

*E-mail: arb@rice.edu (A.R.B.), Qilin.Li@rice.edu (Q.L.).

■ ACKNOWLEDGMENT

Financial support for this work was provided by the US Navy, the Robert A. Welch Foundation, and the University of Wales through the Prince of Wales Visiting Innovator Program (A.R.B.).

■ REFERENCES

(1) Water, sanitation, and hygiene links to health. http://www.who.int/water_sanitation_health/publications/facts2004/en/index.html (accessed month day, year).

(2) Yates, M. V.; Malley, J.; Rochelle, P.; Hoffman, R. Effect of adenovirus resistance on UV disinfection requirements. *J. Am. Water Works Assoc.* **2006**, *98*, 93–106.

(3) *Photocatalysis: Science and Technology*; Kaneko, M., Okura, I. E., Eds.; Springer: New York, 2002.

(4) Hoffmann, M. R.; Martin, S. T.; Choi, W.; Bahnemann, D. W. Environmental applications of semiconductor photocatalysis. *Chem. Rev.* **1995**, *95*, 69–96.

(5) Chen, X.; Mao, S. S. Titanium dioxide nanomaterials: synthesis, properties, modifications, and applications. *Chem. Rev.* **2007**, *107*, 2891–2959.

(6) Ohno, T.; Sarukawa, K.; Tokieda, K.; Matsumura, M. Morphology of a TiO_2 photocatalyst (Degussa, P-25) consisting of anatase and ruthile crystalline phases. *J. Catal.* **2001**, *203*, 82–86.

(7) Hurum, D. C.; Agrios, A. G.; Gray, K. A.; Rajh, T.; Thurnauer, M. C. Explaining the enhanced catalytic activity of Degussa P25 mixed-phase TiO_2 using EPR. *J. Phys. Chem. B* **2003**, *107*, 4545–4549.

(8) Zhang, M.; Shi, L.; Yuan, S.; Zhao, Y.; Fang, J. Synthesis and photocatalytic properties of highly stable and neutral TiO_2/SiO_2 hydrosol. *J. Colloid Interface Sci.* **2009**, *330*, 113–118.

(9) Sun, J.; Iwasa, M.; Gao, L.; Zhang, Q. Single-walled carbon nanotubes coated with titania nanopaticles. *Carbon* **2004**, *42*, 895–899.

(10) Janus, M.; Morawski, A. W. New methods of improving catalytic activity of commercial Degussa P25 for azo dyes decomposition. *Appl. Catal., B* **2007**, *75*, 118–123.

(11) Cho, M.; Chung, H.; Yoon, J. (2005). Different inactivation behaviors of MS-2 phage and Escherichia coli in TiO_2 photocatalytic disinfection. *Appl. Environ. Microbiol.* **2005**, *71*(1), 270-275.

(12) Adams, M. H. *Bacteriophages*; Interscience: New York, 1959.

(13) Jafry, H. R.; Liga, M. V.; Li, Q.; Barron, A. R. Single walled carbon nanotubes (SWNTs) as templates for the growth of TiO_2: the effect of silicon in coverage and the positive and negative synergies for the photocatalytic degradation of Congo red dye. *New J. Chem.* **2011**, DOI: 10.1039/CoNJ00604A.

(14) Apblett, A. W.; Barron, A. R. Cleavage of poly(siloxanes) by trimethylaluminum. *Organometallics* **1990**, *9*, 2137–2141.

(15) Apblett, A. W.; Barron, A. R. Design and synthesis of polymeric precursors to aluminosilicates. *Ceram. Trans.* **1991**, *19*, 35–41.

(16) Landry, C. C.; Davis, J. A.; Apblett, A. W.; Barron, A. R. Siloxy-substituted alumoxanes: their synthesis from polydialkylsiloxanes and trimethylaluminium, and application as aluminosilicate precursors. *J. Mater. Chem.* **1993**, *3*, 597–602.

(17) Gao, X.; Wachs, I. E. Titania-silica as catalysts: molecular structural characteristics and physic-chemical properties. *Catal. Today* **1999**, *51*, 233–254.

(18) Fu, X.; Clark, L. A.; Yang, Q.; Anderson, M. A. Enhanced Photocatalytic performace of titania-based binary metal oxides: TiO_2/SiO_2 and TiO_2/ZrO_2. *Environ. Sci. Technol.* **1996**, *30*, 647–653.

(19) Periyat, P.; Baiju, K. V.; Mukundan, P.; Pillai, P. K.; Warrier, K. G. K. High temperature stable mesoporous anatase TiO_2 achieved by silica addition. *Appl. Catal., A* **2008**, *349*, 13–19.

(20) Malinowska, B.; Walendziewski, J.; Robert, D.; Weber, J. V.; Stolarski, M. The study of photocatalytic activities of titania and titania-silica aerogels. *Appl. Catal., B* **2003**, *46*, 441–451.

(21) Aguado, J.; Grieken, R. V.; Lopez-Munoz, M.; Marugan, J. A comprehensive study of the synthesis, characterization and activity of TiO_2 and mixed TiO_2/SiO_2 photocatalysts. *Appl. Catal., A* **2006**, *312*, 202–212.

(22) Anderson, C.; Bard, A. J. An improved photocatalyst of TiO_2/SiO_2 prepared by sol-gel synthesis. *J. Phys. Chem.* **1995**, *99*, 9882–9885.

(23) Anderson, C.; Bard, A. J. Improved catalytic activity and characterization of mixed TiO_2/SiO_2 and TiO_2/Al_2O_3 materials. *J. Phys. Chem. B* **1997**, *101*, 2611–2616.

(24) Whitsitt, E. A.; Barron, A. R. Silica coated fullerenols: seeded growth of silica spheres under acidic conditions. *Chem. Commun.* **2003**, 1042–1043.

(25) Whitsitt, E. A.; Moore, V. C.; Smalley, R. E.; Barron, A. R. LPD silica coating of individual single walled carbon nanotubes. *J. Mater. Chem.* **2005**, *15*, 4678–4687.

(26) Jafry, H. R.; Whitsitt, E. A.; Barron, A. R. Silica coating of vapor grown carbon fibers. *J. Mater. Sci.* **2007**, *42*, 7381–7388.

(27) Sun, J.; Pignatello, J. J. Evidence for a surface dual hole-radical mechanism in the TiO_2 photocatalytic oxidation of 2,4-Dichlorophenoxyacetic acid. *Environ. Sci. Technol.* **1995**, *29*, 2065–2072.

(28) Kaneko, M.; Okura, I. *Photocatalysis: Science and Technology*; Springer: New York, 2002.

(29) Irene, E. A. *Surfaces, Interfaces, and Thin Films for Microelectronics*; Wiley-Interscience: NJ, 2008.

Appendix B

Single walled carbon nanotubes (SWNTs) as templates for the growth of TiO_2: the effect of silicon in coverage and the positive and negative synergies for the photocatalytic degradation of Congo red dye

Huma R. Jafry,[a,b,c] Michael V. Liga,[a,b,d] Qilin Li,[*a,b,d] and Andrew R. Barron[*a,b,c,e]

[a] *Richard E. Smalley Institute for Nanoscale Science and Technology, Rice University, Houston, TX 77005, USA.*

[b] *Center for Biological and Environmental Nanotechnology, Rice University, Houston, TX 77005, USA*

[c] *Department of Chemistry, Rice University, Houston, TX 77005, USA. E-mail address*: arb@rice.edu; Tel: (+1) 713 348 5610

[d] *Department of Civil and Environmental Engineering, Rice University, Houston, TX 77005, USA*

[e] *Department of Mechanical Engineering and Materials Science, Rice University, Houston, TX 77005, USA*

http://pubs.rsc.org/en/Content/ArticleLanding/2011/NJ/C0NJ00604A

New Journal of Chemistry 2011 (35), 400-406

Single walled carbon nanotubes (SWNTs) as templates for the growth of TiO_2: the effect of silicon in coverage and the positive and negative synergies for the photocatalytic degradation of Congo red dye†

Huma R. Jafry,[abc] Michael V. Liga,[abd] Qilin Li*[abd] and Andrew R. Barron*[abce]

Received (in Montpellier, France) 4th August 2010, Accepted 7th October 2010
DOI: 10.1039/c0nj00604a

Single walled carbon nanotubes (SWNTs) are used as scaffolds to grow titania (TiO_2) under a range of different growth conditions. It is found that the titania growth occurring on SWNTs is significantly different in the presence of silica; this is contrary to prior reports, the important controlling factor for obtaining good coverage is not ''nanoscopic HF bubbles''. The silica is either sourced from the reaction vessel if made from glass or may be added in the form of fumed silica: the greater the silicon content the greater the coverage of the SWNT. The adsorption and photocatalysis of organic Congo red dye on these hybrid titania covered SWNT materials are studied; while the adsorption of the dye onto the catalyst may be high, it is only in certain cases wherein it results in superior catalytic performance. The synergy between TiO_2 and SWNTs with regard to photocatalysis is not always positive. The addition of silica promotes the complete coating of SWNT with TiO_2, the resulting materials show very high absorption of Congo red but essentially no catalytic activity. In order to promote catalytic activity, it is necessary to have less full coverage of the SWNTs and the smallest average particle size of the grown titania. Intimate contact between the SWNT and the TiO_2 is needed (rather than a physical mixture) for any catalysis, and the electronic properties of the SWNTs are clearly important since multiwalled carbon nanotubes appear to have little effect on altering the photocatalytic activity.

Introduction

The use of titania (TiO_2) in general, and TiO_2 nanoparticles in particular, as a photocatalyst is extensively documented,[1,2] and the theory behind their activity is relatively well understood.[3] Recently, interest has been focused upon their use as materials for cleaning up water and air pollutants.[4,5] As such, it is desirable to develop catalysts of greater activity and potential specificity, and to meet this goal we have undertaken an investigation of composite or hybrid structures. As the first part of this study we have shown the differences in the growth of TiO_2 on single walled carbon nanotubes (SWNTs). More recently, we have reported that the inclusion of small quantities of silica (SiO_2) into the TiO_2 nanoparticle results in a significant increase in catalytic activity.[6]

The highly hydrophobic nature of carbon nanotubes (CNTs) coupled with their nanostructure, and the potential for their electronic activity (*i.e.*, as a semiconductor), makes them a potentially important catalyst substrate.[7,8] This idea has prompted several studies into methods for growing or mixing TiO_2 with SWNTs, multiwalled carbon nanotubes (MWNTs) and graphene,[9–12] including studies of the photocatalytic activity of the TiO_2–CNT hybrid on the degradation of organic dyes and pollutants.[13] Previous work has shown that the presence of SWNTs or MWNTs in a TiO_2 matrix helps in increasing surface area of the TiO_2 allowing for more organic pollutants to come into contact with the surface of the TiO_2 particle and thus increase the rate of reaction. In addition, the presence of the SWNT or MWNT allows for the transfer of the photoexcited electron from the TiO_2 to the nanotube, thus slowing down the electron–hole recombination and making photocatalysis more efficient.[5,14]

Given our experience with coating carbon nanotubes (CNTs) with oxides,[15–18] chalcogenides,[19] and carbonates,[20] we are interested in determining whether single walled carbon nanotubes (SWNTs) can act as a scaffold for the TiO_2 particle growth and thus create an intimate hybrid material. In addition, we are interested in whether there is any synergistic effect between the SWNT and TiO_2 with regard to catalytic activity. Our initial studies are based upon developing the methodology for growing TiO_2–SWNT hybrids, and determining their activity to the photocatalytic degradation of a model dye system: Congo red.

Experimental

Materials and characterization

P25-TiO_2 (Degussa), fumed silica (14 nm diameter, Sigma-Aldrich), titanium tetrafluoride (TiF_4) (Sigma-Aldrich), EtOH

[a] *Richard E. Smalley Institute for Nanoscale Science and Technology, Rice University, Houston, TX 77005, USA*
[b] *Center for Biological and Environmental Nanotechnology, Rice University, Houston, TX 77005, USA*
[c] *Department of Chemistry, Rice University, Houston, TX 77005, USA. E-mail: arb@rice.edu; Tel: +1 713 348 5610*
[d] *Department of Civil and Environmental Engineering, Rice University, Houston, TX 77005, USA*
[e] *Department of Mechanical Engineering and Materials Science, Rice University, Houston, TX 77005, USA*

† Electronic supplementary information (ESI) available: TEM images of TiO_2-SWNT-PP-21 and TiO_2-SWNT-glass-21. See DOI: 10.1039/c0nj00604a

(Decon Labs), MeOH (Decon Labs), Congo red dye (MP Biomedicals, 85%), and MWNTs (Nanotech Innovations) were obtained from commercial sources and used without further purification. HiPco SWNTs were grown at Rice University and were received as purified (96–97% purified, Batch HPR 181.1). PES syringe filters with a 0.45 μM-pore-size (Whatman) were pre-rinsed by filtering with DI water and purging with air. Unless stated all reactions were carried out in Nalgene® polypropylene (PP) labware.

X-Ray diffraction (XRD) measurements were performed on a Rigaku D/Max Ultima II emitting Cu-K_α radiation. X-Ray photoelectron spectroscopy (XPS) data were collected using a PHI Quantera X-ray photoelectron microscope. Transmission electron microscopy (TEM) images are obtained using a JEM FasTEM multipurpose ultrahigh resolution analytical microscope.

Photocatalytic reactions were carried out using a pre-stabilized Luzchem LZC-4V photoreactor (Luzchem Research, Inc., Ottawa, ON, Canada) fitted with ten 8W UV-A (315–400 nm) lamps with peak emission at 350 nm (Hitachi). The total light intensity used in all experiments was 6.3 mW cm^{-2} as determined by a UV radiometer (Control Company, Friendswood, TX) with a NIST traceable 350 nm photosensor. The dye concentration was measured by determining the absorbance at 497.6 nM with a UV-visible spectrophotometer (Shimadzu UV-2550).

To indicate the different reaction vessels and reaction times, the following format is used to describe each sample: TiO_2–SWNT–glass-21 indicates a material prepared in a glass beaker over a reaction time of 21 h.

TiO_2–SWNT–PP. SWNTs (200 mg) and a solution of TiF_4 (0.04 M in DI H_2O) were placed in a polypropylene (PP) beaker. The beaker was covered with Parafilm secured with a rubber band, and a syringe is used to make a few pinholes to allow for any vapor to escape during heating. The beaker was placed in an oil bath and the mixture heated to 60 °C. After the allotted reaction time (21 or 48 h), the reaction mixture was centrifuged for 15 min at 4400 rpm. After discarding the supernatant, the solid product was washed three times with EtOH : MeOH (90 mL, 4 : 1). The composition of the TiO_2–SWNT–PP reacted for 21 h (*i.e.*, TiO_2–SWNT–PP-21) was determined by XPS (Table 1).

TiO_2–SWNT–glass. Prepared using the same procedure as TiO_2–SWNT–PP, except for the use of a glass beaker, and using reaction times of 10 or 21 h. The composition of the TiO_2–SWNT–glass reacted for 21 h (*i.e.*, TiO_2–SWNT–glass-21) was determined by XPS (Table 1).

TiO_2–SWNT–SiO_2. SWNTs (200 mg) and a solution of TiF_4 (0.04 M in DI H_2O) were placed in a polypropylene beaker. To this mixture, fumed silica (13 mg, 1 wt% of TiF_4) was added. The beaker was covered with parafilm secured with a rubber band, and a few pinholes added to allow vapor to escape. The beaker was placed in an oil bath (60 °C) and the reaction mixture was stirred for 21 h. The reaction mixture was centrifuged for 15 min at 4400 rpm. After discarding the supernatant, the solid product was washed three times with EtOH : MeOH (90 mL, 4 : 1). The composition of TiO_2–SWNT–SiO_2-21 was determined by XPS (Table 1).

Table 1 XPS analysis (%) for TiO_2-coated SWNTs

Sample	C	O	Ti	Si
TiO_2–SWNT–PP-21	79.4	15.1	5.1	—
TiO_2–SWNT–glass-21	78.8	16.5	4.7	<0.1
TiO_2–SWNT–SiO_2-21	68.4	23.7	7.7	0.2

Photocatalysis and adsorption

Photocatalytic activity of nanomaterials was investigated using Congo red dye as a model pollutant for degradation under UV irradiation. The particles were suspended in ultrapure water (pH 4) in a 50 mL Pyrex beaker and dispersed by probe sonication. An aliquot of Congo red stock solution (1 g L^{-1} in H_2O) was then added to achieve a dye concentration of 150 mg L^{-1}. The beaker was covered and magnetically stirred to achieve adsorption equilibrium. The beaker containing the reaction mixture was placed on a magnetic stir plate in the photoreactor and samples were taken at timed intervals. The catalyst was separated from the dye solution by centrifugation and filtration of the supernatant, followed by the measurement of the dye concentration.

TiO_2–SWNT–PP nanoparticles were tested at 500 mg L^{-1}. After being combined with the Congo red, the reaction mixture was stirred in the dark for 1 h before being placed in the photoreactor. As a comparison P25-TiO_2 was tested at 134 mg L^{-1}, which corresponds to the TiO_2 content of approximately 5% on the coated tubes.

TiO_2–SWNT–glass-10 was initially tested for Congo red adsorption at 500 mg L^{-1} catalyst concentration. Subsequent adsorption and photocatalytic data using this material and the TiO_2–SWNT–glass-10 material were tested at 250 mg L^{-1} catalyst concentration. P25-TiO_2 was tested at 69 mg L^{-1}, which corresponds to the TiO_2 content of approximately 5% on the coated tubes.

P25-TiO_2 and SWNTs were tested at 250 mg L^{-1} when determining the amount of dye removed by adsorption only on each material. After being combined with the dye, they were stirred in the dark for 21 hours before measuring the dye concentration in solution.

A pre-sonicated suspension of P25-TiO_2 and either SWNTs or MWNTs were combined and added to a Congo red solution to achieve a final total catalyst concentration of 250 mg L^{-1} (69 mg L^{-1} or 5% Ti on 250 mg composite), 181 mg L^{-1} SWNTs (or MWNTs) and 150 mg L^{-1} Congo red. The mixtures were stirred in the dark for 21 hours to achieve adsorption equilibrium before beginning the photocatalytic reaction.

Results and discussion

Growth of TiO_2 on SWNTs

Our initial starting point was to replicate the synthesis of Zeng and Liu[14] in coating SWNTs with TiO_2. The formation of TiO_2 is based upon the hydrolysis of titanium tetrafluoride (eqn (1)).

$$TiF_4 + 2\,H_2O \rightarrow TiO_2 + 4\,HF \quad (1)$$

Unsurfacted purified SWNTs were placed in a polypropylene (PP) reaction vessel in DI water with TiF_4. However, TEM analysis of TiO_2 growth on SWNTs for 21 h. Fig. 1a shows incomplete growth with significant portions of the SWNTs still exposed. This is very different from the growth achieved previously,[14] where they reported complete coverage of the SWNT with TiO_2 in only 20 h. In fact, in our hands the reaction needed to proceed for 48 h in order to obtain complete coverage of the SWNTs by TiO_2 (see Fig. 1b).

Upon further investigation, we discovered that while, based upon our prior experiences with HF generating reactions,[18] we had used a polypropylene reaction vessel, Zeng and Liu[14] had used a glass beaker. We therefore repeated the reaction using a glass beaker. As may be seen from the TEM images in Fig. 2 it takes almost half the time to achieve the TiO_2 coverage on SWNTs using a glass beaker, compared to that of a polypropylene beaker (*i.e.*, Fig. 1a *versus* Fig. 2a).

The well-connected growth of TiO_2 on the SWNTs was previously attributed to the formation of nanoscopic HF bubbles that were trapped onto the TiO_2 crystallites.[14] It was proposed that this solid–gas interface prevented the TiO_2 crystallites from growing above a certain size by terminating the supply of TiF_4 to the crystal surface. As a consequence new growth must take place at any available solid–liquid interface (*i.e.*, the uncoated SWNT surface) resulting in a connected mesocrystalline growth. Based upon our results of growth in a polypropylene beaker this explanation cannot be true, since the same nanoscopic HF bubbles would be present in our system. An alternative explanation must be developed.

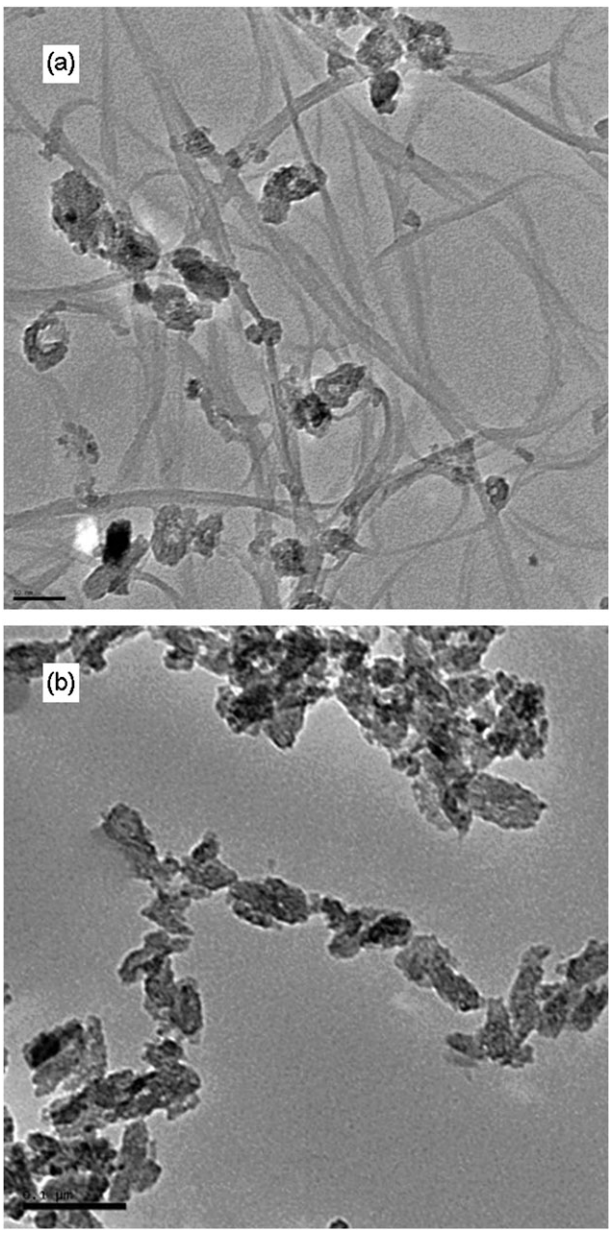

Fig. 1 TEM image of (a) TiO_2–SWNT–PP-21 (scale = 50 nm) and (b) TiO_2–SWNT–PP-48 (scale = 0.1 μm).

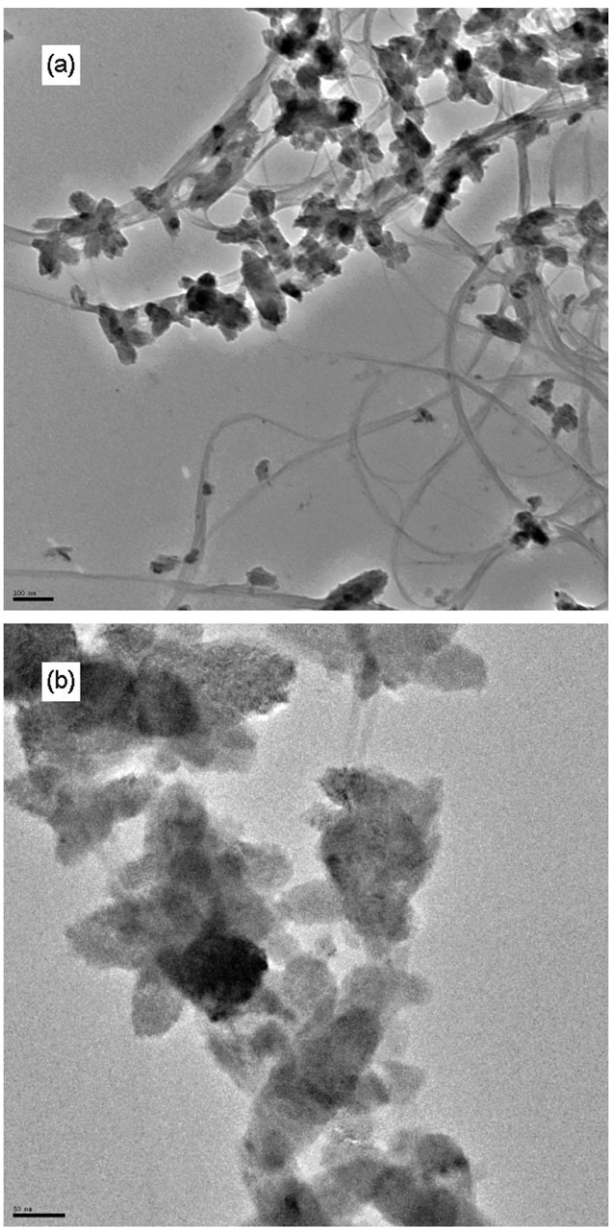

Fig. 2 TEM images of (a) TiO_2–SWNT–glass-21 (scale = 100 nm) and (b) TiO_2–SWNT–glass-10 (scale = 50 nm).

XPS analysis of the TiO_2–SWNT–glass samples shows the presence of detectable amounts of silicon (<1%) not observed in the TiO_2–SWNT–PP samples. Since it is well known that HF will etch silicon and silica glass,[21] and based on eqn (1), it is clear that the HF in the TiO_2 growth solution could be responsible for the inclusion of silicon into the TiO_2–SWNT–glass samples. Previous studies on TiO_2 nanoparticles doped by metals or metal oxides have shown a change in the growth of the TiO_2 crystals. For example, the addition of niobium to a TiO_2 growth solution inhibits the process of nucleation and growth of TiO_2 crystallites.[22] Other studies have shown that the presence of SiO_2 in the growth solution decreases the size of the TiO_2 nanoparticle by reducing the nucleation sites on the grain boundary, thus preventing the TiO_2 particles from aggregating and growing too big.[23–25] It has also previously been described that the presence of SiO_2 in a TiO_2 nanoparticle creates Lewis acid sites,[26] which under heat treatment or irradiation form hydroxyl radicals, which slow the growth of the TiO_2 grain.[27]

Based upon these results we propose that the formation of well-connected growth of TiO_2 on the SWNTs is not a function of "nanoscopic HF bubbles", but the incorporation of small quantities of silica into the TiO_2 as a consequence of the etching of the glass container during the reaction. Although XPS shows a very small presence of silicon (Table 1), a high resolution XPS of the TiO_2–SWNT–glass sample shows that silicon is present in the form of silica or silica bound to TiO_2 (Table 2). This silica is involved in limiting the growth of the TiO_2 crystals, and hence promoting the coverage of the SWNT by TiO_2.

In order to further understand the role of SiO_2 in the growth of TiO_2 on SWNTs, we added fumed SiO_2 into the TiO_2 growth solution. The TEM image of the resulting material (TiO_2–SWNT–SiO_2) is shown in Fig. 3. As can be observed, the SWNT substrate is covered with smaller but many more TiO_2 particles, giving complete coverage of the SWNT. This is in contrast to the image shown in Fig. 1a. In fact, the coverage for the reaction with added SiO_2 is even greater than an equivalent reaction time in glass. Thus, for any given set of reaction conditions, the greater the silicon content (Table 1) the greater the coverage of the SWNT by TiO_2. We believe this demonstrates the idea that the silica plays an important part in controlling the relative rates of grain growth and new growth of TiO_2 on SWNTs. A high resolution XPS performed on this sample shows a similar chemical makeup and presence of silica and silica bound to TiO_2 as the TiO_2–SWNT–glass sample (Table 3). Therefore, in both TiO_2–SWNT–glass and TiO_2–SWNT–SiO_2 samples, the mechanism by which silica is incorporated into the TiO_2 nanocrystals appears to be similar. The only difference between the two samples is in the total amount of silica present in the growth solution.

Table 2 High resolution Si XPS of the TiO_2–SWNT–glass-21 sample

Binding energy/eV	%	Chemical composition
101.64	30.95	$(TiO_2)_x(SiO_2)_y$
102.2	40.53	$(TiO_2)_x(SiO_2)_y$
103.0	28.53	SiO_2

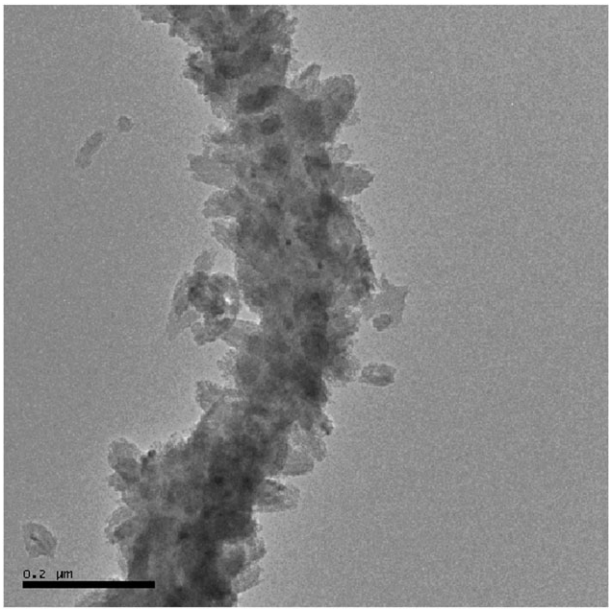

Fig. 3 TEM image of TiO_2–SWNT–SiO_2-21 (scale = 0.2 µm).

Table 3 High resolution Si XPS of the TiO_2–SWNT–SiO_2 sample

Binding energy/eV	%	Chemical composition
101.4	30.28	$(TiO_2)_x(SiO_2)_y$
102.1	38.92	$(TiO_2)_x(SiO_2)_y$
103.1	30.80	SiO_2

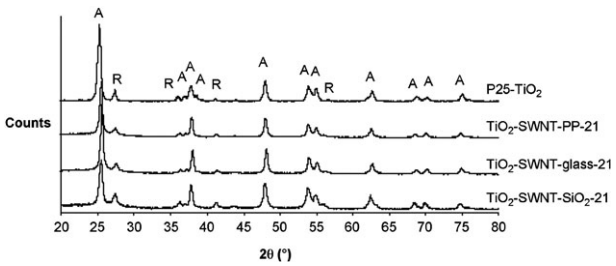

Fig. 4 XRD showing the anatase (A) and rutile (R) phases of commercial P25-TiO_2 as compared to TiO_2–SWNT–PP-21, TiO_2–SWNT–glass-21, and TiO_2–SWNT–SiO_2-21.

Fig. 4 shows the XRD data for the different phases of TiO_2 formed on the TiO_2–SWNT–polypropylene, TiO_2–SWNT–glass, and TiO_2–SWNT–SiO_2 as compared to P25-TiO_2, a commercially available TiO_2 nanoparticle of known high photoreactivity.[28] The XRD data confirm the presence and formation of both anatase and rutile phases for the as grown TiO_2. However, it is interesting to note that the anatase : rutile ratio is dependant on the amount of silica present. The TiO_2 for TiO_2–SWNT–PP and TiO_2–SWNT–glass is slightly richer in anatase than found in P25-TiO_2, while TiO_2–SWNT–SiO_2 has much less anatase than found in P25-TiO_2.

Adsorption of Congo red

Congo red (Fig. 5) is a polycyclic aromatic hydrocarbon dye that is commonly used as a model for photocatalytic

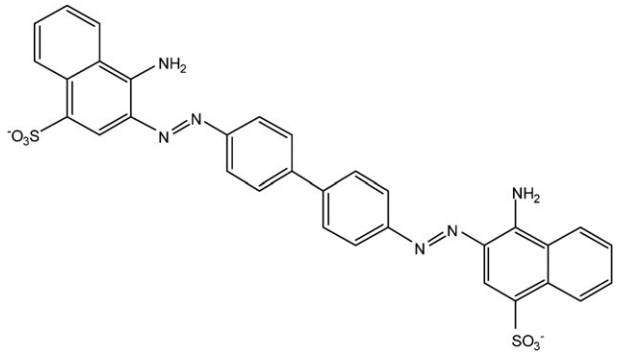

Fig. 5 Chemical structure of Congo red dye.

degradation studies. We have previously found that in studying the degradation of Congo red it is important to determine the adsorption in the dark to provide an accurate initial concentration (C_0) for the photocatalytic measurements. This is particularly important given that the polycyclic aromatic structure of Congo red promotes strong π–π stacking interaction with SWNTs, giving rise to high adsorptive removal. Thus, the percent removal of Congo red after 1 hour dark stirring was measured using an initial dye concentration 150 mg L^{-1} and a catalyst concentration of either 500 mg L^{-1} or 250 mg L^{-1}.

As is shown in Fig. 6 TiO_2–SWNT–PP-21 and TiO_2–SWNT–PP-48 both show significantly greater adsorption as compared to P25-TiO_2, with the greatest adsorption being associated with the lower coverage of the SWNT. The low coverage TiO_2–SWNT–glass-10 shows almost total adsorption (Fig. 6) as do unfunctionalized SWNTs. Given the huge adsorption of the dye on TiO_2–SWNT–glass-10 sample using 500 mg L^{-1} catalyst, it would be impossible to test for catalysis as all the dye would be adsorbed onto the catalyst, making it difficult to measure the degradation of the dye left in solution. Therefore, a low concentration (250 mg L^{-1}) was used for further tests on the TiO_2–SWNT–glass samples and the raw SWNTs (Fig. 7). At a 250 mg L^{-1} catalyst concentration, the TiO_2–SWNT–glass materials still had significant adsorption of Congo red; however, once again the lower adsorption for TiO_2–SWNT–glass-48 as compared to TiO_2–SWNT–glass-21 indicates that complete coverage with TiO_2 can reduce the absorbance capacity.

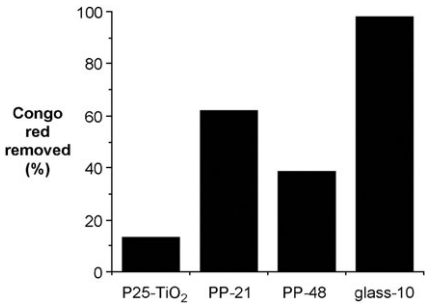

Fig. 6 Percent removal of Congo red after 1 hour dark stirring by P25-TiO_2, TiO_2–SWNTs–PP-21 (PP-21), TiO_2–SWNTs–PP-48 (PP-48), and TiO_2–SWNTs–glass-10 (glass-10) with a catalyst concentration of 500 mg L^{-1} and an initial dye concentration 250 mg L^{-1}.

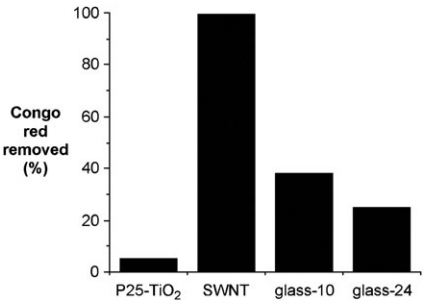

Fig. 7 Percent removal of Congo red after 1 hour dark stirring by P25-TiO_2, SWNTs, TiO_2–SWNTs–glass-10 (glass-10), and TiO_2–SWNTs–glass-21 (glass-21) with a catalyst concentration of 250 mg L^{-1} and an initial dye concentration 150 mg L^{-1}.

Photocatalytic decomposition of Congo red

The photocatalytic decomposition of Congo red was studied for the different hybrid materials in comparison with P25-TiO_2. In each case the samples were stirred in the dark (1 h for TiO_2–SWNT–PP samples and 21 h for TiO_2–SWNT–glass samples), and the initial concentration is defined as C_0, which is the concentration after dark stirring. The C/C_0 values were determined as a function of irradiation time.

A comparison of the photocatalytic activity of TiO_2–SWNT–PP-21 and TiO_2–SWNT–PP-48 is shown in Fig. 8. The TiO_2–SWNT–PP-21 material showed better catalysis than the TiO_2–SWNT–PP-48 material, indicating that complete coverage of the tubes by TiO_2 does not result in enhanced photocatalysis. For the first 80 min of the reaction time, the catalytic results for the TiO_2–SWNT–PP-21 sample were similar to that of P25-TiO_2 nanoparticles tested at the equivalent TiO_2 concentration (134 mg L^{-1}). However, after 80 min the dye degradation by TiO_2–SWNT–PP-21 material proceeded faster than the degradation by P25-TiO_2, *i.e.*, 82% of the dye was removed from solution by the TiO_2–SWNT–PP-21 *versus* only 54% removed by P25-TiO_2 after 165 min of reaction time. We propose that this increase in activity with time is associated with the strong binding of the Congo red reagent to the exposed SWNT.

While the TiO_2–SWNT–glass was found to strongly adsorb Congo red from solution, the material possessed limited to no photocatalytic activity for this particular dye (Fig. 9), whereas P25-TiO_2 tested as a comparison was found to degrade 34% of

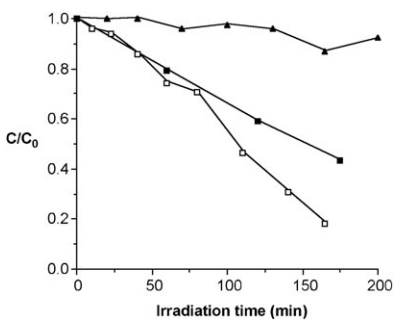

Fig. 8 Normalized photocatalytic degradation of Congo red by TiO_2–SWNTs–PP-21 (□), TiO_2–SWNTs–PP-48 (▲) and P25-TiO_2 (■). C_0 is the dye concentration after dark stirring.

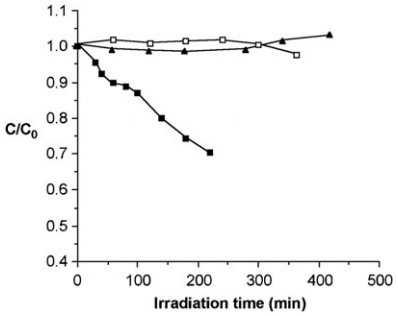

Fig. 9 Normalized photocatalytic degradation of Congo red by TiO_2–SWNTs–glass-10 (▲), TiO_2–SWNTs–glass-21 (□), and P25-TiO_2 (■). C_0 is the dye concentration after dark stirring.

the dye after 220 min irradiation. It is especially surprising that the materials made in glass demonstrate no photocatalytic activity, especially when XRD analysis confirms that the TiO_2 exists mostly as anatase and rutile, which are both photoactive crystalline phases. This result is especially surprising when considering that several other studies have shown enhanced catalysis by TiO_2 when coated onto CNTs.[29–32] Furthermore, studies have shown that doping TiO_2 nanoparticles with silicon or zirconium enhances the photocatalysis.[33] It is possible that, with such strong absorbance to the catalyst, the dye was being degraded on the catalyst surface and not desorbed back into solution. In this way the free dye concentration would not change in solution but the concentration on the particle surface would decrease.

Since the SWNTs appeared to improve TiO_2 activity in one case (TiO_2–SWNT–PP-21) and decrease the TiO_2 activity in all other cases, we decided to investigate whether the presence of SWNTs or MWNTs in solution would hinder or enhance the photocatalytic removal of Congo red from solution by P25-TiO_2. As shown in Fig. 10, the presence of SWNTs was found to eliminate the photocatalytic activity of P25-TiO_2, while the presence of MWNTs slightly slowed the reaction as compared to TiO_2 used without any CNTs. The small reduction when MWNTs are used may simply be due to a shielding of the UV radiation by the MWNTs, while the SWNTs likely inhibit TiO_2 photocatalysis by some other mechanism since the result is so much worse than with MWNTs.

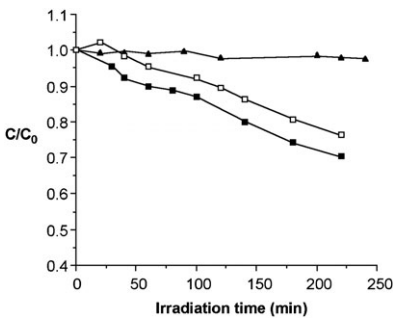

Fig. 10 Normalized photocatalytic degradation of Congo red by a physical mixture of P25-TiO_2 with SWNTs (▲) or MWNTs (□) in comparison with P25-TiO_2 (■). C_0 is the dye concentration after dark stirring.

Conclusion

We have shown that SWNTs do act as templates for the growth of TiO_2. Unlike previously suggested, the important controlling factor for obtaining good coverage is not "nanoscopic HF bubbles", but rather the presence of silica. The silica is either sourced from the reaction vessel if made from glass or may be added in the form of fumed silica: the greater the silicon content the greater the coverage of the SWNT.

While the addition of silica promotes the complete coating of SWNT with TiO_2, the resulting materials show very high absorption of Congo red and essentially no catalytic activity. This is a surprise since P25-TiO_2–SiO_2 has been shown to show a significantly higher catalytic activity than P25-TiO_2 itself. Based upon the adsorption studies we propose a number of requirements in the present system. It is necessary to have less than 70% initial absorption. Any higher absorption and the reactants and/or product are not desorbed and no catalysis occurs. Nevertheless, it also appears necessary that less than full coverage of the SWNTs be attained. It is also worth noting that the highest activity occurs with the small average particle size. We have shown that intimate contact between the SWNT and the TiO_2 is needed (rather than a physical mixture) for any catalysis, presumably since the SWNTs strongly absorb the Congo red and preclude further reaction. However, the electronic properties of the SWNTs (including semiconducting tubes) are clearly important since MWNTs appear to have little effect on altering the photocatalytic activity of P25-TiO_2.

The forgoing results indicate that while there is a synergy between TiO_2 and SWNTs with regard to photocatalysis it is not always positive. In other words, under some conditions the presence of SWNTs inhibits catalysis, and it is only with certain structures (*i.e.*, TiO_2–SWNT–PP-21) that the combination of materials shows an enhancement over the constituent parts. We are furthering our studies to determine whether such a dichotomy is a result of the strong hydrophobic interactions with the particular model system (Congo red) or a general feature of the composite structures.

References

1 A. Fujishima, T. N. Rao and D. A. Tryk, *J. Photochem. Photobiol., C*, 2000, **1**, 1.
2 Y. Ao, J. Xu, D. Fu and C. Yuan, *Electrochem. Commun.*, 2008, **10**, 1812.
3 X. Chen and S. S. Mao, *Chem. Rev.*, 2007, **107**, 2891.
4 H. Choi, A. C. Sofranko and D. D. Dionysiou, *Adv. Funct. Mater.*, 2006, **16**, 1067.
5 Y. Yao, G. Li, S. Ciston, R. M. Lueptow and K. A. Gray, *Environ. Sci. Technol.*, 2008, **42**, 4952.
6 H. R. Jafry, M. V. Liga, Q. Li and A. R. Barron, *Environ. Sci. Technol.*, in press.
7 J. M. Planeix, N. Coustel, B. Coq, V. Brotons, P. S. Kumbhar, R. Dutartre, P. Geneste, P. Bernier and P. M. Ajayan, *J. Am. Chem. Soc.*, 1994, **116**, 7935.
8 W. Li, C. Liang, W. Zhou, J. Qiu, Z. Zhou, G. Sun and Q. Xin, *J. Phys. Chem. B*, 2003, **107**, 6292.
9 J. Sun, M. Iwasa, L. Gao and Q. Zhang, *Carbon*, 2004, **42**, 895.
10 M. Pender, L. Sowards, J. D. Hartgerink, M. O. Stone and R. R. Naik, *Nano Lett.*, 2006, **6**, 40.
11 E. Llobet, E. H. Espinosa, E. Sotter, R. Ionescu, X. Vilanova, J. Torres, A. Felten, J. J. Pireaux, X. Ke, G. V. Tendeloo, F. Renaux, Y. Paint, M. Hecq and C. Bittencourt, *Nanotechnology*, 2008, **19**, 375501.

12 Y.-J. Liu, Z.-M. Wang, M. Aizawa, W.-Q. Peng and T. Hirotsu, *Mater. Lett*., 2009, **63**, 260.
13 K. Woan, G. Pyrgiotakis and W. Sigmund, *Adv. Mater*., 2009, **21**, 2233.
14 B. Liu and H. C. Zeng, *Chem. Mater*., 2008, **20**, 2711.
15 E. A. Whitsitt and A. R. Barron, *Chem. Commun*., 2003, 1042.
16 E. A. Whitsitt, V. C. Moore, R. E. Smalley and A. R. Barron, *J. Mater. Chem*., 2005, **15**, 4678.
17 R. Colorado, Jr. and A. R. Barron, *Chem. Mater*., 2004, **16**, 2691.
18 H. R. Jafry, E. A. Whitsitt and A. R. Barron, *J. Mater. Sci*., 2007, **42**, 7381.
19 R. Loscutova and A. R. Barron, *J. Mater. Chem*., 2005, **15**, 4346.
20 R. E. Anderson and A. R. Barron, *Main Group Chem*., 2005, **4**, 279.
21 G. W. Trucks, K. Raghavachari, G. S. Higashi and Y. J. Chabal, *Phys. Rev. Lett*., 1990, **65**, 504.
22 S. B. Aldabergenova, A. Ghicov, S. Albu, J. M. Macak and P. Schmuki, *J. Non-Cryst. Solids*, 2008, **354**, 2190.
23 C. He, B. Tian and J. Zhang, *Microporous Mesoporous Mater*., 2009, **126**, 50.
24 M. Zhang, L. Shi, S. Yuan, Y. Zhao and J. Fang, *J.Colloid Interface Sci*., 2009, **330**, 113.
25 J. Kim, K. C. Song, S. Foncillas and S. E. Pratsinis, *J. Eur. Ceram. Soc*., 2001, **21**, 2863.
26 P. Periyat, K. V. Baiju, P. Mukundan, P. K. Pillai and K. G. K. Warrier, *Appl. Catal., A*, 2008, **349**, 13.
27 P. Cheng, M. Zheng, Y. Jin, Q. Huang and M. Gu, *Mater. Lett*., 2003, **57**, 2989.
28 D. C. Hurum, A. G. Agrios, K. A. Gray, T. Rajh and M. C. Thurnauer, *J. Phys. Chem. B*, 2003, **107**, 4545.
29 Y. Yao, G. Li, S. Ciston, R. M. Lueptow and K. A. Gray, *Environ. Sci. Technol*., 2008, **42**, 4952.
30 H. Wang, H. L. Wang, W. F. Jiang and Z. Q. Li, *Water Res*., 2009, **43**, 204.
31 B. Liu and H. C. Zeng, *Chem. Mater*., 2008, **20**, 2711.
32 G. An, W. Ma, Z. Sun, Z. Liu, B. Han, S. Miao, Z. Miao and K. Ding, *Carbon*, 2007, **45**, 1795.
33 X. Fu, L. A. Clark, Q. Yang and M. A. Anderson, *Environ. Sci. Technol*., 1996, **30**, 647.

Appendix C

Alumoxane/Ferroxane Nanoparticles for the Removal of Viral Pathogens: The Importance of Surface Functionality to Nanoparticle Activity†‡

Samuel J. Maguire-Boyle,[a,b] Michael V. Liga,[a,c] Qilin Li,[a,c]* and Andrew R. Barron[a,b,d,e]*

[a] Richard E Smalley Institute for Nanoscale Science and Technology, Rice University, Houston, Texas 77005, USA. E-mail: arb@rice.edu; qilin.li@ rice.edu; Tel: +1-713-348-5610

[b] Department of Chemistry, Rice University, Houston, Texas 77005, USA

[c] Department of Civil and Environmental Engineering, Rice University, Houston, Texas 77005, USA

[d] Department of Mechanical Engineering and Materials Science, Rice University, Houston, Texas 77005, USA

[e] College of Engineering, Swansea University, Singleton Park, Swansea SA2 8PP, Wales UK

† Financial support for this work was provided by the US Navy and the Robert A. Welch Foundation (C-0002).

‡ Electronic supplementary information (ESI) available: SEM, EDX, and TEM images, XPS spectra, apparatus, and TGA/DTA. See DOI: 10.1039/c2nr31117h

http://pubs.rsc.org/en/content/articlelanding/2012/nr/c2nr31117h

Nanoscale 2012 (4), 5627-5632

Nanoscale

Dynamic Article Links ►

Cite this: DOI: 10.1039/c2nr31117h

www.rsc.org/nanoscale

PAPER

Alumoxane/Ferroxane Nanoparticles for the Removal of Viral Pathogens: The Importance of Surface Functionality to Nanoparticle Activity†

Samuel J. Maguire-Boyle,[a,b] Michael V. Liga,[a,c] Qilin Li,[a,c]* and Andrew R. Barron[a,b,d,e]*

Received 6th May 2012, Accepted 4th July 2012
DOI: 10.1039/c2nr31117h

A bi-functional nano-composite coating has been created on a porous Nomex® fabric support as a trap for aspirated virus contaminated water. Nomex® fabric was successively dip-coated in solutions containing cysteic acid functionalized alumina (alumoxane) nanoparticles and cysteic acid functionalized iron oxide (ferroxane) nanoparticles to form a nanoparticle coated Nomex® (NPN) fabric. From SEM and EDX the nanoparticle coating of the Nomex® fibers is uniform, continuous, and conformal. The NPN was used as a filter for aspirated bacteriophage MS2 viruses using end-on filtration of aspirated viruses was measured. All measurements were repeated to give statistical reliability. The NPN fabrics show a large decrease as compared to Nomex® alone or alumoxane coating. An increase in the ferroxane content results in an equivalent increase in virus retention. This suggests that it is the ferroxane that has an active role in either deactivating or binding the virus. Heating the NPN to 160 °C results in the loss of cysteic acid functional groups (without loss of the iron nanoparticles) and the resulting fabric behaves similar to that of untreated Nomex®, showing that the surface fuctionalization of the nanoparticles is vital for the surface collapse of aspirated water droplets and the absorption and immobilization of the MS2 viruses. Thus, for virus immobilization it is not sufficient to have nanoparticles per se, but the surface functionality of a nanoparticle is vitally important in ensuring functionality.

Introduction

Contamination of water by viral pathogens is endemic in many parts of the world. Sources of contamination include industrial and agricultural wastes, sewage and other forms of pollution. Sewage levels of approximately 7,000 viruses per liter are common, and can be more than 500,000 virus particles per liter.[1] Inhalation of this aspirated water can lead to serious infections and intoxications through exposure of mucous membranes in the eyes (conjunctiva), nose (rhinal) and mouth. In many cases gastroenteritis, respiratory disease, or eye, ear and nose infections result. However, more serious consequences and life-threatening complications can occur. To overcome this, a viral filter for aspirated viruses would be of great utility.

The use of iron oxide nanoparticles as a component of a filter is reasonable since iron oxide and oxyhydroxides human toxicity is low,[2] and it has also been shown that Fe(O)OH and Fe_2O_3 are more resistant to acidic, corrosive, and oxidant conditions than other anti viral materials (e.g., silver).[3] The affinity for binding of iron nanoparticles to virus pathogens was envisaged as it has been observed in nature,[4] where it has been shown that viruses interact and act as nucleation sites for the adsorption and precipitation of dissolved metals especially iron.[5] Up to 50% of "dissolved iron" in sea water is between 30 nm and 100 nm in diameter.[6,7,8] Between 90% and 99% of iron particulates are strongly chelated by organic ligands.[7,8] Viral-lepidocrocite binding has been observed in sea water systems. Since virus adsorption is a function of surface area as well as surface activity, nanoparticles should show enhanced performance. However, an important

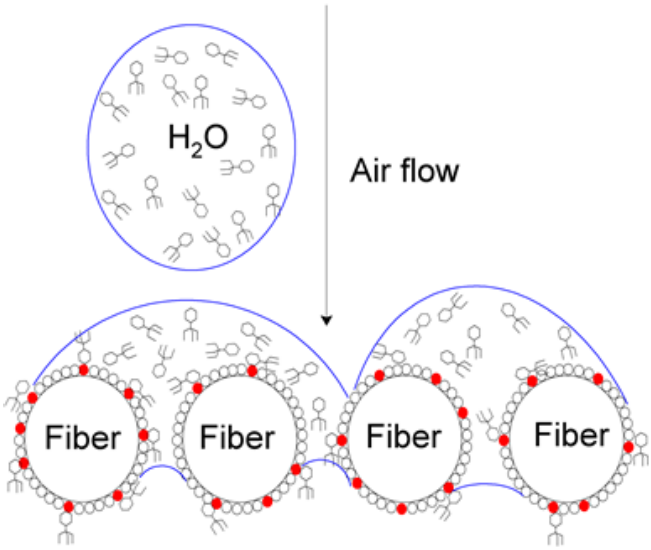

Fig.1 Schematic diagram of alumoxane/ferroxane viral trap showing the collapsed water droplet containing the virus on the fibers coated with both ferroxane (iron oxide) nanoparticles (dark circle) and alumoxane (alumina) nanoparticles (open circles).

question to answer is whether any such performance is simply a function of the "nano" nature of the iron oxide nanoparticle, or a consequence of the surface functionality in concert with the nano scale. The present research is aimed at understanding how the surface functionality of a nanoparticle can alter the efficacy of the nanoparticle activity.

Despite the efficacy of iron oxides, and the potential of nanocrystaline iron oxides, there is a second important component of any trap for aspirated viruses; it is necessary to provide a surface onto which water droplets will collapse. We have previously shown that coating Nomex® or similar fabric with cysteic acid [$HO_2CCH(NH_2)CH_2SO_3H$] functionalized alumina nanoparticles (cysteic-alumoxane) results in a superhydrophilic surface that allows for the passage of water,[9] but not hydrocarbons. In the present application the function of the superhydrophilic surface as measured by an extremely low contact angle (<3°) is to "collapse" airborne water droplets onto the surface, if this hydrophilic surface is combined with functionalization to trap and immobilize viruses then a combined system for removal of airborne or aspirated viruses may be achieved (Fig. 1). As noted above binding efficiency of iron oxides for viruses has been well documented suggesting that an iron oxide containing surface should be ideal as the trap. Thus, we propose that the creation of a bi-functional nano-composite coating on a porous support should provide a suitable test bed as a trap for aspirated virus contaminated water. The cysteic acid functionalized nanoparticles (alumina or iron oxide) should both cause the collapse of the water droplets, while the greater the iron content should trap and immobilize higher concentrations of viruses. Nomex® fabric was chosen as a convenient nanoparticle scaffold because of the uniformity of the fibers (providing a homogeneous support) and the large weave of the fabric (sufficient to allow viruses to pass through). In addition, its use in protective garments in hazardous locations[10] and its tolerance to harsh conditions[11] make it a suitable practical substrate.

We have shown previously that carboxylic acid functionalized iron oxide nanoparticles (ferroxanes), are readily prepared from rust-like materials and propose the combination of a hydrophilic surface alumoxane nanoparticles and viral binding functionalization ferroxane nanoparticles should make an effective hybrid material.[12]

Experimental section

1. Materials and methods

Cysteic acid, $FeCl_2.4H_2O$, EtOH and acetone (Sigma-Aldrich) were used as received. Pseudoboehmite Catapal B was provided by Sasol North America Inc. Nomex® fabric was obtained from Pegasus Auto Racing Supplies, and was washed sequentially with EtOH and acetone to remove excess dye molecules. Energy dispersive spectroscopy (EDS) studies were performed on a FEI Quanta 400 ESEM. The samples were attached to a metal mount using carbon tape. Thermogravimetric/differential thermal analyses (TG/DTA) were obtained on a Q-600 Simultaneous TGA/DSC TA Instruments machine using a carrier gas of either dry argon or air. Scanning electron microscopy (SEM) studies were performed on a FEI Quanta 400 ESEM. A 5 nm layer of gold was sputtered onto the samples to provide a conducting surface. The samples were mounted on carbon tape. Transition electron microscopy (TEM) studies were performed on a JEOLl 1230 HC-TEM 120kV. Dilute solutions of nanoparticles were sonicated in DI water, and drop cast onto 300 mesh copper grids the excess solution being wicked away. Samples containing MS2 were subsequently stained with 2% uranyl acetate (SPI-CHEM). The grids were received from Ted Pella with amorphous carbon surface and Formvar coating with the Formvar coating being removed by immersion of the grid in Chloroform for thirty seconds and air drying just before drop casting. XPS studies were conducted on a PHI Quantera XPS machine. Samples were mounted onto the platen using double-sided carbon tape. Atomic force microscopy (AFM) measurements were conducted on a multimode AFM in tapping mode. The microscope was equipped with a Nanoscope IIIa scanning probe microscope controller and an Optizoom microscope from Digital Instruments. AFM tips were from K-TEK nanotechnology, which were SPM probe model: TETA/Au (15) with an Au conductive coating and a resonant frequency of 300 Hz.

Bacteriophage MS2 (ATCC 15597-B1) and the host bacteria, *E. coli* (ATCC 15597) were originally obtained from the ATCC, LB-Lennox media and sodium bicarbonate were purchased from Fisher Scientific, and Bacto™ agar was purchased from Difco Laboratories. Ultrapure water was obtained from a Barnstead E-Pure system. All materials were sterilized by autoclave, 70% EtOH, or filtration through a 0.22 μM membrane. Bacteriophage MS2 was used as a surrogate pathogenic virus in this study and was propagated using *E. coli*. in LB-Lennox media (Fisher Scientific). 200 μL of MS2 stock solution was combined with 800 μL of an incubation of *E. coli*. This was combined with 3 mL of molten (45 °C) LB-Lennox media containing 0.7% Bacto™ Agar (Difco Laboratories) and poured onto a Petri dish containing solid LB-Lennox media with 1.5% Bacto™ Agar. The plates were incubated overnight and subsequently filled with 15 mL of 100 mM $NaHCO_3$ solution (Fisher Scientific) and gently rocked for 3 hours.[13] The buffer was withdrawn, centrifuged at 10,900 x g for 15 minutes, and the supernatant passed through a 0.22 μM-pore-size syringe filter. The virus solution measured ~7 x 10^9 PFU/mL and was stored at 4 °C until use in the virus removal experiments.

2. Synthesis

2.1. Synthesis of cysteic acid alumoxane nanoparticles

In a modification of the literature procedures[14] pseudoboehmite (100 g) was vigorously stirred in DI H_2O (80 mL) to this was slowly added an aqueous 1 M solution of cysteic acid (80 mL). The resulting solution was allowed to stir overnight, and then centrifuged at 4500 rpm for 1 h. The supernatant was evaporated under vacuum and the resulting solid was used for coatings. Ceramic yield: 55%. Average particle size: 18 nm.

2.2. Synthesis of cysteic acid ferroxane nanoparticles

In a modification of the literature procedure[12] a 1M solution $FeCl_2.4H_2O$ (100 mL) was mixed with 1.67 M solution of NaOH (100 mL). The ratio R = $[FeCl_2.4H_2O]/[NaOH]$ = 0.6 favors the formation of a pure lepidocrocite. To this was slowly added an aqueous 1 M solution of cysteic acid (80 mL). The resulting

suspension was centrifuged at 4400 rpm for 30 mins and the volatiles were removed in a vacuum at 90 °C. The resulting solid was used for subsequent coating experiments. Ceramic yield: 30%. Average particle size: 100 nm.

2.3. Formation of alumoxane/ferroxane hybrid material

A sample of Nomex® fabric (18 mL) was washed sequentially with EtOH and acetone to remove excess dye molecules. The fabric was then vacuum dried to remove all volatiles. The fabric was dip-coated in an aqueous solution of L-cysteic acid-alumoxane 20 wt% (10 g in 50 mL) and held there for 2 – 5 s. The dip-coat was allowed to oven dry (100 °C) before repeating the procedure three times. Loading of L-cysteic acid functionalized ferroxane 5 wt% (1.0 g in 20 mL DI H_2O) onto the L-cysteic acid alumoxane coated Nomex® resulted in the nanoparticle coated Nomex® (NPN) fabric, which was tested against aspirated MS2 bacteriophage for virus filtration. In order

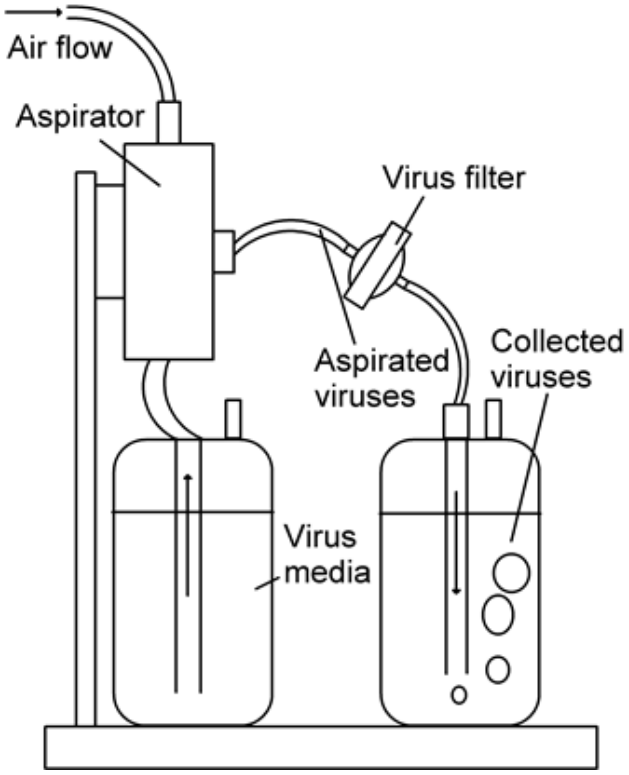

Fig. 2 Schematic diagram of the viral adsorption apparatus.

to limit potential nanoparticle shedding a similar sample was annealed to partially convert the nanoparticles to ceramic by heating the filter to 160 °C for 2 hrs in an argon atmosphere (NPN-160). Increased loading of cysteic ferroxane 20 wt% (5.0 g in 20 mL) was the undertaken onto an alumoxane functionalized 18 cm^2 piece of Nomex® fabric (NPN-4x). The above membranes were characterized via XPS, SEM-EDS and tested as virus filter against MS2 bacteriophage.

3. Viral absorption studies

The virus filtration experiments were conducted by generating an aerosolized virus stream, passing the output through a Nomex® fabric composite membrane the synthesis of which is outlined above, and collecting and enumerating the viruses that are completely transported through the system (Fig. 2 and Fig. S1‡). The aerosolized virus stream was generated using a TSI Constant Output Atomizer (model 3076, Shoreview, MN) operating in recirculation mode. The system was sterilized by operating with 70% EtOH followed by rinsing and operation with sterile ultrapure water prior to each experiment. To conduct an experiment, the virus stock was combined with 300 mL ultrapure water (final titer ~10^6 PFU/mL) in the feed reservoir, which was placed in an ice bath and connected to the atomizer. A 25 mm diameter piece of fabric was cut and placed in a reusable Swinnex® filter holder (Millipore, Billerica, MA) which was then attached to the discharge of the atomizer. The output of the filter holder was connected to a tube, which discharged through a stone diffuser into 150 mL of ultrapure water in a tall glass jar. The discharge water was sampled before each test and every 10 minutes up to 1 hour. Viruses in the samples were enumerated by the agar overlay method.[15]

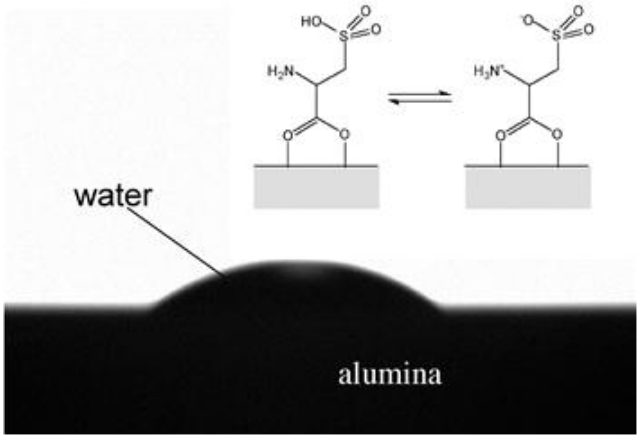

Fig. 3 Photographic images of water droplet on cysteic acid functionalized alumina surface taken immediately upon dropping on the surface since within a few seconds the droplet completely wets the surface. The Zwitter ionic forms of the cysteic acid are shown inset.

Results and Discussion

The strategy of our filters was to immobilize the nanoparticles onto a porous fabric scaffold (Fig. 1). To accomplish this, a fabric support with hydrophilic alumoxane and hydrophilic ferroxane nanoparticle was functionalized and subjected this filter to viral screening. Reduction in concentrations of viruses passing through the functionalized filter compared to the un-functionalized filter was by an order of magnitude.

Our previous work has shown that carboxylic acid functionalization of alumina surfaces can change the surface properties of the alumina.[9] We have previously undertaken the study of many carboxyilic acid functionalized hydrophilic surfaces. These effects were related to the hydrophilicity, as indicated by the contact angle of water on the surface. It was observed that cysteic acid functionalized alumina coated wafers were extremely hydrophilic, achieving complete wetability when in contact with water.[9] In fact the extent of wetting is such that complete wetting of the surface results which is attributed to the hydrogen bonding abilities of both sulfonyl and amine moieties

on functionalized cysteic acid and its Zwitter ionic form (Fig. 3).

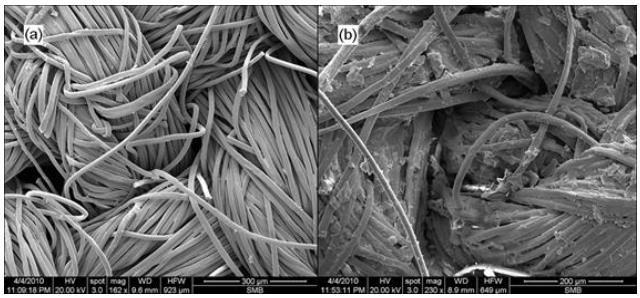

Fig. 4 SEM image of (a) uncoated Nomex fabric and (b) alumoxane/ferroxane composite coated fabric (NPN-2).

Based on these results cysteic acid was chosen as the best candidate for the creation of our highly hydrophilic alumoxane-ferroxane Nomex® composite membrane.

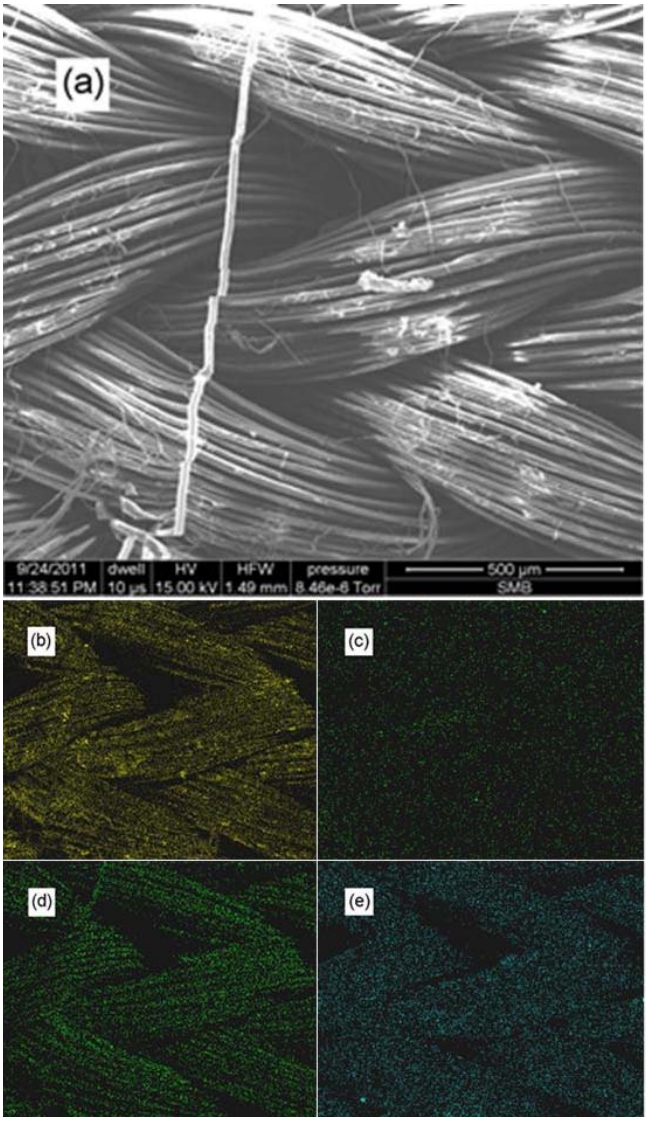

Fig. 5 SEM (a) and associated EDS maps of alumoxane/ferroxane nanoparticle coated fiber (NPN-2): (b) aluminum, (c) iron, (d) nitrogen, and (e) sulfur.

We havepreviously reported that carboxylic acid functionalized alumina and lepidiocrocite nanoparticles (carboxylate alumoxanes and ferroxane) can be used to coat a range of fabrics and fibers.[16] In the present case our goal was to deposit a thin layer of cysteic acid alumoxane onto a suitable support, anneal to 100 °C to provide a cysteic acid functionalized alumina surface on the support. Then repeat the process with ferroxane. TG/DTA analysis of the ferroxane nanoparticles (Fig. S4‡) shows that eating to 100 °C results in loss of adsorbed water without loss of the cysteic acid functional groups.

In contrast to our previous membrane work,[17] the resulting nanoparticle coated fabric (NPN) surface is not designed to act as a membrane on its own, but to be the sidewalls of a particle filtration membrane (10^3 - 10^6 nm pore size). SEM images indicated that deposition of the hydrophilic alumoxane and the viral active ferroxane nanoparticle occurred evenly across the fibers (Fig. 4).

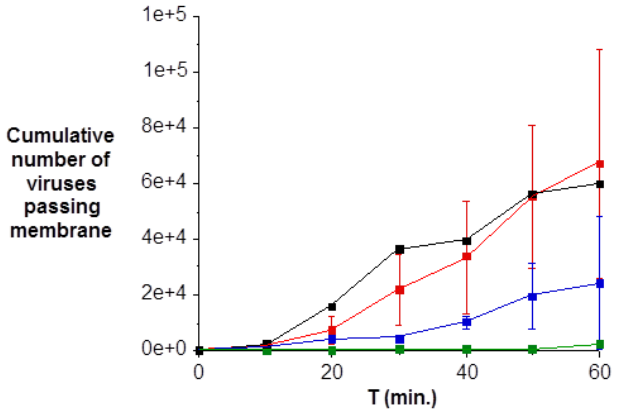

Fig. 6 Plot of cumulative number of viruses passing through the Nomex®-derived filters as a function of exposure time for MS2 bacterage adsorption studies: untreated Nomex® (■), NPN (■), NPN-4x (■), and NPN heated to 160 °C for 2 hours (■).

This observation is confirmed by EDS mapping of individual fibers (Fig. 5) showing a continuously uniformly coated single fiber as demonstrated by the overlap of the aluminum and iron EDS maps (Fig. 5b and c) with the SEM image of a fiber (Fig. 5a). The lower intensity of the iron signal is consistent with the lower concentration of the ferroxane. It is also important to note that the nitrogen and sulfur EDS maps (Fig. 5d and e) are identical since the sulfur is due to the cysteic acid functional group, while the nitrogen is due to both both the cysteic acid functional group and the Nomex® aramid structure. If there were areas of the fibers not coated then the sulfur and nitrogen maps would be expected to be dissimilar. Uniform layering allows for passages of air with deposition of water droplets containing the target virus. Furthermore, from Fig. 3 it can be seen that there is no extensive webbing that would preclude flow through the filter or act such that the fabric pore sizes are decreased.

The reason we chose to use Nomex® fabric as a support was that the large weave of the fabric cannot facilitate screening and thus it must be the surface of the fibers not pore size that is responsible for virus separation. Fabrication of the filter is achieved by first bringing the surface of the support into contact with a solution of cysteic acid functionalized alumoxane. The solution is drawn into the surface pores of the support by capillary forces. The surface coating thickness is controlled by the concentration of the cysteic acid alumoxane and ferroxane precursors and the pH of the solution. Size exclusion experiments

using Dextrans determined that pore throat size of the functionalized membranes were sufficiently large as to not be an issue.[9] Especially when considering that the Brownian motion of an aspirated water droplet as in its aerodynamic motion if less than 1 μm in diameter is significantly larger than its diameter.[18] This ensures that in the application of our membrane for aspirated virus removal within an air-way the air flux is large while still ensuring capture of the aerosol water droplet.

Testing of virus filtration was undertaken using bacteriophage MS2; this is a single stranded (+) RNA virus with an icosahedral capsid about 25 nm in diameter.[19] MS2 is similar to some water borne pathogenic viruses and has been used as a surrogate in several disinfection studies.[20] Compared to other bacteriophage, MS2 has been shown to be more resistant to UV disinfection.[21] In disinfection studies using chlorine and chloramines, MS2 was found to be comparable or resistant compared to Hepatitis A virus[22] and Poliovirus.[23] MS2 has also been recommended by the EPA as an indicator for viral inactivation processes.[24] MS2 is particularly convenient to work with, as its propagation and enumeration are relatively simple when compared to procedures required with pathogenic human viruses. Investigation of the screening properties for MS2 of the functionalized membranes and unfuntionalized membranes were investigated, using end-on filtration of aspirated viruses was measured. All virus trapping measurements were repeated to give statistical reliability.

Fig. 6 shows a plot of the cumulative number of viruses passing through each coated fabric as a function of time. It may clearly be seen that the alumoxane/ferroxane nanoparticle coated fabrics (NPN and NPN-4x) show a large decrease as compared to Nomex® alone. A Log plot is shown in Fig. S9‡. It is particularly noteworthy that an increase in the ferroxane content (i.e., sample NPN-4x versus sample NPN) results in an equivalent increase in virus retention. This suggests that it is the ferroxane that has an active role in either deactivating or binding to the virus.

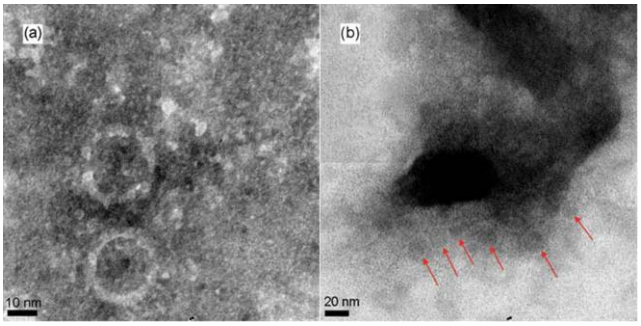

Fig. 7 TEM of (a) MS2 bacteriophage and (b) MS2 (arrowed) bound to cysteic acid-functionalized ferroxane nanoparticle.

In order to confirm this result we have investigated the interaction of MS2 with individual ferroxane particles by TEM. Fig. 7a shows a TEM image of two MS2 viruses for comparison, while in the center of Fig. 7b is a representative example of a ferroxane particle to which is associated with multiple MS2 viruses (TEM images of ferroxane particles in the absence of MS2 are shown for comparison in Fig. S6‡). In the entire TEM sample of NPN/MS2 all the ferroxane nanoparticles were observed "binding", i.e., being in close proximity to at least one if not multiple MS2 viruses.

From Fig. 6 it may be seen that the Nomex® fabric alone provides some barrier to transport of aspirated MS2 bacteriophage in comparison to no fabric at all. This provides a simple measure of the physical barrier that any porous fabric would provide. Although previous work has suggested that iron oxides should act as efficient traps for viruses such as MS2, the coated fabric that was heated to 160 °C (NPN-160) shows essentially that the same results as for untreated Nomex®, suggestive that the ferroxane is deactivated.

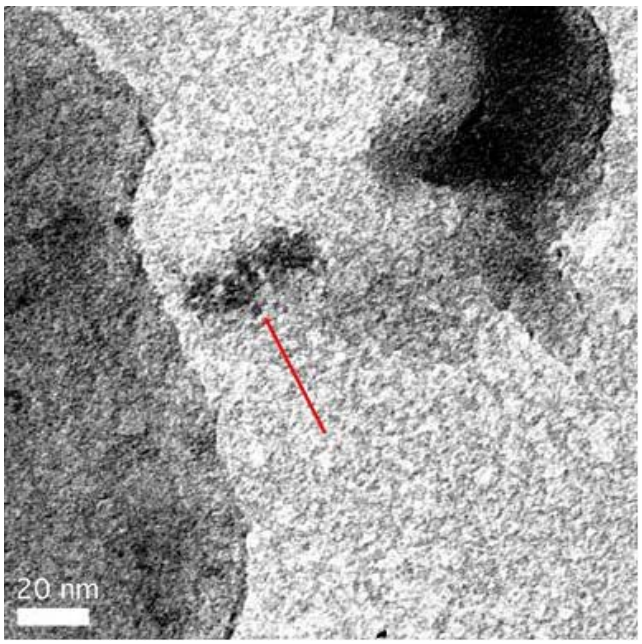

Fig. 8 TEM of MS2 bacteriophage (arrowed) bound to cysteic acid-functionalized ferroxane nanoparticle (left) that has been pretreated by heating to 160 °C for 2 hours.

However, TEM images of a sample of cysteic acid ferroxane heated to 160 °C and then mixed in the presence of MS2 bacteriophage shows particles associated with multiple MS2 viruses (Fig. 8) indicating that the binding of MS2 to the iron oxide nanoparticle is possible.

These results are indicative of two issues. First, the nanoparticle coating process does not significantly alter the porosity of (or flow through) the fabric, since NPN-160 and Nomex® alone behave identically, and hence the results for NPN and NPN-4x are not a consequence of smaller pore/weave sizes. Second, TGA data indicates that annealing either cysteic acid alumoxane or ferroxane to 160 °C (Fig. S4‡) results in the partial loss of functional groups on the nanoparticles without sintering of the individual nanoparticles and lowering the surface area.[14,25] This suggests that the surface fuctionalization of the nanoparticles (i.e, the hydrophilic surface due to the cysteic acid functional groups) is vital for the surface collapse of aspirated water droplet and the subsequent absorption and immobilization of the MS2 viruses. Thus we can conclude that a nanoparticle surface functionalization is far more important in the present process than the actual nanoparticle nature of the coating per se.

Conclusions

We have synthesized and characterized a permeable hydrophilic fabric-based filter with high flux for air flow and high virus

binding capabilities, derived from simple hydrophilic principles and natural virus binding mechanisms found in nature. The benign nature of synthesis of the membrane composite ensures that future functionalization of any component within an air-way system is possible with regards to virus inactivation. The concept of this membrane maybe utilized in the future for functionalizing multiple components. While it is reasonable to propose that the ferroxane-MS2 interaction is essentially the same as in nature with regards to virus binding to lepidiocrocite, the important result from this work is that it is not sufficient to have nanoparticles per se, but their surface functionality is important in ensuring functionality. In the present case this means the use of hydrophilic surface functionalization that ensures the collapse of aspirated water droplets and the wetting of the surface to allow exposure of the viruses to the "active" component of the surface.

Notes and references

[a] *Richard E Smalley Institute for Nanoscale Science and Technology, Rice University, Houston, Texas 77005, USA. Tel.: +1-713-348-5610; E-mail: arb@rice.edu, qilin.li@rice.edu*
[b] *Department of Chemistry, Rice University, Houston, Texas 77005, USA*
[c] *Department of Civil and Environmental Engineering, Rice University, Houston, Texas 77005, USA*
[d] *Department of Mechanical Engineering and Materials Science, Rice University, Houston, Texas 77005, USA*
[e] *College of Engineering, Swansea University, Singleton Park, Swansea SA2 8PP, Wales UK*
† Financial support for this work was provided by the US Navy and the Robert A. Welch Foundation (C-0002).
‡ Electronic supplementary information (ESI) available: SEM, EDX, and TEM images, XPS spectra, apparatus, TGA/DTA. See DOI: 0.1039/c2nr31117h

1 W. Renate, W. Macht, J. Durkop, R. Hecht, U. Hornig, and P Schulze, *Water Res.*, 1989, **23**, 133-136.
2 R. M. Cornell and U. Schwertmann. *The iron oxides*, VCH, New York (1996).
3 M. Pourbaix, *Atlas d'Equilibre Electrochimiques*, Gauthier-Villars, Paris (1963).
4 C. J. Daughney, X. Chatellier, A. Chan, P. Kenward, D. Fortin, C. A. Suttle and D. A. Fowle, *Mar. Chem.*, 2004, **91**, 101-115.
5 L. A. Warren and F. G. Ferris, *Environ. Sci. Technol.*, 1998, **32**, 2331-2337; X. Chatellier, D. Fortin, M. M. West, G. G. Leppard, and F. G. Ferris, *Eur. J. Mineral*., 2001, **13**, 705-714; C. J. Daughney, D. A. Fowle, and D. Fortin, *Geochim. Cosmochim. Acta.*, 2001, **65**, 1025-1035; J. B. Fein, S. Scott, and N. Rivera, *Chem. Geol.*, 2002, **182**, 265-273.
6 M. L. Wells and E. D. Goldberg, *Mar. Chem.*, 1992, **40**, 5-18; L. Wells and E. D. Goldberg, *Mar. Chem.*, 1993, **41**, 353-358; M. L. Wells and E. D. Goldberg, *Limnol. Oceanogr.* 1994, **39**, 286-302.
7 J. Wu and G. W. Luther III, *Limnol. Oceanogr.*, 1994, **39**, 1119-1129; J. Wu and G. W. Luther III, *Mar. Chem*., 1995, **50**, 159-177; J. Wu and G. W. Luther III, *Geochim. Cosmochim. Acta.*, 1996, **60**, 2729-2741; J. Wu, E. Boyle, W. Sunda, and L. –S. Wen, *Science*, 2001, **292**, 847-849.
8 J. Nishioka, S. Kakeda, C. S. Wong, and W. K. Johnson, *Mar. Chem.*, 2001, **74**, 157-179.
9 S. J. Maguire-Boyle and A. R. Barron, *J. Membrane Sci.,* 2011, **382**, 107-115.
10 R. S. Villar, A. A. Martinez, and J. M. D. Tascon, *J. Therm. Anal. Calorim.*, 2005, **79**, 529-532; L. T. Hasty, *Engineer*., 2003, **33**, 37; H. Gu, *Proc. Inst. Mech. Eng. S.*, 2009, **30**, 4324-4326.
11 Y. Sun and G. Sun., *Ind. Eng. Chem. Res.*, 2004, **43**, 5015-5020; A. Akdag, H. B. Kocer, S. D. Worley, R. M. Broughton, T. R. Webb, and T. H. Bray, *J. Phys. Chem. B.*, 2007, **111**, 5581-5586.
12 J. Rose, M. M. Cortalezzi-Fidalgo, S. Moustier, C. Magnetto, C. D. Jones, A. R. Barron M. R. Wiesner, and J. –Y. Bottero, *Chem. Mater.*, 2002, **14**, 621-628; M. M. Cortalezzi-Fidalgo, J. Rose, G. F. Wells, J. –Y. Bottero, A. R. Barron, and M. R. Wiesner, *J. Membrane Sci.*, 2003, **227**, 207-217; J. Rose, M. R. Wiesner, and A. R. Barron, *US Patent* 6,770,773 (2004).
13 M. Cho, H. Chung and J. Yoon. *Appl. Environ. Microbiology*, 2005, **71**, 270-275.
14 R. L. Callender, C. J. Harlan, N. M. Shapiro, C. D. Jones, D. L. Callahan, M. R. Wiesner, D. B. MacQueen, R. Cook, and A. R. Barron. *Chem. Mater*., 1997, **9**, 2418-2433.
15 M. H. Adams *Bacteriophages*; Interscience: New York, **1959**.
16 R. L. Callender and A. R. Barron, *J. Mater Sci.*, 2001, **36**, 4977-4987; R. L. Callender and A. R. Barron, *Ceramic Trans.*, 2000, **115**, 435-454; R. L. Callender and A. R. Barron, *J. Mater. Res*., 2000, **15**, 2228-2237.
17 C. D. Jones, M. Fidalgo, M. R. Wiesner, and A. R. Barron, *J. Membr. Sci.*, 2001, **193**, 175-184; D. A. Bailey, C. D. Jones, A. R. Barron, and M. R. Wiesner, *J. Membr. Sci.*, 2000, **176**, 1-9; K. A. DeFriend, M. R. Wiesner and A. R. Barron, *J. Membr. Sci.*, 2003, **224**, 11-28; K. A. DeFriend and A. R. Barron, *J. Membr. Sci.*, 2003, **212**, 29-38.
18 S. –S. Lu, X. Wang, H. Hirano, T. Tagawa, and H. Ozoe, *J. Appl. Phys.*, 2005, **98**, 114906-114909.
19 M. T. Madigan and J. M. Martinko. *Brock Biology of Microorganisms*. Pearson Prentice Hall, Upper Saddle River, NJ (2006).
20 M. A. Butkus, *Appl. Environ. Microbiol.*, 2004, **70**, 2848-2853; Y. Koizumi and M. Taya, *Biochem. Eng. J.*, 2002, **12**, 107-116; E. D. Mackey, *J. Am. Water Works Assoc.*, 2002, **94**, 62-69.
21 R. Sommer, *Water Res.*, 2001, **35**, 3109-3116.
22 M. D. Sobsey, T. Fuji, and P.A. Shields. *Water Sci. Technol.*, 1988, **20**, 385-391.
23 J. A. Tree, M. R. Adams and D. N. Lees, *Appl. Environ. Microbiol.*, 2003, **69**, 2038-2043.
24 M. Pirnie, *Guidance manual for compliance with the filtration and disinfection requirements for public water systems using surface water sources.* USEPA (1991).
25 R. L. Callender and A. R. Barron, *Adv. Mater*., 2000, **12**, 734-738.

